

MINERALOGY AND PETROLOGY  
OF THE  
HAM KIMBERLITE, SOMERSET ISLAND  
N.W.T., CANADA

By



Bruce Craig Jago

Submitted in Partial Fulfillment  
of the requirements for the degree of  
Master of Science

Faculty of Science  
Lakehead University  
Thunder Bay, Ontario, Canada

May, 1982

ProQuest Number: 10611674

All rights reserved

INFORMATION TO ALL USERS

The quality of this reproduction is dependent upon the quality of the copy submitted.

In the unlikely event that the author did not send a complete manuscript and there are missing pages, these will be noted. Also, if material had to be removed, a note will indicate the deletion.



ProQuest 10611674

Published by ProQuest LLC (2017). Copyright of the Dissertation is held by the Author.

All rights reserved.

This work is protected against unauthorized copying under Title 17, United States Code  
Microform Edition © ProQuest LLC.

ProQuest LLC.  
789 East Eisenhower Parkway  
P.O. Box 1346  
Ann Arbor, MI 48106 - 1346

THH BFC

W 5c

1982

524

(c) Bruce Craig Jago 1982

295227

## ABSTRACT

The Ham diatreme and dyke are post-late Silurian intrusions located in north-central Somerset Island and are the most northerly known kimberlites in the Somerset Island kimberlite province. The Ham diatreme, which consists of three petrographically distinct varieties of kimberlite, formed as a series of fluidized intrusions at the intersection of several regional fracture sets. Type 1A kimberlite is petrographically similar to the Ham dyke (a single intrusion located 1.5 km to the east) and forms the flanks of the Ham diatreme. This dark, massive rock contains phenocrysts and xenocrysts of garnet, olivine, chrome-diopside, phlogopite, spinel and carbonate in a serpentine-carbonate groundmass containing carbonate and serpentine emulsion textures. Type 1B kimberlite, which occupies the central portion of the Ham diatreme, is a highly altered, light green, serpentine-carbonate-rich rock formed by the prograde serpentinization and carbonatization of Type 1A kimberlite. This alteration occurred during the degassing of structurally lower portions of the Ham diatreme. Type 2 kimberlite is a carbonate-rich mineralogical equivalent of Type 1A kimberlite and formed as a late stage dyke within the Ham diatreme.

Pre-fluidization phenocrysts include Mg-rich olivine ( $\text{Fo}_{89-93}$ ), low Cr, ( $<3.5$  wt. %  $\text{Cr}_2\text{O}_3$ ), high Ti ( $>0.3$  wt. %  $\text{TiO}_2$ ) pyrope-garnet, Al-rich, Ti-poor ( $<2.00$  wt. %  $\text{TiO}_2$ ) aluminous-magnesium chromite ( $\text{Cr}/\text{Cr}+\text{Al}=0.18-0.85$ ) and Ti-rich phlogopite ( $1.0-4.6$  wt. %  $\text{TiO}_2$ ). Post-fluidization microphenocrysts include Mg-rich olivine ( $\text{Fo}_{89-93}$ ), Ti-rich phlogopite ( $2.5-4.0$  wt. %  $\text{TiO}_2$ ) and spinel which evolved from Ti-bearing ( $2.00$  wt. %  $\text{TiO}_2$ ), titan-magnesium-aluminous-chromite to  $\text{Fe}^{3+}$ - and Ti-rich (max.  $17.0$  wt. %  $\text{TiO}_2$ ) magnesium-ulvöspinel- ulvöspinel-magnetite. Atoll spinels, formed prior to the complete crystallization of the kimberlite groundmass are present in the Ham dyke but extensive resorption of magnesium-ulvöspinel- ulvöspinel-magnetite and titan-magnesium-aluminous-chromite in the Ham diatreme has precluded their persistence.

Xenocrysts formed by the disaggregation of garnet and spinel lherzolites include Cr-rich ( $3.5-10.0$  wt. %  $\text{Cr}_2\text{O}_3$ ), Ti-poor ( $<0.30$  wt. %  $\text{TiO}_2$ ) pyrope-garnet, Mg-rich olivine and chrome-diopside. Pressure temperature estimates from garnet lherzolite xenoliths range from  $36$  to  $37$  kb and  $1031$  to  $1146^\circ\text{C}$  corresponding to a depth of origin of  $110$  to  $120$  km.

Multiple discriminant analysis demonstrates that cluster analysis can only distinguish between

garnets of grossly different chemistry and paragenesis and that major and minor element variation diagrams are required to separate statistically, chemically similar garnets within a paragenesis.

Geophysical studies may be used to delineate kimberlite subcrop patterns and structural elements which may have controlled the intrusion of the kimberlite.

This thesis is dedicated to the early explorers of Canada's vast Arctic wilderness; to those who perished during the long, cold, lonely Arctic nights and to those who survived to see this hinterland flourish beneath the midnight sun.

## ACKNOWLEDGEMENTS

I sincerely wish to thank Dr. Roger Mitchell for suggesting and supervising this study and inspiring my career interests in kimberlites.

Ron Bennett and Sam Spivak are thanked for technical advice. Without Les Mayes and Bonnie Morton the enigmas of fortran would still be unresolved. Keith Pringnitz and Allan MacKenzie are thanked for technical assistance in the chemical instrumentation laboratory. Annabelle Downton provided excellent typing services.

Field assistance given by Valerie Dennison is appreciated. Mary, thank you for those long, late night discussions and for your untiring encouragement and understanding.

This study was supported financially by N.S.E.R.C. grants to Dr. R. H. Mitchell and myself and in the field, in part by the Polar Continental Shelf Project.

## Table of Contents

	<u>Page</u>
ABSTRACT	i
DEDICATION	iv
ACKNOWLEDGEMENTS	v
LIST OF FIGURES	ix
LIST OF TABLES	xii
LIST OF PLATES	xv
CHAPTER 1	
INTRODUCTION	1
GEOLOGY	3
FIELD GEOLOGY	3
FIELD PETROLOGY	5
PETROGRAPHY	9
Type 1A Kimberlite	9
Type 1B Kimberlite	11
Type 2 Kimberlite	11
CHAPTER 2	
OLIVINES	13
CHEMISTRY	13
CONCLUSIONS	24
CHAPTER 3	
MICAS	26
CHEMISTRY	27
CONCLUSIONS	34
CHAPTER 4	
GARNETS	35
The Compositional Variation of Ham Garnets	35
Classification of Ham Garnets	45
Statistical Classification	48

Table of Contents - cont'd

Cluster Analysis	53
Multiple Discriminant Analysis (MDA)	53
Principal Component Analysis (PCA)	56
The Statistical Classification and Analysis of Ham Garnets	58
CONCLUSIONS	78
CHAPTER 5	
CLINOPYROXENE	81
Comparison with other Somerset Island Pyroxenes	88
CONCLUSIONS	94
PYROXENE GEOTHERMOMETRY	94
GEOBAROMETRY	98
Temperature and Pressure Estimate for Ham Pyroxenes	99
CONCLUSIONS	99
CHAPTER 6	
HAM SPINELS	101
Aluminous Magnesian Chromite (AM-Chromite)	101
Titan Magnesian Aluminous Chromite	104
Atoll Spinel	104
Magnesian Ulvospinel Ulvospinel Magnetite	108
CHEMISTRY	108
Aluminous Magnesian Chromite (AM-Chromite)	111
Titan Magnesian Aluminas Chromite	118
Magnesian Ulvospinel Ulvospinel Magnetite	122
Atoll Spinel	123
A COMPARISON OF SPINEL EVOLUTIONARY TRENDS	127
Aluminous Magnesian Chromite (AM-Chromite)	127
Titan Magnesian Aluminous Chromite	130
Magnesian Ulvospinel Ulvospinel Magnetite	132
CONCLUSIONS	135

Table of Contents - cont'd

CHAPTER 7

CARBONATE AND SERPENTINE MINERALS	137
CARBONATE	137
Petrology	137
Carbonate in Kimberlite	138
SERPENTINES	141
Models of Prograde and Retrograde Serpentinization	141
Serpentine Petrography in the Ham Kimberlite	150
Type 1A Kimberlite	150
Type 1B Kimberlite	151
Type 2 Kimberlite	153
GEOCHEMICAL STUDIES	154
SERPENTINES IN KIMBERLITE	160
CARBONIZATION AND SERPENTINIZATION OF THE HAM KIMBERLITE	165

CHAPTER 8

MISCELLANEOUS MINERALS	168
PEROVSKITE	168
RUBY	169
CONCLUSIONS	175

CHAPTER 9

HEAVY MINERAL DISPERSION PATTERN	177
----------------------------------	-----

CHAPTER 10

MAGNETIC EXPRESSION AND STRUCTURAL CONTROL	188
STRUCTURAL CONTROL	194

CHAPTER 11

SUMMARY	200
---------	-----

REFERENCES	204
------------	-----

APPENDIX A - HAM DIATREME AND DYKE GARNETS	216
APPENDIX B - HAM DIATREME CLINOPYROXENES	225
APPENDIX C - CLUSTER ANALYSIS PROGRAM FOR HAM GARNETS	226
APPENDIX D - MULTIPLE DISCRIMINANT ANALYSIS PROGRAM FOR HAM GARNETS	234
APPENDIX E - MICROPROBE OPERATING CONDITIONS	235

### List of Figures

- Figure 1 - Geology map of the Ham kimberlite
- Figure 2 - Histogram of olivine composition (mol. % Fo)
- Figure 3 - Zonation trends in Ham olivines (mol. % Fo) and (wt. % NiO.)
- Figure 4 - NiO (mol. %) vs Fo (mol. %) variation diagram for Ham olivines
- Figure 5 - Comparison of the compositional variation of olivines from Somerset Island, Greenland and South African kimberlites
- Figure 6 - TiO<sub>2</sub> vs Cr<sub>2</sub>O<sub>3</sub> variation diagram for Ham micas (classification of Ham micas)
- Figure 7 - NiO vs Mg/Mg+Fe variation diagram for Ham micas
- Figure 8 - Mg-Fe-Ca ternary plot for Ham garnets - Ham diatreme
- Figure 9 - TiO<sub>2</sub> vs Cr<sub>2</sub>O<sub>3</sub> variation diagram for Ham diatreme garnets
- Figure 10 - Mg-Fe-Ca ternary plot for Ham garnets - Ham dyke
- Figure 11 - TiO<sub>2</sub> vs Cr<sub>2</sub>O<sub>3</sub> variation diagram for Ham dyke garnets
- Figure 12a - Histogram of canonical discriminant functions for clusters of Ham diatreme garnets generated by cluster analysis
- Figure 12b - Histogram of canonical discriminant functions for clusters of Ham dyke garnets generated by cluster analysis
- Figure 13 - Histogram of canonical discriminant functions for groups of Ham diatreme garnets generated by major and minor element plots
- Figure 14 - Histogram of canonical discriminant functions for groups of Ham dyke garnets generated by major and minor element plots

List of Figures con'd.

- Figure 15a - Histogram of canonical discriminant functions for groups of Ham diatrema and dyke garnets generated by major and minor element plots
- Figure 15b - Histogram of canonical discriminant functions for groups of Ham and Elwin Bay garnets
- Figure 16a - Orthogonal, 3-D plot of principle axes (PCA) of variation for groups of Ham diatrema garnets generated by major and minor element plots
- Figure 16b - Orthogonal, 3-D plot of principle axes (PCA) of variation for groups of Ham dyke garnets generated by major and minor element plots
- Figure 17 - Compositional variation of Ham pyroxenes in the pyroxene quadrilateral
- Figure 18 - A comparison of Ham pyroxenes and Somerset Island lherzolite pyroxenes in the pyroxene quadrilateral
- Figure 19 - A comparison of Ham pyroxenes and Somerset Island lherzolite pyroxenes in a Cr-Na-Al ternary plot
- Figure 20 - A comparison of Ham pyroxenes and pyroxenes from lherzolite xenoliths and groundmass pyroxenes in the Al vs Cr variation diagram
- Figure 21 - Histogram of canonical discriminant functions for Ham pyroxenes, pyroxenes from lherzolite xenoliths and groundmass pyroxenes
- Figure 22a - Compositional variation of Ham dyke spinels in the "reduced" spinel prism
- Figure 22b - Compositional variation of Ham diatrema Type 1A kimberlite spinels in the "reduced" spinel prism
- Figure 22c - Compositional variation of Ham diatrema Type 1B kimberlite spinels in the "reduced" spinel prism

List of Figures con'd.

- Figure 22d - Compositional variation of Ham diatrema Type 2 kimberlite spinels in the "reduced" spinel prism
- Figure 23 -  $MgAl_2O_4$ - $Mg_2TiO_4$ - $MgCr_2O_4$  ternary plot -Ham kimberlite spinels
- Figure 24 - Histogram of Ti-rich spinels
- Figure 25 - Univariant compositional variation diagram ( $TiO_2$  wt. %) for Ham spinels
- Figure 26 - Compositional variation trends in MU-magnetite in the Ham kimberlite
- Figure 27 - Histogram of Fe/Fe+Mg ratios for Ham serpentines
- Figure 28 -  $Fe^{2+}$  vs  $Mg^{2+}$  variation diagram for Ham serpentines
- Figure 29 -  $SiO_2$ - $MgO$ - $FeO$  ternary plot for Ham serpentines
- Figure 30 - Alteration paths in the Ham diatrema
- Figure 31a - Magnetic expression of the Ham kimberlite
- Figure 31b - Geological and structural interpretation of the Ham kimberlite (overlay)
- Figure 32 - Magnetic cross-sections of the Ham diatrema and dyke
- Figure 33 - Magnetic cross-sections of the Batty Bay kimberlites

### List of Tables

- Table 1 - Modal analyses (volume %) of the Ham Kimberlites
- Table 2 - Representative analyses of Ham olivines
- Table 3 - Representative analyses of Ham micas
- Table 4 - Representative analyses of Ham garnets
- Table 5A - Means, ranges and standard deviations for groups of Ham diatreme garnets generated on the basis of major and minor element compositional variation
- Table 5B - Statistical classification of Ham diatreme garnets by methods of Dawson and Stephens (1975)
- Table 6A - Means, ranges and standard deviations for groups of Ham dyke garnets generated on the basis of major and minor element compositional variation
- Table 6B - Statistical classification of Ham dyke garnets by methods of Dawson and Stephens (1975)
- Table 7A - Statistical classification of Ham diatreme garnets by methods of Danchin and Wyatt (1979)
- Table 7B - Statistical classification of Ham dyke garnets by methods of Danchin and Wyatt (1979)
- Table 7C - Danchin and Wyatt's (1979) classification scheme for garnets
- Table 8A - Means, ranges and standard deviations for clusters of Ham diatreme garnets generated by cluster analysis
- Table 8B - Means, ranges and standard deviations for clusters of Ham dyke garnets generated by cluster analysis
- Table 8C - Summary table of Wilks' lambda and F-ratios for Ham diatreme garnet clusters generated by cluster analysis

Tables con'd.

- Table 8D - Summary table of Wilks' lambda and F-ratios for Ham dyke garnet clusters generated by cluster analysis
- Table 9A - Summary table of Wilks' lambda and F-ratios for Ham diatreme garnet groups generated by major and minor element plots
- Table 9B - Summary table of Wilks' lambda and F-ratios for Ham dyke garnet groups generated by major and minor element plots
- Table 10 - Summary table of Wilks' lambda and F-ratios for a composite analysis of groups of Ham garnets
- Table 11 - Representative analyses of Ham clinopyroxenes
- Table 12 - Representative analyses of Ham clinopyroxenes and orthopyroxenes in garnet lherzolite xenoliths with a pressure-temperature estimate of equilibration
- Table 13 - A comparison of Ham pyroxenes with other Somerset Island Pyroxenes from Garnet and Spinel lherzolite xenoliths
- Table 14 - A comparison of Ham pyroxenes with pyroxene megacrysts and groundmass pyroxenes from North American and South African kimberlites
- Table 15 - Summary table of Wilks' lambda and F-ratios for Ham pyroxenes, pyroxenes from lherzolite xenoliths and groundmass pyroxenes
- Table 16 - Representative analyses of Ham spinels
- Table 17A- Compositional variation of Somerset Island AM-Chromites
- Table 17B- Compositional variation of chromite in spinel-bearing mantle xenoliths
- Table 18A- Representative analyses of titaniferous magnesium aluminous chromites - Somerset Island
- Table 18B- Representative analyses of titaniferous magnesium aluminous chromites - South Africa

Tables con'd.

- Table 19A- Representative analyses of Somerset Island MU-magnetite
- Table 19B- Representative analyses of South African MU-magnetite
- Table 20 - Representative analyses of Ham carbonate
- Table 21 - X-ray diffraction data for Ham serpentines
- Table 22 - Representative analyses of opaques in serpentine
- Table 23 - Representative analyses of Ham serpentines
- Table 24 - Representative analyses of Somerset Island and South African serpentines
- Table 25 - REE content of Ham perovskite
- Table 26 - Representative analyses of Ham rubies
- Table 27 - X-ray diffraction data of Ham rubies
- Table 28 - Distinctive characteristics of heavy minerals
- Table 29 - Concentrations of indicator minerals in stream sediment samples
- Table 30 - Grain morphologies of indicator minerals in stream sediment samples
- Table 31 - Comparison of grain morphologies and mineral abundances with data from Russian and Australian kimberlites
- Table 32 - Magnetic intensities of Somerset Island, American, South African and Russian kimberlites

## List of Plates

- 1 - Aerial view of the Ham diatreme from the southwest
- 2 - Ham dyke viewed from the southwest
- 3 - Type 1A kimberlite
- 4 - Type 1B kimberlite
- 5 - Type 2 kimberlite
- 6a-6f - Scanning x-ray photographs of the major element distribution in a Ham spinel
- 7a-7f - Scanning x-ray photographs of the major element distribution in a Ham atoll spinel
- 8a-8f - Scanning x-ray photographs of the major element distribution in a Ham atoll spinel
- 9a - Coarse bladed lizardite in a retrograde serpentine pseudomorph
- 9b - Spherulitic prograde serpentine in a carbonate emulsion texture
- 10a - Chrysotile rods in a carbonate (leached by HCl) emulsion texture
- 10b - Chrysotile rods with coarse bladed lizardite
- 11a - Antigorite blades protruding into a carbonate (leached by HCl) emulsion texture
- 11b - Interlocking antigorite blades in the kimberlite groundmass

## Appendices

- A - Ham garnet analyses
- B - Ham clinopyroxene analyses
- C - Cluster analysis program
- D - Multiple discriminant analysis program
- E - Microprobe operating conditions

## Location Map

See back pocket.

CHAPTER 1INTRODUCTION

The Ham Kimberlite, the most northerly known kimberlite (Map 1) of the Somerset Island kimberlite province (Mitchell 1976) intrudes Ordovician limestones which were deposited on the flanks of Precambrian Boothia granulite terrains exposed on the west coast of Somerset Island, N.W.T. The intrusion of the kimberlite is believed to pre-date Cenozoic volcanic activity associated with Eurekan rifting and to be post-late Silurian in age (Mitchell 1976). During intrusion, mantle-derived ultrabasic xenoliths and abundant country rock fragments were incorporated into the kimberlite magma.

The Ham diatreme (Plate 1) is exposed as frost-heaved regolith on a gently sloping plain adjacent to the Cunningham River in north-central Somerset Island (Map 1). The Ham dyke (Plate 2) is a northeast-southwest trending intrusion exposed approximately 1.5 kilometres to the northeast.

This study describes in detail the petrography, mineralogy, magnetic expression, structural control and mineral dispersion pattern of the Ham Kimberlite.

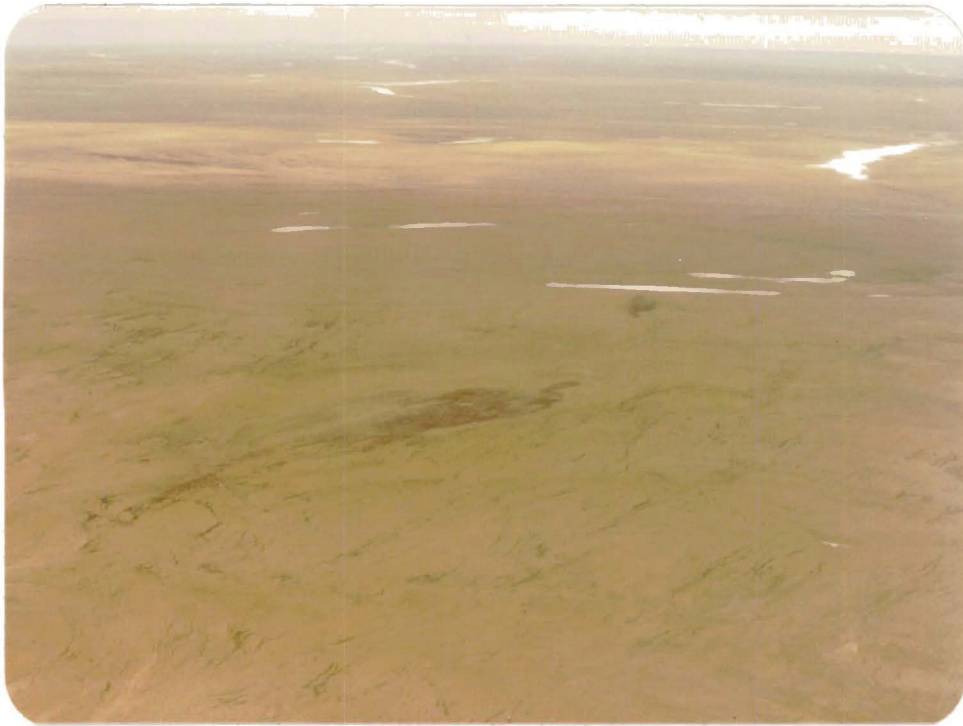


Plate 1:  
Aerial view of the Ham diatrema from the southwest

Plate 2:  
Ham dyke viewed from the southwest

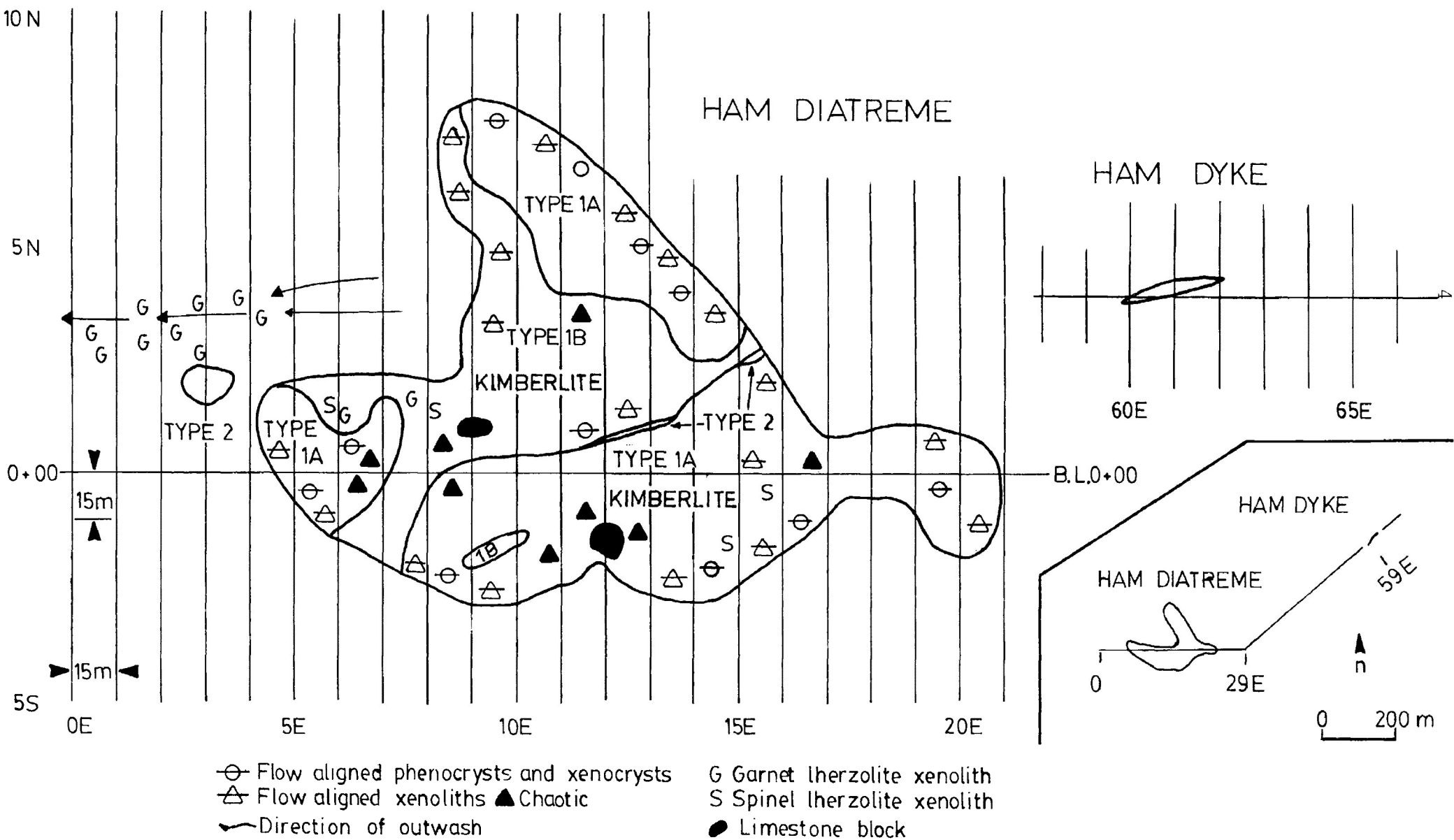


GEOLOGYFIELD GEOLOGY

Regolith mapping techniques can be applied at the Ham Kimberlite because little or no lateral transport of vertically frost-heaved kimberlite fragments has occurred. Field mapping distinguished three petrographically distinct varieties of kimberlite within the Ham diatreme. The diatreme predominantly consists of Type 1A kimberlite with subordinate Type 1B and Type 2 kimberlite. The Ham dyke is petrographically similar to diatreme Type 1A kimberlite.

Field relations illustrated in Figure 1 indicate that the Ham diatreme forms a roughly bell-shaped concentration of kimberlite regolith approximately 270m long and up to 165m wide. Several concentrations of limestone regolith are interpreted to be large blocks of country rock which have slumped in the kimberlite. The northern and southern flanks and the apex of the diatreme consists of Type 1A kimberlite. Type 1B kimberlite occupies the central portion of the diatreme and appears to cross-cut the northern and southern flanks. Type 2 kimberlite forms a small, circular concentration of kimberlite regolith 10 metres west of the diatreme and occurs as two isolated

FIGURE 1  
GEOLOGY MAP OF THE HAM KIMBERLITE



concentrations of regolith within the northern and southern flanks of the diatreme. These are interpreted to represent a discontinuous dyke.

Field relations and geophysical studies (Chapter 10) of the Ham Kimberlite indicate that it does not represent the upper portions of a fluidized diatreme (Dawson 1967) but probably represents a series of "blows" or enlarged fluidized fissure intrusions along several intersecting fracture sets which eventually coalesced to form a roughly bell-shaped intrusion. The Ham dyke is interpreted to be a single, fluidized fissure intrusion. Time relations cannot be ascertained between the Ham diatreme and dyke and geophysical studies indicate these are separate intrusive systems.

#### FIELD PETROLOGY

Type 1A kimberlite (Plate 3) in the Ham diatreme and dyke is a black, massive to weakly foliated, porphyritic rock containing fresh to strongly altered, small (<5mm long), rounded, olivine megacrysts and abundant carbonate in rounded to cusp-shaped emulsion textures (see Chapter 7) and tiny veinlets in a fine to medium-grained carbonate- and serpentine-rich groundmass. Rounded megacrysts of phlogopite and garnets with alteration (kelyphite) rims



Plate 3:  
Type 1A kimberlite

are scarce. Angular to subrounded limestone xenoliths, which occur throughout the diatreme and dyke, are weakly to moderately altered. Megacrysts and xenoliths demonstrate flow alignment throughout the Ham dyke and adjacent to the margins of the northern and southern flanks of the diatreme.

Type 1B kimberlite (Plate 4) is a light reddish-green, massive to porous rock, containing highly altered limestone xenoliths and small (<3mm long), massive to porous, oblong patches of dark green serpentine or serpentine plus carbonate, within a fine-grained groundmass. Petrographic examination reveals that the oblong patches of serpentine are pseudomorphs after rounded olivine megacrysts. Groundmass carbonate and emulsion textures and veins are scarce to moderately abundant.

Type 2 kimberlite (Plate 5) is a grey to light blue-grey, massive, porphyritic rock containing abundant fresh to strongly altered, small (<3mm long), rounded olivine megacrysts and scarce, large (<5mm long), rounded phlogopite megacrysts in a very fine-grained carbonate-rich groundmass. Country rock fragments, which are small, sub-angular to sub-rounded fragments of limestone, are strongly altered and commonly flow aligned parallel to olivine megacrysts. Carbonate veins and emulsion textures are very scarce.



Plate 4:  
Type 1B kimberlite

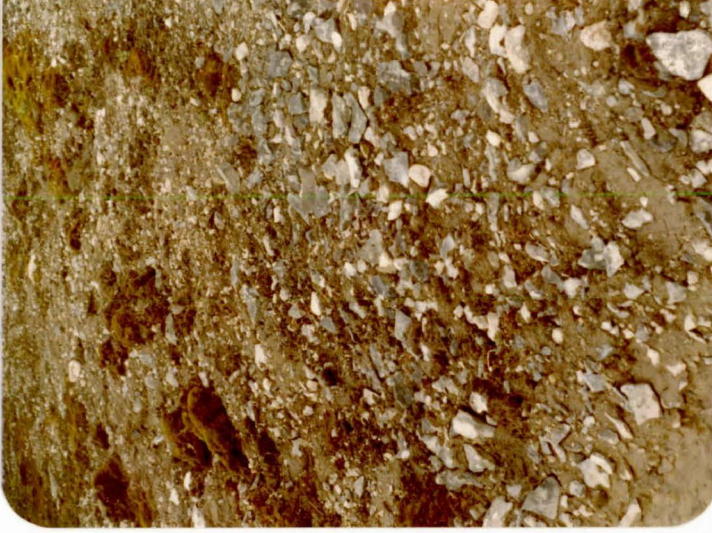


Plate 5:  
Type 2 kimberlite

The rounded aspect of some ultrabasic xenoliths and some country rock fragments and kimberlite megacrysts is interpreted to be a result of fluidized transport in the kimberlite magma. Fluidization (Reynolds 1954 and Dawson 1967) is an intrusive process during which megacrysts and cognate and accidental xenoliths are rounded and abraided by a moving, gas-charged medium prior to crystallization.

#### PETROGRAPHY

Petrographic examination indicates that Hamiatreme Type 1A, Type 1B and Type 2 kimberlites are petrographically distinct kimberlite varieties. Hamdiatreme and dyke Type 1A kimberlite are similar petrographically, although minor textural and petrographic distinctions can be discerned. Table 1 gives the modal abundance of kimberlite minerals.

#### Type 1A Kimberlite

Type 1A kimberlite is a massive to weakly foliated, porphyritic rock containing two generations of olivine, phlogopite and spinel in a fine-grained groundmass of serpentine, carbonate, spinel, perovskite and apatite. Heavy mineral separation indicates the presence of pyrope-garnet, chrome-diopside and ruby. Serpentine and

Table 1

## Modal Analysis (Volume %) of Ham Kimberlites

Minerals	Type 1A	Type 1B	Type 2
Olivine <sup>1</sup>	40	40	40
Mica	<1	<1	<1
Garnet	<1	<1	<1
Cr-Diopside	<1	<1	<1
Spinel	<1	<1	<1
Carbonate <sup>2</sup>	10-15	n.r.	15-20
Serpentine <sup>3</sup>	45-50	n.r.	37-42
Perovskite	<1	<1	<1
Apatite	<1	<1	<1
Secondary Minerals <sup>2</sup>			
Carbonate <sup>4</sup>	3	5-10	1
Serpentine <sup>5</sup>	15	50-65	<1

- 1 - includes fresh olivine and serpentine pseudomorphs after olivine
- 2 - includes carbonate in emulsion textures and as groundmass laths
- 3 - includes serpentine in the groundmass and serpentine in emulsion textures
- 4 - includes carbonate as olivine pseudomorphs and groundmass replacement
- 5 - includes serpentine in olivine pseudomorphs and as a groundmass replacement
- n.r. - information not recorded due to obliteration of primary features

carbonate form rounded (Ham dyke) to cusp-shaped (Ham diatrema) emulsion textures in the groundmass. Serpentine and less commonly serpentine and carbonate form incipient to complete pseudomorphs after olivine and groundmass crystals of phlogopite. Ham dyke Type 1A kimberlite may be distinguished from diatrema Type 1A kimberlite by a more diverse suite of spinels and less intense serpentinization of olivines and groundmass minerals .

#### Type 1B Kimberlite

Type 1B kimberlite is a massive to porous, highly serpentinized and weakly carbonatized rock, containing two generations of olivine and spinel, in a fine-grained groundmass of serpentine, carbonate, spinel and perovskite. Serpentine and carbonate occur predominantly as alteration minerals after olivine and country rock fragments and in emulsion textures and veinlets. Type 1B kimberlite is a serpentinized and weakly carbonatized equivalent of Type 1A kimberlite, in which olivines are wholly pseudomorphed by serpentine and second generation spinels are extensively corroded.

#### Type 2 Kimberlite

Type 2 kimberlite is a massive, carbonate-rich, serpentine-poor kimberlite, containing two generations of

fresh to incipiently altered olivine and spinel and scarce phlogopite megacrysts. Groundmass minerals include spinel, perovskite, carbonate and minor serpentine. Carbonate forms in cusp-shaped emulsion textures and serpentine occurs as scarce crosscutting veins and rims on olivine. Type 2 kimberlite is a carbonate-rich, serpentine poor, relatively unaltered equivalent of Types 1A and 1B kimberlite, in which second generation spinel is relatively scarce and second generation phlogopite is lacking.

Further details of the petrography are given in the discussion of individual minerals in Chapters 2 to 3.

CHAPTER 2OLIVINES

Olivine in the Ham diatreme and dyke kimberlite occurs as small (<0.75mm long), euhedral to subhedral, post-fluidization microphenocrysts and, as large (<6mm long), rounded, anhedral, pre-fluidization megacrysts. Megacryst olivines may exhibit cataclastic textures and undulatory extinction.

Fresh olivine microphenocrysts and megacrysts are found only in Type 2 kimberlite and are absent in Type 1B kimberlite. Fresh megacrysts are present in Type 1A kimberlite although fresh microphenocrysts are absent. Therefore, no chemical data is available for microphenocrysts in Types 1A or 1B kimberlite, or for megacrysts in Type 1B kimberlite.

The nature of the olivine alteration is discussed in detail in Chapter 7. In brief, olivine microphenocrysts and megacrysts may be incipiently to wholly replaced by serpentine + magnetite or serpentine and carbonate + magnetite.

CHEMISTRY

Representative analyses of Ham olivines are given in Table 2 and their compositional variation (mol. % Forsterite) is illustrated in Figure 2.

Inspection of Figure 2 reveals that Ham olivines range in composition from Fo<sub>88-94</sub>. Figure 2B indicates that olivine microphenocrysts in Type 2 kimberlite cannot be distinguished chemically from megacryst olivines in Type 1A or Type 2 kimberlite although both microphenocrystal and megacryst olivines can be distinguished chemically from large, rounded, "porphyroclastic" olivines (Fo<sub><89</sub> mol. %). Table 2 indicates that the nickel contents of the olivine megacrysts and the microphenocrysts are similar.

Zonation trends plotted in Figure 3 reveal that both olivine megacrysts and microphenocrysts are zoned toward iron-rich (approx. 1 mol. % Fa) and nickel-depleted (approx. 0.15 mol. % Ni-ol) margins although some crystals are not zoned and some demonstrate reverse zoning.

Inspection of Figure 4 reveals that olivine megacrysts from Type 1A kimberlite exhibit a broad range of nickel-olivine contents ( $\text{Ni}_2\text{SiO}_4 = 0.00-0.25$ ) and a restricted range in forsterite contents (Fo<sub>91.5-92.5</sub>).

In contrast, olivine microphenocrysts and megacrysts from Type 2 kimberlite exhibit a broader range in forsterite (Fo<sub>89.5-93.5</sub>) contents and a more restricted range in nickel-olivine ( $\text{Ni}_2\text{SiO}_4 = 0.25-0.05$ ) contents. These olivines demonstrate poor negative and positive correlations between magnesium and nickel, respectively.

Table 2A  
Representative Analyses of Ham Olivines

OXIDE	1	2	3	4	5	6	7	8	9	10
SiO <sub>2</sub>	40.96	41.02	41.20	40.24	41.62	41.23	41.60	41.23	41.77	41.27
FeO*	7.46	7.57	7.69	10.75	7.31	7.35	6.51	6.98	7.48	8.32
MgO	51.23	51.29	51.05	48.37	50.71	51.36	51.77	51.65	50.57	50.07
CaO	0.05	0.01	0.02	0.04	0.02	0.00	0.04	0.02	0.00	0.02
MnO	0.00	0.00	0.00	0.00	0.00	0.00	0.00	0.00	0.12	0.02
NiO	0.29	0.13	0.17	0.08	0.14	0.16	0.09	0.13	0.15	0.07
Total	99.99	100.01	100.13	99.46	99.80	100.11	100.02	100.01	100.09	99.77
Fo(mol. %)	92.5	92.4	92.2	88.9	92.6	92.6	93.5	93.0	92.3	91.5
OXIDE	11	12	13	14	15	16	17	18	19	20
SiO <sub>2</sub>	41.41	40.15	40.46	41.08	41.25	40.57	40.66	41.30	40.27	40.52
FeO*	7.67	10.13	10.79	8.45	7.14	8.43	9.45	6.85	9.84	9.85
MgO	50.76	48.08	48.11	50.85	51.84	49.92	49.51	51.68	49.72	49.92
CaO	0.02	0.07	0.03	0.07	0.01	0.09	0.09	0.09	0.09	0.11
MnO	0.01	0.00	0.05	0.00	0.00	0.00	0.00	0.00	0.00	0.03
NiO	0.13	0.20	0.12	0.18	0.13	0.20	0.08	0.17	0.20	0.27
Total	100.01	99.34	99.55	100.64	100.36	99.20	99.80	100.08	100.11	100.70
Fo(mol. %)	92.3	89.6	88.9	91.5	92.8	91.4	90.4	93.1	90.0	90.0

Analyses 1-11 Large Rounded Olivines (<6mm) - Type 1A kimberlite  
 Analyses 12-13 Large Rounded Strained Olivines (<6mm) - Type 2 kimberlite  
 Analyses 14-20 Small Euhedral Olivines (<0.75mm) - Type 2 kimberlite

\*-Total Iron as FeO

Table 2B  
Ranges in Forsterite, NiO and CaO Contents of Ham Olivines  
Rounded Olivines Euhedral Olivines

OXIDE	CORE	MARGIN	CORE	MARGIN
Forsterite (% Fo)	93.5-88.9	92.8-88.8	93.1-90.0	92.0-90.0
NiO (wt. %)	0.32-0.05	0.24-0.00	0.32-0.08	0.25-0.12
CaO (wt. %)	0.06	-	0.15	-
		0.00		0.05

## FIGURE 2

### HISTOGRAM OF OLIVINE COMPOSITIONS (mol.%Fo)

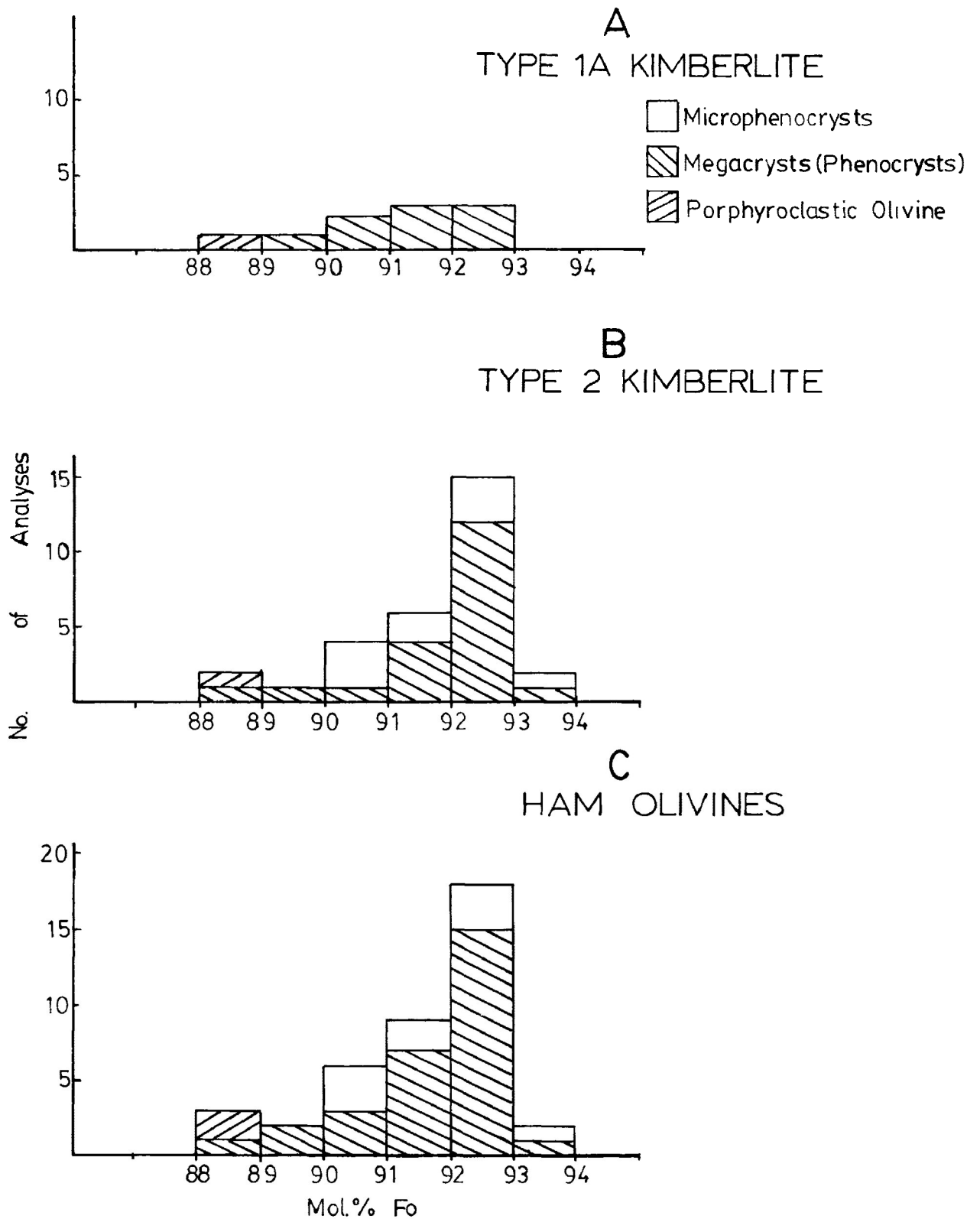
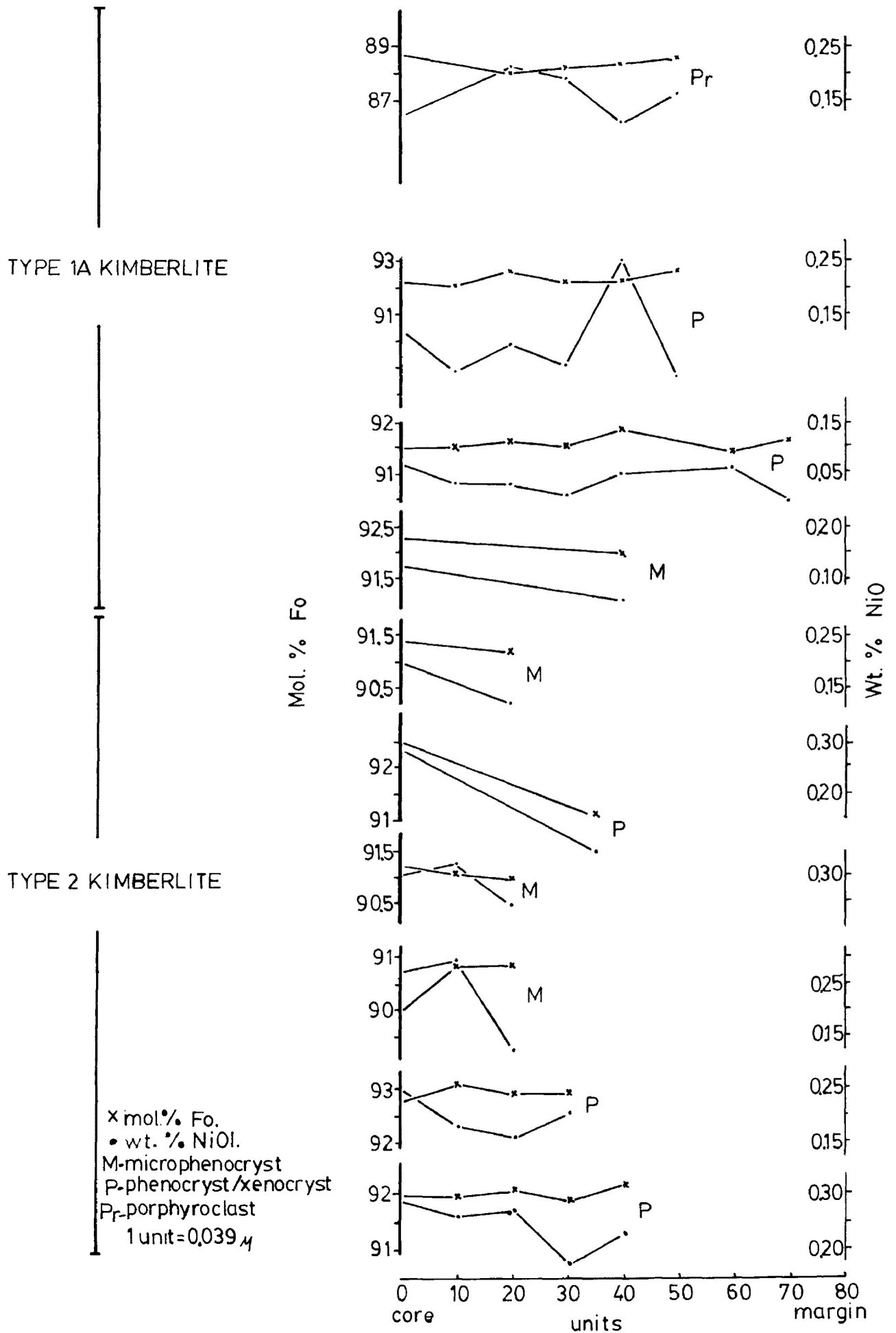
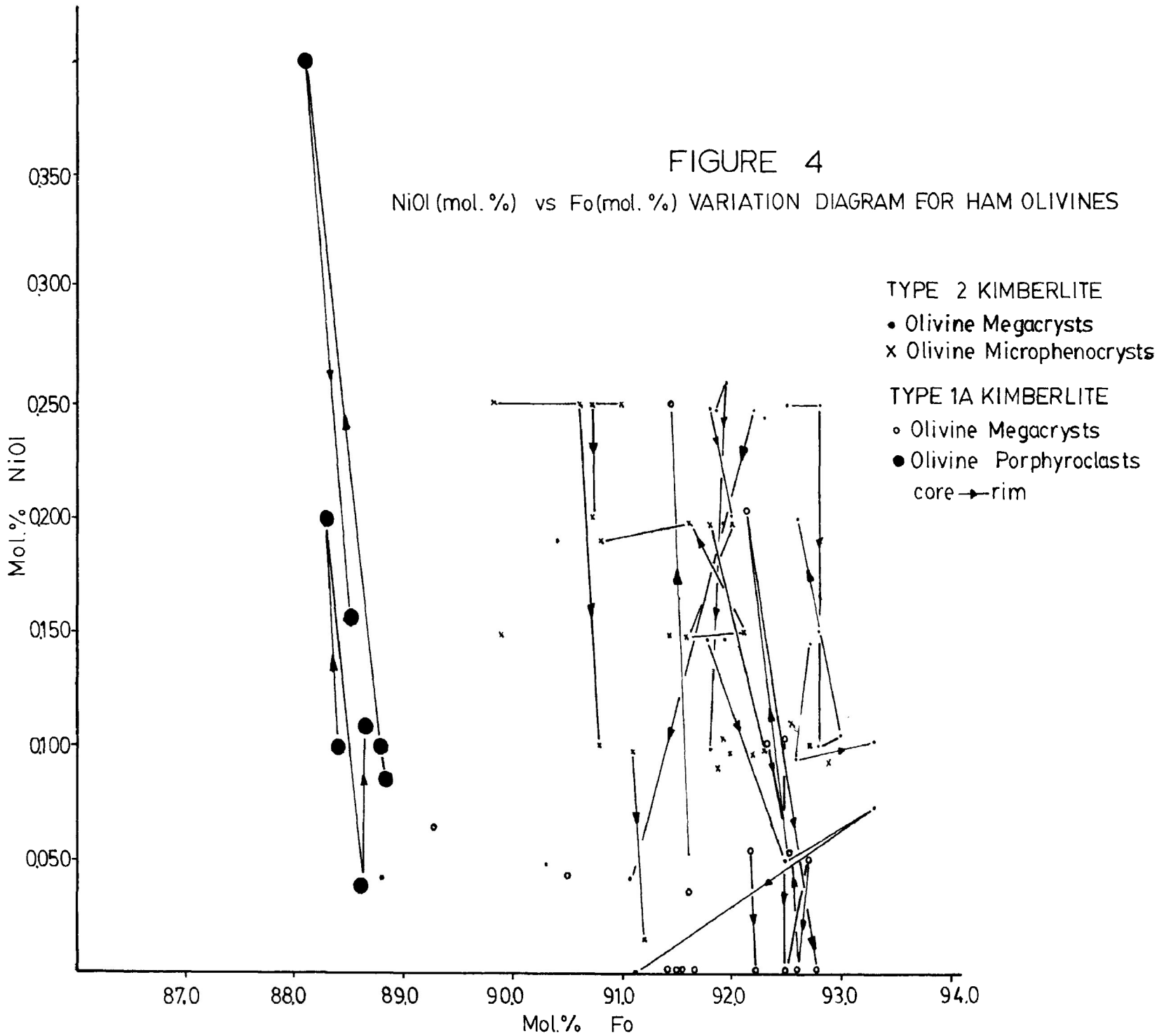


FIGURE 3  
ZONATION TRENDS IN HAM OLIVINES (mol.% Fo) AND (wt.% NiO)



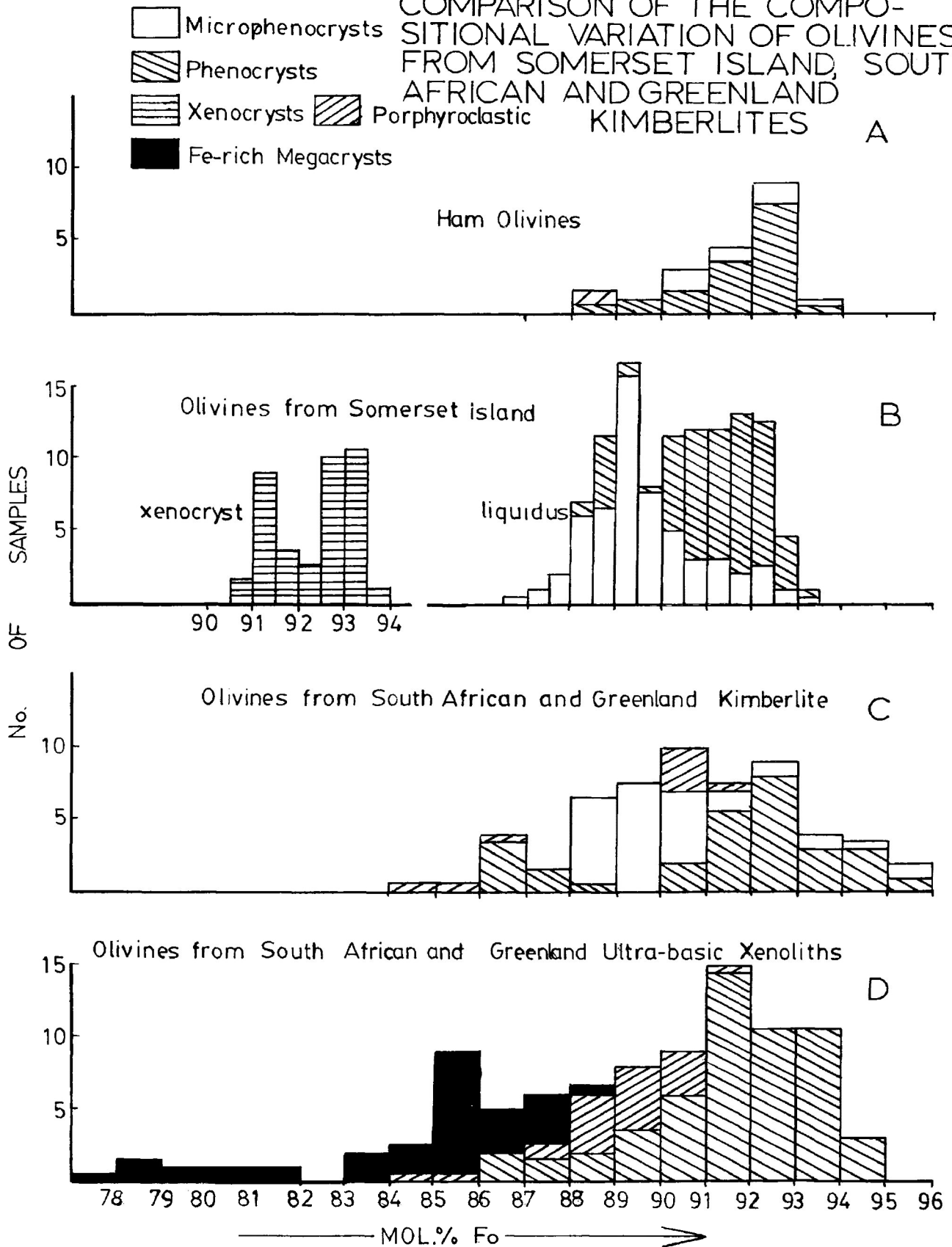


Porphyroclastic olivines have a limited range in composition ( $\text{Fo}_{88-89}$ ) but a broad range of nickel-olivine ( $\text{Ni}_2\text{SiO}_4=0.40 - 0.05$ ) contents.

A comparison of Figures 2 and 5 demonstrate that the compositional variation of Ham olivines ( $\text{Fo}_{88.0-93.5}$ ) is similar to that of olivines from other Somerset Island kimberlites ( $\text{Fo}_{86.0-93.5}$ , Mitchell and Fritz 1972, Mitchell 1978a, 1979a). Ham olivines do not show the bimodal distribution of compositions that olivine microphenocrysts and megacrysts display in the Peuyuk (Mitchell and Fritz 1972), Tunraq (Mitchell 1979a) or Jos kimberlites (Mitchell and Meyer 1980). The unimodal distribution demonstrated by Elwin Bay olivines (Mitchell 1978a) encompasses the compositional variation of Ham olivines.

Olivine microphenocrysts and megacrysts from the Ham Kimberlite are compositionally similar to olivine megacrysts from other Somerset Island kimberlites but contain olivine microphenocrysts which are more magnesium than microphenocrysts from the Peuyuk (Mitchell and Fritz 1972) or Tunraq (Mitchell 1979a) kimberlites. The paucity of microphenocryst analyses less magnesium than  $\text{Fo}_{90}$  indicates that these olivines crystallized from a magnesium-enriched kimberlite magma rather than a magma depleted in magnesium by the fractional crystallization of pre-fluidization olivine megacrysts. Mitchell

FIGURE 5  
COMPARISON OF THE COMPOSITIONAL VARIATION OF OLIVINES FROM SOMERSET ISLAND, SOUTH AFRICAN AND GREENLAND KIMBERLITES A



postulates a similar origin for olivine microphenocrysts in the Elwin Bay (Mitchell 1978a) and Jos kimberlites (Mitchell and Meyer 1980).

Inspection of Table 2 and Figures 3 and 4 reveal that Ham olivines demonstrate complex zonation patterns which include combinations of reverse and normal zoning. In general, zonation patterns are similar to those described by Mitchell and Fritz (1972) and Mitchell (1978a, 1979a) who show that olivines from Somerset Island kimberlite are zoned toward iron-rich (approximately 1 mol. % Fa) and nickel-depleted grain margins. CaO contents of Ham olivines (max. 0.15 wt % CaO) are similar to calcium contents of olivines from other Somerset Island kimberlites (max. 0.20 wt %). Olivine megacrysts and microphenocrysts from the Ham diatreme may be distinguished on the basis of their CaO contents; the former contains up to approximately 0.60 wt. percent CaO and the latter bears between 0.05 and 0.15 wt. percent CaO. A similar relationship was established by Mitchell (1979a) for olivines from the Tunraq kimberlite.

A comparison of Figures 5A and 5C indicate olivine megacrysts from the Ham kimberlite are compositionally similar to olivine megacrysts from South African and Greenland kimberlites although olivine microphenocrysts

from the Ham kimberlite are more forsterite-rich than the majority of olivine microphenocrysts in the latter kimberlites.

Chemical zonation trends determined for Ham olivines are similar to zonation trends found in olivines from the DeBeers (Boyd and Clement 1977), Wesselton Mine and Ison Creek (Mitchell 1973), Benfontein (Dawson and Hawthorne 1973) and South-west Greenland (Emeleus and Andrews 1975) kimberlites. These kimberlites demonstrate positive and negative correlations between magnesium and nickel and manganese, respectively (Simkin and Smith 1970), in crystals which may demonstrate normal or reverse zoning of magnesium and nickel toward grain margins. Magnesium zonation according to Boyd and Clement (1977) and Emeleus and Andrews (1975) converges on a compositional band between  $\text{Fo}_{87-91}$ . MnO contents are uniformly low, which agrees with data for forsterite-rich olivines given by Simkin and Smith (1970). Calcium contents, in agreement with data presented by Warner and Luth (1973) for the  $\text{Mg}_2\text{SiO}_4$ - $\text{CaMgSiO}_4$  solvus are low (<0.10 wt. % CaO). Simkin and Smith (1970) suggest that low calcium contents characterize a plutonic origin for olivine and that higher calcium contents (>0.10 wt. % CaO) suggest a hypabyssal to extrusive origin.

A comparison of Figures 5A, B, C and D reveal that the majority of olivine megacrysts are forsterite-rich ( $>Fo_{90}$ ) compared to olivine microphenocrysts ( $Fo_{87-90}$ ) although Mitchell (1973), Boyd and Clement (1977), Mitchell (1979a) and Mitchell and Meyer (1980) indicate that magma mixing may be responsible for the occurrence together of forsterite-rich ( $Fo_{90-94}$ ) and relatively fayalite-rich ( $Fo_{77-89}$ ) olivine megacrysts. The former olivines cannot be distinguished chemically from forsterite-rich olivine phenocrysts. Inspection of Figure 5D reveals that olivines from mantle-derived ultra-basic xenoliths are compositionally similar to kimberlite olivines and have a compositional maxima which closely coincides with the compositional maxima of forsterite-rich olivine phenocrysts and some olivine microphenocrysts (e.g. Ham olivines, this study, and Elwin Bay Mitchell 1978a). Mitchell (1973), Boyd and Clement (1977) and Nixon et al (1963) have attempted to distinguish between olivines derived from the fragmentation of ultra-basic xenoliths and olivines which have crystallized as pre-fluidization phenocrysts and post-fluidization microphenocrysts from a kimberlite magma. The chemical similarity of these three varieties of olivines is further complicated by the textural similarity of

rounded, pre-fluidization olivine phenocrysts and rounded olivines from ultra-basic xenoliths which may not demonstrate cataclastic textures. Mitchell (1973) suggests that the vast numbers of large, rounded olivines observed in kimberlites precludes their derivation solely from fragmented ultra-basic xenoliths, which, in some kimberlites are scarce or lacking (Davidson 1964). In addition, Mitchell (1973) indicates that a kimberlite magma which crystallized abundant post-fluidization olivine microphenocrysts should have been able to crystallize pre-fluidization olivine phenocrysts during the ascent of the magma throughout the upper mantle.

#### CONCLUSIONS

Petrographic examination of Ham kimberlite reveals that two generations of olivine crystals are present; a large, rounded, pre-fluidization olivine megacryst, which may demonstrate cataclastic textures and a post-fluidization microphenocryst. Geochemical studies suggest that olivine megacrysts ( $\text{Fo}_{89-94}$ ) and microphenocrysts ( $\text{Fo}_{90-94}$ ) cannot be distinguished chemically, but, are more forsterite-rich than porphyroclastic olivines ( $\text{Fo}_{88-89}$ ). Major (Mg, Fe) and minor (Ni, Ca, Mn) element distribution patterns in Ham

olivines are similar to distribution patterns in olivines from other kimberlites, although the sometimes complex distribution of magnesium, iron and nickel indicates magma mixing has occurred. Petrographic and geochemical studies reveal that olivine megacrysts which may have crystallized from a kimberlite magma cannot be distinguished from strain-free olivines, which may have been derived from the fragmentation of ultrabasic xenoliths.

CHAPTER 3MICAS

The Ham Kimberlite contains two generations of phlogopite:

- 1) Large (max. 5mm across), rounded and corroded, anhedral megacrysts
- and 2) Microphenocrysts as tiny (<0.1 mm long) euhedral laths.

Phlogopite megacrysts are commonly broken, exhibit strained extinction and are pleochroic light tan brown to dark tan brown to dark orange brown. Optical zonation was not observed although a single, corroded crystal was overgrown by a thin (<0.05mm thick), corroded mantle of tan brown phlogopite. Grain margins may be bleached colourless and incipiently replaced by chlorite and/or carbonate. Megacrysts are pseudomorphed by serpentine in Type 1B kimberlite.

Phlogopite microphenocrysts are inclusion and strain-free and exhibit colourless to light brown to tan brown pleochroism. Crystals may be slightly corroded in the Ham dyke but are completely replaced by septechlorite and serpentine in the Ham diatreme Type 1A and Type 1B kimberlite. Microphenocrysts were not observed in Type 2 kimberlite.

CHEMISTRY

Representative analyses of Ham phlogopites are given in Table 3. Low totals are a result of partial chloritization of mica megacrysts and microphenocrysts. The compositional variation is illustrated in Figures 6 and 7.

Table 3 and Figures 6 and 7 suggest that phlogopite megacrysts in the Ham diatreme and dyke are compositionally similar in their major and minor element contents although Ham dyke megacrysts have a higher range of  $TiO_2$  (0.25-4.0 wt. %) and lower range of  $Cr_2O_3$  (0.10-1.6 wt. %) contents than do Ham diatreme megacrysts ( $TiO_2=2.25-4.5$  wt. %,  $Cr_2O_3=0.00-2.1$  wt. %). NiO contents are similar and vary from 0.00 to 0.23 and 0.04 to 0.26 weight percent, respectively. Individual crystals demonstrate normal and reverse zoning in  $TiO_2$  and  $Cr_2O_3$  contents.

Mica megacrysts from the Ham Kimberlite are compositionally similar (Figure 7) to Type B micas from the Jos kimberlite (Mitchell and Meyer 1980) and Ti-Cr-rich micas from the Tunraq kimberlite (Mitchell 1979a) although Jos micas have a more limited range in Cr contents (0.00 to 0.50 wt. %  $Cr_2O_3$ ) and Tunraq micas have higher Ti contents (5.0 to 5.6 wt. %  $TiO_2$ ). Ham micas have

Table 2  
Representative Analyses of Ham Miccas

	1	2	3	4	5	6	7	8	9	10	11	12
SiO <sub>2</sub>	39.05	39.52	39.00	35.12	39.35	38.46	40.36	37.45	38.70	39.21	37.63	36.22
TiO <sub>2</sub>	4.15	4.27	4.47	4.46	3.58	3.50	2.64	2.44	4.19	4.20	3.51	3.58
Al <sub>2</sub> O <sub>3</sub>	13.48	12.89	12.66	11.68	14.03	13.74	13.34	11.89	12.69	12.52	13.74	15.75
Cr <sub>2</sub> O <sub>3</sub>	1.07	1.16	0.56	0.56	1.69	1.77	1.50	1.29	0.25	0.33	1.93	1.16
FeO*	4.49	4.16	4.42	4.35	3.67	3.37	3.68	3.39	4.09	3.84	3.70	4.04
MgO	21.18	21.02	21.55	20.35	22.07	21.59	24.23	22.28	21.65	21.77	20.61	21.53
CaO	0.00	0.00	0.00	0.01	0.00	0.02	0.00	0.03	0.00	0.00	0.01	0.02
MnO	0.07	0.07	0.04	0.05	0.00	0.06	0.07	0.06	0.04	0.00	0.05	0.06
NiO	0.19	0.21	0.13	0.13	0.17	0.17	0.26	0.20	0.08	0.15	0.25	0.08
Na <sub>2</sub> O	0.21	0.36	0.18	0.17	0.38	0.37	0.30	0.09	0.35	0.01	0.23	0.28
K <sub>2</sub> O	10.27	9.39	9.89	9.06	9.33	9.04	9.86	8.78	9.30	9.13	8.78	8.65
Total	94.16	93.05	92.90	85.94	94.27	92.09	96.24	87.90	91.34	91.16	90.44	91.37

	13	14	15	16	17	18	19	20	21	22	23	24	25	26	27	28
SiO <sub>2</sub>	36.97	36.02	38.50	36.98	39.32	40.71	32.78	33.51	35.96	36.86	36.94	37.33	26.39	30.74	22.37	23.45
TiO <sub>2</sub>	3.12	3.85	0.75	0.71	0.60	0.63	3.38	3.45	3.71	3.82	3.58	3.29	0.00	0.00	0.00	0.01
Al <sub>2</sub> O <sub>3</sub>	13.96	16.00	13.39	13.35	12.08	11.96	16.14	14.60	12.84	12.82	12.75	12.69	11.54	9.58	16.08	13.46
Cr <sub>2</sub> O <sub>3</sub>	0.61	0.69	1.08	1.13	0.85	0.91	0.72	0.47	0.15	0.21	0.91	1.06	0.04	0.02	0.04	0.02
FeO*	4.51	4.70	2.61	2.54	2.75	2.64	5.04	5.58	4.56	4.67	4.35	3.95	3.63	4.01	1.34	2.55
MgO	24.48	21.79	24.09	24.39	24.92	25.18	22.13	22.22	23.00	23.01	22.53	22.21	38.24	35.78	38.62	39.50
CaO	0.01	0.06	0.00	0.00	0.04	0.10	0.04	0.11	0.03	0.03	0.02	0.02	0.11	0.27	0.25	0.12
MnO	0.01	0.08	0.02	0.04	0.05	0.03	0.06	0.06	0.01	0.04	0.05	0.04	0.11	0.11	0.04	0.06
NiO	0.09	0.05	0.21	0.17	0.13	0.18	0.05	0.13	0.05	0.04	0.15	0.13	0.08	0.15	0.04	0.17
Na <sub>2</sub> O	0.39	0.21	0.32	0.46	0.32	0.11	0.05	0.08	0.20	0.12	0.02	0.00	7.07	4.54	8.29	9.10
K <sub>2</sub> O	6.66	8.34	8.66	8.54	8.75	8.96	6.79	6.53	6.62	7.68	7.33	6.77	0.42	0.97	0.41	0.38
Total	90.81	91.79	89.63	88.31	89.81	91.41	87.18	86.74	87.13	89.30	88.64	87.42	87.63	86.17	87.48	87.88

Analyses 1-12, Ham Diatrene Megacrysts, (1-2, 3-4, 5-6, 7-8, 9-10, 11-12, core-rim analyses)

Analyses 13-18, Ham Dyke Megacrysts, (13-14, 15-16, 17-18, core-rim analyses)

Analyses 19-24, Ham Dyke Microphenocrysts, (19-20, 21-22, 23-24, core-rim analyses)

Analyses 25-28, Septechlorites replacing microphenocrysts

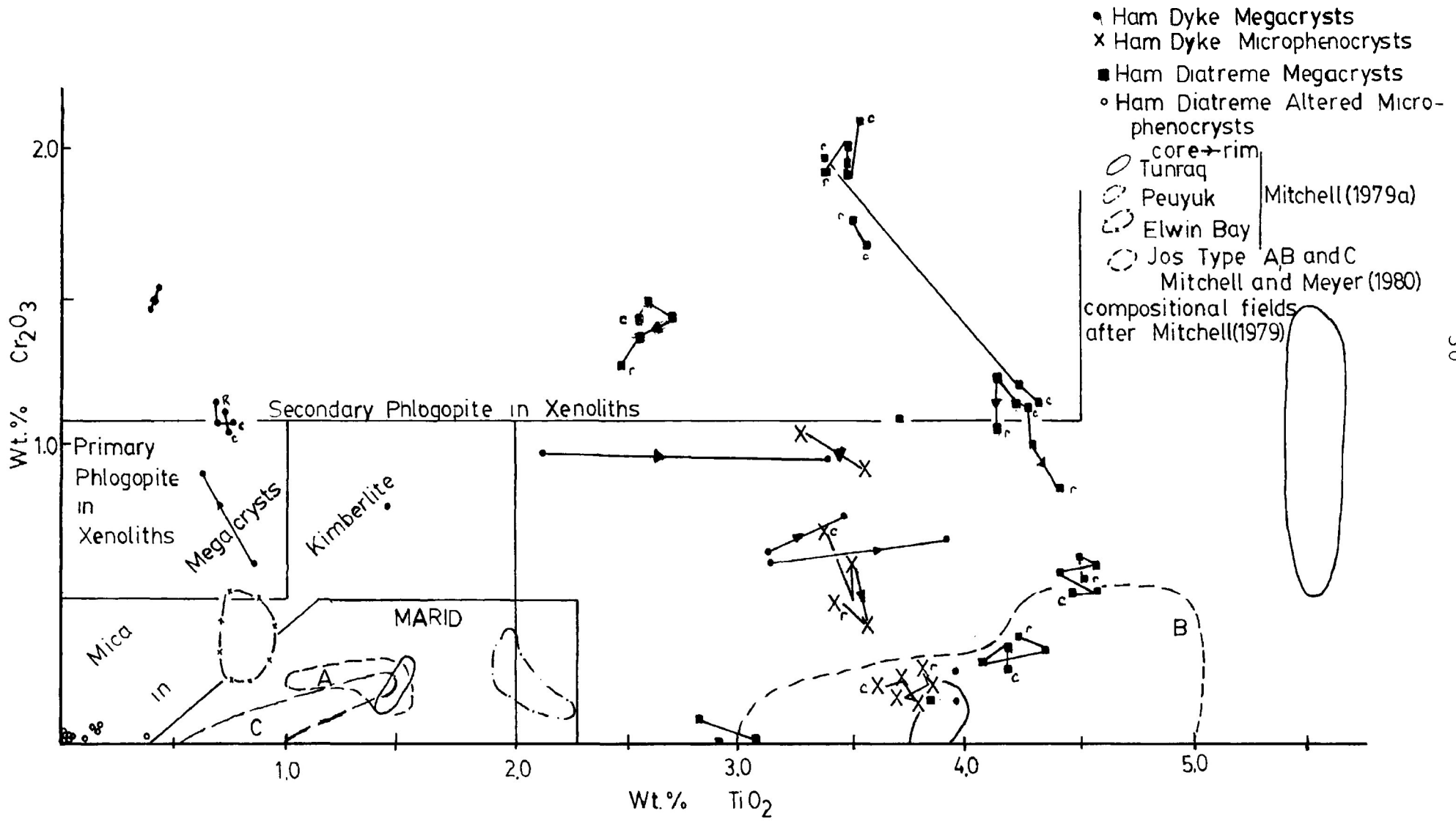
\*Total iron as FeO

higher Ti and Cr contents than megacrysts in the Elwin Bay kimberlite (Mitchell 1978a), the Peuyuk kimberlite (Mitchell 1975) and Type A megacrysts in the Jos kimberlite (Mitchell and Meyer 1980). Figure 7 indicates that Ham micas demonstrate a broader range in Mg/Mg+Fe ratios and NiO contents than megacrysts in the Tunraq (Mitchell 1979) or Jos (Mitchell and Meyer 1980) kimberlite.

Inspection of Figure 6 indicates that Ham megacrysts lie outside the field of mica megacrysts as defined by Dawson and Smith (1975) and contain considerably higher  $TiO_2$  and  $Cr_2O_3$  contents such that several analyses plot within the field of secondary micas. Derivation from a secondary source is unlikely as petrographic examination of 60 garnet lherzolite xenoliths from the Ham Kimberlite failed to locate any secondary phlogopite. This study and data from Mitchell (1979a) indicate that the mica megacryst field should be extended up to at least 6.0 weight percent  $TiO_2$ . Inspection of Figure 7 indicates that Ham phlogopites have NiO contents and Mg/Mg+Fe ratios similar to Dawson and Smith's (1977) megacryst micas.

Phlogopite microphenocrysts in the Ham diatreme are pseudomorphed by septechlorite (Table 3, Anal. 25

FIGURE 6  
 TiO<sub>2</sub> vs Cr<sub>2</sub>O<sub>3</sub> VARIATION DIAGRAM FOR HAM MICAS



to 28). These contain very low  $\text{TiO}_2$  (0.00 to 0.38 wt. %) and  $\text{Cr}_2\text{O}_3$  (0.00 to 0.10 wt. %) contents with high Mg/Mg+Fe ratios (0.91 to 0.98) compared to Ham dyke microphenocrysts. These latter micas are essentially compositionally homogenous, high Ti (3.25 to 3.80 wt. %  $\text{TiO}_2$ ), high Cr (0.10 to 1.0 wt. %) phlogopites (Mg/Mg+Fe=0.90 to 0.88). Microphenocrysts may be distinguished chemically from Ham diatreme and dyke megacrysts by having a higher mean FeO content (4.89 wt. % compared to 3.79 wt. %). Microphenocrysts have lower  $\text{Cr}_2\text{O}_3$  contents for a given  $\text{TiO}_2$  content than dyke megacrysts and a lower mean  $\text{TiO}_2$  content than diatreme megacrysts.

Ham microphenocrysts have higher Ti, Cr and Ni contents than microphenocrysts in the Elwin Bay (Mitchell 1978a) or Jos (Mitchell and Meyer 1980) kimberlite but are compositionally similar to Type B megacrysts in the Jos (Mitchell and Meyer 1980) kimberlite.

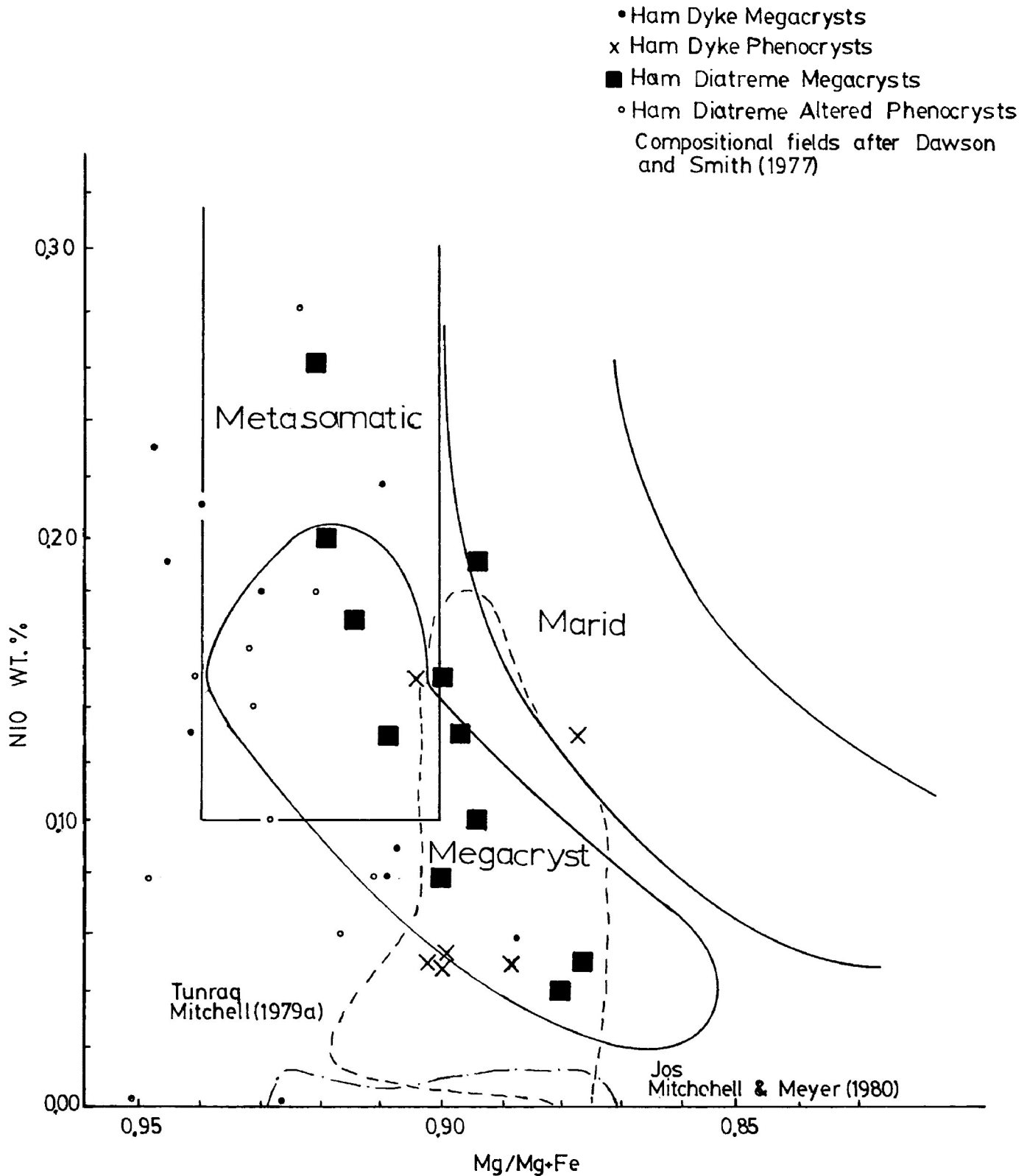
Ham microphenocrysts are compositionally similar to Type II micas examined by Smith et al. (1978) which are rich in Mg (Mg/Mg+Fe=0.93-0.80), Ti ( $\text{TiO}_2$ =0.07-4.0 wt. %) and Cr ( $\text{Cr}_2\text{O}_3$ =0.05-1.4 wt. %) but contain more Cr ( $\text{Cr}_2\text{O}_3$ =0.0-0.3 wt. %) and less Fe (FeO=21.7-6.3 wt. %, Mg/Mg+Fe=0.45-0.65) than their Type I micas. Ni contents of Ham microphenocrysts are similar to Type II micas (NiO=0.00-0.25 wt. %) and are

considerably greater than Ni contents of Type I micas ( $\text{NiO}=0.00-0.05$  wt. %).

Inspection of Figures 6 and 7 reveals that Ham micas do not demonstrate any systematic compositional variation between megacrysts and microphenocrysts and that no chemical evolutionary trends can be established for any single mica variety. In contrast, micas in the Elwin Bay (Mitchell 1978a) and Tunraq (Mitchell 1979a) kimberlite evolve toward lower  $\text{TiO}_2$  and higher  $\text{Cr}_2\text{O}_3$  contents. Micas in the Jos (Mitchell and Meyer 1980) kimberlite demonstrate complex mantling relationships in which Type A micas (low Ti, low Cr) are overgrown by Ti-Cr-rich Type B which may be overgrown by Cr-poor, Ti-rich Type C micas or by Ti-Cr-poor Type C micas. Mitchell and Meyer (1980) attribute this complex mantling relationship and the wide spread in  $\text{TiO}_2$  contents of Type B micas to a crystal fractionation-magma mixing model. Smith et al. (1978) indicate that the complex compositional variation in South African micas may result from the intrusion of another magma just prior to the intrusion of the kimberlite and the onset of the crystallization of mica microphenocrysts.

Similarly, the broad range in the compositional variation of Ham diatreme megacrysts may have resulted from the periodic mixing of magmas of slightly

FIGURE 7  
NiO-Mg/Mg+Fe Variation Diagram for Ham Micras



different compositions. The compositional similarity of Ham dyke megacrysts and microphenocrysts indicate that magma mixing may have occurred just prior to the intrusion of the kimberlite. These processes are similar to those discerned for Ham olivines (Chapter 2).

### CONCLUSIONS

Two generations of phlogopite occur in the Ham diatreme and dyke. Mica megacrysts which occur as large, rounded and corroded crystals are interpreted to have crystallized from a kimberlite magma prior to intrusion, when small, euhedral microphenocrysts formed. The paucity of chemical evolutionary trends between and within mica varieties, the compositional similarity of Ham dyke megacrysts and microphenocrysts and the broad compositional range of Ham diatreme megacrysts is attributed to magma mixing. The chloritization and serpentization of Ham micas occurred during late stage crystallization of the kimberlite magma.

CHAPTER 4GARNETS

Approximately 450 orange, brown and deep red to purple garnets were recovered from heavy mineral concentrates from the Ham kimberlite. Scarce, rounded, deep red garnets were observed in regolith samples, in garnet lherzolite xenoliths and in concentrates from kimberlite regolith. Crystals in handspecimen are commonly enveloped in a kelyphite (spinel + enstatite + hornblende + mica + chlorite) reaction rim (Nixon et al. 1963) formed between a garnet and the transporting fluid (Mitchell 1970). Frosted grain surfaces developed during the fluidized intrusion of the diatreme were observed on garnets from the regolith.

The Compositional Variation of Ham Garnets

All 450 garnets were analyzed by electron microprobe for 11 elements using energy dispersive spectroscopy at Dalhousie University. So that Ham analyses would be directly comparable to garnet analyses from other Somerset Island kimberlites obtained by this microprobe, the same standards and operating conditions were utilized (See Appendix E).

Representative analyses of Ham garnets are given in Table 4; all analyses are given in Appendix A.

The compositional variation is illustrated in Figures 8, 9, 10 and 11.

Examination of Table 4 reveals that all the Ham garnets are Cr-pyropes ( $>0.5$  wt. %  $\text{Cr}_2\text{O}_3$ , O'Hara and Mercy 1966). The variation in colour from orange to deep-red corresponds to increasing amounts of  $\text{MgO}$ ,  $\text{Cr}_2\text{O}_3$  and  $\text{CaO}$  and to decreasing amounts of  $\text{FeO}$ .

Figures 8 and 10 show that Ham garnets may be grouped into two independent compositional variation trends based on major element (Fe-Mg-Ca) contents in which:

- (A)  $\text{Mg}/\text{Mg}+\text{Fe}$  varies from 0.78 to 0.84 and  $\text{CaO}$  (4.80 wt. %) is approximately constant,
- and (B)  $\text{Mg}/\text{Mg}+\text{Ca}$  varies from 0.77 to 0.88 and  $\text{FeO}$  (5.57 wt. %) is approximately constant.

In general, Al, Fe and Ti decrease and Ca increases with increasing Cr content. Inspection of Figures 9 and 11 show that Trend A is characterized by relatively Ti-rich, Cr-poor garnets and that Trend B is characterized by relatively Ti-poor, Cr-rich garnets. However, relatively Ti-poor, Cr-rich and Ti-rich, Cr-rich garnets may occur in Trend A and Trend B, respectively.

TABLE 4

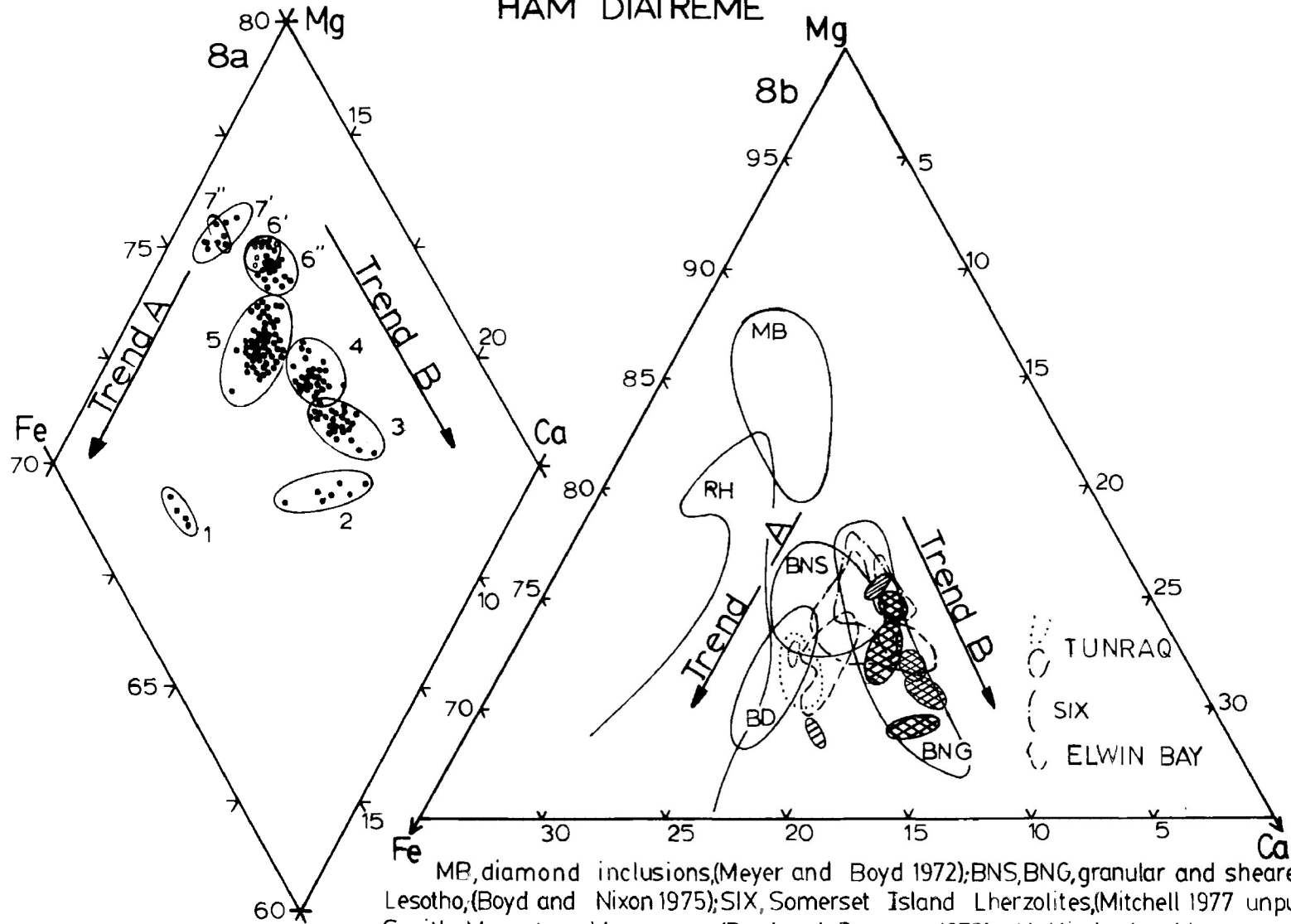
## Representative Analyses of Ham Garnets

Diatreme Clusters*	HW1	HW2	HW3	HW4	HW5	HW6	HW7
SiO <sub>2</sub>	40.68	40.88	40.53	40.95	41.72	40.94	41.45
TiO <sub>2</sub>	0.80	0.00	0.49	0.32	0.13	0.33	0.42
Al <sub>2</sub> O <sub>3</sub>	20.65	18.61	17.94	19.21	20.03	20.47	22.62
Cr <sub>2</sub> O <sub>3</sub>	2.53	6.70	7.09	5.94	5.04	4.01	0.59
FeO**	9.09	7.01	6.71	6.77	7.31	6.15	7.29
MnO	0.36	0.49	0.25	0.34	0.38	0.18	0.34
MgO	19.81	19.54	19.98	20.24	20.02	21.11	21.60
CaO	5.31	6.36	6.04	5.72	5.34	5.49	4.35
TOTAL	99.23	99.59	99.03	99.49	99.97	98.68	98.66
Dyke Clusters*	HD1	HD2	HD3	HD4	HD5	HD6	HD7
SiO <sub>2</sub>	40.03	40.74	40.84	41.57	41.10	40.88	40.57
TiO <sub>2</sub>	1.48	0.23	0.21	0.35	0.28	0.24	0.69
Al <sub>2</sub> O <sub>3</sub>	19.33	21.54	20.97	21.52	19.74	17.84	15.66
Cr <sub>2</sub> O <sub>3</sub>	2.56	2.38	3.43	1.77	4.76	8.05	9.99
FeO**	9.01	9.14	8.45	7.58	7.29	6.45	6.26
MnO	0.29	0.47	0.43	0.28	0.45	0.43	0.41
MgO	20.17	19.17	20.12	21.39	20.60	19.58	19.92
CaO	6.55	5.09	5.14	4.77	5.44	7.18	7.08
TOTAL	99.42	98.76	99.59	99.23	99.66	100.65	100.58

\*Data for clusters generated using major and minor element plots.

\*\*Total iron as FeO

FIGURE 8  
Fe-Mg-Ca Ternary Plot for Ham Garnets  
HAM DIATREME



MB, diamond inclusions, (Meyer and Boyd 1972); BNS, BNG, granular and sheared garnet lherzolite, Lesotho, (Boyd and Nixon 1975); SIX, Somerset Island Lherzolites, (Mitchell 1977 unpub. data); BD, Frank Smith-Monastery Megacrysts, (Boyd and Dawson 1972); RH, Kimberley Megacrysts, (Reid and Hanor 1970); ELWIN, Elwin Bay Megacrysts, (Mitchell 1978); TUNRAQ, Tunraq Garnets, (Mitchell 1979a)

FIGURE 9  
 $TiO_2$  vs  $Cr_2O_3$  Compositional Variation Diagram  
 for  
 Ham Diatreme Garnets

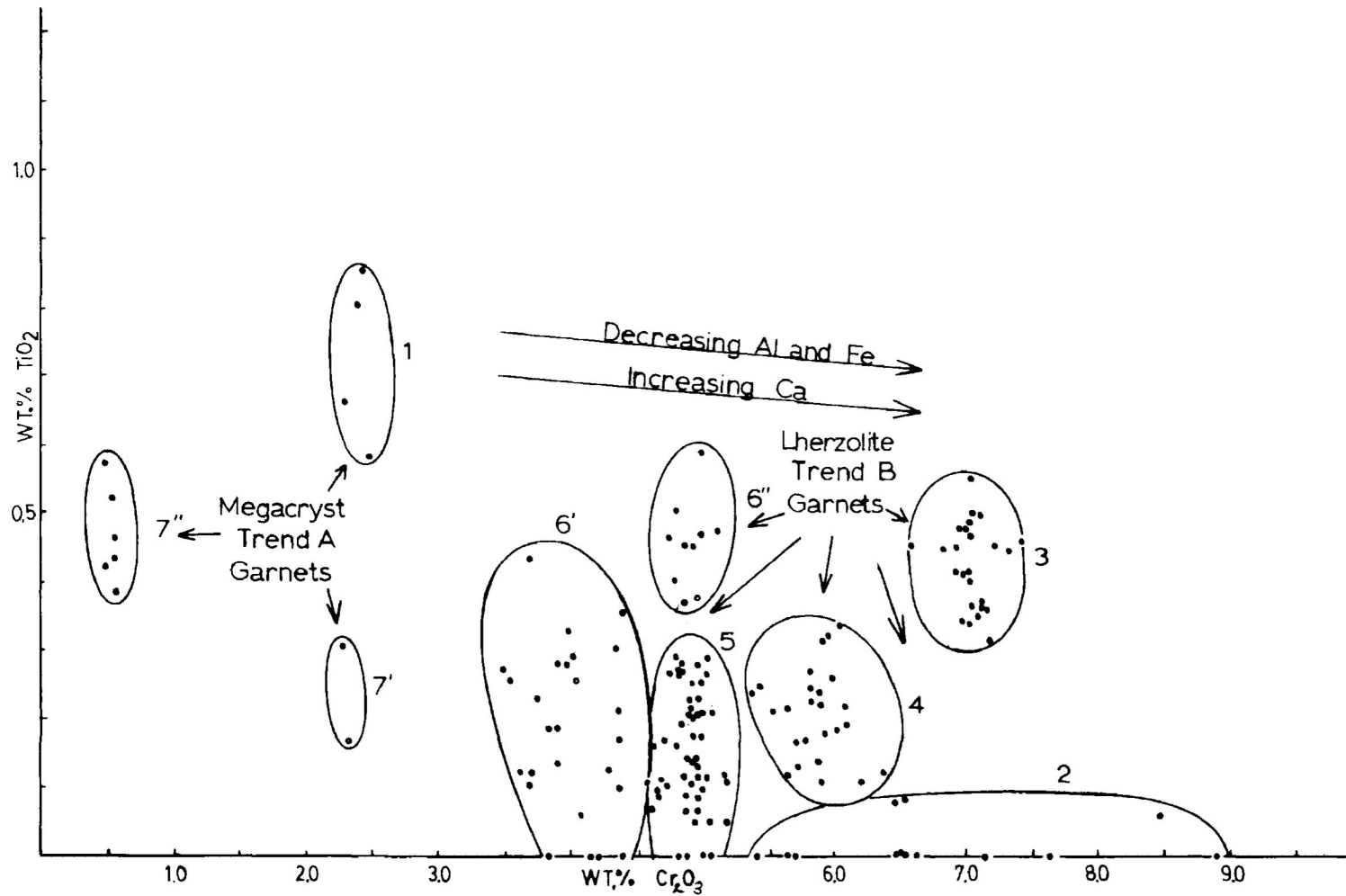
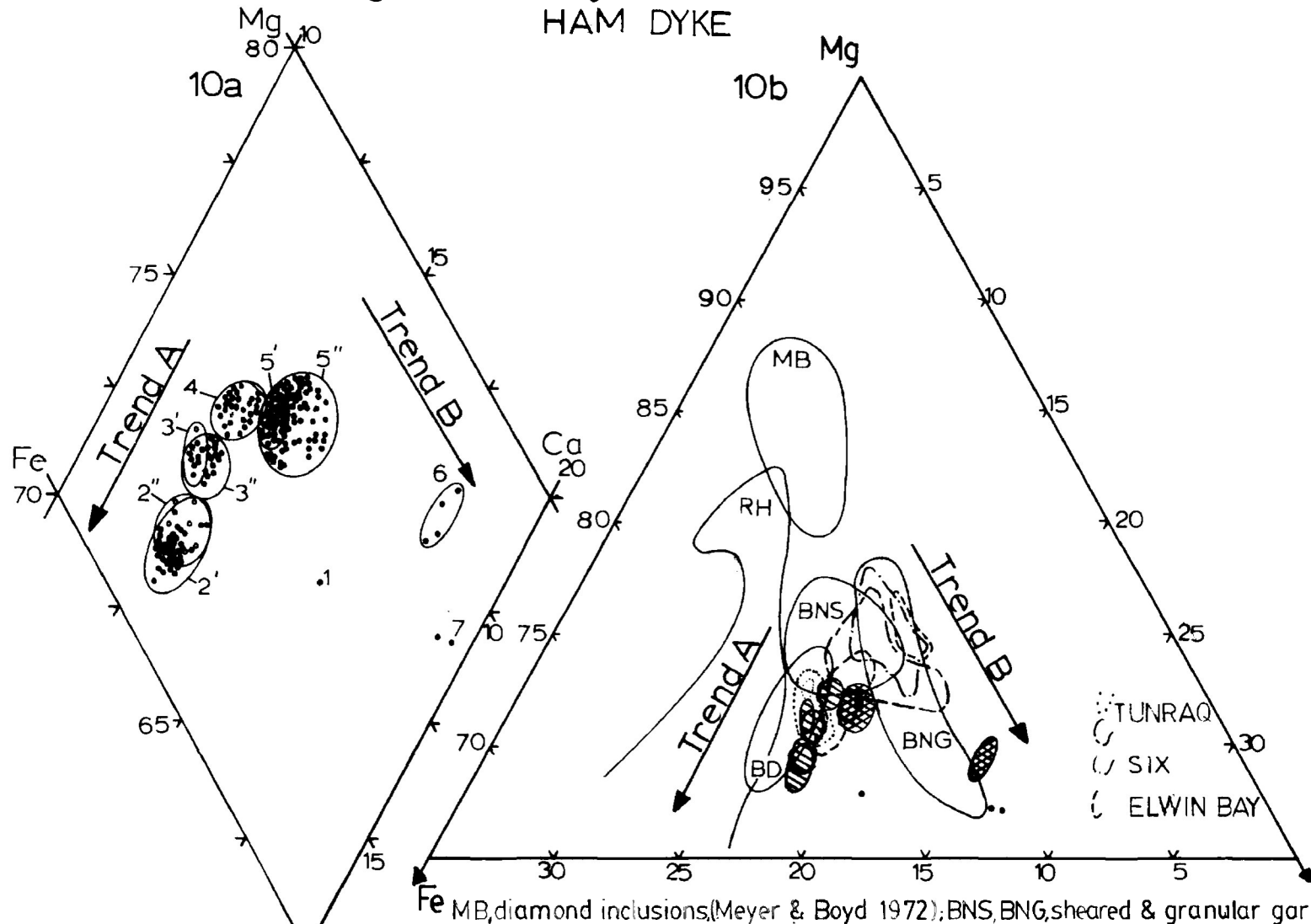


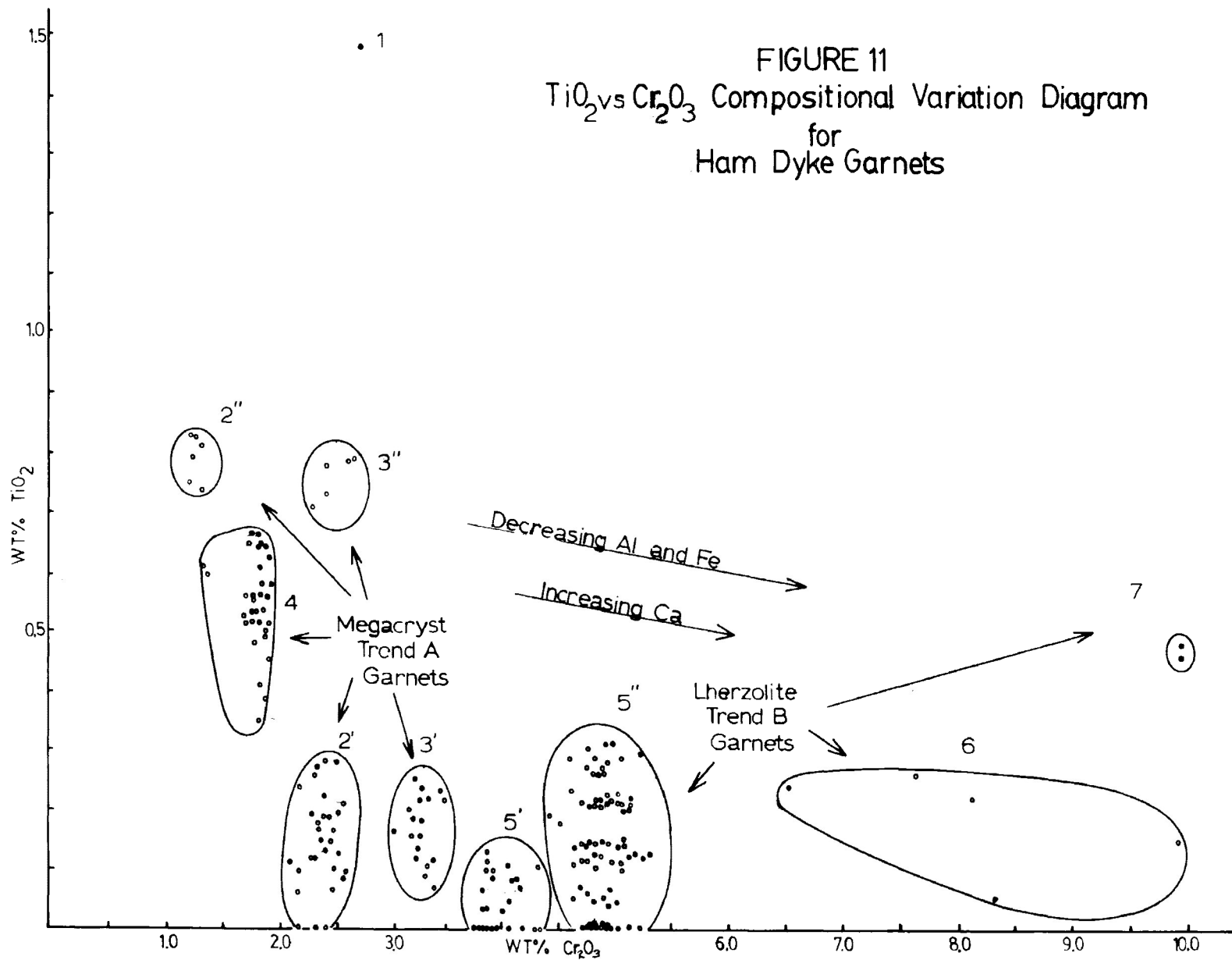
FIGURE 10

Fe-Mg-Ca Ternary Plot for Ham Garnets  
HAM DYKE



MB, diamond inclusions, (Meyer & Boyd 1972); BNS, BNG, sheared & granular garnet lherzolite, Lesotho, (Boyd & Nixon 1975); SIX, Somerset Island lherzolite (Mitchell 1977 & unpub data); BD, Frank Smith-Monastery Megacrysts, (Boyd & Dawson 1972); RH, Kimberley Megacrysts, (Reid & Hanor 1970); ELWIN Elwin Bay Megacrysts (Mitchell 1978a); TUNRAQ, Tunraq Garnets, (Mitchell 1979a)

FIGURE 11  
TiO<sub>2</sub> vs Cr<sub>2</sub>O<sub>3</sub> Compositional Variation Diagram  
for  
Ham Dyke Garnets



Further examination of Figures 8, 9, 10 and 11 shows that Ham garnets in Trend A and B can be further subdivided into sub-groups based on major (Fe-Mg-Ca) and minor ( $\text{TiO}_2\text{-Cr}_2\text{O}_3$ ) element contents. These are listed in Tables 5 and 6.

A review of Figures 8 and 9 show that garnets in Groups HW 2, 3, 4, 5 and 6 (Trend B) are Ca- and Cr-rich and Ti-poor relative to garnets in Groups 1 and 7 (Trend A). Group 2 garnets can be distinguished from garnets in Group 3 and 4 by having lower Ti and higher Ca contents. Although the garnets in Group 3 and 4 appear to form a continuum in Figure 8a (Fe-Mg-Ca plot), the maximas for the compositional variation ( $\text{Ca}/\text{Ca}+\text{Mg}$ ) and the higher Ti and Cr contents of the former group can be used to separate them. Garnets in Group 4 are Ca- and Cr-rich compared to Group 5 garnets which demonstrate a greater variation in  $\text{Fe}/\text{Fe}+\text{Mg}$  ratios than Group 4 garnets. Group 6 garnets may be distinguished from relatively iron-poor Group 5 garnets by a broader range in Ti and Cr contents, a bi-modal distribution of Ti and Cr and a wide spread in the maximas for the major element variation ratio ( $\text{Fe}/\text{Fe}+\text{Mg}$ ).

Figures 10 and 11 show that Trend A garnets predominate in the Ham dyke and that groupings

are more easily discerned based upon minor element contents than in the Ham diatreme. Trend B garnets in Groups HD 5, 6 and 7 can be distinguished from other garnets by their relatively Ca- and Cr-rich nature. Garnets in Group 7 are Ti-rich relative to Cr-rich, Ti-poor garnets in Groups 5 and 6. Garnets in Group 5 demonstrate a bi-modal distribution of Ti and Cr and are Ca- and Mg-rich relative to garnets in Groups 2 and 3 and Group 4, respectively. These garnets appear to form a continuum (major element variation, Figure 10), however, compositional maxima (Fe/Fe+Mg ratios) and Ti and Cr contents (Figure 11) serve to distinguish between them. Group 2 and 3 garnets demonstrate a bi-modal distribution of Ti and Cr contents, containing relatively Ti-rich, Cr-poor and Ti-poor, Cr-rich sub-groups.

Statistical analysis (see below) shows that these groups, based on major and minor contents, are statistically, significantly different.

Figures 8B and 10B show that Trend B garnets are compositionally similar to relatively Fe-poor, Ca-rich garnets in the Tunraq (Mitchell 1979a) and Elwin Bay (Mitchell 1978a) kimberlites. These are compositionally similar to garnets from garnet lherzolite xenoliths in the Elwin Bay (Mitchell 1978a) and other

Somerset Island kimberlites (Mitchell 1977) and are interpreted to be garnets from such fragmented xenoliths (Mitchell 1979a). In contrast, garnets in Trend A are compositionally similar to Ca-poor garnets with variable iron contents ( $Mg/Mg+Fe = 0.76$  to  $0.83$ , Mitchell 1979a) from the Elwin Bay (Mitchell 1978a) and Tunraq (Mitchell 1979a) kimberlites. These garnets exceed one centimetre in diameter (i.e. are larger than garnets in garnet lherzolites) and are compositionally different to garnets in garnet lherzolite xenoliths. Mitchell (1979a) contends that these megacrysts are true kimberlite phenocrysts and are not of xenocrystal origin.

Trend B garnets are compositionally similar to Fe-poor, Ca-rich garnets from granular garnet lherzolites (Boyd and Nixon 1975) from Lesotho but are slightly iron-poor relative to garnets in sheared garnet lherzolite (Boyd and Nixon 1975). Trend A garnets are compositionally similar to Ca-poor megacrysts in the Frank Smith and Monastery kimberlites (Boyd and Dawson 1972) but are richer in Ca than Kimberley megacrysts (Reid and Hanor 1970) and Fe, than garnets in sheared garnet lherzolite (Boyd and Nixon 1975). All Trend A and Trend B garnets are Mg-poor relative to garnet inclusions in diamond (Meyer and Boyd 1972).

### Classification of Ham Garnets

Classification schemes proposed by Dawson and Stephens (1975) and Danchin and Wyatt (1979) are useful as an exploration guide in the search for kimberlite diatremes. The classification schemes attempt to distinguish between garnet sources in a random sample of garnets, which, may originate from diverse paragenesis and not all of which may be associated with kimberlites. It is important, therefore, to characterize garnets associated with kimberlite magma genesis, upper mantle xenoliths and diamond-bearing kimberlites, so that exploration programs will not be misdirected. The statistical methods employed by Dawson and Stephens (1975) and Danchin and Wyatt (1979) are discussed below (see Statistical Methods and Classification).

A review of Tables 5B and 6B show that Ham garnets fall into 2 groups using the statistical classification scheme of Dawson and Stephens (1975). Trend A (megacryst garnets) fall into Group 1, dominated by high-Ti, low-Cr, titan-pyropes and Trend B (lherzolite garnets) belong to Group 9, and are low-Ti, chrome-pyropes which are transitional toward low-Ca chrome-pyrope (Group 10) and titan-uvarovite-pyrope (Group 11) (Dawson and Stephens

TABLE 5A  
Means, Ranges and Standard Deviations for Groups of Ham Diatrene Garnets Generated  
on the Basis of Major and Minor Element Compositional Variation

Cluster	TiO <sub>2</sub>			Al <sub>2</sub> O <sub>3</sub>			Cr <sub>2</sub> O <sub>3</sub>			FeO*			MgO			CaO		
	Mean	Range	σ	Mean	Range	σ	Mean	Range	σ	Mean	Range	σ	Mean	Range	σ	Mean	Range	σ
1	0.73	0.59-0.85	0.12	20.61	20.46-20.70	0.11	2.54	2.48-2.61	0.05	9.02	8.93-9.09	0.07	19.76	19.59-19.83	0.11	5.31	5.19-5.43	0.10
2	0.02	0.00-0.09	0.03	18.60	16.71-20.54	1.13	6.91	5.70-8.91	1.06	7.06	6.58-7.67	0.40	19.55	18.84-19.61	0.64	6.52	5.97-7.77	0.79
3	0.46	0.33-0.68	0.14	18.16	17.83-19.23	0.30	7.07	6.21-7.49	0.32	6.83	6.56-7.17	0.14	20.21	19.74-20.87	0.26	6.08	5.57-6.46	0.21
4	0.21	0.12-0.35	0.06	19.16	18.35-19.42	0.24	5.92	5.57-6.09	0.20	6.89	6.64-7.15	0.16	20.49	20.15-20.79	0.18	5.71	5.35-5.85	0.15
5	0.18	0.00-0.55	0.09	19.88	17.98-21.15	0.26	4.88	1.89-6.79	0.14	7.12	6.62-7.60	0.22	20.78	20.16-21.39	0.23	5.24	4.62-6.21	0.12
6**	0.23	0.00-0.51	0.15	20.38	17.98-21.07	0.63	4.28	3.51-5.05	0.44	6.80	5.85-7.65	0.35	21.27	20.37-22.23	0.40	5.06	4.22-5.49	0.30
6'	0.16	0.00-0.33	0.10	20.62	20.25-21.07	0.23	4.04	3.51-4.41	0.25	6.26	5.85-7.65	0.45	21.32	20.37-22.23	0.39	5.01	4.22-5.49	0.29
6''	0.41	0.34-0.51	0.06	19.66	17.98-20.74	0.70	4.86	4.67-5.05	0.11	6.80	6.55-7.28	0.24	21.14	20.61-21.72	0.35	5.20	4.94-5.44	0.19
7**	0.41	0.17-0.57	0.13	22.04	19.85-22.63	0.97	1.08	0.59-2.39	0.77	7.24	6.98-7.52	0.18	21.48	21.23-21.61	0.13	4.42	4.27-4.62	0.12
7'	0.24	0.17-0.31	0.06	21.72	21.63-21.81	0.09	2.23	2.26-2.39	0.07	7.48	7.44-7.52	0.04	21.32	21.23-21.41	0.09	4.57	4.52-4.62	0.05
7''	0.46	0.38-0.57	0.07	22.14	19.85-22.63	1.03	0.66	0.59-0.77	0.06	7.16	6.98-7.29	0.12	21.51	21.42-21.61	0.07	4.37	4.27-4.52	0.09

\*Total iron as FeO

\*\*Clusters 6 and 7 are a combination of subclusters 6' and 6'' and 7' and 7'', respectively.

TABLE 5B  
Classification of Ham Diatrene Garnets by Methods of Dawson and Stephens (1975)  
Dawson and Stephens' Classification Scheme

Means of Critical Oxides

Ham Clusters	Group	TiO <sub>2</sub>	Cr <sub>2</sub> O <sub>3</sub>	FeO	MgO	CaO	Origin*
1 7 7' 7''	1	0.58	1.34	9.32	20.0	4.82	K, GL, GOW, D
2 3	9-11 11 9-10 10	0.51 0.04	9.55 7.73	7.54 6.11	15.89 23.16	10.27 2.13	K, GL, GW, D K, GS, D
4 5 6 6' 6''	9	0.17	3.47	8.01	20.01	5.17	K, GL, GOW, GH, EC, D

\* K = kimberlite garnet, GL = garnet lherzolite, GOW = garnet olivine websterite, GH = garnet harzburgite, EC = eclogite, D = Diamond, GW = garnet websterite, GS = garnet serpentinite

TABLE 6A  
Means, Ranges and Standard Deviations for Groups of Ham Dyke Garnets Generated  
on the Basis of Major and Minor Element Compositional Variation

Cluster	TiO <sub>2</sub>			Al <sub>2</sub> O <sub>3</sub>			Cr <sub>2</sub> O <sub>3</sub>			FeO			MgO			CaO		
	Mean	Range	σ	Mean	Range	σ	Mean	Range	σ	Mean	Range	σ	Mean	Range	σ	Mean	Range	σ
1	1.48	-	-	19.33	-	-	2.56	-	-	8.01	-	-	19.17	-	-	6.55	0	-
2	0.23	0.00-0.83	0.23	21.46	21.14-21.90	0.17	2.28	1.20-2.63	0.39	9.26	8.74-9.75	0.18	19.48	19.17-19.90	0.19	5.04	4.81-5.23	0.10
2'	0.15	0.00-0.40	0.09	21.49	21.14-21.90	0.17	2.43	2.19-2.63	0.10	9.32	9.06-9.75	0.14	19.47	19.17-19.90	0.18	5.04	4.81-5.23	0.10
2''	0.79	0.74-0.83	0.28	21.28	21.19-21.37	0.22	1.28	1.20-1.36	0.05	8.98	8.74-9.19	0.15	19.60	19.19-19.85	0.24	4.10	5.01-5.18	0.06
3	0.29	0.06-0.79	0.25	20.95	20.62-21.23	0.13	3.11	2.34-3.43	0.35	8.29	7.58-8.62	0.26	20.13	19.70-20.61	0.25	5.01	4.77-5.23	0.13
3'	0.18	0.06-0.31	0.09	20.99	20.76-21.23	0.11	3.28	3.10-3.43	0.07	8.35	8.10-8.57	0.13	20.08	19.70-20.43	0.21	4.98	4.77-5.14	0.11
3''	0.75	0.70-0.79	0.40	20.80	20.62-20.84	0.20	2.46	2.34-2.66	0.11	8.07	7.58-8.62	0.45	20.30	19.85-20.61	0.35	5.13	4.97-5.23	0.11
4	0.53	0.35-0.65	0.07	21.37	21.02-21.85	0.16	1.89	1.77-2.08	0.09	7.93	7.58-9.29	0.29	20.68	20.42-21.39	0.19	5.03	4.77-5.25	0.09
5'	0.13	0.00-0.32	0.09	20.16	19.54-21.02	0.36	4.70	3.76-5.17	0.38	7.37	6.82-7.79	0.21	20.38	19.88-21.33	0.27	5.44	4.84-7.25	0.19
5'	0.07	0.00-0.19	0.06	20.78	20.08-21.02	0.20	3.95	3.76-4.93	0.19	7.52	7.32-7.74	0.10	20.34	19.94-20.60	0.17	5.31	5.11-5.53	0.10
5''	0.15	0.00-0.32	0.09	19.43	19.54-20.88	0.38	4.73	3.77-5.17	0.25	7.34	6.82-7.79	0.21	20.24	19.88-21.23	1.69	5.42	4.84-7.25	0.45
6	0.27	0.06-0.69	0.22	17.13	15.49-18.56	1.11	8.45	6.61-9.99	1.33	6.47	5.99-7.00	0.34	19.85	18.80-20.32	0.27	7.03	6.37-7.73	0.32
7	0.57	0.45-0.69	0.12	15.58	15.49-15.66		9.95	9.91-9.99	0.04	6.58	6.26-6.89	0.31	19.36	18.80-19.92	0.56	7.41	7.08-7.77	0.33

TABLE 6B  
Classification of Ham Dyke Garnets by Methods of Dawson and Stephens (1975)  
Dawson and Stephens' Classification Scheme

Means of Critical Oxides

Ham Clusters	Group	TiO <sub>2</sub>	Cr <sub>2</sub> O <sub>3</sub>	FeO	MgO	CaO	Origin
1 2 3 4	1	0.58	1.34	9.32	20.00	4.82	K, GL, GOW, D
5 6 7	9	0.17	3.47	8.01	20.01	5.17	K, GL, GOW, GH, EC, D

K = kimberlite, GOW = garnet-olivine websterite, GL = garnet lherzolite  
GH = garnet harzburgite, EC = eclogite, D = diamond

1975, 1976).

Table 7 shows that Ham garnets may be classified as Ti-poor peridotitic garnets (Groups 16 and 33) and Ti-rich peridotitic garnets (Groups 22, 26 and 37) based upon the classification scheme of Danchin and Wyatt (1979). The former groups are dominated by "kimberlite" (megacryst) and lherzolite garnets and the latter groups are dominated by "kimberlite" garnets and scarce lherzolite garnets.

#### Statistical Classification

The statistical classification of garnets from kimberlite, utilizing cluster analysis, augmented by the prior knowledge of the garnet paragenesis, has been attempted by Dawson and Stephens (1975) (Wards method, Wishart 1969) and by Danchin and Wyatt (1979) (Park's method, 1970) with varying degrees of success. A review of Figure 6 of Dawson and Stephens (1975) and Tables 1, 2 and 3 of Danchin and Wyatt (1979) indicate that considerable compositional overlap exists between their clusters and that in both classification schemes, the classification category "kimberlite garnets" includes garnets of both phenocrystal and xenocrystal origin; the two paragenesis which form the clearly distinct compositional variation trends

TABLE 7A

Statistical Classification of Ham Diatrema Garnets by  
Methods of Danchin and Wyatt (1979)

HAM DIATREME GARNETSSUMMARY - PROBABILITIES

	> .80	0.70-0.80	0.60-0.70	0.50-0.60	TOTAL
GROUP 13	1				1
GROUP 16	34	8	26	16	84
GROUP 20		1			1
GROUP 21			1	1	2
GROUP 22	3	2	1	2	8
GROUP 26		2			2
GROUP 33	20	5	2	3	30
GROUP 37	8	3	7	6	24
GROUP 44				1	1
GROUP 47	2			2	4

TABLE 7B

Statistical Classification of Ham Dyke Garnets by Methods  
of Danchin and Wyatt (1979)

HAM DYKE GARNETSSUMMARY - PROBABILITIES

	> .80	0.70-0.80	0.60-0.70	0.50-0.60	TOTAL
GROUP 16	119	22	18	6	165
GROUP 19			4	4	8
GROUP 20		1	10	14	25
GROUP 22	27	4	1		32
GROUP 26		4	4		8
GROUP 32	1				1
GROUP 33	2		1	1	4
GROUP 37		2	2	3	7
GROUP 46	1		1		2
GROUP 50	1				1

TABLE 7C  
Danchin and Wyatt's Classification Scheme for Garnets

TABLE 1 THE COMPOSITION OF GARNETS BELONGING TO CHROMIUM-RICH CLUSTER GROUPS\*

GROUP	COMPOSITION (wt. %)						CLASSIFICATION											
	NO	TiO <sub>2</sub>	Cr <sub>2</sub> O <sub>3</sub>	FeO	MgO	CaO	EC	DI	DX	GEC	PX	SPX	K	GWB	GL	GGL	DGL	GE
<u>Ti-Poor Peridotitic Garnets - Increasing Cr</u>																		
19	52	0.07	1.11	9.48	19.54	4.68	3			2	1	5	20	9	8	4		
20	125	0.09	2.36	7.65	20.47	4.79	3				4	8	56	4	22	22	1	3
16	219	0.11	4.72	7.05	20.62	4.99	3	8	10		17	1	69	3	35	26	23	24
33	66	0.09	7.28	6.53	20.37	5.40	1	5	1		4		22	2	10	5	9	7
<u>Ti-Rich Peridotitic Garnets - Increasing Cr</u>																		
24	52	1.00	1.13	9.33	20.50	4.54	7						41		1			3
26	102	0.90	1.45	8.98	20.58	4.52	2	1			2		72	1	1			22
22	52	0.49	2.30	8.05	20.78	4.63	1	2			8		26	3	9			3
27	16	0.41	3.80	12.17	17.38	5.18		1		1			2	7	5			
37	55	0.41	4.42	6.79	21.03	4.97	1	2	3		2		24		10	1		10
49	40	1.51	4.96	7.09	21.13	5.20					6							21
47	13	0.91	5.80	6.95	20.92	5.24					1		1		3			5
46	23	0.78	10.53	7.20	18.61	7.00					1		12		7	3		
<u>Diamond Inclusions and Harzburgites - Increasing Ca</u>																		
31	51	0.02	9.96	5.94	23.79	1.42		41	3				7					
34	55	0.02	6.99	5.91	23.77	1.47		32	4		3		15					1
45	16	0.06	13.58	6.07	23.21	1.76		14					2					
35	25	0.04	3.86	5.77	23.27	2.47		1	2		4		15		1			2
42	10	0.17	11.80	6.45	21.20	4.01		3	4				1					2
32	23	0.13	9.40	6.96	19.97	5.41		5	1		2		12		1			1

EC = eclogites, GEC = graphite bearing eclogites, DI = diamond inclusions, DX = diamond bearing xenoliths (includes diamond intergrowths), PX = polymict xenoliths, SPX = spinel bearing xenoliths, GWB = garnet websterites, GL = undefined garnet lherzolites, GGL = granular garnet lherzolites, DGL = deformed garnet lherzolites, GH = garnet harzburgites, K = Xenocrysts and kimberlite concentrate garnets, NO = Number of grains.

\*Danchin and Wyatt (1979)

discerned above. Further, Mitchell (1978a and 1979a) notes that Dawson and Stephens' (1975) classification fails to separate satisfactorily garnets in Groups 1, 2, and 9 (the latter into Cr-rich and Cr-poor garnets) and that further subdivision based upon  $\text{Cr}_2\text{O}_3$  and  $\text{CaO}$  should be attempted. These conclusions were amplified by the difficulty encountered during the classification of Ham garnets in this study, in which, a bi-modal distribution of Ti and Cr was encountered in several clusters (see above). Danchin and Wyatt (1979) indicate that Dawson and Stephens' (1975) classification scheme is limited as a paragenetic indicator because the sample size (353 cases) is not large enough to be representative, and also, some localities are overly represented. However, Danchin and Wyatt's (1979) classification scheme suffers from similar drawbacks; the sample size being only 1777 cases and not representative of a world wide distribution of garnets in kimberlite. Mitchell (1979a) contends that these classification schemes are too general and that because differences may occur in the paragenesis of garnet suites between diatremes, within the same kimberlite province, it is important initially to characterize the garnet suites within each province prior to attempting a classification scheme based

upon a world wide distribution of random samples. This may result in the diffusion and overlap of originally, chemically and statistically distinct garnet clusters from one kimberlite province with those derived from another.

In this study, cluster analysis, multiple discriminant analysis (MDA) and principal component analysis (PCA) were utilized in an attempt to classify statistically Ham garnets into chemically homogeneous groups based solely on major ( $\text{Al}_2\text{O}_3$ ,  $\text{MgO}$ ,  $\text{FeO}$  and  $\text{CaO}$ ) and minor ( $\text{TiO}_2$  and  $\text{Cr}_2\text{O}_3$ ) element contents.  $\text{SiO}_2$  and  $\text{MnO}$  were omitted from the classification attempt because they contribute little to the total variance of the garnet population as concluded by Dawson and Stephens (1975).

Cluster analysis (see below) was initially performed on unclassified data to derive chemically homogeneous clusters. The statistical significance (see below) of these clusters and clusters generated by plotting garnet data in an Fe-Mg-Ca ternary and a  $\text{TiO}_2$ - $\text{Cr}_2\text{O}_3$  plot was tested by multiple discriminant analysis to determine which classification method is most useful.

### Cluster Analysis

Cluster analysis is a statistical procedure in which some measure of resemblance or similarity can be computed for every pair of objects in a matrix of  $n$  objects with  $m$  measureable characteristics (Davis 1973). The heirarchical method of cluster analysis (Wishart 1969) forms clusters by the fusion of sample with sample and sample with cluster at successively higher levels of dissimilarity. A coefficient of dissimilarity may be calculated, utilizing, for example, a correlation or distance matrix of similarity (Davis 1973) for all cases. This coefficient is multiplied by each variable in a sample and then summed for all samples to determine the greatest similarity between any two cases. The most similar two cases are then fused to form a single case and the process repeated until all cases are fused with a progressively decreasing coefficient of similarity (Davis 1973). In this study, cluster analysis was performed using Davis' (1973) program (see Appendix C) modified for use on the Lakehead University VAX computer.

### Multiple Discriminant Analysis (MDA)

Multivariate analysis allows changes in several variables in a given sample to be monitored

simultaneously. Pearce (1974) indicates that the simplest approach to this is the analysis of the standard deviations of variables in data sets within and between groups. In this manner, it is possible to identify the variable most likely and/or least likely to contribute to the variation between groups. Pearce (1974) outlines the procedure of variance analysis utilizing F-ratios (where  $F = A/B$  and A is the within groups variance and B is the between groups variance), in which calculated and empirical F-ratios are compared for the null hypothesis, "that the means of each analysis are the same", could be rejected at the 0.01 significance level (see below) (i.e. 1 chance in 100, 1%) at the appropriate number of degrees of freedom. If calculated F-ratios are greater than empirical F-ratios, the likelihood that that variable will be a good discriminator is high. The relatively higher F-ratios correspond to variables with the greatest discriminating power (Pearce 1974). Wilks' Lambda ( $\lambda$ ) is a test for the statistical significance of the discriminating information which has not yet been removed by a discriminate function (Klecka 1975). The magnitude of the test inversely accompanies the F-ratio, such that a high F-ratio is accompanied by a low Wilks' Lambda. The significance of the F-ratio

and Wilks' Lambda is a measure of the chance of obtaining a higher F-ratio (i.e. better discriminating power) or lower Wilks' Lambda (i.e. that less information is required to make a statistically sound discrimination) for a given data set. A significance level of 0.0500 (i.e. 500 chances in 10,000 or 5%) and 0.0100 (i.e. 100 chances in 10,000 or 1%) represent statistically significant and highly significant tests, respectively.

For example, a review of Table 9A shows that  $\text{Cr}_2\text{O}_3$  has the highest F-ratio and lowest Wilks' Lambda of all variables used in the discriminant analysis. This indicates that  $\text{Cr}_2\text{O}_3$  is the best discriminating variable and that potentially more discrimination between data sets can be made with this variable than any other. The chance of obtaining a higher F-ratio or lower Wilks' Lambda (i.e. better discrimination with less information using this variable) is 0.0000 or 0 chances in 10,000. It is also evident from Table 9A that  $\text{TiO}_2$  is the least useful discriminating variable.

MDA performed on Ham garnet clusters made no prior assumptions as to the variation within or between data sets so that all variables had an equal chance to contribute to the discriminate analysis.

In order to represent graphically, the discrimination between clusters derived using 6 oxides, 6 axes, in 6 dimensional space would be required. Pearce (1974) explains that a single axis (linear discriminant function) can be selected, which, combines the discriminating power of all variables, for a given case, into a linear function, in which, the discriminating power of each variable, in each case, is maximized by canonical correlation (Cooley and Lohnes 1962, Klecka 1975) and summed to form a single, linear, canonical discriminant function for that case. The mean of all linear discriminant functions for a data set is located at the group centroid, which is the typical location of a case, from that group. The distance away from the group centroid of any case, is therefore, a function of the dissimilarity of that case with the group as a whole (Klecka 1975, Cooley and Lohnes 1962).

The multiple discriminant analysis program used in this study is documented in Appendix D (Klecka 1975).

#### Principal Component Analysis (PCA)

Principal component analysis is a variance analysis technique which is used to determine the minimum number of independent dimensions needed to

account for most of the variance in a given data set (Cooley and Lohnes 1962). Davis (1973) explains, that the summation of eigenvectors in a correlation matrix, for a data set, equals the total variance. Because the variance of a data set can be expressed in the form of an  $m \times m$  matrix, each element of the matrix can be regarded as defining points, on an  $m$ -dimensional ellipsoid, in which, the lengths of the principal axes are represented by the magnitude of the constituent eigenvectors. Therefore, the magnitude and orientation of the principal axes is a function of the proportion of variance each variable in the data set contributes toward the total variance. Inevitably, at least one of the principal axes (representing a variable with the most variance) will be more efficient in terms of accounting for the total variance than any of the others.

In this manner, PCA reduces the complexity of variance analysis and reduces the number of divariant variation diagrams (oxide vs oxide) needed to express the compositional variation, of all 11 variables (oxides), in each analysis, for each sample, to a single, three dimensional, orthogonal plot, which usually accounts for greater than 95% of the total variance for each case (Le Maitre 1968).

In Figure 16, ellipsoids representing at least 95% of the total variation within individual garnet clusters are presented. These were generated utilizing Equation (1) (Le Maitre 1968, Le Maitre person. comm) and the three, unrotated, principal eigenvectors (components) which were extracted by PCA from the correlation matrices for groups of garnets by the "SCSS package" documented by Kim (1975).

$$Z_i = (X_i - \bar{X}_i) V_i S_i \quad \text{Equation (1)}$$

In equation (1),  $X_i$  is the  $i^{\text{th}}$  oxide,  $\bar{X}_i$  is the mean of the  $i^{\text{th}}$  oxide,  $S_i$  is the standard deviation of the  $i^{\text{th}}$  oxide and  $V_i$  is the  $i^{\text{th}}$  term of the eigenvector.

#### The Statistical Classification and Analysis of Ham Garnets

Inspection of Tables 8A and 8B shows that considerable overlap occurs in clusters generated by cluster analysis for Ham garnets and that the seven clusters generated from diatreme garnets and the six clusters generated from dyke garnets may be combined into three clusters, based primarily upon  $TiO_2$  and  $Cr_2O_3$ ; FeO, MgO and CaO demonstrating little variation between clusters. The three clusters which emerge for the Ham diatreme are characterized by garnets with; 1) low Ti, high Cr and moderately high Ca contents, 2) high Ti,

TABLE 8A  
Means, Ranges and Standard Deviations for Clusters of Ham Diatreme Garnets Generated  
by Cluster Analysis

	TiO <sub>2</sub>			Al <sub>2</sub> O <sub>3</sub>			Cr <sub>2</sub> O <sub>3</sub>			FeO			MgO			CaO		
	Mean	Range	σ	Mean	Range	σ	Mean	Range	σ	Mean	Range	σ	Mean	Range	σ	Mean	Range	σ
1	0.10	0.06-0.15	0.05	19.43	19.03-20.07	0.56	5.87	5.17-6.58	0.71	7.05	6.91-7.26	0.19	20.54	20.25-20.76	0.26	5.30	5.18-5.49	0.17
2	0.04	0.00-0.21	0.09	19.21	18.17-19.81	0.68	6.05	5.07-7.35	0.94	7.18	6.77-7.67	0.35	19.82	19.26-20.58	0.63	5.79	5.03-6.56	0.64
3	0.17	0.00-0.35	0.16	19.45	17.99-20.92	0.46	5.53	4.24-7.21	0.92	7.23	6.70-7.67	0.09	20.31	19.61-20.91	0.59	5.81	4.95-6.92	0.81
4	0.28	0.00-1.04	0.18	19.65	16.71-22.76	1.09	5.11	0.62-8.91	1.52	7.00	6.06-9.09	0.39	20.71	18.86-21.89	0.55	5.46	4.32-7.77	0.50
5	0.28	0.00-0.66	0.17	19.35	17.83-22.63	1.19	5.44	0.77-7.49	1.73	7.02	5.85-9.02	0.62	20.55	19.59-21.51	0.50	5.56	4.52-6.29	0.47
6	0.24	0.00-0.48	0.34	19.37	17.98-20.75	1.96	5.54	3.96-7.12	2.23	6.72	6.68-6.76	0.06	20.65	19.91-21.39	1.05	5.56	4.93-6.19	0.89
7	0.41	-	-	17.91	-	-	7.15	-	-	6.85	-	-	20.34	-	-	6.15	-	-

TABLE 8B  
Means, Ranges and Standard Deviations for Clusters of Ham Dyke Garnets Generated  
by Cluster Analysis

	TiO <sub>2</sub>			Al <sub>2</sub> O <sub>3</sub>			Cr <sub>2</sub> O <sub>3</sub>			FeO			MgO			CaO		
	Mean	Range	σ	Mean	Range	σ	Mean	Range	σ	Mean	Range	σ	Mean	Range	σ	Mean	Range	σ
1	0.66	0.35-1.48	0.38	20.90	19.33-21.52	0.83	2.18	1.36-3.77	0.79	7.79	6.79-8.74	0.58	20.50	19.17-21.39	0.74	5.28	4.77-6.55	0.60
2	0.54	0.50-0.61	0.61	21.43	21.37-21.46	0.05	1.93	1.87-1.98	0.06	7.85	7.79-7.91	0.06	20.72	20.59-20.81	0.11	5.03	4.98-5.11	0.07
3	0.64	0.51-0.83	0.10	21.26	21.13-21.37	0.07	1.76	1.26-2.08	0.33	8.20	7.67-9.19	0.57	20.34	19.19-20.73	0.60	5.08	5.00-5.18	0.07
4	0.17	0.00-0.82	0.14	20.39	15.49-21.84	0.88	4.21	1.31-9.99	0.31	7.74	5.99-9.75	0.76	20.20	18.80-21.23	0.43	5.37	4.76-7.73	0.40
5	0.63	0.41-0.81	0.17	21.13	20.62-21.46	0.31	2.04	1.26-2.66	0.45	2.04	1.26-2.66	0.49	20.39	19.55-20.76	0.40	5.07	4.93-5.23	0.11
6	0.62	-	-	21.41	-	-	1.91	-	-	7.93	-	-	20.68	-	-	4.99	-	-

TABLE 8C

Summary Table of Wilks' Lambda and F-Ratios for Ham  
Diatreme Garnet Clusters Generated by Cluster Analysis

<u>VARIABLE</u>	<u>WILKS' LAMBDA</u>	<u>F</u>	<u>SIGNIFICANCE</u>
TiO <sub>2</sub>	0.92649	2.142	0.0513
Al <sub>2</sub> O <sub>3</sub>	0.97486	0.6962	0.6530
Cr <sub>2</sub> O <sub>3</sub>	0.96991	0.8378	0.5424
FeO	0.97834	0.5977	0.7319
MgO	0.91101	2.637	0.0182
CaO	0.97203	0.7768	0.5892

TABLE 8D

Summary Table of Wilks' Lambda and F-Ratios for Ham Dyke  
Garnet Clusters Generated by Cluster Analysis

<u>VARIABLE</u>	<u>WILKS' LAMBDA</u>	<u>F</u>	<u>SIGNIFICANCE</u>
TiO <sub>2</sub>	0.54408	45.25	0.0000
Al <sub>2</sub> O <sub>3</sub>	0.92912	4.119	0.0013
Cr <sub>2</sub> O <sub>3</sub>	0.77918	15.30	0.0000
FeO	0.98301	0.9333	0.4598
MgO	0.96816	1.776	0.1180
CaO	0.95830	2.350	0.0413

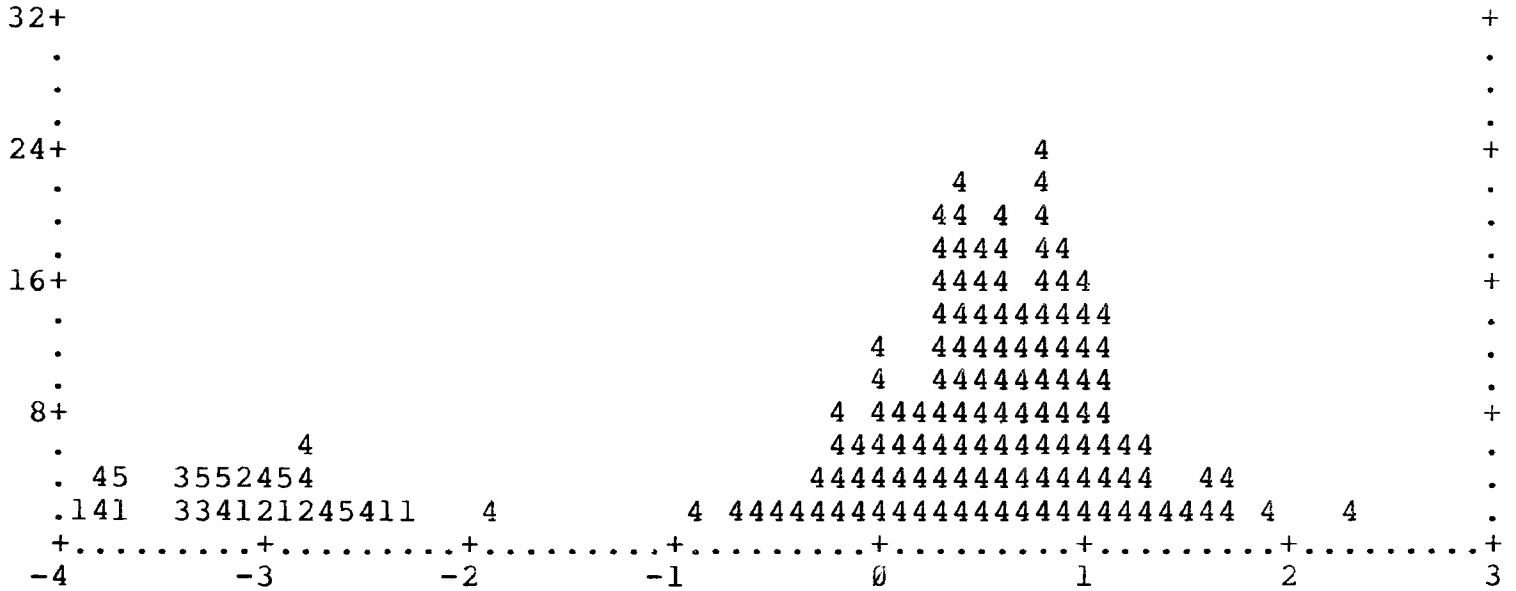
low Cr and moderately low Ca contents relative to (1) and 3) high Ti, Cr and Ca contents relative to (1) or (2). Table 8B shows that similar clusters emerge for Ham dyke garnets which are characterized by; 1) low Ti, high Cr and relatively low Fe contents, 2) high Ti, low Cr and highly variable Fe contents relative to (1) and 3), high Ti and Fe and low Cr and Ca contents relative to (1) or (2). Low Ti, high Cr garnets and high Ti, low Cr garnets are compositionally similar to Trend A and Trend B garnets, respectively.

In contrast, a review of Tables 5 and 6 (see above) shows that groups generated by major and minor plots (Figures 8, 9, 10 and 11) do not exhibit compositional overlap and are characterized by a specific compositional variation.

The results of multiple discriminant analysis for clusters generated by cluster analysis are presented in Tables 8C and 8D and illustrated in Figures 12A and 12B for Ham diatreme and dyke garnets, respectively. Inspection of Table 8C shows that MgO and  $TiO_2$  are statistically the best discriminating oxides for diatreme garnets, although Figure 12A shows that these clusters are virtually indistinguishable and that the compositional overlap (see Table 8A) is extensive. However, garnets in



FIGURE 12B  
 HISTOGRAM OF CANONICAL DISCRIMINANT FUNCTIONS FOR CLUSTERS  
 OF HAM DYKE GARNETS GENERATED BY CLUSTER ANALYSIS



CANONICAL DISCRIMINANT FUNCTIONS EVALUATED AT GROUP CENTROIDS

SYMBOL	GROUP	LABEL	GROUP	DISCRIMINANT FUNCTION
1	1	1	HDA	-3.66571
2	2	2	HDB	-2.95002
3	3	3	HDC	-3.38072
4	4	4	HDD	0.36152
5	5	5	HDE	-3.31649
6	6	6	HDF	-3.17040

LHERZOLITE GARNETS	FUNCTION	MEGACRYST GARNETS	FUNCTION
HDD	0.36152	HDA	-3.66571
		HDB	-2.95002
		HDC	-3.38072
		HDE	-3.31649
		HDF	-3.17040

Cluster 2, which are compositionally similar to Trend A megacrysts (see above), are distinguished from Trend B xenocrysts, by having a strongly negative canonical discriminant function. Similarly, Figure 12B shows that Trend A megacrysts and Trend B xenocrysts are compositionally different, the former with strongly negative discriminate functions relative to the latter. Table 8D shows that  $TiO_2$ ,  $Cr_2O_3$ ,  $Al_2O_3$  and CaO are statistically the best discriminating oxides for dyke garnets.

Although Figure 12 shows that cluster analysis can generate clusters of garnets belonging to two distinct paragenesis, it is evident from the compositional overlap between clusters, given in Tables 8A and 8B and illustrated in Figure 12, that cluster analysis cannot statistically separate compositionally similar garnets in the same paragenesis. Cluster analysis is undoubtedly useful for regional mineral prospecting as garnets of very different composition can be classified unambiguously (i.e. eclogite and lherzolite) but it is not useful for dealing with subtle differences within a population of garnets of similar compositions.

The results of multiple discriminant analysis (MDA) for groups (Tables 5 and 6) of garnets

generated on the basis of major (Figure 8 and 10) and minor (Figure 9 and 11) element contents are shown in Table 9A and 9B and illustrated in Figures 13 and 14. A comparison of Tables 9A and 9B shows that the  $\text{Cr}_2\text{O}_3$  content of Ham garnets is the most useful discriminating oxide between groups and that  $\text{Al}_2\text{O}_3$ ,  $\text{CaO}$ ,  $\text{MgO}$ ,  $\text{FeO}$  and  $\text{TiO}_2$  are successively less useful. Figures 13 and 14 show that the groups which make up the two compositional trends, A and B (see above), may be distinguished using a linear, canonical discriminant function and that the discriminant function for Trend A (megacryst) and Trend B (xenocryst) garnets is less than and greater than 0.0000 respectively, in the Ham dyke and -4.0000 respectively, in the Ham diatreme. The broad compositional variation of several diatreme clusters (HW2, 3, 4, 5 and 6) contrasts with the relatively narrow compositional variation of most dyke clusters. This suggests that garnets in these clusters crystallized over a broader composition range than garnets in groups which form discrete clusters. Dyke clusters HD3 and 4 demonstrate a similar relationship. That several clusters (HW6 and 7 and HD2, 3 and 5) have a bi-modal compositional variation (see Tables 5 and 6) is well illustrated by the skewed or bi-modal nature of their respective portions of Figures 13 and 14.

TABLE 9A

Summary Table of Wilks' Lambda and F-Ratios for Ham  
Diatreme Garnet Groups Generated by Major and  
Minor Element Plots

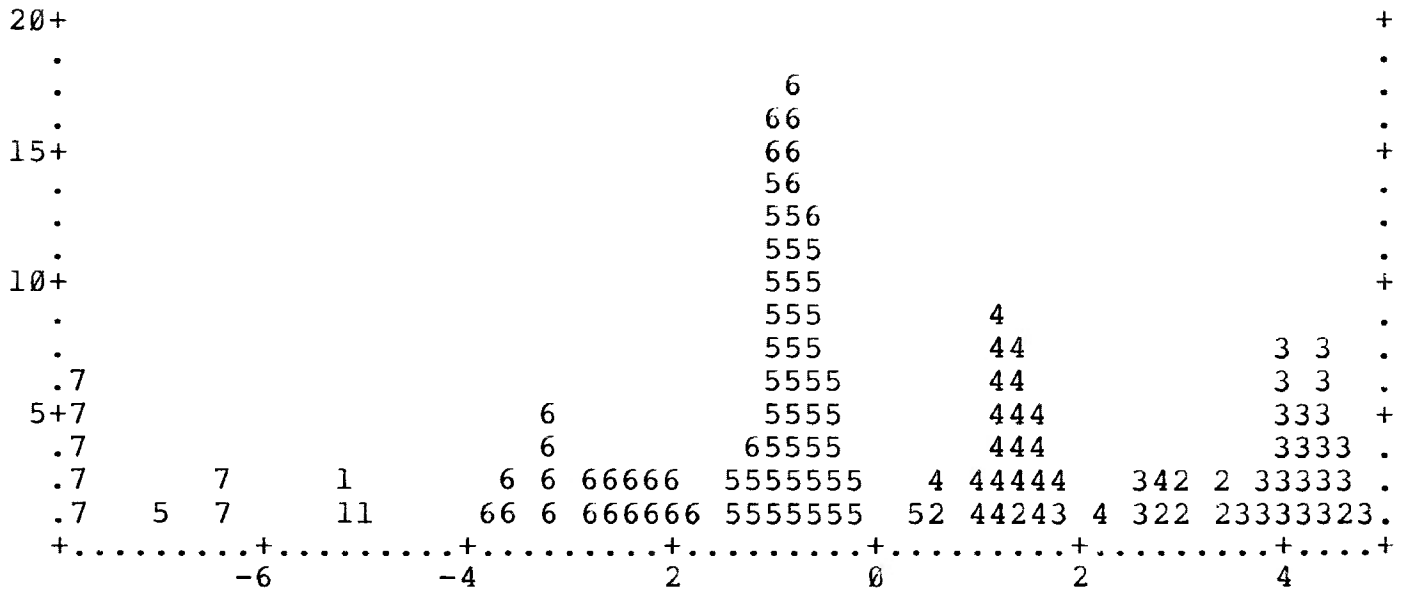
<u>VARIABLE</u>	<u>WILKS' LAMBDA</u>	<u>F</u>	<u>SIGNIFICANCE</u>
TiO <sub>2</sub>	0.37065	45.00	0.0000
Al <sub>2</sub> O <sub>3</sub>	0.19415	110.0	0.0000
Cr <sub>2</sub> O <sub>3</sub>	0.08960	269.3	0.0000
FeO	0.31749	56.97	0.0000
MgO	0.26319	74.19	0.0000
CaO	0.21413	97.26	0.0000

TABLE 9B

Summary Table of Wilks' Lambda and F-Ratios for Ham Dyke  
Garnet Groups Generated by Major and Minor Element  
Plots

<u>VARIABLE</u>	<u>WILKS' LAMBDA</u>	<u>F</u>	<u>SIGNIFICANCE</u>
TiO <sub>2</sub>	0.44762	55.33	0.0000
Al <sub>2</sub> O <sub>3</sub>	0.13990	275.6	0.0000
Cr <sub>2</sub> O <sub>3</sub>	0.07993	516.0	0.0000
FeO	0.10253	392.5	0.0000
MgO	0.32727	92.16	0.0000
CaO	0.19453	185.6	0.0000

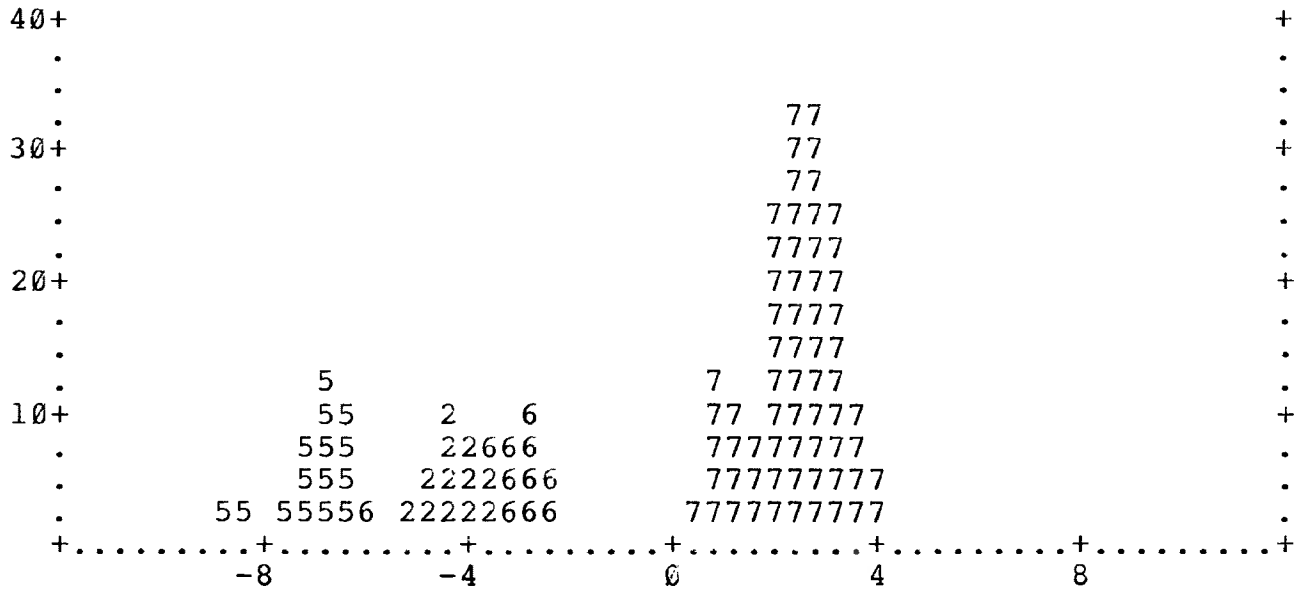
FIGURE 13  
 HISTOGRAM OF CANONICAL DISCRIMINANT FUNCTIONS FOR GROUPS OF  
 HAM DIATREME GARNETS GENERATED BY MAJOR AND MINOR ELEMENTS PLOTS



CANONICAL DISCRIMINANT FUNCTIONS EVALUATED AT GROUP CENTROIDS					
SYMBOL	GROUP	LABEL	GROUP	DISCRIMINANT FUNCTION	
1	1	HW1	1	-5.12403	
2	2	HW2	2	3.76444	
3	3	HW3	3	4.09303	
4	4	HW4	4	1.41309	
5	5	HW5	5	-0.88652	
6	6	HW6	6	-2.25895	
7	7	HW7	7	-8.83481	

LHERZOLITE GARNETS		FUNCTION	MEGACRYST GARNETS		FUNCTION
HW2		3.76444	HW1		-5.12403
HW3		4.09303	HW7		-8.83481
HW4		1.41309			
HW5		-0.88652			
HW6		-2.25895			

FIGURE 14  
 HISTOGRAM OF CANONICAL DISCRIMINANT FUNCTIONS  
 FOR GROUPS OF HAM DYKE GARNETS GENERATED BY MAJOR AND  
 MINOR ELEMENT PLOTS



CANONICAL DISCRIMINANT FUNCTIONS EVALUATED AT GROUP CENTROIDS

SYMBOL	GROUP	LABEL	GROUP	DISCRIMINANT FUNCTION
1	1	HD1	1	-3.55641
2	2	HD4	2	-4.20677
3	3	HD7	3	12.97172
4	4	HD6	4	10.84919
5	5	HD2	5	-7.03040
6	6	HD3	6	-3.16380
7	7	HD5	7	2.41355

LHERZOLITE GARNETS  
 HD5  
 HD6  
 HD7

DISCRIMINANT FUNCTION  
 2.41355  
 10.84919  
 12.97172

MEGACRYST GARNETS  
 HD1  
 HD2  
 HD3  
 HD4

DISCRIMINANT FUNCTION  
 -3.55641  
 -7.03040  
 -3.16380  
 -4.20677

Table 10 shows that  $\text{Cr}_2\text{O}_3$  is the most useful discriminating oxide to distinguish between megacryst and lherzolite garnets in a composite analysis of both diatreme and dyke garnets. Figure 15A shows that megacryst and lherzolite garnets are successfully separated by MDA and that some compositional variation within paragenetic types is apparent.

To test the validity of this classification, MDA was used to assign garnets of known paragenesis (Elwin Bay, Mitchell 1978b and unpubl. data) to the classification scheme generated for Ham garnets. Figure 15B shows that MDA correctly classified megacryst and lherzolite garnets from the Elwin Bay kimberlite and shows that the paragenetic classification scheme developed for Ham garnets is correct. Therefore, MDA is an efficient method of distinguishing paragenesis and can separate xenocryst and phenocryst garnets from a random sample of garnets to facilitate the study of chemical evolutionary trends in kimberlite magmas.

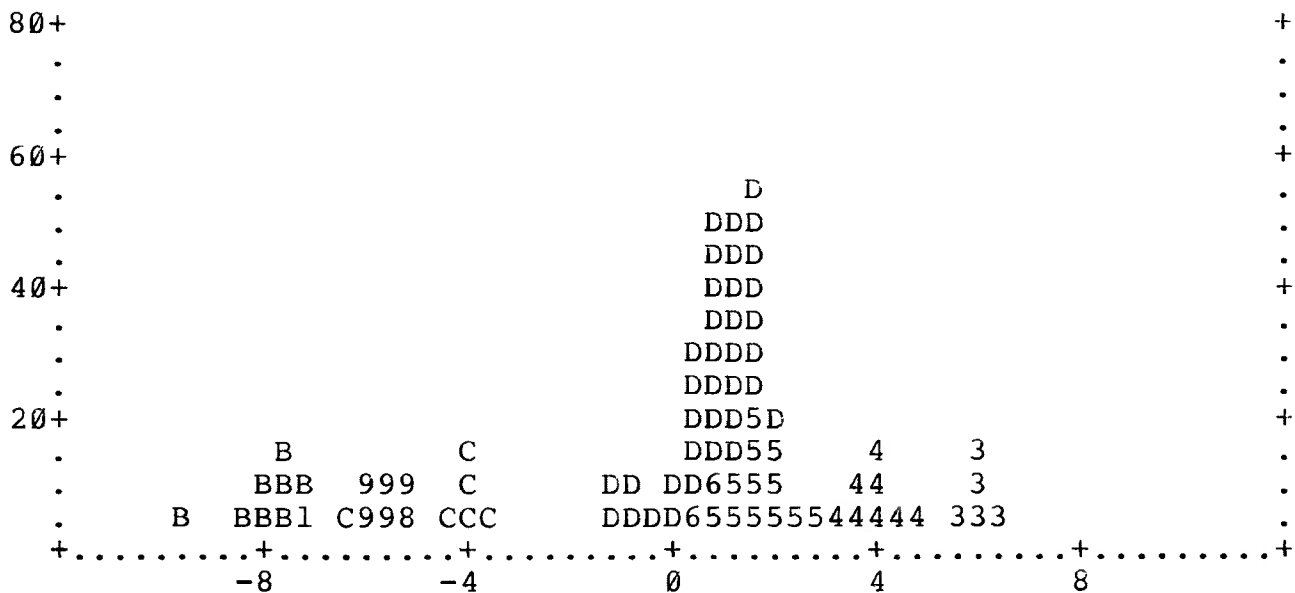
Inspection of Figure 16A shows that principal component analysis (PCA) delineated 2 trends for the principal axes of variation characterized by groups HW1, 2, 5 and 7 (Trend 1) and HW3, 4 and 6 (Trend 2). A comparison of Figures 16A and Figure 8A shows that

TABLE 10

Summary Table of Wilks' Lambda and F-Ratios for a composite analysis of groups of Ham garnets

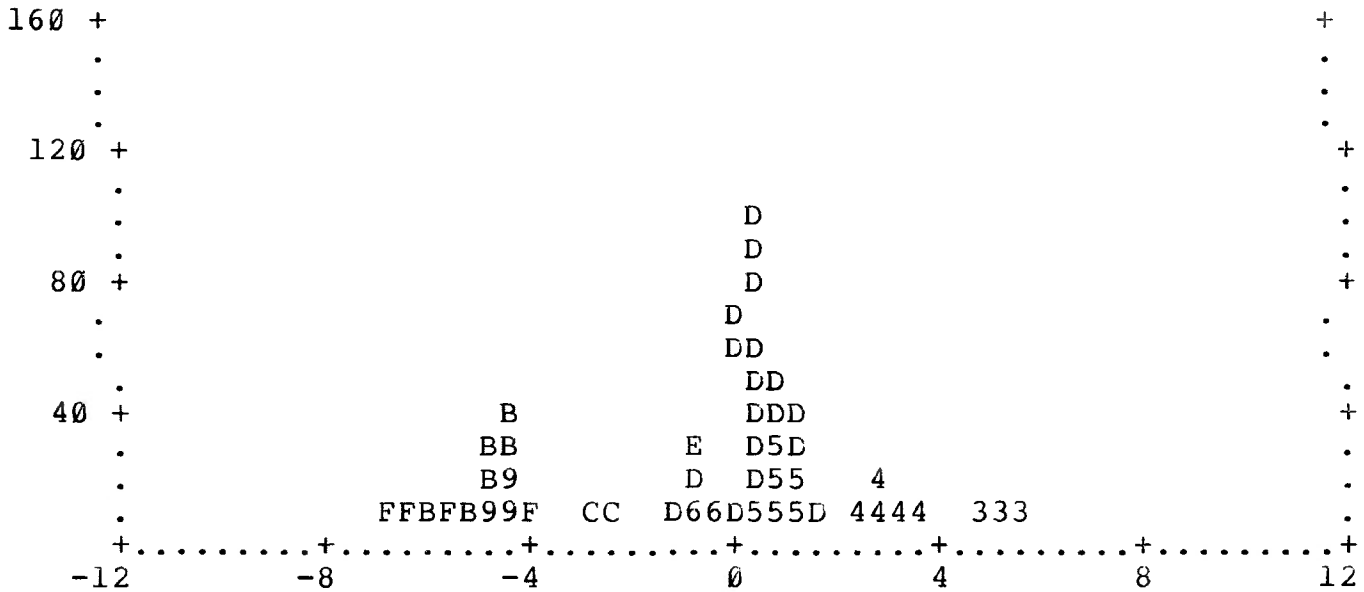
<u>VARIABLE</u>	<u>WILKS' LAMBDA</u>	<u>F</u>	<u>SIGNIFICANCE</u>
TiO <sub>2</sub>	0.41771	45.89	0.0000
Al <sub>2</sub> O <sub>3</sub>	0.13731	206.8	0.0000
Cr <sub>2</sub> O <sub>3</sub>	0.07149	427.6	0.0000
FeO	0.10382	284.2	0.0000
MgO	0.25522	96.08	0.0000
CaO	0.20085	131.0	0.0000

FIGURE 15A  
 HISTOGRAM OF CANONICAL DISCRIMINANT FUNCTIONS FOR  
 GROUPS OF HAM DIATREME AND DYKE GARNETS GENERATED  
 BY MAJOR AND MINOR ELEMENT PLOTS



CANONICAL DISCRIMINANT FUNCTIONS EVALUATED AT GROUP CENTROIDS				LHERZOLITE GARNETS		FUNCTION
SYMBOL	GROUP	LABEL	GROUP FUNCTION			
1	1	HW1	-7.10431	HW2		5.29307
2	2	HW2	5.29307	HW3		6.03412
3	3	HW3	6.03412	HW4		3.88185
4	4	HW4	3.88185	HW5		1.54206
5	5	HW5	1.54206	HW6		1.26516
6	6	HW6	1.26516	HD5		0.75297
7	7	HW7	-5.52066	HD6		8.58637
8	8	HD1	-5.01449	HD7		11.41648
9	9	HD4	-5.42890			
0	10	HD7	11.41648	MEGACRYST GARNETS		FUNCTION
A	11	HD6	8.58637	HW1		-7.10431
B	12	HD2	-7.94696	HW7		-5.52066
C	13	HD3	-4.23910	HD1		-5.50149
D	14	HD5	0.75297	HD2		-7.94696
				HD3		-4.23910
				HD4		-5.42890

FIGURE 15B  
HISTOGRAM OF CANONICAL DISCRIMINANT FUNCTIONS  
FOR HAM AND ELWIN BAY GARNETS



CANONICAL DISCRIMINANT FUNCTIONS EVALUATED AT GROUP CENTROIDS

SYMBOL	GROUP	LABEL	GROUP	FUNCTION	LHERZOLITE GARNETS
1	1	HW1	1	-3.91711	HW2 5.10513
2	2	HW2	2	5.10513	HW3 5.40362
3	3	HW3	3	5.40362	HW4 3.26795
4	4	HW4	4	3.26795	HW5 1.21401
5	5	HW5	5	1.21401	HW6 0.46253
6	6	HW6	6	0.46253	HD7 10.44260
7	7	HW7	7	-5.21983	HD6 7.47775
8	8	HD1	8	-2.26554	HD5 0.95599
9	9	HD4	9	-4.01975	ELWLHZ 2.18824
0	10	HD7	10	10.44260	
A	11	HD6	11	7.47775	MEGACRYST GARNETS
B	12	HD2	12	-4.54281	HW1 -3.91711
C	13	HD3	13	-2.44668	HW7 -5.21983
D	14	HD5	14	0.95599	HD1 -2.26554
E	15	ELWLHZ	15	2.18824	HD4 -4.01975
F	16	ELWMEG	16	-5.39215	HD2 -4.54281
					HD3 -2.44668
					ELWMEG -5.39215

the former trend may be correlated with garnets in clusters characterized by a variable Mg/Mg+Ca ratio at an approximately constant FeO content.

Inspection of Figure 16B shows that PCA delineated a single principal axis of variation approximately parallel to that delineated for Trend 1 above. A comparison of Figure 10 and 16B shows that the major composition variation correlatable with this trend, is the variation in the Fe/Fe+Mg ratios within individual clusters. The bi-modal nature of the compositional variation illustrated by HD5 (Table 6A), is shown in the relatively polarized nature of the data plot (Figure 16B). This trend is also illustrated by clusters HW2, 6 and 7 (Table 6A). This is not illustrated by HD2 or HD3 which indicates that the chemical variation within these bi-modal clusters may not be significant. A comparison of Figure 16B and Figure 11 shows that the relatively dispersed nature of a PCA data plot may be a function of the highly variable nature of the major or minor element contents (e.g. HD6, highly variable Cr<sub>2</sub>O<sub>3</sub> content) of the constituent garnets. The paucity of data for clusters HD1 and 7 precludes analysis by PCA.

Contrary to conclusions reached by Le Maitre (1968), PCA did not provide additional information

FIGURE 16A

ORTHOGONAL 3-D PLOT OF PRINCIPAL AXES (PCA) OF VARIATION FOR GROUPS OF GARNETS GENERATED BY MAJOR AND MINOR ELEMENT PLOTS

HAM DIATREME

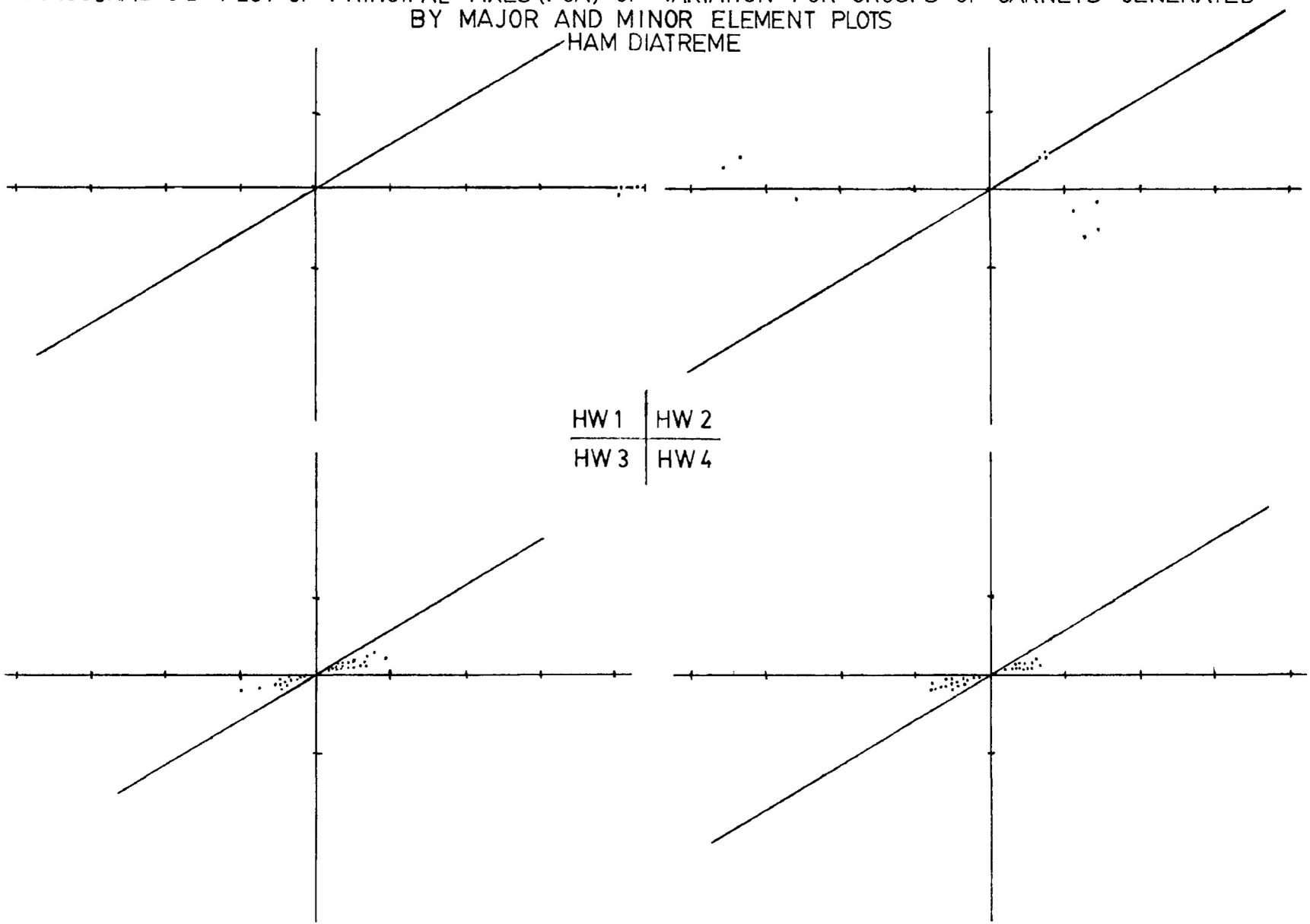


FIGURE 16A CONT'D

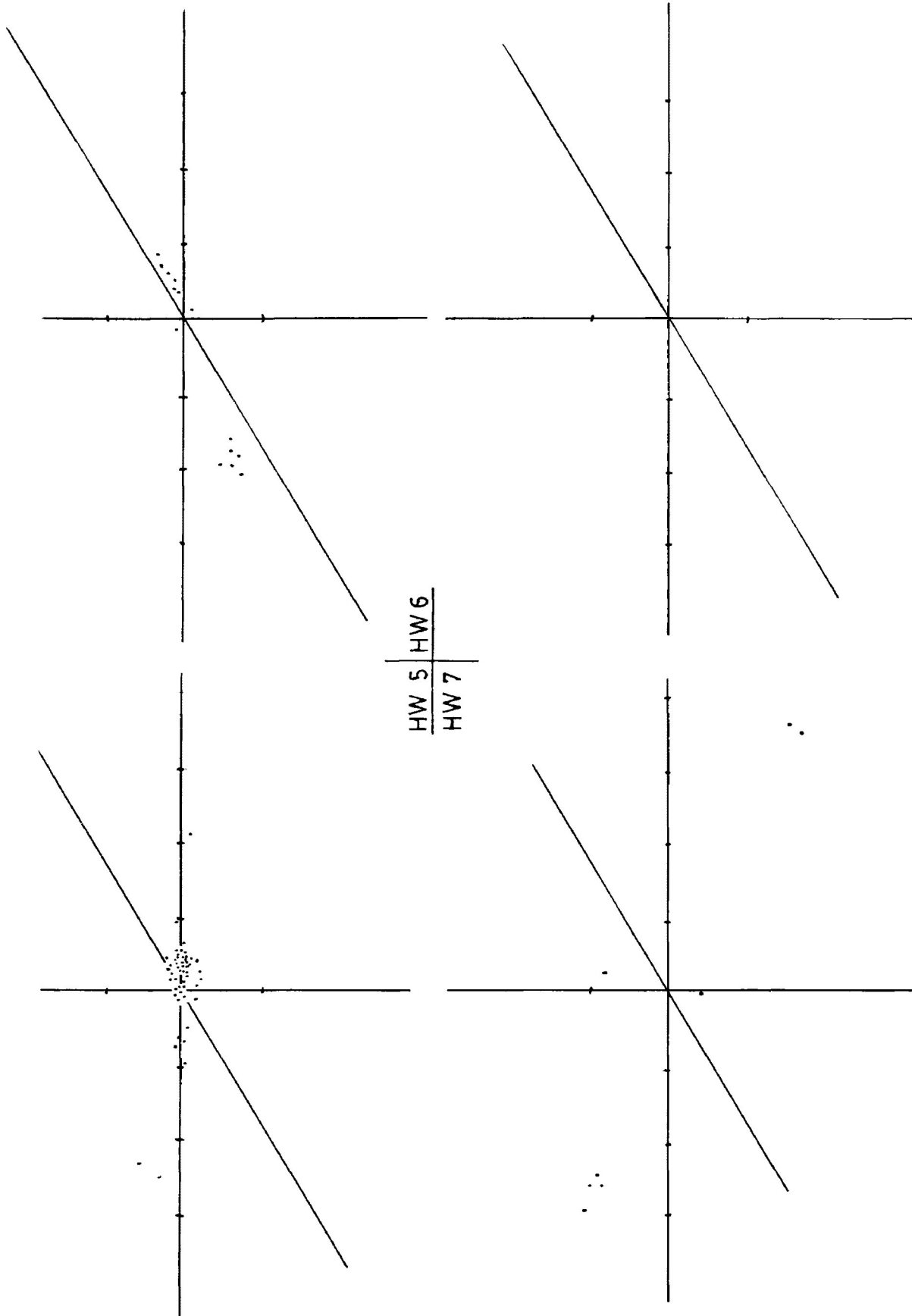


FIGURE 16B  
ORTHOGONAL 3D PLOT OF PRINCIPAL AXES (PCA) OF VARIATION FOR GROUPS OF GARNETS GENERATED  
BY MAJOR AND MINOR ELEMENT PLOTS

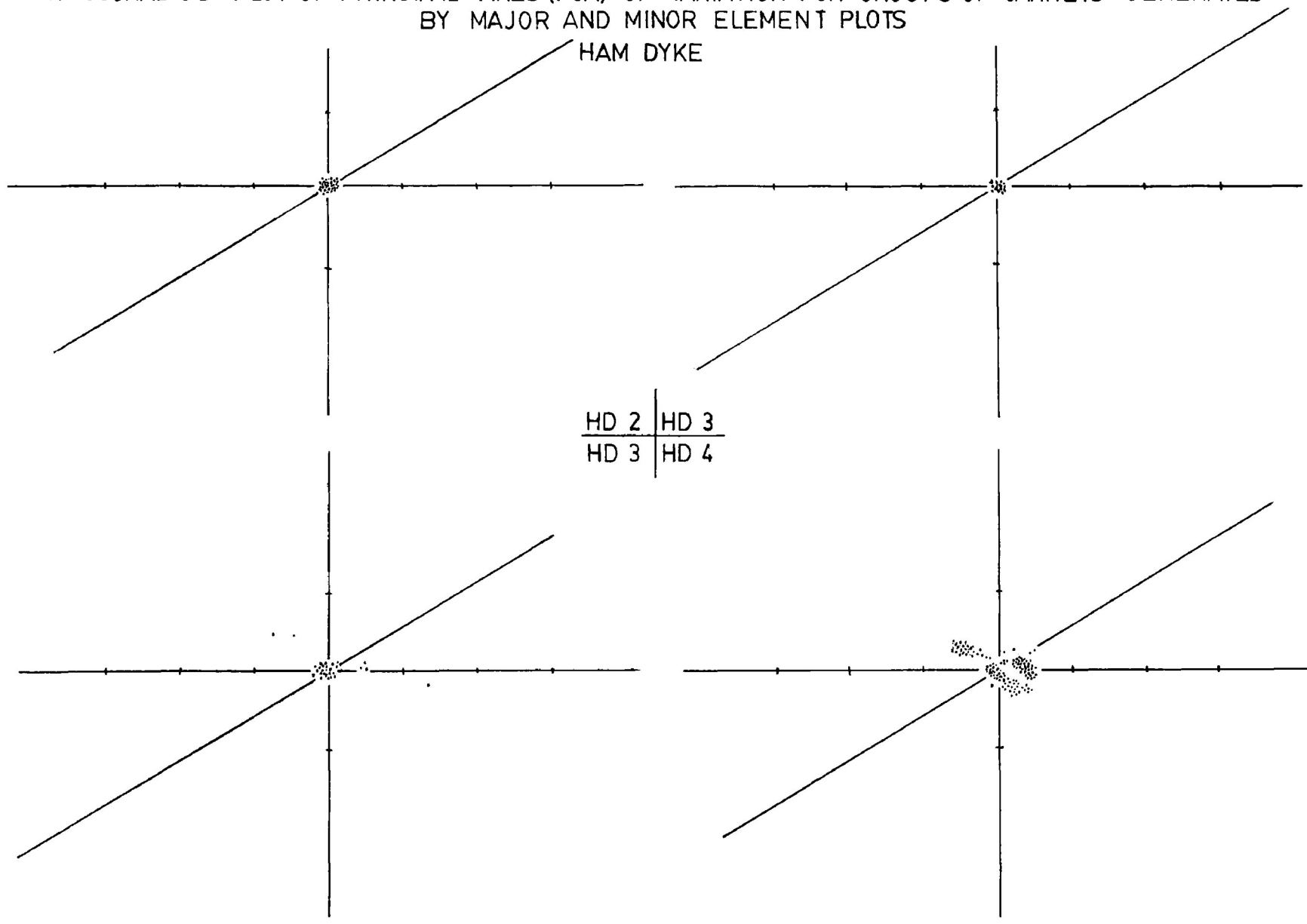
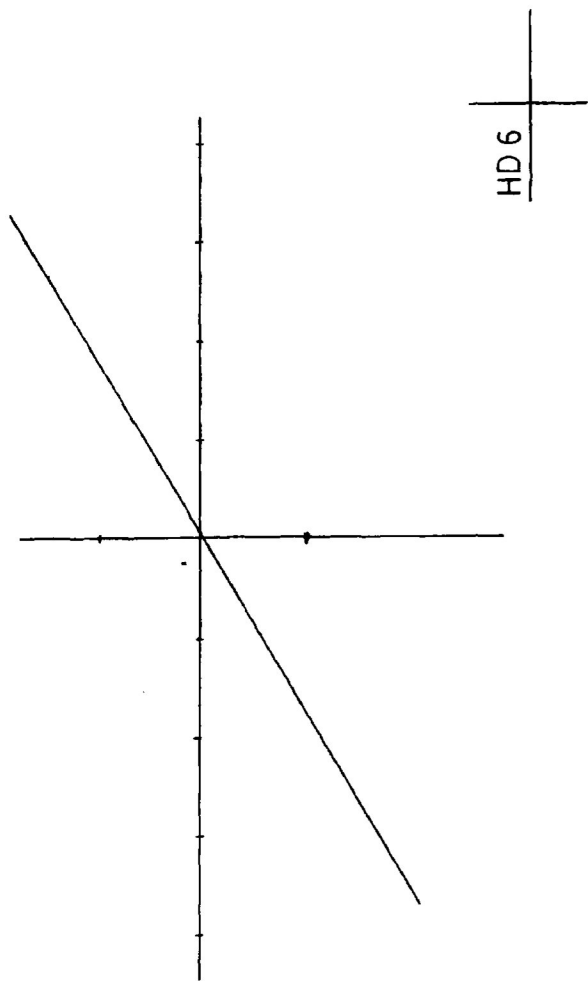


FIGURE 16B CONT'D



concerning the compositional variation in or between clusters for Ham garnets. The two trends delineated for the principal axes of variation within the ellipsoids of variation appear to reflect only the bi-modal nature of the compositional variation discerned for Ham garnets in Figures 9 and 11.

### CONCLUSIONS

Major and minor element variation diagrams divide Ham garnets into two paragenesis; Trend A garnets are compositionally similar to kimberlite megacrysts (phenocrysts) and Trend B garnets are compositionally similar to garnets in garnet lherzolite xenoliths from Somerset Island and South African kimberlites. These garnets are compositionally similar to Dawson and Stephens (1975) titan-pyropes (Group 1) and chrome-pyropes (Group 9) and Danchin and Wyatts' (1979) Ti-rich peridotite garnets and Ti-poor peridotitic garnets, respectively. No eclogite or iron-rich metamorphic garnets similar to those found in the Peuyuk kimberlite were encountered in the Ham kimberlite.

Major element compositional variation diagrams show that there is chemical variation between and within paragenetically distinct garnets from

kimberlites in the same kimberlite province. This suggests that existing classification schemes for garnets, which are based on a world wide distribution of garnets in kimberlite, are too general for classification within individual garnet provinces, and, that chemically distinct groups, generated for individual diatremes may become diffuse in nature when successively combined with garnets of a similar paragenesis from diatremes, in another kimberlite province.

The contrast in garnet assemblages between the Ham diatreme and dyke suggests that petrogenetic conditions in the latter kimberlite enhanced the crystallization of garnet phenocrysts and that intrusive events in the upper mantle and crust favoured the incorporation and fragmentation of garnet lherzolite xenoliths into the Ham diatreme. This suggests that the feeder system for the Ham diatreme is more extensive than that for the Ham dyke and that the intrusion of the former was more dynamic than the latter.

The statistical analysis (MDA) of Ham garnets shows that although cluster analysis can separate garnets into distinct paragenesis, the degree of separation is not satisfactory (see Figure 12A) and statistically significant separation is not achieved for clusters within individual paragenesis.

Cluster analysis, therefore, yields garnet clusters with considerable compositional overlap. In contrast, statistical analysis (MDA) of groups of garnets generated by major and minor element plots, shows, that statistically significant separation can be obtained between and within paragenesis, by this method of classification. In addition, MDA shows that if two chemically similar groups are compared, no statistical difference will be discerned for the two. It is, therefore, suggested that the initial classification of garnets from a kimberlite should be based solely upon major and minor element compositional variation and that multiple discriminant analysis should be used to determine if these groups are significantly distinct. Any new data for that kimberlite should be included in a separate statistical analysis to determine to which group it belongs.

Principal component analysis of Ham garnets does not add any additional information to that obtained by multiple discriminant analysis.

CHAPTER 5  
CLINOPYROXENE

Green clinopyroxene (<1.5mm in diameter) occurs as rounded, pitted and frosted grains in heavy mineral concentrates from the Ham kimberlite. Crystallization prior to the fluidized intrusion of the Ham kimberlite is indicated by the rounded and abraded nature of the pyroxene grains. Petrographic examination of the Ham kimberlite revealed that clinopyroxene did not crystallize from the kimberlite magma.

Representative analyses of clinopyroxenes from kimberlite concentrates are given in Table 11; all analyses are listed in Appendix B. Table 12 gives analyses and temperatures and pressures of equilibration for co-existing clinopyroxene and orthopyroxene in two garnet lherzolite xenoliths. The compositional variation of Ham clinopyroxenes is illustrated in Figures 17 to 20.

The major element compositional variation of Ham pyroxenes and pyroxenes in garnet lherzolite xenoliths from the Ham diatreme is illustrated in the pyroxene quadrilateral (Figure 17, Poldervaart and Hess 1951). This plot indicates that 91 percent of Ham pyroxenes including the two lherzolite pyroxenes are diopsides. One grain plots above the diopside-hedenbergite join and four grains plot within the endiopside field ( $En_{55-75}$ ,  $Fs_{0-10}$ ,  $Wo_{25-45}$ ).



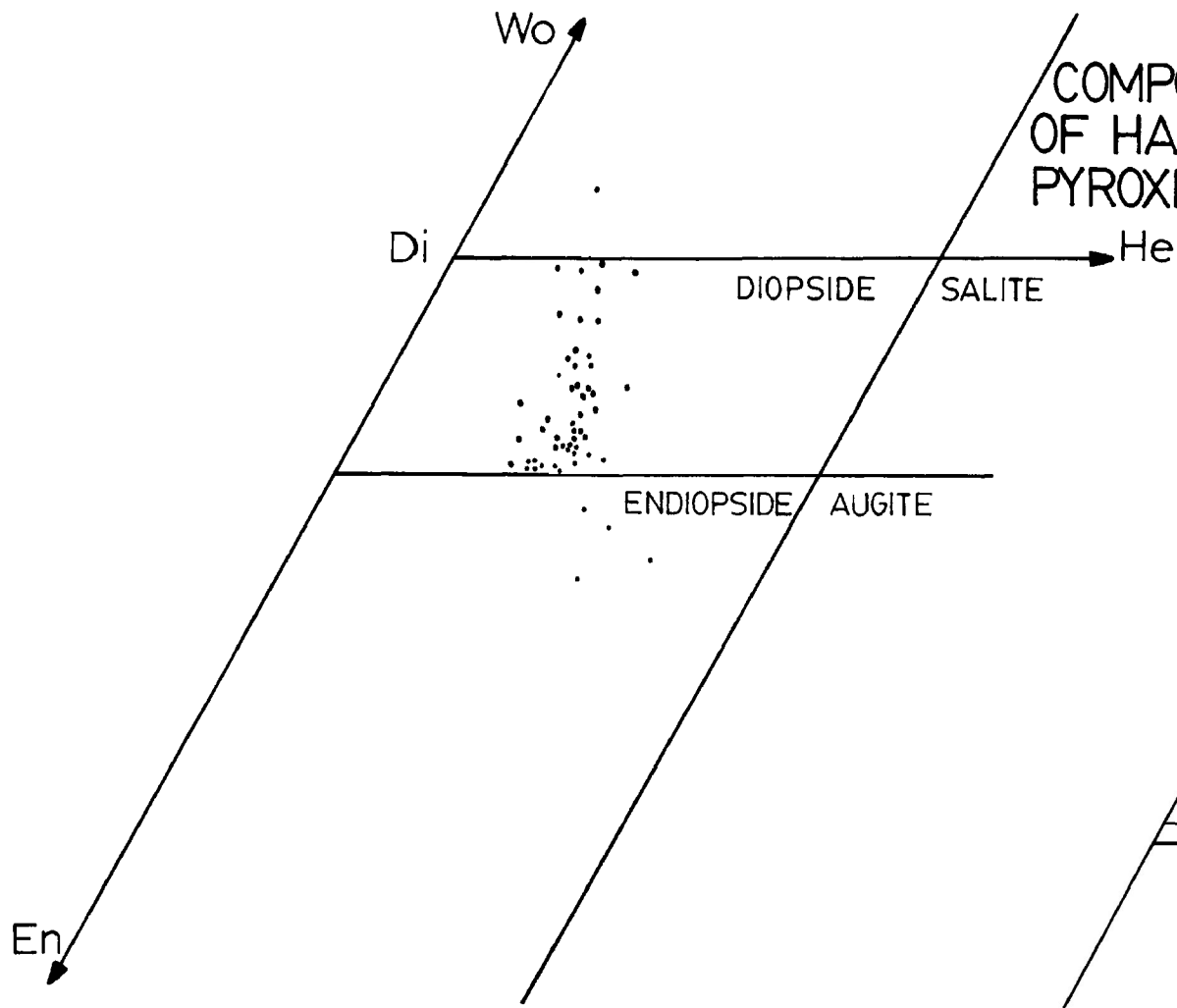
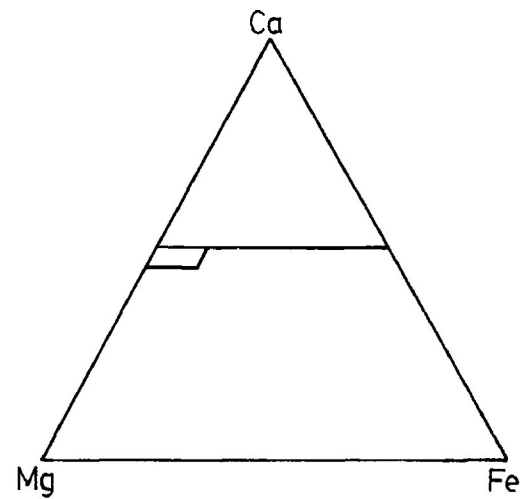


FIGURE 17  
COMPOSITIONAL VARIATION  
OF HAM PYROXENES IN THE  
PYROXENE QUADRILATERAL



Pyroxene fields after Poldervaart and Hess (1951)

Table 12  
 Representative Analyses of Clinopyroxenes and Orthopyroxenes  
 in Garnet Lherzolite Xenoliths with a Pressure-Temperature  
 Estimate of Equilibration

	Ø2		14	
	Cpx	Opx	Cpx	Opx
SiO <sub>2</sub>	54.30	57.39	54.10	57.12
TiO <sub>2</sub>	0.28	0.13	0.45	0.23
Al <sub>2</sub> O <sub>3</sub>	2.51	1.08	2.53	1.48
Cr <sub>2</sub> O <sub>3</sub>	1.75	0.45	1.20	0.40
FeO*	2.51	5.12	3.60	6.40
MnO	0.09	0.13	0.13	0.08
MgO	16.98	34.77	18.33	33.90
CaO	18.80	0.61	17.68	1.13
Na <sub>2</sub> O	1.92	0.11	1.43	0.18
K <sub>2</sub> O	0.0	0.0	0.0	0.0
NiO	0.04	0.05	0.06	0.06
TOTAL	99.18	99.84	99.51	100.98
Fe/Fe+Mg	0.076	0.076	0.099	0.096
Mg/Mg+Fe	0.923	0.924	0.901	.904
Ca/Ca+Mg	0.443	0.012	0.409	0.023
Cr/Cr+Al	0.319	0.219	0.241	0.153
Wells T°C	1031°C		1146°C	
Pressure	36.0 Kb		39.0 Kb	
Depth	110 km		120 km	

\*Total iron as FeO

Ø2 - Granular garnet lherzolite

14 - Mosaic porphyroclastic garnet lherzolite

Table 13  
A Comparison of Ham Pyroxenes with Other Somerset Island Pyroxenes from  
Garnet and Spinel Lherzolite Xenoliths

	Ham		Elwin Bay <sup>1</sup>		Nanorluk <sup>2</sup>		Ameyersuk <sup>3</sup>	
	Kimberlite Xenocrysts	Garnet Lherzolite	Garnet Lherzolite	Spinel Lherzolite	Garnet Lherzolite	Spinel Lherzolite	Garnet Lherzolite	Spinel Lherzolite
Fe/Fe+Mg								
Range	0.04-0.10	0.08-0.10	0.06-0.08	0.03-0.05	0.07-0.09	0.04-0.05	0.07-0.09	0.08
Mean	0.07	0.09	0.07	0.04	0.07	0.045	0.08	-
Ca/Ca+Mg								
Range	0.39-0.50	0.41-0.44	0.42-0.48	0.48-0.50	0.42-0.49	0.49-0.52	0.39-0.45	0.51
Mean	0.43	0.43	0.43	0.49	0.44	0.50	0.42	-
Cr/Cr+Al								
Range	0.02-0.59	0.24-0.31	0.26-0.56	0.16-0.24	0.22-0.39	0.06-0.26	0.23-0.43	0.13
Mean	0.35	0.28	0.35	0.19	0.30	0.17	0.33	-

1 Mitchell (1977, 1978b)

2 Mitchell (1978b)

3 Mitchell (1978b)

FIGURE 18  
 A COMPARISON OF HAM PYROXENES  
 AND SOMERSET ISLAND LHERZOLITE  
 PYROXENES IN THE PYROXENE QUADRI-  
 LATERAL

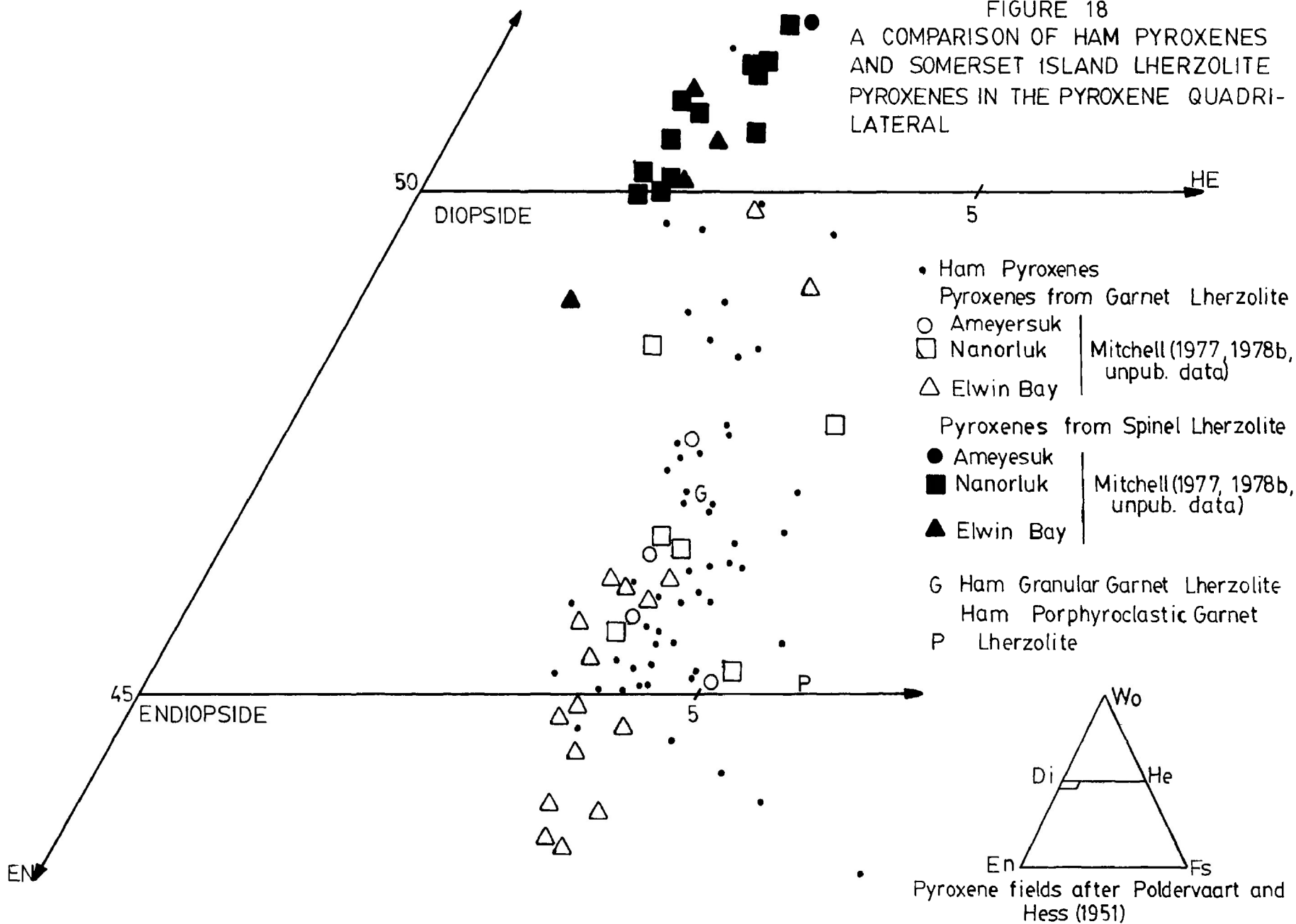
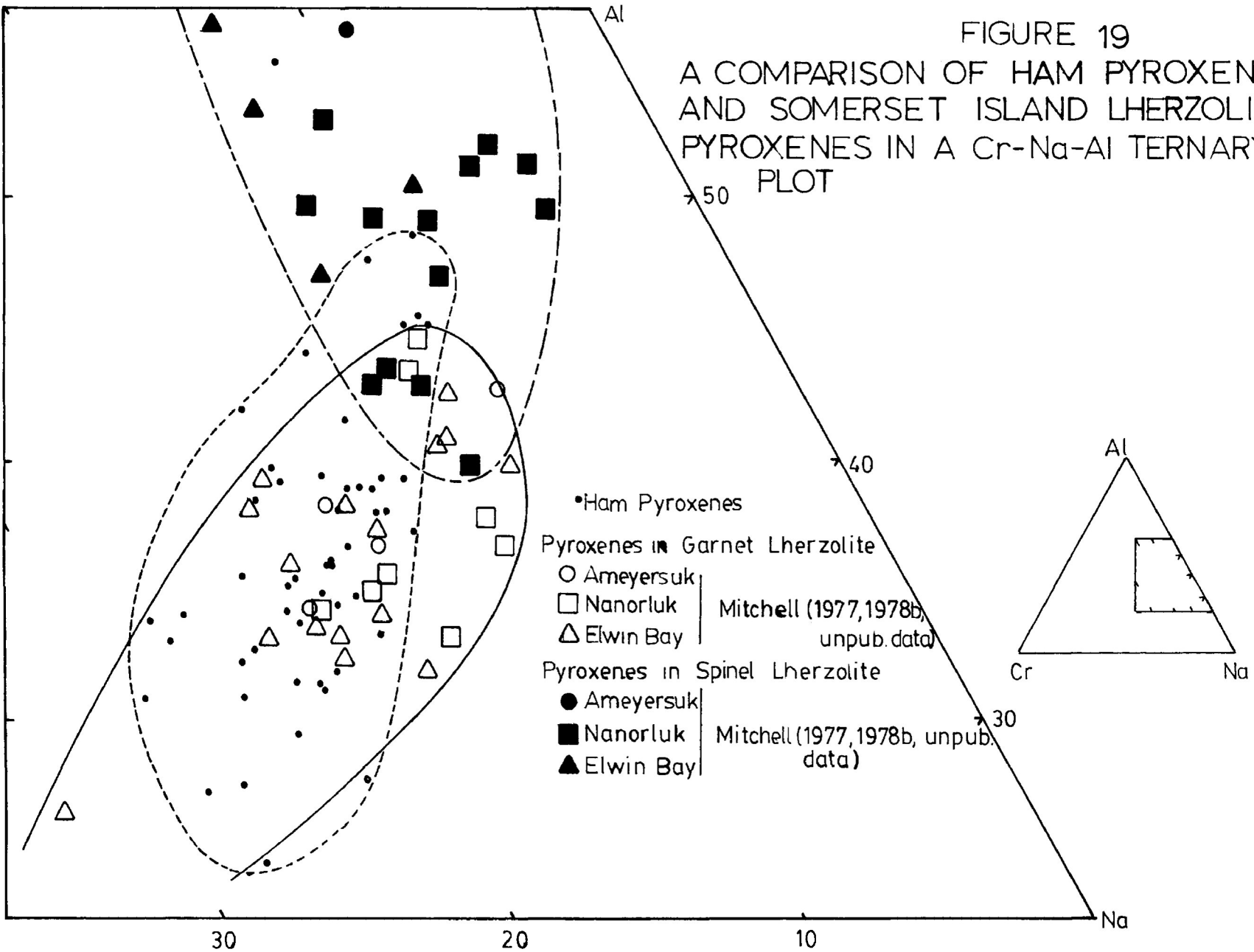


FIGURE 19

A COMPARISON OF HAM PYROXENES AND SOMERSET ISLAND LHERZOLITE PYROXENES IN A Cr-Na-Al TERNARY PLOT



Stephens and Dawson's (1977) classification of pyroxenes indicates that Ham pyroxenes fall into three groups based upon their  $TiO_2$ ,  $Al_2O_3$ ,  $Cr_2O_3$ ,  $FeO$ ,  $MgO$ ,  $CaO$  and  $Na_2O$  contents (Table 11). Ninety percent are chrome-diopsides (Group 5, 0.21-2.81 wt. %  $Cr_2O_3$ ) including the two clinopyroxenes in Ham garnet-lherzolite xenoliths. Two grains are transitional between chrome-diopside and ureyitic-diopside (Group 6) and two grains are ureyitic-diopsides (Group 6, 1.72-6.15 wt. %  $Cr_2O_3$ ). Two grains are diopsides (Group 2, 0.13 to 0.99 wt. %  $Cr_2O_3$ ).

#### Comparison with other Somerset Island Pyroxenes

A comparison of Table 12 and Table 13 and Figures 18, 19 and 20 demonstrate the major and minor element similarity between Ham pyroxenes and pyroxenes in mantle-derived garnet lherzolite xenoliths from the Ham diatrema and other Somerset Island kimberlites (Mitchell 1977, 1978b). Figures 18 and 20 demonstrate that Ham pyroxenes may be distinguished from pyroxenes in spinel lherzolite xenoliths based on Ca, Cr, Al and Na contents; the latter pyroxenes having greater Ca and Al and less Cr and Na.

Table 14 and Figure 20 indicate that Ham pyroxenes may be distinguished chemically from groundmass

Table 14  
A Comparison of Ham Pyroxenes with Pyroxene Megacrysts and Groundmass  
Pyroxenes from North American and South African Kimberlite

	Ham Kimberlite	Monastery Mine <sup>1</sup> Megacrysts	Monastery Mine <sup>1</sup> Megacryst with Garnet	Premier Mine <sup>2</sup>	Schuller Pipe <sup>3</sup> Groundmass Pyroxene	Prairie Creek <sup>4</sup>
Fe/Fe+Mg						
Range	0.04-0.10	0.12-0.17	0.14-0.16	0.08-0.18	0.20-0.34	0.02-0.12
Mean	0.07	0.15	0.15	0.13	0.27	0.07
Ca/Ca+Mg						
Range	0.39-0.50	0.32-0.42	0.41-0.45	0.52-0.58	0.58-0.74	0.42-0.51
Mean	0.43	0.37	0.44	0.56	0.63	0.49
Cr/Cr+Al						
Range	0.02-0.59	0.01-0.09	0.23-0.41	0.03-0.92	0.09-0.18	0.03-1.00
Mean	0.35	0.05	0.32	0.57	0.26	0.65

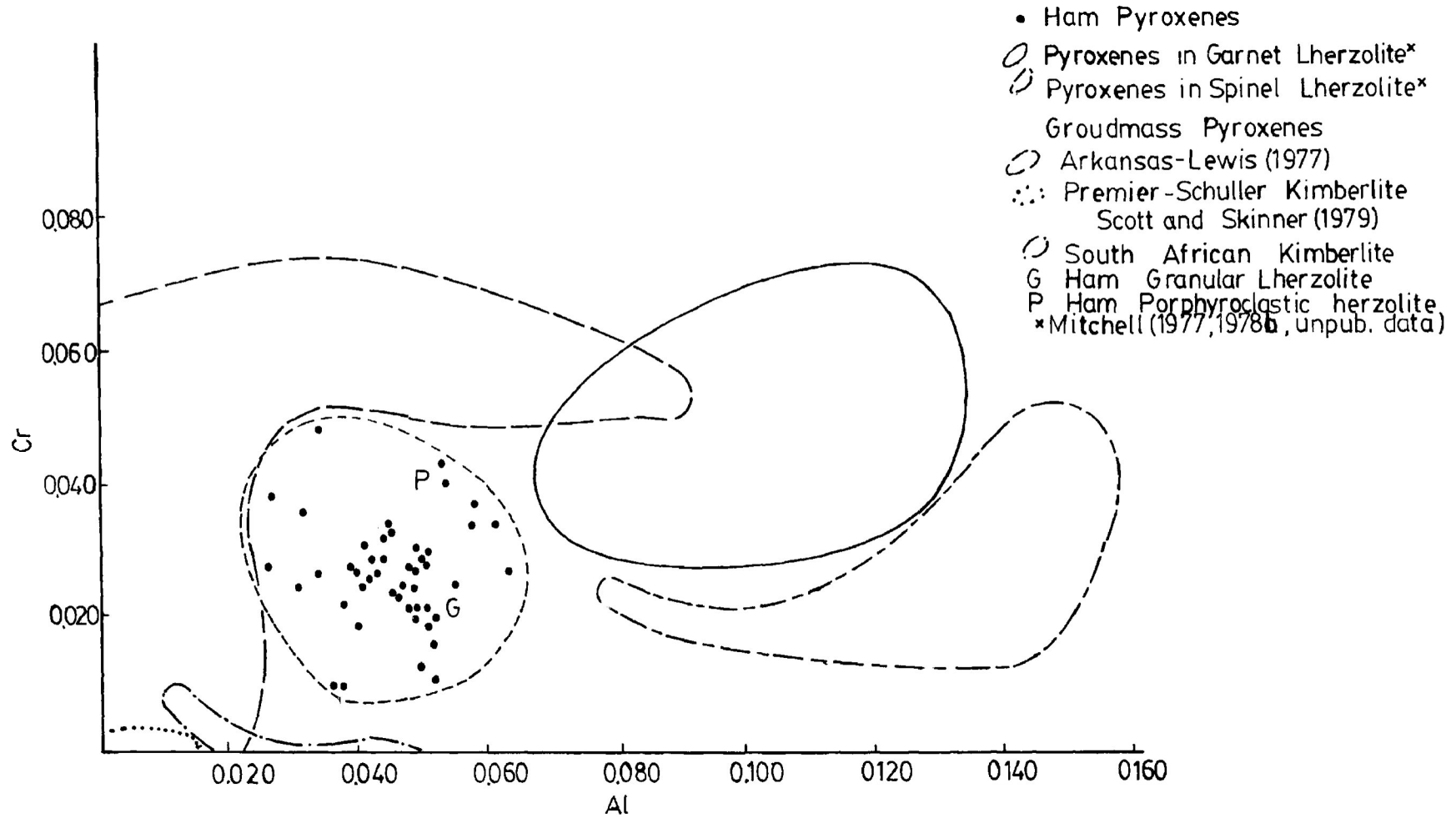
1 Gurney, Jacob and Dawson (1979)

2-3 Scott and Skinner (1979)

4 Lewis (1977)

FIGURE 20

A COMPARISON OF HAM PYROXENES AND PYROXENES FROM LHERZOLITE AND GROUNDMASS PYROXENES IN THE Al vs Cr VARIATION DIAGRAM

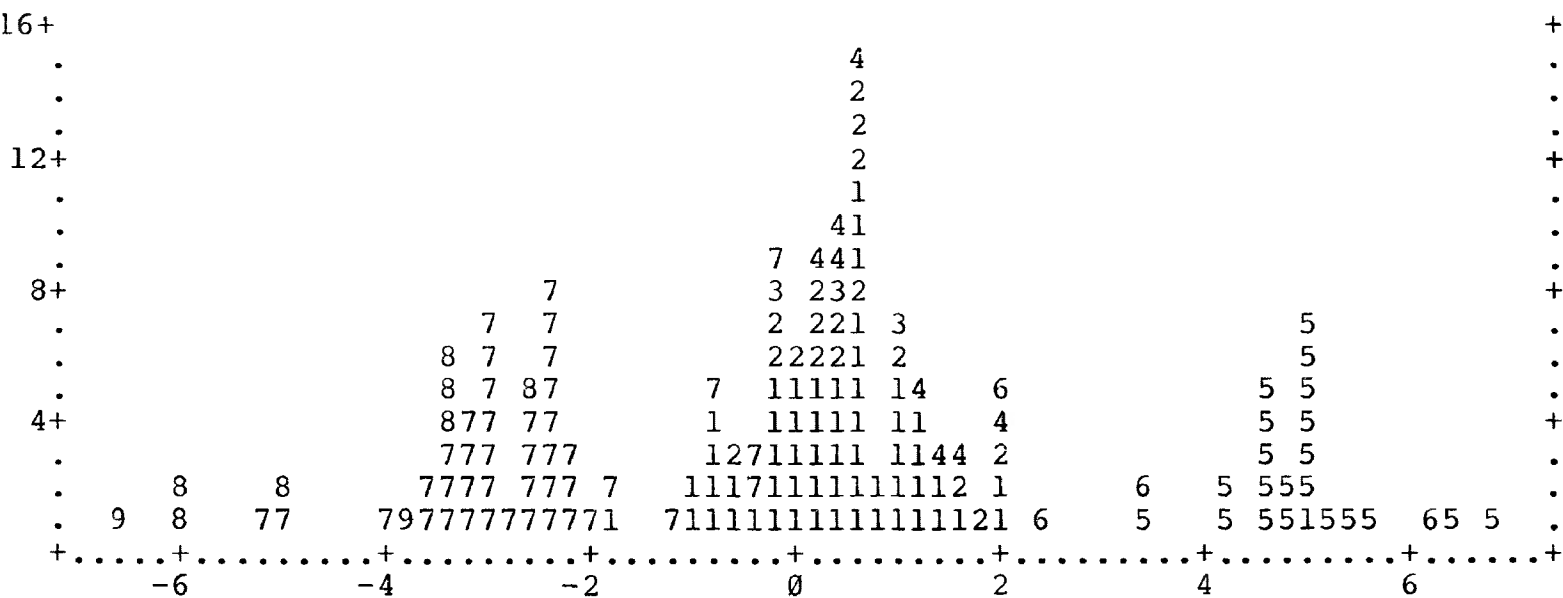


pyroxenes (Scott and Skinner 1979, Lewis 1980) on the basis of major and minor element contents. Groundmass pyroxenes have higher  $TiO_2$  and  $CaO$  contents and lower  $Cr_2O_3$ ,  $Al_2O_3$  and  $Na_2O$  contents. This is reflected in their higher  $Ca/Ca+Mg$  and  $Cr/Cr+Al$  ratios.  $Fe/Fe+Mg$  ratios are variable; those from the Premier Mine and Schuller Pipe (Scott and Skinner 1979) being greater than the  $Fe/Fe+Mg$  ratios of Arkansas groundmass pyroxenes or Ham pyroxenes.

Inspection of Table 14 indicates that Ham pyroxenes are chemically distinct from pyroxene megacrysts and pyroxene megacrysts with garnet (Nixon and Boyd 1973a, discrete nodule suite). Ham pyroxenes are characterized by lower  $Fe/Fe+Mg$  ratios and a broader range of  $Cr/Cr+Al$  ratios than those exhibited by pyroxene megacrysts.  $Ca/Ca+Mg$  ratios are similar.

Inspection of Figure 21 and Table 15 reveal that multiple discriminant analysis (see Chapter 4) may be used to distinguish between pyroxenes from garnet lherzolite xenoliths, spinel lherzolite xenoliths and in the kimberlite groundmass. Table 15 indicates that pyroxenes from garnet lherzolite may be distinguished from pyroxenes from spinel lherzolite and the kimberlite groundmass based on  $TiO_2$ ,  $Al_2O_3$  and  $Na_2O$  and  $FeO$ ,  $MgO$  and  $NiO$ , respectively. Pyroxene from spinel lherzolite

FIGURE 21  
 CANONICAL DISCRMINANT FUNCTIONS AT GROUP CENTROIDS FOR HAM PYROXENES  
 AND PYROXENES FROM GARNET AND SPINEL LHERZOLITE AND THE GROUNDMASS



GROUP CENTROIDS  
 HAM PYROXENES DISCRM. FUNCT.  
 GROUP 1 0.43620

GARNET LHZER. PYX.  
 GROUP 2 0.53348  
 GROUP 3 0.38030  
 GROUP 4 1.00264

GROUP CENTROIDS  
 SPINEL LHERZ. PYX. DISCRM. FUNCT.  
 GROUP 5 4.94671  
 GROUP 6 3.43077

GROUNDMASS PYX.  
 GROUP 7 -2.65425  
 GROUP 8 -4.31482  
 GROUP 9 -6.30642

Table 15  
 Summary Table of Wilks' Lambda and F-ratios for Ham  
 Pyroxenes, Pyroxenes from Lherzolite Xenoliths and  
 Groundmass Pyroxenes

VARIABLE	WILKS' LAMBDA	F RATIO	SIGNIFICANCE	BETWEEN	GROUPS
TiO <sub>2</sub>	0.64392	38.157	0.0000	1	2
Al <sub>2</sub> O <sub>3</sub>	0.19558	283.790	0.0000	1	2
Cr <sub>2</sub> O <sub>3</sub>	0.57269	51.484	0.0000	2	3
FeO	0.48435	73.459	0.0000	1	3
MgO	0.65627	36.140	0.0000	1	3
CaO	0.33400	137.590	0.0000	2	3
Na <sub>2</sub> O	0.45215	83.603	0.0000	1	2
NiO	0.78865	18.491	0.0000	1	3

Group 1 Pyroxenes from garnet lherzolite xenoliths  
 Group 2 Pyroxenes from spinel lherzolite xenoliths  
 Group 3 Groundmass pyroxenes

and groundmass pyroxenes may be distinguished by their  $\text{Cr}_2\text{O}_3$  and  $\text{CaO}$  contents.

#### CONCLUSIONS

In conclusion, Ham chrome-diopsides are compositionally similar to chrome-diopside from Ham and other Somerset Island garnet lherzolite xenoliths, and are undoubtedly derived by the fragmentation of such xenoliths during kimberlite intrusion.

#### PYROXENE GEOTHERMOMETRY

Pyroxene solvus geothermometry can be used to estimate temperatures of equilibration for co-existing pyroxenes from Ham garnet lherzolite xenoliths. Two xenoliths (Table 12), Ham 02, a granular garnet lherzolite xenolith and Ham 14, a mosaic, porphyroclastic garnet lherzolite xenolith were chosen. Mitchell (1977) indicates that textural and mineralogical variations between xenoliths are paralleled by variations in the compositions of the pyroxenes. These reflect variations in the temperatures of equilibration (see below), which, in conjunction with pressures of equilibration may be used to define a geotherm.

Pyroxene solvus geothermometry is based upon the temperature dependent equilibrium between coexisting orthopyroxene and clinopyroxene given in equation (1).



According to Mitchell et al. (1980) and Carswell and Gibb (1980), Wells' (1977) formulation of the pyroxene geothermometer is more realistic than methods employed by others, such as Davis and Boyd (1966), Wood and Banno (1973) and Boyd (1973). Wells (1977) demonstrates that at high temperatures, the diopside limb of the diopside-enstatite miscibility gap is slightly pressure dependent, but, that for the pressure range applicable to kimberlite (1bar to 40 kbar), the pressure effects can be ignored because experimental errors are as large or larger.

Equation (2) gives the equilibrium condition for Equation 1 where  $\Delta G_{P,T}^{\circ}$  is Gibb's free energy of formation at P and T.

$$\Delta G_{P,T}^{\circ} = RT \ln K = -RT \ln \left[ \frac{\text{cpx}}{\text{opx}} \frac{a_{\text{Mg}_2\text{Si}_2\text{O}_6}}{a_{\text{Mg}_2\text{Si}_2\text{O}_6}} \right] \quad \text{Equation (2)}$$

Wells (1977) indicates that most of the experimental data for the two-pyroxene miscibility gap can be fitted to a linear relation between  $\ln K$  and  $1/T$

using the ideal two-site mixing model of Wood and Banno (1973). The optimum solution to equation 2 is given by equation 3 (Wells 1977).

$$\ln K = -\frac{\Delta H^{\circ}}{RT} + \frac{\Delta S^{\circ}}{R} = -\frac{7341}{T} + 3.355 \quad (\text{Equation 3})$$

Using T-X data (where X is molecular proportion of iron in orthopyroxene) for 43 multicomponent, two-pyroxene assemblages, Wells (1977) calibrated the iron-dependence of  $\ln K$ , extending the original work by Wood and Banno (1973).  $\ln K$  is strongly dependent on the iron content of the pyroxenes; the Ca content of the clinopyroxene decreasing progressively with increasing iron at constant temperature and pressure (Wells 1977). Experimental data (Figures 2 and 3, Wells 1977) can be fitted to the empirical linear relation given in equation (4) (Wells 1977).

$$\ln K - 3.355 + \frac{7341}{T} = A = 2.44 \cdot X_{\text{Fe}}^{\text{opx}} \quad (\text{Equation 4})$$

$$\text{where } X_{\text{Fe}}^{\text{opx}} = \frac{\text{Fe}^{2+}}{\text{Fe}^{2+} + \text{Mg}^{2+}}$$

This equation can be rearranged to give an expression for temperature (Wells 1977), equation (5).

$$T = \frac{7341}{3.355 + 2.44 \cdot X_{\text{Fe}}^{\text{opx}} - \ln K} \quad (\text{Equation 5})$$

$$\text{where } \ln K = \frac{a_{\text{Mg}_2\text{Si}_2\text{O}_6}^{\text{cpx}}}{a_{\text{Mg}_2\text{Si}_2\text{O}_6}^{\text{opx}}}$$

where  $a_X^Y$  is the activity of component X in phase y,

$$a_{\text{Mg}_2\text{Si}_2\text{O}_6}^{\text{cpx}} = \left[ \frac{\text{Mg}_{m_2}}{(\text{Ca Mg Fe})_{m_2}} \right] \cdot \left[ \frac{\text{Mg}_{m_1}}{(\text{Fe}^{3+} \text{Al Cr Mg Fe}^{2+} \text{Ti})_{m_1}} \right]$$

and  $a_{\text{Mg}_2\text{Si}_2\text{O}_6}^{\text{opx}} = \left[ \frac{\text{Mg}_{m_2}}{(\text{Ca Mg Fe})_{m_2}} \right] \cdot \left[ \frac{\text{Mg}_{m_1}}{(\text{Fe}^{3+} \text{Al Cr Mg Fe}^{2+} \text{Ti})_{m_1}} \right]$

Experimental data by O'Hara and Schairer (1963), Boyd (1970) and Akella (1976) indicate that substitution of Al for Mg and Si on M1 and tetrahedral sites, respectively, in clinopyroxene, with complete coupling between octahedral and tetrahedral Al to maintain charge balance, considerably reduces the activity of the  $\text{Mg}_2\text{Si}_2\text{O}_6$  component in ortho- and clinopyroxene. Recent experimental data by Wells (1977) indicates that for  $\text{Al}_2\text{O}_3$  contents up to 12 weight percent that  $\log \left( \frac{a_{\text{Mg}_2\text{Si}_2\text{O}_6}^{\text{cpx}}}{a_{\text{Mg}_2\text{Si}_2\text{O}_6}^{\text{opx}}} \right)$  is not consistently related to the amount of Al in pyroxenes.

Wells' (1977) Table 1 shows that experimental equilibration temperatures are very similar to those calculated using equation 5 and that 90 percent of the calculated temperatures lay within  $70^\circ\text{C}$  of the experimental temperatures.

In summary, Wells' (1977) equation 5 produces results accurate to  $\pm 70^\circ\text{C}$  over the temperature range

785 to 1500°C and compositional ranges of  $X_{\text{Fe}}^{\text{opx}} = 0.0$  to 1.0 and  $\text{Al}_2\text{O}_3^{\text{cpx}} = 0.00$  to 10.0 weight percent.

### GEOBAROMETRY

Mitchell et al. (1980) reviewed current garnet-enstatite geobarometry methods which are based upon the experimental work of MacGregor (1974). She showed that the solubility of the potential garnet molecule in pyroxene coexisting with garnet decreases with increasing pressure for a given temperature. Therefore, if a temperature estimate can be obtained, pressure may be calculated from the  $\text{Al}_2\text{O}_3$  content of the orthopyroxene. The accuracy of the method is dependent upon the method used to generate a temperature estimate and the presence of Na, Cr, Fe and Ca in the assemblage. These will reduce the activity of Al in the pyroxenes and lead to an overestimation of pressure. The effectiveness of Wood's (1977) semi-empirical correction for Cr is inconsistent, but in general, it reduces calculated pressures relative to those calculated without the correction. In conjunction with solvus temperatures formulated using Mori and Green's (1978) method, Mitchell et al. (1980) contend that calculated pressures for Cr-rich ( $\text{Cr}/\text{Cr}+\text{Al} = 12.4 - 24.6$ ) Pipe 200

assemblages, without the Wood (1974) Cr correction, are marginally superior to those calculated using it. However, they conclude that there is no way as yet to assess the validity of the Cr-correction in xenolith assemblages with widely varying Cr contents.

#### Temperature and Pressure Estimate for Ham Pyroxenes

Temperature and pressure estimates for Ham pyroxenes given in Table 12 show that xenolith 14, a mosaic, porphyroclastic garnet lherzolite equilibrated at higher temperatures and pressures than xenolith 02, a granular lherzolite. This contrast is consistent for perturbed mantle geotherms defined by pressure-temperature estimates using granular, porphyroclastic and fluidal textured xenoliths by Mitchell (1977) and Hearne and Boyd (1975) for North American geotherms, although the paucity of data from the Ham kimberlite precludes any definite conclusions.

#### CONCLUSIONS

Green clinopyroxene in heavy mineral concentrates is chemically similar to clinopyroxene in Ham and other Somerset Island garnet lherzolite xenoliths and was probably liberated from such xenoliths during the

fluidized intrusion of the Ham kimberlite. Temperatures and pressures of equilibration correspond to a depth of origin between 110 (36 kbs) and 120 km (39 kb) and a temperature range of 1031 to 1146°C.

CHAPTER 6  
HAM SPINELS

The Ham diatrema and dyke contain two distinct spinel assemblages which may be subdivided according to their crystal habit into pre-fluidization and post-fluidization types. Spinel which formed prior to the fluidized intrusion of the kimberlite are anhedral and rounded. Those spinels which crystallized after the intrusion are generally euhedral and may form euhedral mantles upon cores of pre-fluidization types.

Petrographic examination indicates that the Ham diatrema and dyke contain three textural varieties of spinel;

- 1) Pre-fluidization, aluminous magnesian chromite (AM-chromite),
  - 2) Post-fluidization, titan magnesian aluminous chromite (titan-MA-chromite),
- and 3) Post-fluidization, atoll spinels.

In addition, the Ham dyke contains a texturally distinct spinel variety;

- 4) Post-fluidization, magnesian ulvöspinel ulvöspinel magnetite (Mu-magnetite).

Aluminous Magnesian Chromite (AM-chromite)

AM-chromite occurs as discrete, rounded and corroded, anhedral, transparent, reddish-orange crystals

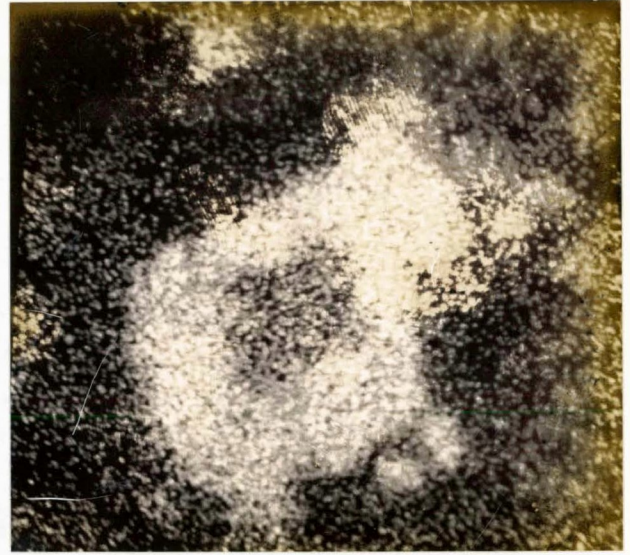
up to 0.35 mm in diameter. Individual crystals are commonly overgrown by a blocky, euhedral mantle of perovskite or form the cores of a complexly zoned spinel as illustrated in Plates 6a to 6f. Plate 6a illustrates the sub-rounded habit of the Cr-rich AM-chromite core. This is overgrown by an Fe-Ti-rich euhedral mantle of titan-MA-chromite (Plates 6b to 6e).

Rarely, large (1.6 mm diameter), euhedral, transparent, reddish-orange AM-chromite is poikilitically enclosed in rounded pre-fluidization olivine crystals. The presence of these large, euhedral spinel crystals and the morphology of discrete, AM-chromite crystals suggests that this phase crystallized early in the evolution of the magma. The rounded, anhedral to subhedral habit of individual crystals indicates a pre-fluidization origin for this spinel, and rounded, cusp-shaped grains indicate that once larger crystals were broken and rounded during intrusion. Spinels of all three habits are similar in composition (see below). The chemical similarity and the pre-fluidization nature of the spinel grains and the presence of euhedral AM-chromite in pre-fluidization olivine suggests a deep-seated origin for AM-chromite. This conclusion agrees with that of Mitchell and Clarke (1976) who suggest that AM-chromites found as inclusions in pyrope were part of a high pressure

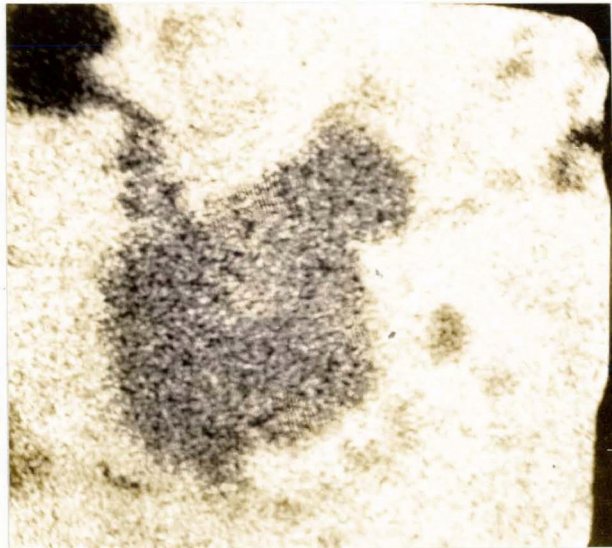
X-ray Scanning Photograph of the Major  
Element Distribution in Ham Spinels



6a. Chromium



6b. Iron



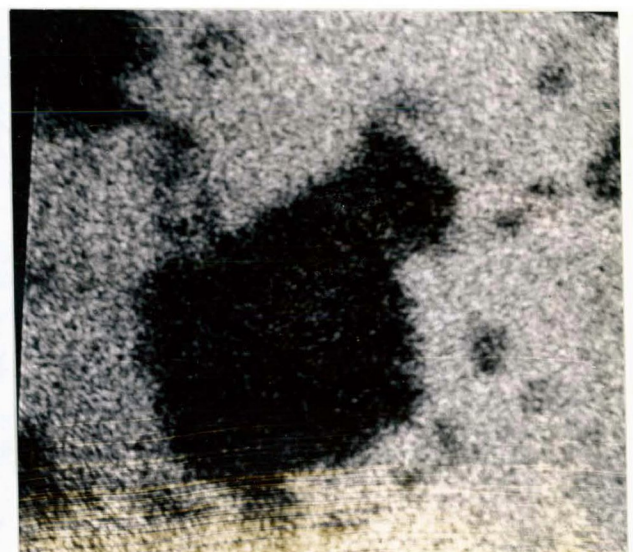
6c. Magnesium



6d. Aluminum



6e. Titanium



6f. Silica

X650

phenocrystal spinel suite formed in the mantle prior to the fluidized intrusion of the kimberlite.

#### Titan Magnesian Aluminous Chromite (Titan-MA-Chromite)

Titan-MA-chromite occurs as discrete, partially resorbed, subhedral to euhedral, opaque groundmass crystals. Crystals within the Ham dyke range up to 0.30 mm in diameter while those in the Ham diatrema range up to 0.07 mm in diameter. Titan-MA-chromite is commonly overgrown by a highly resorbed, anhedral to euhedral opaque mantle of MU-magnetite or a spongy, corroded, opaque mantle of rutile-free, Ti-Al-Cr-poor magnetite. Perovskite occurs as blocky euhedral overgrowths on discrete crystals or as tiny euhedral crystals distributed about the periphery of the spinel grains.

#### Atoll Spinels

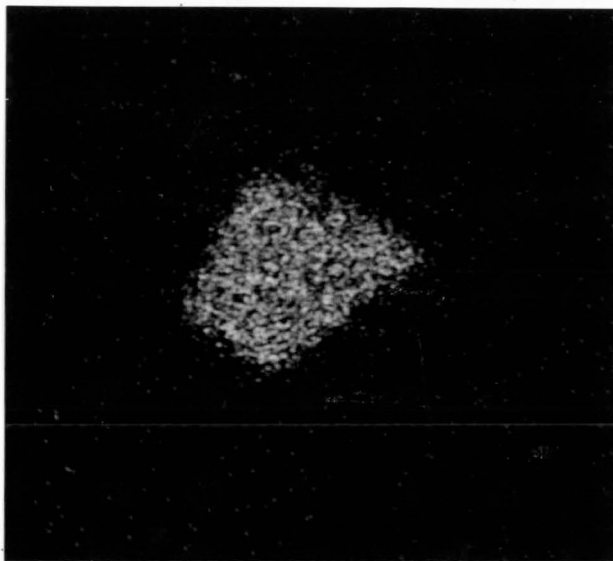
Atoll spinels (Mitchell and Clarke 1976) are developed on rounded cores of AM-chromite or subhedral to euhedral cores of titan-MA-chromite. Atoll spinels developed upon cores of AM-chromite are mantled by a thin (<0.005 mm thick), opaque, corroded subhedral overgrowth of titan-MA-chromite, followed by a thin (<0.005 mm thick) zone of silicate, essentially serpentine and carbonate and an outer, highly corroded, anhedral, partially resorbed mantle of rutile-free, Ti-Al-Cr-poor

magnetite. The habit of the magnetite parallels that of the titan-MA-chromite mantle and is commonly intergrown with tiny perovskite crystals. Atoll spinels developed on titan-MA-chromite cores demonstrate a similar distribution of mineral phases from core to rim.

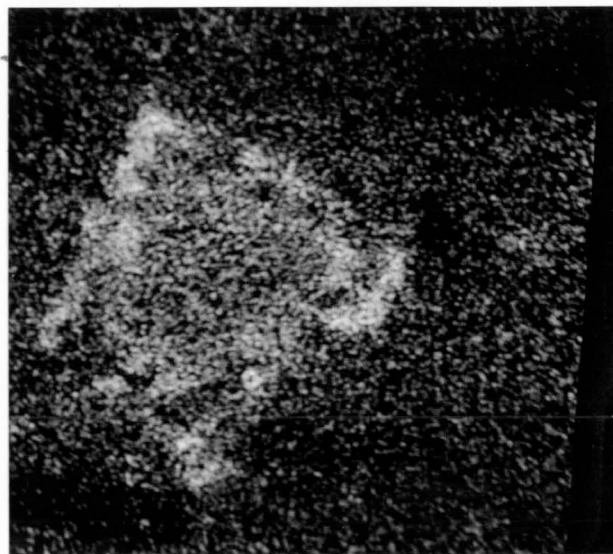
Plates 7a to 7f and 8a to 8f are x-ray scanning photographs of atoll spinels developed on AM-chromite and titan-MA-chromite cores, respectively. These plates illustrate the major element distribution within a single spinel crystal. Plates 7a and 7d illustrate the distribution of Cr and Al within the rounded AM-chromite core. Plate 7b illustrates the distribution of iron within this complexly zoned spinel. Fe is concentrated in the inner, corroded, subhedral titan-MA-chromite mantle and in the outer, corroded, anhedral, partially resorbed magnetite mantle. Plates 7c and 7f illustrate the distribution of Mg and Si within the zone of silicate, essentially serpentine and carbonate between the two spinel mantles and the groundmass.

The atoll spinel characterized by a core of titan-MA-chromite is illustrated in Plates 8a to 8f. The euhedral core spinel is characterized by a homogenous distribution of chromium (Plate 8a) and a progressive enrichment in iron (Plate 8b) toward the crystal margin.

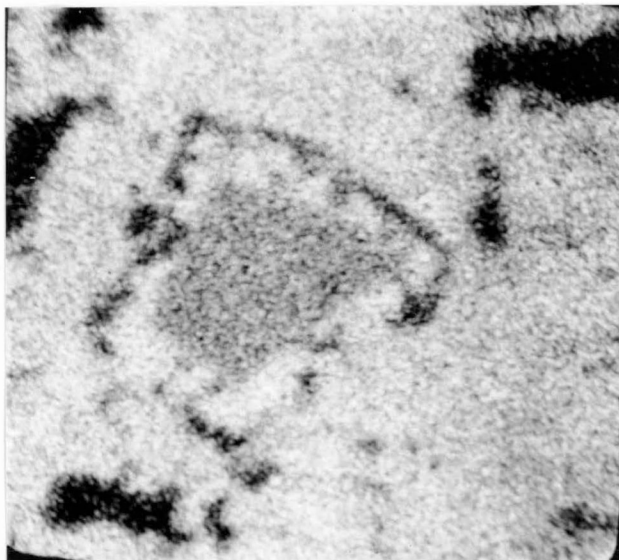
100  
Plate 7  
X-ray Scanning Photograph of the Major  
Element Distribution in Ham Atoll Spinels



7a. Chromium



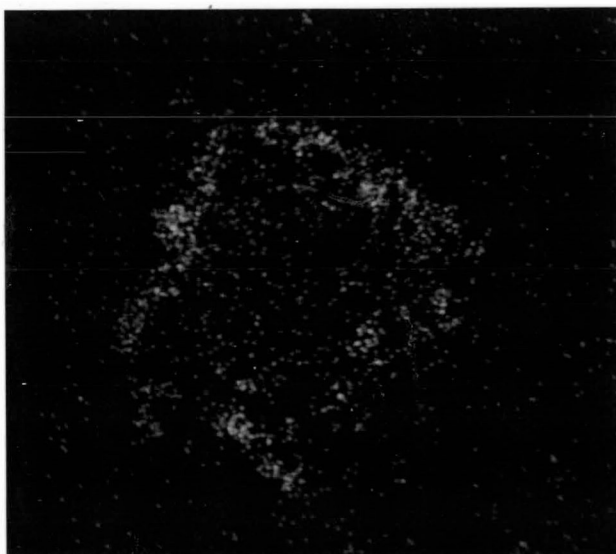
7b. Iron



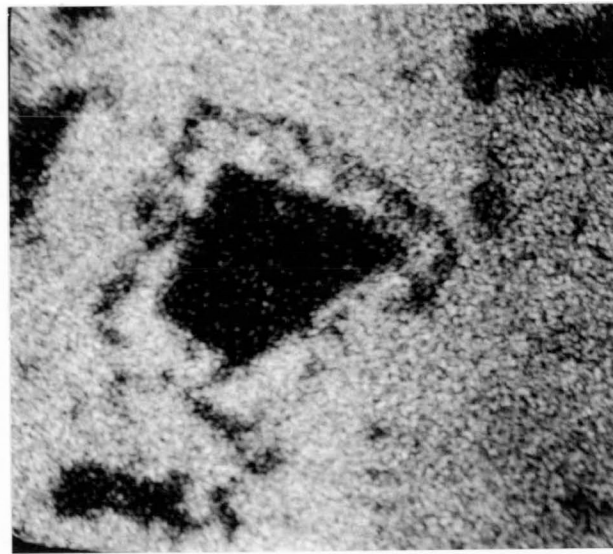
7c. Magnesium



7d. Aluminum



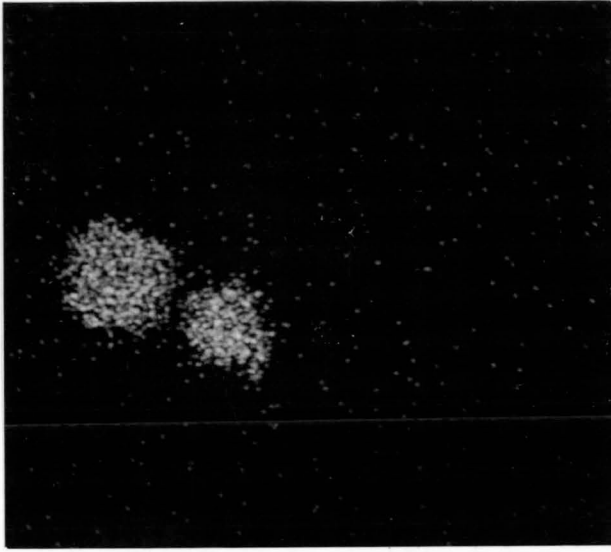
7e. Titanium



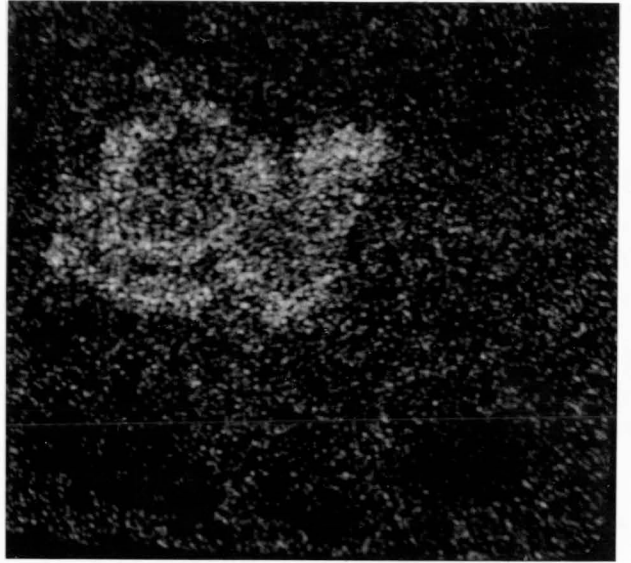
7f. Silica

X450

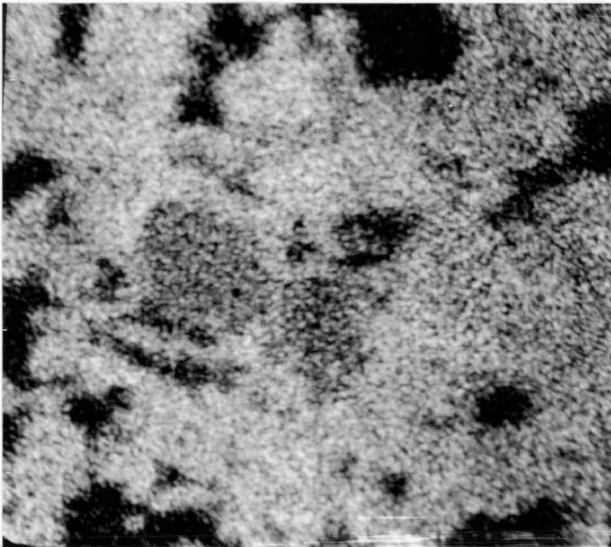
107  
Plate 8  
X-ray Scanning Photograph of the Major  
Element Distribution in Ham Atoll Spinels



8a. Chromium



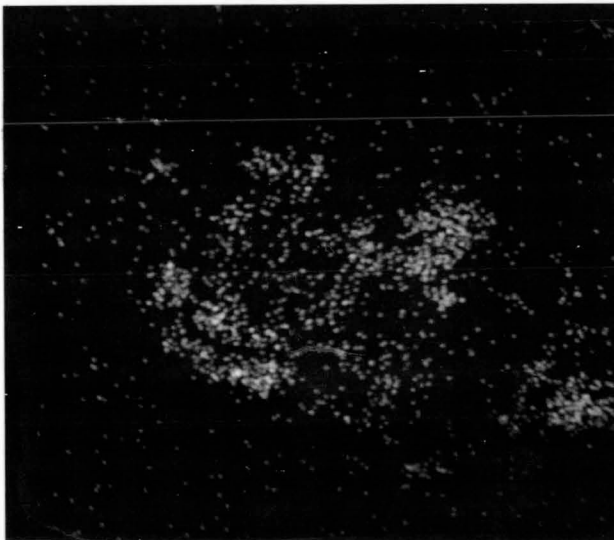
8b. Iron



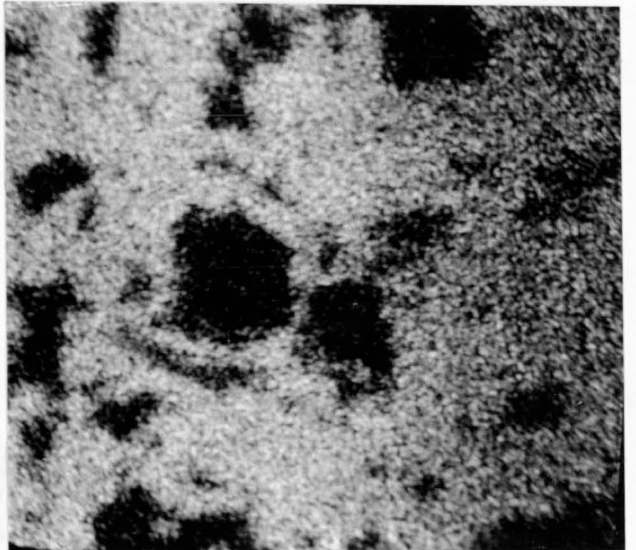
8c. Magnesium



8d. Aluminum



8e. Titanium



8f. Silica

X450

Alumina (Plate 8d) demonstrates a complex zonation pattern within the titan-MA-chromite core. This core spinel is separated from the outer, corroded, subhedral mantle of Fe-Ti-rich MU-magnetite (Plates 8b and 8e) by a corroded, spongy, Mg-Si-rich zone of silicate (Plates 8c and 8f). This silicate zone is essentially serpentine and carbonate.

Magnesian Ulvöspinel Ulvöspinel Magnetite (MU-Magnetite)

MU-magnetite occurs as opaque, partially resorbed, subhedral to euhedral groundmass crystals up to 0.10 mm in diameter and as partially resorbed, subhedral to euhedral mantles on AM-chromite or titan-MA-chromite cores. Individual crystals may be mantled by a blocky, euhedral overgrowth of perovskite or a thin, spongy, partially resorbed mantle of rutile-free, Ti-Al-Cr-poor magnetite.

CHEMISTRY

Representative analyses of Ham spinels are given in Table 16. Ferric iron was calculated by Carmichael's (1967) method. The major element compositional variation is illustrated using the "reduced" spinel prism (Haggerty 1973) in Figures 22a to 22d. This graphical means of depicting spinel compositional variation

(Johnston prism) was used by Irvine (1965) to study the value of chrome spinel as a petrogenetic indicator. Haggerty's (1972) study of Lunar spinels required modification of the Johnston prism to take into account the highly reducing conditions under which Lunar spinels formed. The  $\text{Fe}^{+3}$ -bearing spinels,  $\text{MgFe}_2\text{O}_4$  (magnesian ferrite) and  $\text{Fe}_3\text{O}_4$  (magnetite) placed at the "oxidized" prism apex were replaced by  $\text{Mg}_2\text{TiO}_4$  (magnesian ulvöspinel) and  $\text{Fe}_2\text{TiO}_4$  (ulvöspinel). This modified "reduced" spinel prism in which total iron is calculated as FeO is useful for plotting the chemical variation of kimberlite spinels. These spinels are believed to have formed under relatively reducing conditions (Haggerty 1973, Mitchell 1973). Utilization of the "reduced" spinel prism does not illustrate possible variations in the  $\text{MgFe}_2\text{O}_4$  and  $\text{Fe}_3\text{O}_4$  contents of kimberlite spinels, however, all elements which were determined are plotted. Spinel compositions were plotted by the methods of Irvine (1965).

The spinel prism is based upon the extensive solid-solution between spinel end-members. The base of the prism is defined by solid-solutions involving  $\text{FeCr}_2\text{O}_4$  (chromite),  $\text{MgCr}_2\text{O}_4$  (picrochromite),  $\text{FeAl}_2\text{O}_4$  (hercynite) and  $\text{MgAl}_2\text{O}_4$  (spinel). Chemical variation is defined by changes in the Cr/Cr+Al and Fe/Fe+Mg

ratios. The apices of the prism are defined by solid-solutions between  $\text{Mg}_2\text{TiO}_4$  (magnesian ulvöspinel) and  $\text{Fe}_2\text{TiO}_4$  (ulvöspinel). Chemical variation between these two end-members is defined by changes in the Fe/Fe+Mg ratio. Chemical variation between the base and apex of the prism is defined by changes in the Ti/Ti+Cr+Al ratio.

Figure 23, a ternary section through the "reduced" spinel prism with coordinates  $\text{Mg}_2\text{TiO}_4$ - $\text{MgAl}_2\text{O}_4$ - $\text{MgCr}_2\text{O}_4$ , distinguishes between highly aluminous and alumina deficient kimberlite spinels as well as illustrating the spinel evolutionary trend toward magnesian-ulvöspinel-ulvöspinel-magnetite. Figure 25 is a univariate frequency distribution plot of spinel crystal cores and rims of specific  $\text{TiO}_2$  contents. This figure defines the compositional limits of the various spinel varieties based on  $\text{TiO}_2$  content and grain textures. Figure 26 is a compositional variation plot of continuously zoned magnesian ulvöspinel ulvöspinel magnetite crystals and mantles upon pre-fluidization cores of AM-chromite and post-fluidization cores of titan-MA-chromite.

Spinel from the Ham diatreme vary from Al-rich, aluminous magnesium chromites to titan magnesian aluminous chromites. These assemblages reflect a concomitant increase in the Cr/Cr+Al and Fe/Fe+Mg ratio and a chemical evolution from a Mg-Al-rich spinel to a

Ti-bearing Fe-Cr-rich spinel. Spinel from the Ham dyke vary from aluminous magnesium chromites to titan magnesian aluminous chromites to magnesian ulvöspinel ulvöspinel magnetite.

The chemical evolutionary path of the Ham dyke spinels reflects a limited increase in the Cr/Cr+Al ratio at an approximately constant Fe/Fe+Mg ratio. The Ham dyke spinels reflect a chemical evolution from Mg-Al-rich spinels to Ti-bearing, Fe-Cr-rich spinels to Fe-Ti-rich spinels.

#### Aluminous Magnesian Chromite (AM-chromite)

Representative analysis of AM-chromite are given in Table 16, analyses 1 to 8. The compositional variation is illustrated in Figures 22a to 22d and Figures 25 and 26 and Table 17a. Cr/Cr+Al ratios for AM-chromite from Ham diatreme Type 1A, 1B and Type 2 kimberlite and Ham dyke Type 1A kimberlite range from 0.18 to 0.83, 0.68 to 0.81, 0.57-0.78 and from 0.57 to 0.79, respectively. Fe/Fe+Mg ratios range from 0.22 to 0.46, 0.32 to 0.44, 0.34 to 0.45 and from 0.32 to 0.49 in diatreme Type 1A, 1B and Type 2 kimberlite and in Ham dyke Type 1A kimberlite. TiO<sub>2</sub> contents in this compositionally homogenous phase range up to approximately 2.00 weight percent. The

TABLE 16  
Representative Analyses of Ham Spinels

ANAL.	1	2	3	4	5	6	7	8	9	10	11
TiO <sub>2</sub>	0.07	0.09	0.13	0.16	0.16	0.50	0.50	0.78	2.40	2.42	2.52
Al <sub>2</sub> O <sub>3</sub>	16.66	18.30	34.57	34.71	33.91	33.84	12.38	12.29	16.75	16.14	14.28
Cr <sub>2</sub> O <sub>3</sub>	53.04	51.11	30.85	34.29	35.06	30.75	56.21	55.73	43.30	45.54	46.54
FeO	15.16	14.30	18.72	13.15	13.29	18.38	15.54	18.00	18.80	19.12	20.39
MnO	0.52	0.42	0.28	0.27	0.30	0.26	0.42	0.35	0.37	0.39	0.49
MgO	13.55	14.82	15.02	16.73	16.29	16.53	14.28	13.22	15.57	15.27	14.74
TOTAL	99.00	99.04	99.57	99.31	99.01	100.26	99.33	100.37	97.19	98.88	99.96
Recalculated Analysis											
Fe <sub>2</sub> O <sub>3</sub>	2.15	2.90	4.88	1.69	1.38	6.67	3.87	4.08	7.77	7.02	7.82
FeO	13.23	11.69	14.33	11.63	12.05	12.38	12.06	14.33	14.10	12.80	13.35
TOTAL	99.22	99.33	100.06	99.48	99.15	100.95	99.72	100.78	100.26	99.58	99.74
MgAl <sub>2</sub> O <sub>4</sub>	30.6	32.9	57.4	58.2	57.4	54.9	22.7	22.3	25.4	27.8	24.7
Mg <sub>2</sub> TiO <sub>4</sub>	0.2	0.3	0.4	0.5	0.5	1.5	1.7	2.7	6.3	7.9	8.3
Mn <sub>2</sub> TiO <sub>4</sub>	0.0	0.0	0.0	0.0	0.0	0.0	0.0	0.0	0.0	0.0	0.0
Fe <sub>2</sub> TiO <sub>4</sub>	0.0	0.0	0.0	0.0	0.0	0.0	0.0	0.0	0.0	0.0	0.0
MgCr <sub>2</sub> O <sub>4</sub>	32.0	34.1	5.1	12.0	11.6	10.8	41.0	34.7	24.7	28.0	28.6
MnCr <sub>2</sub> O <sub>4</sub>	1.3	1.0	0.6	0.6	0.7	0.6	1.1	0.9	1.4	0.9	1.2
FeCr <sub>2</sub> O <sub>4</sub>	31.9	26.5	28.6	25.8	27.4	21.6	26.7	32.1	24.6	23.5	24.1
Fe <sub>3</sub> O <sub>4</sub>	3.7	5.0	7.7	2.7	2.2	10.6	6.7	7.1	17.4	11.5	12.9

ANALYSIS 1-8 Aluminous-Magnesian Chromite  
 9-18 Titaniferous-Aluminous-Magnesian Chromite  
 19-22 Titaniferous-Magnesian Chromite (TMC)  
 23-36 Magnesian-Ulvöspinel-Ulvöspinel Magnetite  
 37-38 Magnetite

ANAL	12	13	14	15	16	17	18	19	20	21	22
TiO <sub>2</sub>	2.69	3.08	3.26	3.83	3.83	3.93	4.96	3.02	5.05	5.11	5.84
Al <sub>2</sub> O <sub>3</sub>	16.91	11.23	26.16	13.90	12.09	24.34	17.38	9.75	9.12	11.50	7.34
Cr <sub>2</sub> O <sub>3</sub>	44.39	52.25	28.97	42.98	44.61	28.50	33.68	52.67	44.82	39.98	43.88
FeO	18.95	17.66	23.30	23.59	24.87	24.87	26.13	18.73	24.79	26.99	26.24
MnO	0.37	0.34	0.33	0.41	0.45	0.28	0.42	0.38	0.59	0.52	0.57
MgO	15.71	15.00	16.70	14.55	14.43	17.09	15.99	14.44	14.50	14.54	14.22
TOTAL	99.02	99.56	98.72	99.26	100.28	99.01	98.56	98.99	98.87	98.64	98.09
Recalculated Analysis											
Fe <sub>2</sub> O <sub>3</sub>	7.10	4.88	11.58	9.58	15.38	13.07	13.31	5.67	10.77	12.77	11.66
FeO	12.56	13.27	12.88	14.97	9.23	13.11	14.16	13.63	15.10	15.50	15.75
TOTAL	99.73	100.05	99.88	100.22	102.02	100.32	99.90	99.56	99.95	99.92	99.26
MgAl <sub>2</sub> O <sub>4</sub>	28.8	19.7	29.1	23.4	18.3	38.2	27.9	17.3	15.4	19.0	12.4
Mg <sub>2</sub> TiO <sub>4</sub>	8.7	10.3	9.9	12.3	11.1	11.8	15.2	10.2	16.3	16.2	18.9
Mn <sub>2</sub> TiO <sub>4</sub>	0.0	0.0	0.0	0.0	0.0	0.0	0.0	0.0	0.0	0.0	0.0
Fe <sub>2</sub> TiO <sub>4</sub>	0.0	0.0	0.0	0.0	0.0	0.0	0.0	0.0	0.0	0.0	0.0
MgCr <sub>2</sub> O <sub>4</sub>	27.2	33.1	12.3	22.1	41.3	13.1	16.7	33.8	24.7	20.2	23.2
MnCr <sub>2</sub> O <sub>4</sub>	0.9	0.8	0.7	0.9	0.9	0.7	0.9	0.9	1.4	1.2	1.3
FeCr <sub>2</sub> O <sub>4</sub>	22.6	27.6	17.3	25.5	3.0	16.1	18.6	27.9	24.6	22.9	25.2
Fe <sub>3</sub> O <sub>4</sub>	11.6	8.2	17.7	15.4	25.2	19.1	20.4	7.1	17.4	28.2	18.8

TABLE 16 (Cont'd)

ANAL.	23	24	25	26	27	28	29	30	31	32	33
TiO <sub>2</sub>	8.45	13.03	12.47	12.58	12.92	14.21	14.31	14.46	14.48	15.02	15.11
Al <sub>2</sub> O <sub>3</sub>	8.73	8.37	7.21	8.75	8.29	7.18	7.58	8.80	7.73	7.93	8.43
Cr <sub>2</sub> O <sub>3</sub>	0.20	0.00	0.00	0.00	0.18	0.00	1.32	0.68	0.34	0.27	0.68
FeO	62.51	61.90	63.79	62.32	62.47	62.73	58.88	58.29	59.63	60.63	58.61
MnO	0.58	0.52	0.60	0.53	0.45	0.45	0.52	0.51	0.53	0.53	0.57
MgO	14.33	12.16	11.90	12.09	12.39	10.79	12.74	13.51	12.14	12.97	14.01
TOTAL	94.8	95.98	95.97	96.27	96.70	95.36	95.35	96.25	94.85	97.35	97.41
Recalculated Analysis											
Fe <sub>2</sub> O <sub>3</sub>	46.31	40.05	43.04	41.20	41.37	38.38	37.25	37.30	37.16	38.19	37.57
FeO	20.84	25.39	25.06	25.25	25.24	28.20	25.27	24.72	26.20	26.26	24.80
TOTAL	99.44	99.52	100.28	100.40	100.84	99.21	98.99	99.98	98.58	101.17	101.17
MgAl <sub>2</sub> O <sub>4</sub>	12.6	11.6	9.9	12.1	11.4	10.1	10.5	12.1	10.8	10.8	11.4
Mg <sub>2</sub> TiO <sub>4</sub>	23.3	23.2	23.7	22.6	23.7	21.2	25.8	26.1	24.1	25.4	27.4
Mn <sub>2</sub> TiO <sub>4</sub>	0.0	0.7	0.8	0.7	0.6	0.6	0.7	0.0	0.8	0.7	0.0
Fe <sub>2</sub> TiO <sub>4</sub>	0.0	10.5	8.3	9.8	9.5	16.3	11.6	11.1	13.9	12.9	0.0
MgCr <sub>2</sub> O <sub>4</sub>	0.0	0.0	0.0	0.0	0.0	0.0	0.0	0.0	0.0	0.0	0.8
MnCr <sub>2</sub> O <sub>4</sub>	0.0	0.0	0.0	0.0	0.0	0.0	0.0	0.0	0.0	0.0	10.9
FeCr <sub>2</sub> O <sub>4</sub>	0.0	0.0	0.0	0.0	0.1	0.0	1.2	0.6	0.3	0.2	0.6
Fe <sub>3</sub> O <sub>4</sub>	64.0	53.8	57.0	54.5	54.4	51.6	49.9	49.1	49.9	49.8	48.7

ANAL.	34	35	36	37	38
TiO <sub>2</sub>	15.11	15.12	15.47	0.42	0.66
Al <sub>2</sub> O <sub>3</sub>	8.43	7.61	7.63	0.32	0.37
Cr <sub>2</sub> O <sub>3</sub>	0.68	0.17	1.42	0.09	0.08
FeO	58.61	59.26	58.40	91.14	88.48
MnO	0.57	.50	0.57	0.23	0.20
MgO	14.01	12.81	13.25	2.29	3.52
TOTAL	97.41	95.47	96.74	94.49	93.31
Recalculated Analysis					
Fe <sub>2</sub> O <sub>3</sub>	36.09	37.01	36.09	67.53	65.55
FeO	25.92	25.95	25.92	30.38	29.49
TOTAL	100.81	99.17	100.35	101.26	99.87
MgAl <sub>2</sub> O <sub>4</sub>	10.4	10.5	10.4	0.4	0.5
Mg <sub>2</sub> TiO <sub>4</sub>	26.6	25.7	26.6	1.2	1.9
Mn <sub>2</sub> TiO <sub>4</sub>	0.8	0.7	0.8	0.0	0.0
Fe <sub>2</sub> TiO <sub>4</sub>	13.1	13.6	13.1	0.0	0.0
MgCr <sub>2</sub> O <sub>4</sub>	0.0	0.0	0.0	0.0	0.0
MnCr <sub>2</sub> O <sub>4</sub>	0.0	0.0	0.0	0.0	0.0
FeCr <sub>2</sub> O <sub>4</sub>	1.3	0.1	1.3	0.0	0.0
Fe <sub>3</sub> O <sub>4</sub>	47.5	49.1	47.4	98.2	97.4

FIGURE 22A  
 COMPOSITIONAL VARIATION OF HAM DYKE SPINELS IN THE "REDUCED" SPINEL PRISM

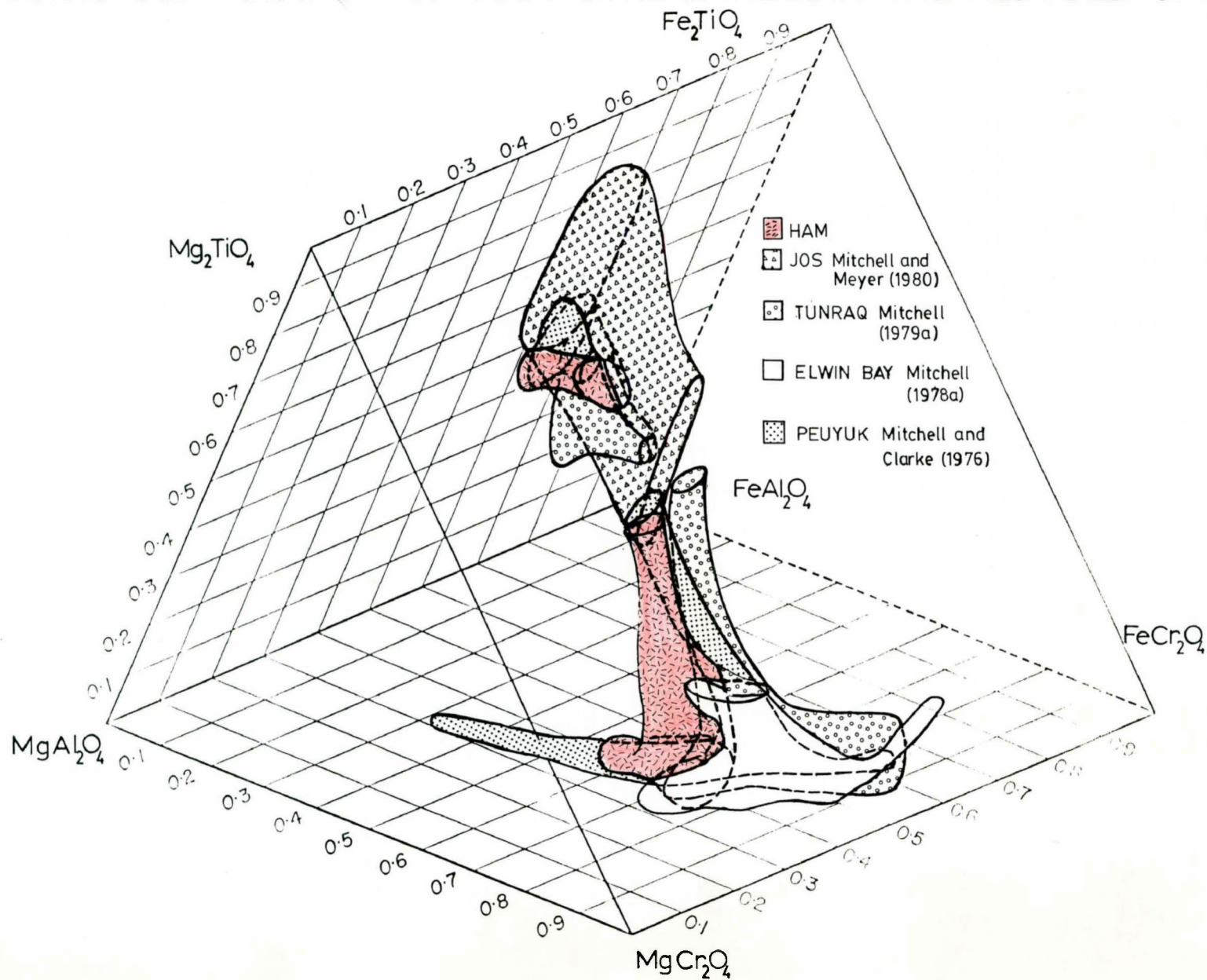


FIGURE 22B  
 COMPOSITIONAL VARIATION OF HAM DIATREME TYPE 1A KIMBERLITE SPINELS IN  
 THE "REDUCED" SPINEL PRISM

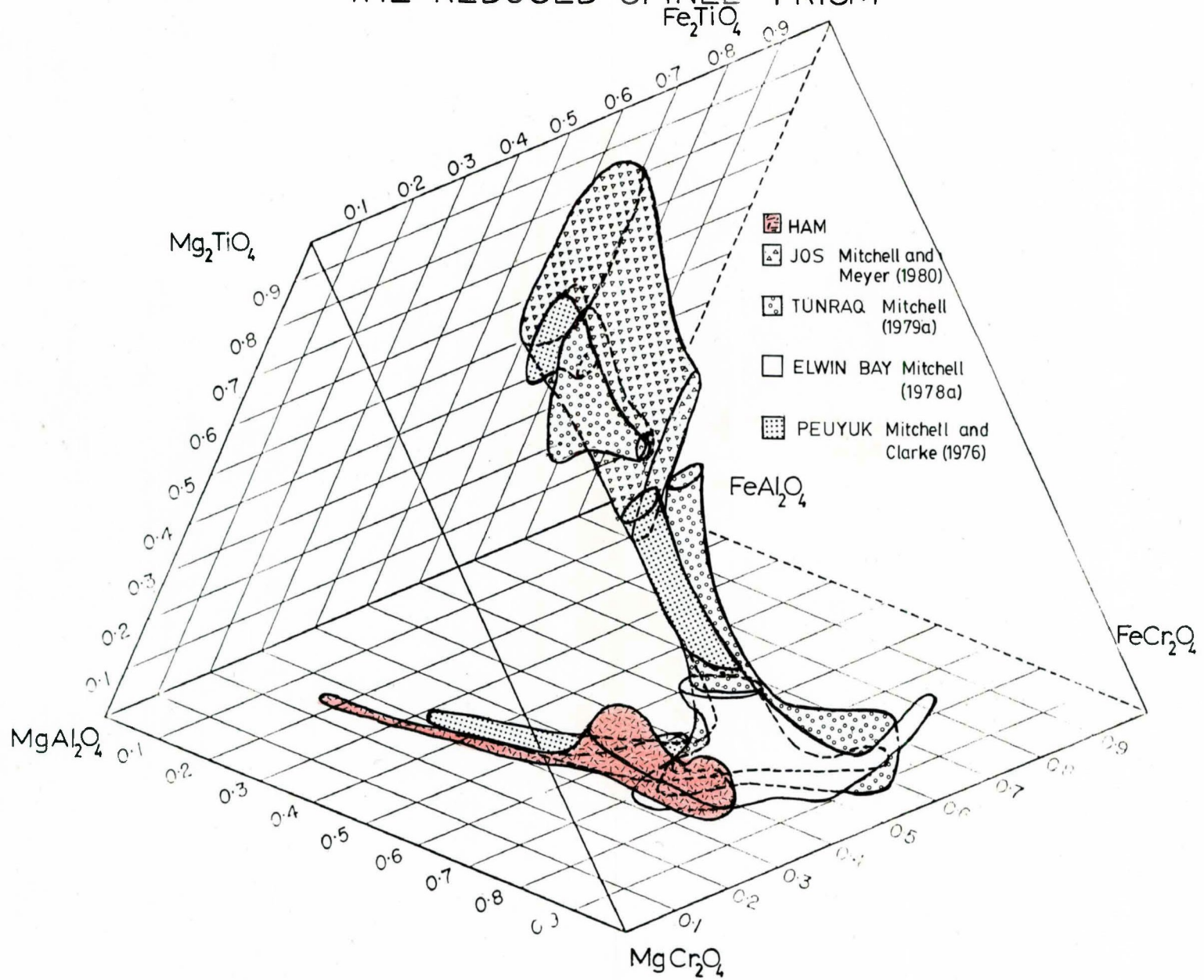


FIGURE 22C  
 COMPOSITIONAL VARIATION OF HAM DIATREME TYPE 1B KIMBERLITE SPINELS IN  
 THE "REDUCED" SPINEL PRISM

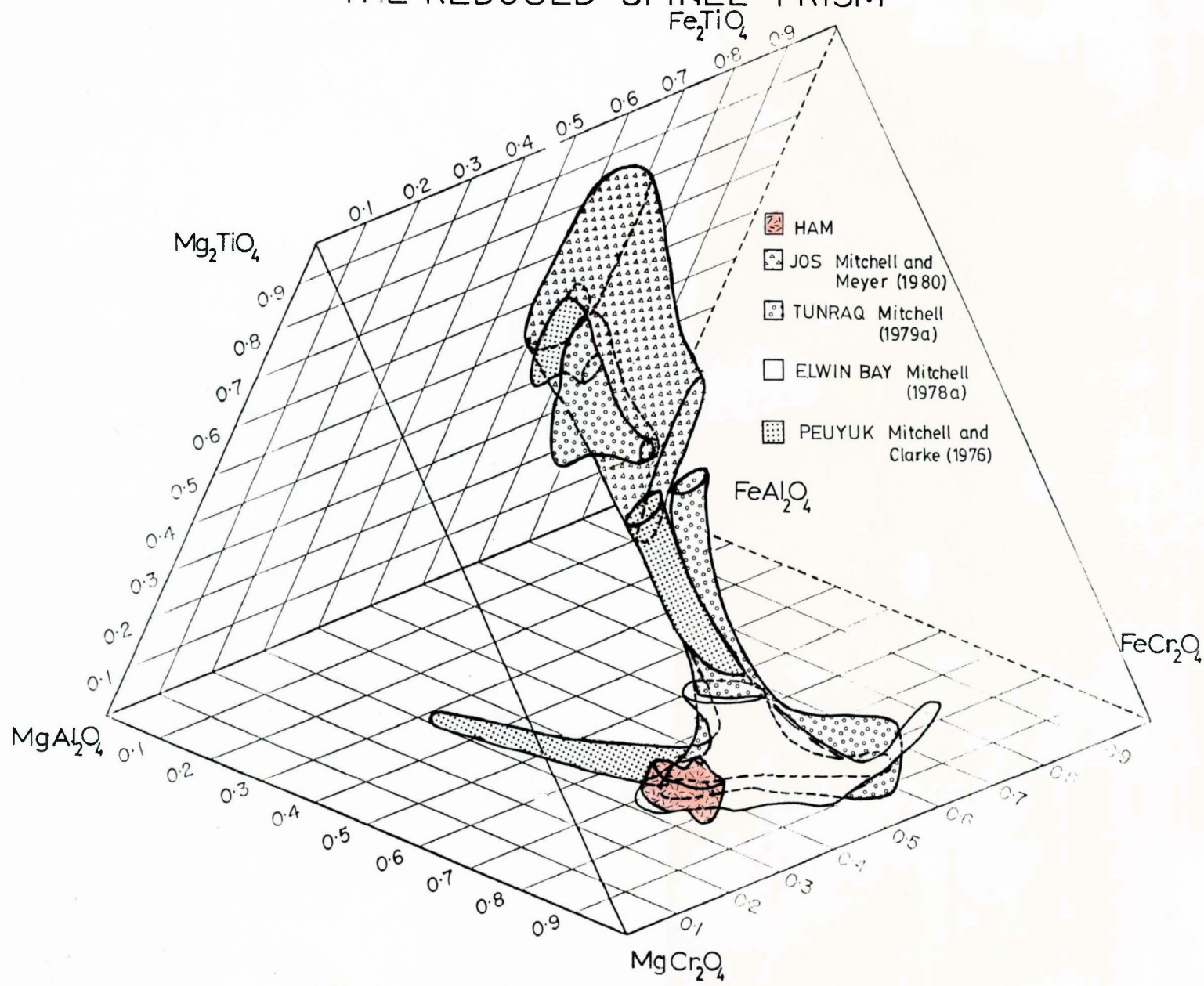
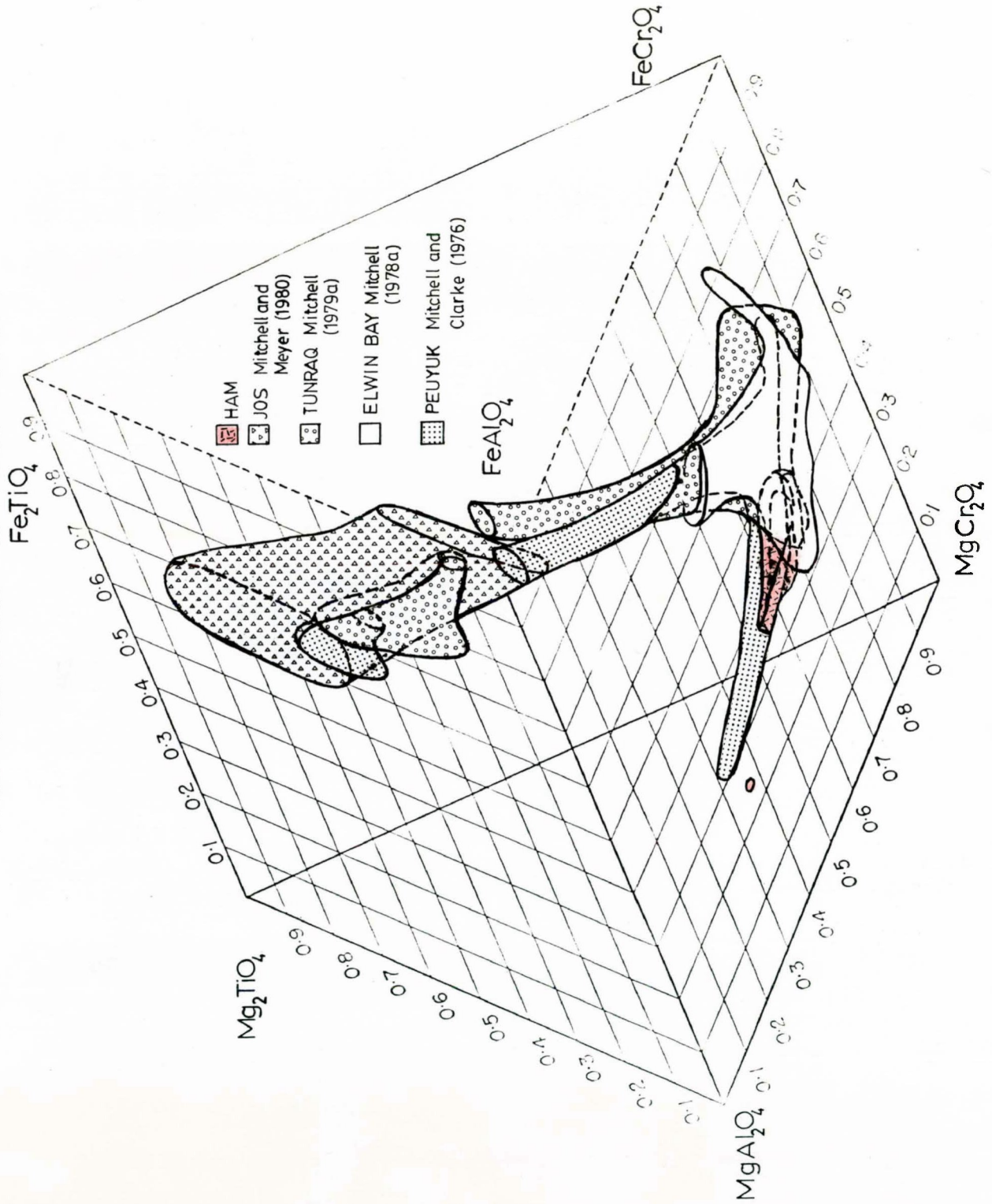


FIGURE 22D  
 COMPOSITIONAL VARIATION OF HAM DIATREME TYPE 2 KIMBERLITE SPINELS IN  
 THE "REDUCED" SPINEL PRISM



upper composition limit is based upon textural-compositional criteria presented in Figure 25. Figures 23 and 24 demonstrates the highly aluminous nature of AM-chromite from Ham diatreme Type 1A kimberlite compared to AM-chromite from other Ham kimberlites and the Penyuk kimberlite (Mitchell and Clarke 1976). Haggerty (1976) suggests that variations in the Cr/Cr+Al ratio along the base of Figure 23 are pressure dependent. Thus, the Cr/Cr+Al ratio would increase with a decrease in pressure during the ascent of the kimberlite magma from the mantle. The increase in the Cr/Cr+Al ratio is manifested as an increase in the proportion of  $MgCr_2O_4$  in the solid solution series  $MgAl_2O_4$ - $MgCr_2O_4$ . These observations agree with petrographic examinations which suggest that AM-chromite found as euhedral inclusions in pre-fluidization olivine (this study) and garnet (Mitchell and Clarke 1976), were part of a high pressure, phenocrystal spinel suite formed in the mantle prior to the fluidized intrusion of the kimberlite.

#### Titan Magnesian Aluminas Chromite (Titan-MA-Chromite)

Representative analyses of titan-MA-chromite are given in Table 16, analyses 9 to 18. The compositional variation is illustrated in Figures 22a to 22d and in Figures 23 and 25 and Table 18a. Cr/Cr+Al ratios and

FIGURE 23  
 $MgAl_2O_4$ - $Mg_2TiO_4$ - $MgCr_2O_4$  TERNARY PLOT-HAM KIMBERLITE SPINELS

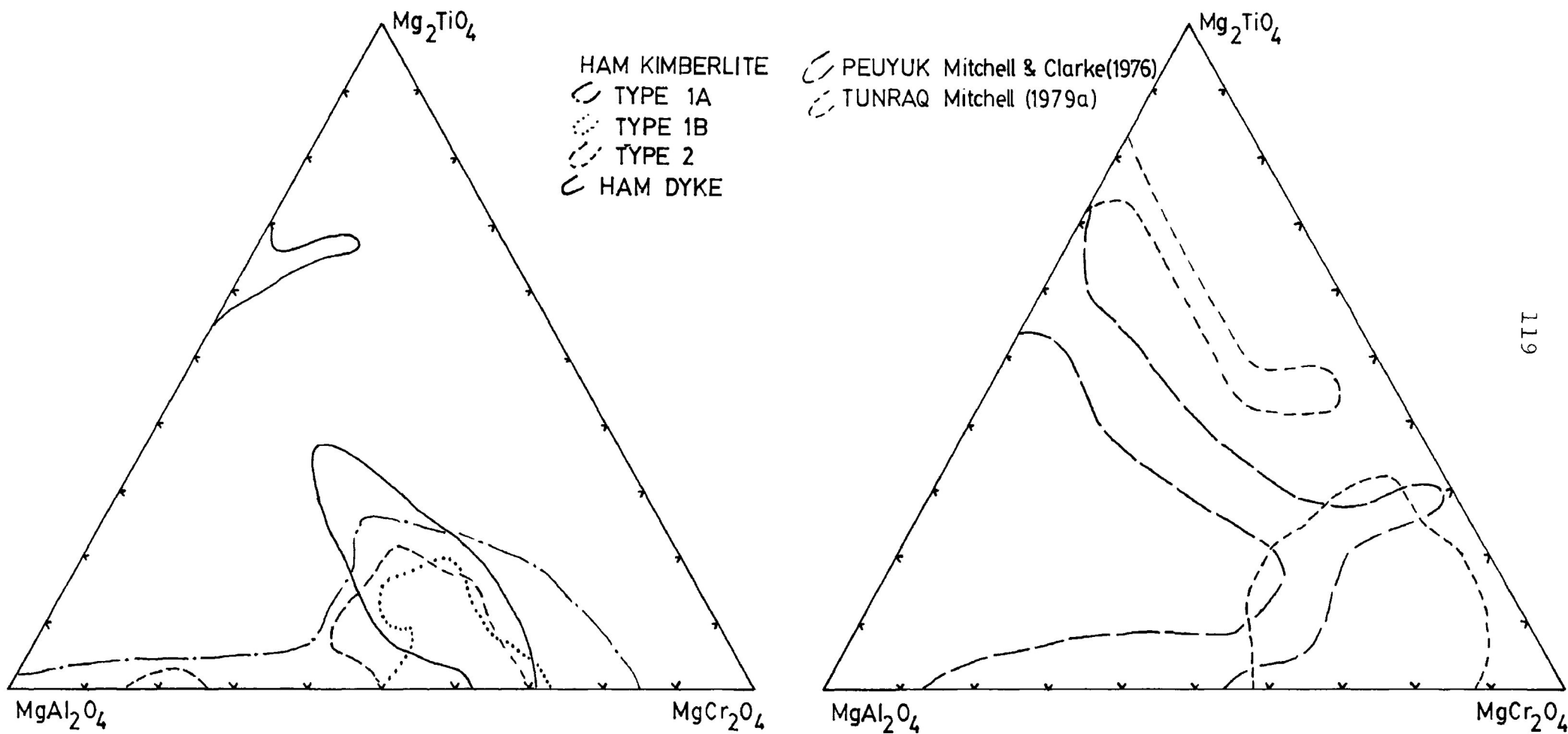


FIGURE 24  
Histogram of Ti-rich Spinels

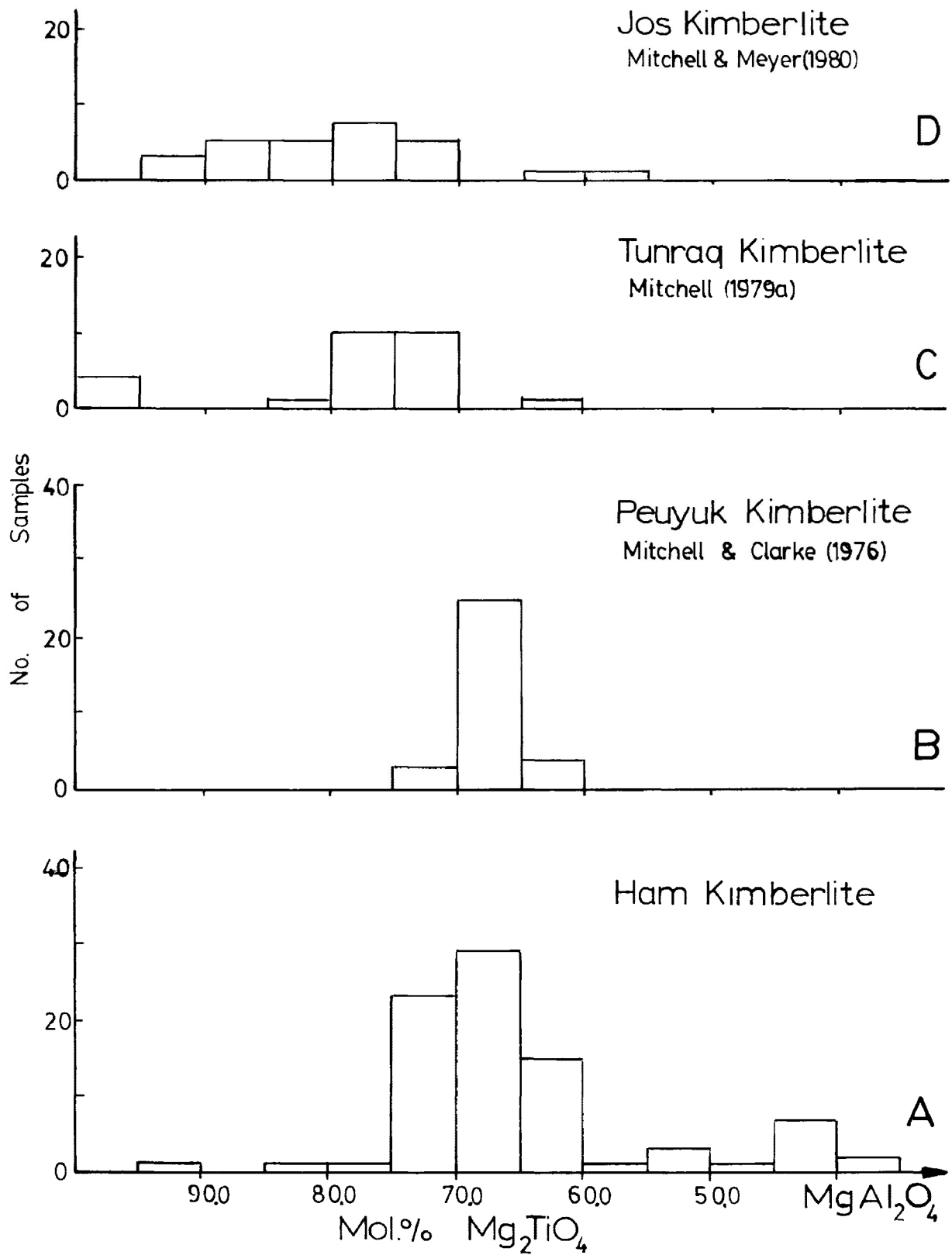
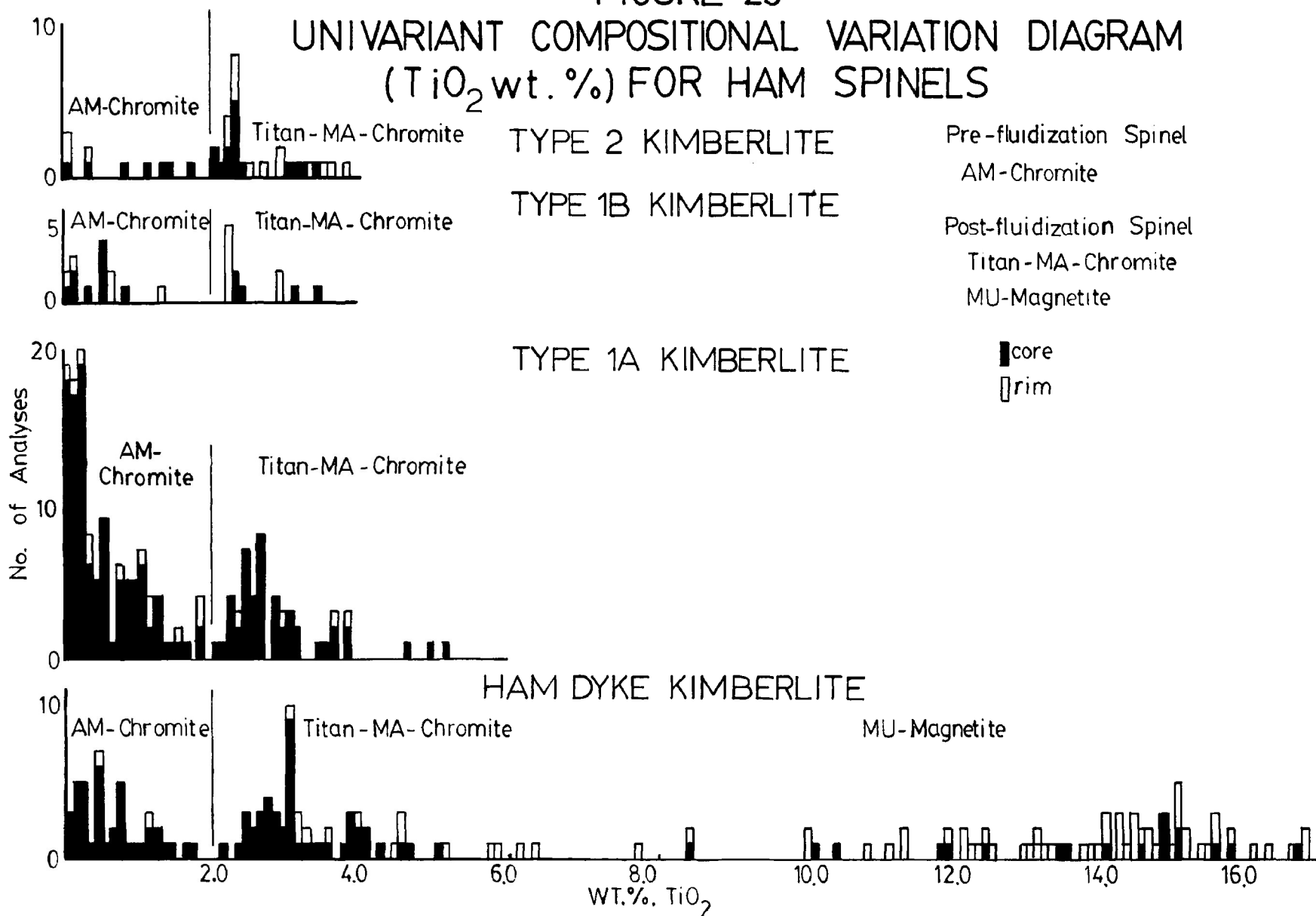


FIGURE 25

UNIVARIANT COMPOSITIONAL VARIATION DIAGRAM  
(TiO<sub>2</sub> wt. %) FOR HAM SPINELS



Fe/Fe+Mg ratios of Ham diatreme titan-MA-chromite (including Type 1A, 1B and Type 2 kimberlite) range from approximately 0.55 to 0.80, 0.68 to 0.79 and 0.57 to 0.78, and, from 0.35 to 0.50, 0.33 to 0.40 and 0.33 to 0.45, respectively.  $TiO_2$  contents of discrete, subhedral to euhedral compositionally homogenous crystals and continuously zoned mantles upon pre-fluidization AM-chromite range from approximately 2.00 to 5.20 weight percent. In contrast, Cr/Cr+Al ratios of titan-MA-chromite from the Ham dyke increase from approximately 0.55 to 0.80 then decrease to approximately 0.25. Fe/Fe+Mg ratios range from 0.32 to 0.58.  $TiO_2$  contents (Figures 23 and 25) are greater than those encountered in Ham diatreme spinels and range from 2.00 to 8.40 weight percent  $TiO_2$  in discrete crystals and continuously zoned mantles. The maximum  $TiO_2$  content was derived from electronprobe traverses (Figure 25) of continuously zoned, euhedral crystals. The paucity of analyses between 6.40 and 8.40 weight percent  $TiO_2$  reflects the corroded nature of discrete crystals and the development of "atoll" structures in continuously zoned crystals.

Magnesian Ulvöspinel Ulvöspinel Magnetite (MU-Magnetite)

MU-magnetite occurs exclusively in the Ham dyke kimberlite. Representative analyses are given in Table

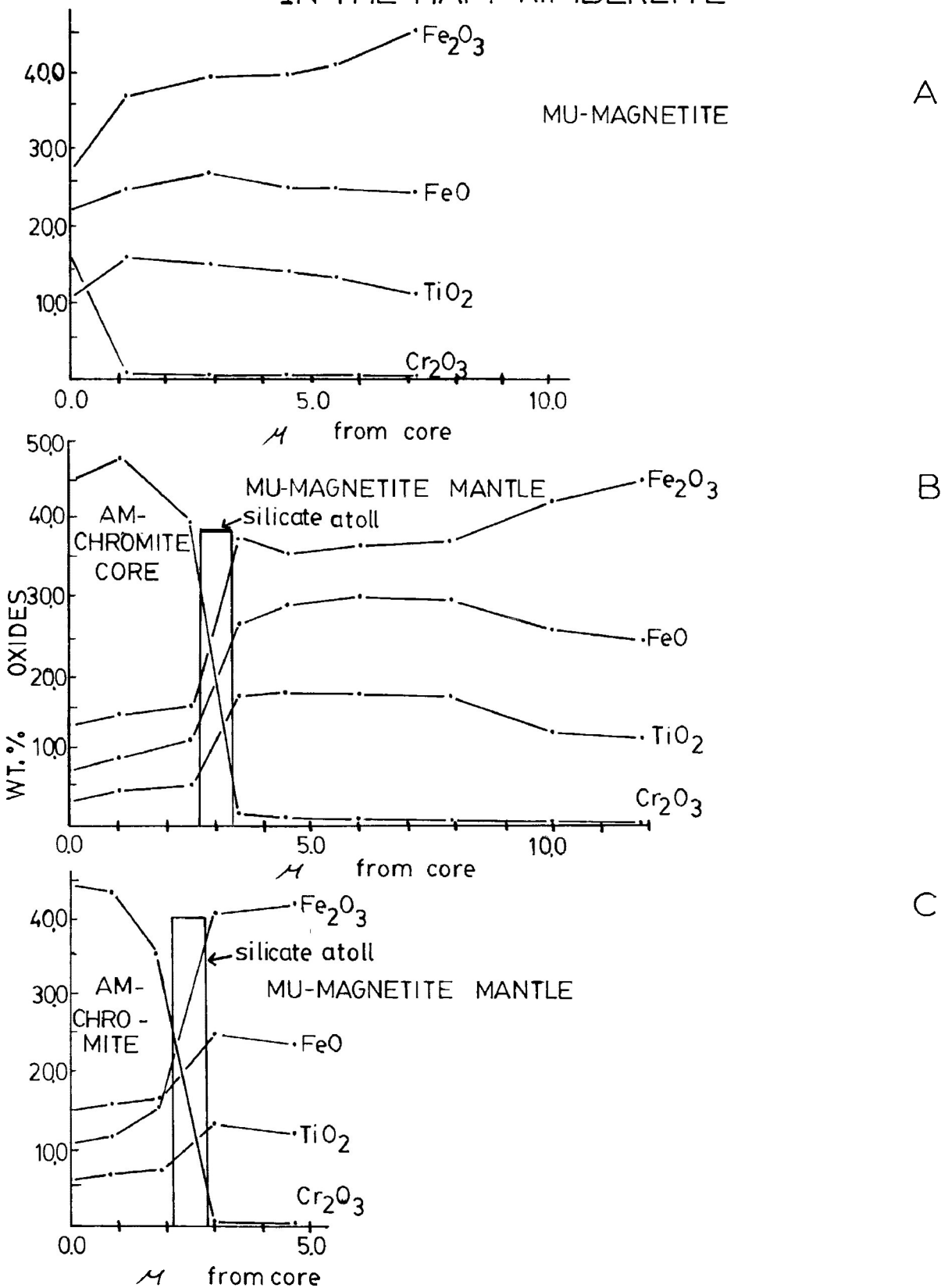
16, analyses 23-36. The compositional variation is illustrated in Figures 22a, 23 and 25. Figure 26 illustrates the compositional variation of discrete, continuously zoned, euhedral MU-magnetite crystals (Figure 26a) and continuously zoned subhedral to euhedral mantles (Figures 26b and c) upon Am-chromite crystals. Cr/Cr+Al ratios in continuously zoned crystals and mantles decrease from approximately 0.32 to 0.00 with a concomitant increase in the Fe/Fe+Mg ratio from 0.58 to 0.70. TiO<sub>2</sub> contents of small, discrete, compositionally homogenous crystals ranges from approximately 10.20 to 16.60 weight percent TiO<sub>2</sub>. In contrast, TiO<sub>2</sub> contents in continuously zoned mantles (Figures 26b and 26c) increases from approximately 10.20 to 16.60 weight percent TiO<sub>2</sub>, then decreases to approximately 10.90 weight percent TiO<sub>2</sub> at grain margins.

#### Atoll Spinel

The development of the atoll spinel is best illustrated in the Ham dyke kimberlite. Plates 7a to 7f and 8a to 8f illustrate the compositional variation from grain core to margin.

Haggerty (1973), Mitchell and Clarke (1976) and Pasteris (1980) demonstrate that kimberlite spinels evolve from AM-chromite to titan-MA-chromite to

FIGURE 26  
COMPOSITIONAL VARIATION TRENDS IN MU-MAGNETITE  
IN THE HAM KIMBERLITE



MU-magnetite. The compositional trend of atoll spinels in Ham dyke kimberlite are similar to those of kimberlite spinels described above except that a Si-Mg-rich silicate zone occupies a portion of the evolutionary trend bounded by  $TiO_2$  contents of 6.40 and 10.00 weight percent  $TiO_2$  (Figure 25). The inner and outer boundaries of this silicate zone are in corroded contact with a continuously zoned core of titan-MA-chromite and a continuously zoned mantle of MU-magnetite (Plates 7 and 8). The outer mantle of MU-magnetite is commonly mantled by a spongy, anhedral overgrowth of Ti-poor magnetite (Table 16, analyses 37 and 38). The appearance of the silicate zone suggests that prior to complete crystallization of the kimberlite groundmass, atoll structures did not exist and that the outer mantle of MU-magnetite was continuous from the titan-MA-chromite core to MU-magnetite margin.

Mitchell and Clarke (1976) believe that the atoll structure is formed by preferential resorption of a spinel phase after the growth of an outer magnetite mantle. This outer MU-magnetite mantle, both in the Peuyuk (Mitchell and Clarke 1976) and Ham diatrema kimberlite, appear to have crystallized epitaxially upon the titan-MA-chromite mantle (Plates 6a to 6f). Further, increasing  $TiO_2$  contents of Peuyuk Phase C spinels led

to crystallization of discrete magnesian ulvöspinel ulvöspinel magnetite crystals and mantles upon titaniferous chromites. Although no MU-magnetite was found in Peuyuk Phase B kimberlite (or in the Ham diatrema kimberlite), Mitchell and Clarke (1976) believe that Phase B and C spinels initially followed similar chemical evolutionary paths. They conclude that the resorbed spinel may have been MU-magnetite that was resorbed when the spinel grain was in contact with a carbonated groundmass liquid.

These petrologic conditions are similar to those deduced for the Ham kimberlite. Figures 22a to 22d illustrate that initially both the diatrema and dyke evolved along similar chemical evolutionary trends. Dyke spinels, however, evolved to much higher  $TiO_2$  contents. This is reflected in the development of MU-magnetite mantles in dyke atoll spinels and the paucity of such mantles on diatrema spinels. Had the two kimberlites followed similar chemical evolutionary paths, a similar suite of spinels would have crystallized. Therefore, it is not unreasonable to assume that the resorbed spinel in atoll structures developed in the Ham dyke kimberlite may have been MU-magnetite and that a similar process was responsible for the complete resorption of MU-magnetite mantles upon titan-MA-chromite in the Ham diatrema kimberlite.

### A Comparison of Spinel Evolutionary Trends

The spinel evolutionary trends established for the Ham kimberlites are similar to trends reported for kimberlite spinels by Haggerty (1973), Mitchell and Clarke (1976), Mitchell (1978a, 1979a), Mitchell and Meyer (1980), Shee (1979) and Pasteris (1980).

### Aluminous Magnesian Chromite (AM-chromite)

Inspection of Figures 22a to 22d and 23 and Table 17a reveal that AM-chromite from the Ham, Peuyuk (Mitchell and Clarke 1976) and Elwin Bay (Mitchell 1978a) kimberlites are similar although the range in Fe/Fe+Mg ratios of AM-chromite from the latter two kimberlites is substantially greater. The range of Cr/Cr+Al ratios of AM-chromite from Ham Type 1A kimberlite is broader than Cr/Cr+Al ratios of AM-chromite from other Ham and Somerset Island kimberlites. Figures 23 and 24 demonstrate the highly aluminous nature of AM-chromite from Type 1A kimberlite compared to other Ham and Somerset Island kimberlites. TiO<sub>2</sub> contents of Elwin Bay AM-chromite (max 1.0 wt. %) and Peuyuk (max. 1.39 wt. %) are less than TiO<sub>2</sub> contents reported for Ham AM-chromite (max. 2.0 wt. %).

Table 17b compares the compositional variation of Ham AM-chromite with spinels found in spinel lherzolite

TABLE 17A  
Compositional Variation of Somerset Island AM-Chromite\*

Kimberlite	Cr/Cr+Al	Fe/Fe+Mg	TiO <sub>2</sub> (wt.%)	Source
Type 1A	0.18-0.83	0.22-0.46	<2.00	This study
Type 1B	0.68-0.81	0.32-0.44	"	"
Type 2	0.57-0.78	0.34-0.45	"	"
Ham Dyke	0.55-0.79	0.32-0.49	<2.00	This study
Peuyuk	0.32-0.89	0.28-0.65	<1.35	Mitchell and Clarke (1976)
Elwin Bay	0.68-0.89	0.29-0.70	<1.00	Mitchell (1978a)
Wesselton Mine	0.50-0.81	0.39-0.60	base of prism	Shee (1979)
DeBeers Pipe	0.49-0.80	0.38-0.68	base of prism	Pasteris (1980)

\* - compositional limits based on projections in the reduced spinel prism

TABLE 17B  
Compositional Variation of Chromite in Spinel-bearing  
Mantle Xenoliths

Xenolith Type	Cr/Cr+Al	Fe/Fe+Mg	TiO <sub>2</sub> (wt.%)	Source
A Spinel Lherzolite	0.20-0.53	0.23-0.66	0.00-0.37	Mitchell (unpubl. data)
B Spinel Lherzolite	0.77-0.94	0.42-0.43	0.27-0.96	Smith and Dawson (1975)
C Spinel Lherzolite	0.09-0.50	0.33-0.70	-	Jackson (1979)
D Garnet-Spinel Lherzolite	0.17-0.72	0.26-0.39	0.34-1.64	Smith and Dawson (1975)
E Garnet-Lherzolite	0.24-0.79	0.22-0.46	0.07-0.59	Carswell, Clarke and Mitchell (1979)
F Garnet-Chromite Lherzolite	0.70-0.73	0.41-0.43	0.00-0.11	" " "
G Chromite Lherzolite	0.83	0.32	0.34	" " "
H Spinel-Rutile Lherzolite	0.87	0.33	2.63	Smith and Dawson (1975)
I Ultra-basic Nodule Suite	0.69-0.76	0.36-0.49	0.05-0.36	Nixon and Boyd (1975)
J Spinel Harzburgite	0.45-0.60	0.34-0.59	0.00-0.11	Smith and Dawson (1975)
K Chromite Harzburgite	0.78-0.84	0.31-0.33	0.00	Carswell, Clarke and Mitchell (1979)
L Spinel Peridotite	0.49-0.79	0.16-0.31	0.00-0.41	MacGregor (1979)

A - Nanorluk - Somerset Island, N.W.T. Canada

B - DeBeers Pipe, Lashaine Kimberlite, S. Africa, Letseng-La-Terae, Lesotho

C - Lipelaneng Kimberlite - Lesotho

D - Bultfontein, Monastery Mine, S. Africa, Letseng-La-Terae, Lesotho

E - Pipe 200 - South Africa

F - Pipe 200 - South Africa

G - Pipe 200 - South Africa

H - Bultfontein - South Africa

I - Thaba Putsoa and Mothae, Lesotho

J - Newlands, Bultfontein and Lashaine, South Africa

K - Pipe 200 - South Africa

L - Kao - South Africa

xenoliths within the Nanorluk kimberlite (Mitchell unpubl. data). The range of Cr/Cr+Al ratios and TiO<sub>2</sub> contents of Ham AM-chromite encompasses the range obtained for Nanorluk lherzolite spinels although the range of Fe/Fe+Mg ratios of the latter spinels is much broader and higher than Fe/Fe+Mg ratios of Ham AM-chromite.

Tables 17A and 17B suggest a compositional similarity between AM-chromite from the Ham kimberlite and spinel from some mantle-derived ultra-basic xenoliths from South African localities. Cr/Cr+Al ratios are similar except for higher ratios reported for Smith and Dawson's (1973) spinel lherzolite and spinel-rutile lherzolite suite and Carswell et al. (1979) chromite lherzolite and chromite-harzburgite suite. Fe/Fe+Mg ratios of AM-chromite from the Wesselton Mine (Shee 1979) and DeBeers Pipe (Pasteris 1980) kimberlite and Smith and Dawson's (1973) spinel-harzburgite suite, Nixon and Boyd's (1973) ultra-basic xenolith suite and Jackson's (1979) spinel-lherzolite suite are greater than Fe/Fe+Mg ratios of Ham AM-chromite. The range of TiO<sub>2</sub> contents of Ham AM-chromite is substantially broader than all South African examples except for Smith and Dawson's (1973) spinel-rutile lherzolite suite.

The presence of AM-chromite in high pressure mantle-derived phenocrysts (olivine and garnet) and the chemical similarity of some Ham AM-chromite to spinel in spinel lherzolite xenoliths indicates that AM-chromite may be both phenocrystal and xenocrystal in origin. Because the compositional range of Ham AM-chromite encompasses that of most spinels in spinel lherzolite xenoliths, chemical distinction between the two paragenesis cannot be made.

#### Titan Magnesian Aluminous Chromite (Titan-MA-Chromite)

Inspection of Figures 22a to 22d and Table 18a indicate that although titan-MA-chromite from the Ham kimberlites and other Somerset Island kimberlites was initially compositionally different, titan-MA-chromite from the Ham dyke, Peuyuk (Mitchell and Clarke 1976) and Tunraq (Mitchell 1979a) kimberlites evolved toward similar Cr/Cr+Al and Fe/Fe+Mg ratios and  $TiO_2$  contents. In general, this spinel evolved toward grain margins enriched in  $TiO_2$  and  $Fe_2O_3$  with a concomitant decrease in the  $Cr_2O_3$  content.

A comparison of Tables 18A and 18B indicate that titan-MA-chromite from South African localities demonstrates a broader range in Cr/Cr+Al and Fe/Fe+Mg ratios than titan-MA-chromite from the Ham kimberlite although  $TiO_2$  contents are similar.

TABLE 18A  
Representative Analyses of  
Titaniferous Magnesium Aluminous Chromites-Somerset Island

	1	2	3	4	5	6	7	8	9
TiO <sub>2</sub>	2.40	3.08	5.05	5.84	3.81	12.90	3.05	6.57	3.20
Al <sub>2</sub> O <sub>3</sub>	12.75	11.23	9.12	7.34	7.67	9.24	9.98	10.07	10.30
Cr <sub>2</sub> O <sub>3</sub>	43.30	52.25	44.82	43.88	47.27	10.84	50.28	33.73	51.60
Fe <sub>2</sub> O <sub>3</sub>	10.77	4.88	10.77	11.66	11.01	28.10	8.75	19.76	7.10
FeO	15.10	13.27	15.10	15.75	15.23	23.28	13.12	13.26	13.00
MnO	0.37	0.34	0.59	0.57	0.44	0.50	0.45	0.53	0.40
MgO	15.57	15.00	14.50	14.22	13.40	13.24	14.95	16.81	15.30
TOTAL	100.26	100.05	99.95	99.26	98.85	98.21	100.50	100.73	100.90
Cr/Cr+Al	0.63	0.76	0.77	0.80	0.80	0.44	0.77	0.69	0.77
Fe/Fe+Mg	0.27	0.29	0.33	0.34	0.35	0.45	0.29	0.27	0.28

Analyses 1-4 - Ham Diatreme and Dyke, this work  
 Analyses 5-6 - Peuyuk Kimberlite - Mitchell and Clarke (1976)  
 Analyses 7-8 - Elwin Bay Kimberlite - Mitchell (1978a)  
 Analysis 9 - Tunraq Kimberlite - Mitchell (1979a)

TABLE 18B  
Representative Analyses of  
Titaniferous Magnesium Aluminous Chromites-South Africa

	1	2	3	4	5	6	7	8	9
TiO <sub>2</sub>	3.02	4.20	8.57	3.20	2.95	4.29	3.30	4.91	8.09
Al <sub>2</sub> O <sub>3</sub>	6.62	7.41	6.74	7.67	9.86	6.00	7.27	11.32	5.87
Cr <sub>2</sub> O <sub>3</sub>	54.57	49.44	38.92	51.90	44.40	50.36	51.21	41.84	44.82
Fe <sub>2</sub> O <sub>3</sub>	6.02	5.36	10.47	8.19	12.10	8.26	8.50	8.87	11.11
FeO	18.53	19.81	22.60	14.40	17.30	18.69	13.54	20.90	12.21
MnO	0.36	0.38	0.28	0.29	0.57	0.35	0.25	0.94	0.91
MgO	10.84	12.55	11.43	14.0	11.80	11.55	14.95	10.46	17.88
TOTAL	99.96	99.15	99.01	99.65	98.98	99.50	99.02	99.24	100.89
Cr/Cr+Al	0.84	0.81	0.79	0.82	0.75	0.85	0.83	0.71	0.84
Fe/Fe+Mg	0.45	0.39	0.48	0.33	0.45	0.43	0.29	0.53	0.28

Analysis 1 - Wesselton Mine, W3 Kimberlite - Shee (1979)  
 Analysis 2 - Wesselton Mine, W7 Kimberlite - Shee (1979)  
 Analysis 3 - Wesselton Mine - Wesselton Sill - Shee (1979)  
 Analysis 4 - Nigerdlikasik Kimberlite - Greenland - Emeleus and  
 Andrews (1975)  
 Analysis 5 - Pyramidefjeld Kimberlite - Greenland - Emeleus and  
 Andrews (1975)  
 Analyses 6-7 - Letseng-La-Terae, Lesotho, Boyd (1973)  
 Analyses 8-9 - DeBeers Pipe Kimberlite - S. Africa - Pasteris (1980)

Magnesian Ulvöspinel Ulvöspinel Magnetite (MU-Magnetite)

Figure 22 a and Table 19a illustrate the compositional similarity between MU-magnetite found in the Ham dyke and Peuyuk (Mitchell and Clarke 1976) kimberlites and to lesser extent the highly evolved Tunraq kimberlite (Mitchell 1979 ) and lesser evolved Jos kimberlite (Mitchell and Meyer 1980). The latter two kimberlites evolved to substantially lower and higher Cr/Cr+Al and Fe/Fe+Mg ratios, respectively.

Figure 24 shows that the Ti-rich spinel MU-magnetite assemblage of the Ham kimberlite is similar to that of the Peuyuk (Mitchell and Clarke 1976) kimberlite but that both of these are rich in the  $MgAl_2O_4$  component relative to Ti-rich spinels in the Tunraq fissile micaceous kimberlite (Mitchell 1979a) or the Jos (Mitchell and Meyer 1980) kimberlite. This supports Mitchell's (1979a) contention that spinels in kimberlite are generally richer in Al than spinels in micaceous kimberlite.

Table 19b reveals that the range of Cr/Cr+Al and Fe/Fe+Mg ratios and  $TiO_2$  contents of MU-magnetite from South African kimberlite encompasses those from the Ham kimberlite.

TABLE 19A  
Representative Analyses of Somerset Island MU-Magnetite

	1	2	3	4	5	6	7	8	9	10	11
TiO <sub>2</sub>	8.45	12.58	14.46	15.47	16.48	16.70	16.70	18.20	11.10	17.10	23.80
Al <sub>2</sub> O <sub>3</sub>	8.73	8.75	8.80	7.63	10.69	7.20	8.70	8.40	11.00	6.40	4.90
Cr <sub>2</sub> O <sub>3</sub>	0.20	0.00	0.68	1.42	1.25	3.80	2.40	1.50	0.70	0.80	1.10
Fe <sub>2</sub> O <sub>3</sub>	49.78	41.20	37.30	36.09	30.61	29.60	32.20	30.50	41.10	36.40	25.40
FeO	17.17	25.25	24.72	25.92	26.61	26.30	23.20	25.90	24.10	23.50	25.70
MnO	0.58	0.53	0.51	0.57	0.47	0.50	0.50	0.50	0.70	0.70	0.90
MgO	14.33	12.09	13.51	13.52	13.57	15.00	15.70	15.00	12.10	16.00	17.60
TOTAL	99.24	100.40	99.98	100.62	99.68	99.10	99.40	100.00	100.90	100.80	99.40
Cr/Cr+Al	0.02	0.00	0.05	0.11	0.07	0.29	0.15	0.11	0.04	0.07	0.13
Fe/Fe+Mg	0.37	0.50	0.46	0.48	0.48	0.37	0.41	0.45	0.49	0.40	0.41

Analyses 1-4 - Ham Diatrema - this work

Analysis 5 - Peuyuk Kimberlite - Mitchell and Clarke (1976)

Analyses 6-8 - Tunraq Kimberlite - Mitchell (1979a)

Analyses 9-11- Jos Kimberlite - Mitchell and Meyer (1980)

TABLE 19B  
Representative Analyses of South African MU-Magnetite

	1	2	3	4	5	6	7	8	9	10	11
TiO <sub>2</sub>	16.10	10.96	16.40	16.90	18.27	19.77	22.82	19.90	19.93	21.89	20.70
Al <sub>2</sub> O <sub>3</sub>	12.50	6.36	8.07	9.21	10.10	9.54	9.28	7.04	3.68	5.85	5.52
Cr <sub>2</sub> O <sub>3</sub>	2.95	2.50	0.03	0.00	0.78	0.82	1.11	2.68	0.30	2.23	4.38
Fe <sub>2</sub> O <sub>3</sub>	27.40	43.60	36.06	34.25	29.85	30.69	24.68	27.81	31.33	25.95	25.12
FeO	26.40	23.50	23.76	25.58	22.51	19.97	15.79	24.60	30.95	26.30	31.02
MnO	0.39	0.54	0.57	0.51	0.73	0.55	0.82	0.94	0.60	0.78	0.77
MgO	13.80	11.70	15.20	14.70	17.72	18.97	24.45	16.43	11.78	16.51	12.74
TOTAL	99.54	99.16	100.09	101.15	99.96	100.31	98.95	99.40	98.35	99.51	100.25
Cr/Cr+Al	0.14	0.21	0.00	0.00	0.05	0.10	0.07	0.20	0.05	0.20	0.35
Fe/Fe+Mg	0.48	0.50	0.43	0.45	0.37	0.35	0.23	0.41	0.55	0.43	0.58

Analysis 1 - Lipelong Kimberlite - Haggerty (1975)  
 Analysis 2 - Kao Kimberlite - Haggerty (1975)  
 Analyses 3-4 - Igvisi Hills Extrusive Kimberlite-Reid et al. (1975)  
 Analyses 5-7 - Green Mountain Kimberlite-Bocter and Meyer (1979)  
 Analysis 8 - Wesselton Mine - W2 Kimberlite - Shee (1979)  
 Analysis 9 - Wesselton Mine - Wesselton Sill - Shee (1979)  
 Analysis 10 - Wesselton Mine - W2 Kimberlite - Shee (1979)  
 Analysis 11 - DeBeers Pipe - Pasteris - (1980)

CONCLUSIONS

Petrographic observations and chemical evolutionary trends suggest that Ham kimberlite spinels are represented by a pre-fluidization aluminous magnesian chromite which varies from a Mg-Al-rich spinel to a Ti-bearing Cr-Fe-rich spinel and by a suite of post-fluidization spinels, which evolved chemically during the crystallization of the kimberlite magma, from Ti-bearing, Cr-Fe-rich titaniferous magnesian aluminous chromite to Cr-poor, Fe-Ti-rich magnesian ulvöspinel ulvöspinel magnetite. Aluminous magnesian chromite which is compositionally similar to spinel found in some mantle-derived, ultrabasic xenoliths is believed to be a member of a high pressure, spinel phenocrystal suite formed in the mantle prior to intrusion of the kimberlite magma and a product of crystallization from the kimberlite magma during its ascent through the mantle. The post-fluidization crystallization of kimberlite spinels is manifested in the crystallization of continuously zoned spinels involving extensive solid solution between titan magnesian aluminous chromite and magnesian ulvöspinel ulvöspinel magnetite. Resorption of a portion of this solid solution is demonstrated by the development of atoll spinels which probably formed when

the spinels were in contact with a carbonated ground-mass liquid prior to complete crystallization of the kimberlite magma.

A comparison of Figures 22a, 22b and 22c suggests that spinels in Type 1A and 1B kimberlite are chemically similar. The paucity of Al- and Ti-rich spinels in the highly altered Type 1B kimberlite may be attributed to their preferential resorption during serpentinization and carbonatization. There is no textural evidence to suggest that spinel in Type 2 kimberlite evolved toward higher Fe and Ti contents than already indicated.

Although there is no chemical evidence to suggest that spinel in the Ham diatreme evolved toward iron and titanium contents similar to Ham dyke spinels (i.e. toward MU-magnetite), textural evidence suggests that more extensive resorption (development of atoll spinel) of titan-MA-chromite in the Ham diatreme may have precluded its preservation and that the Ham dyke and diatreme did evolve along similar chemical evolutionary paths toward grain margins rich in MU-magnetite.

The relatively Ti-poor, Al-rich nature of Ham spinels compared to the Ti-Al-rich nature of Jos (Mitchell and Meyer 1980) and Tunraq (Mitchell 1979a) spinels suggests that the Ham kimberlite did not form from a micaceous kimberlite magma.

CHAPTER 7CARBONATE AND SERPENTINE MINERALS

Carbonate and serpentine occur as primary and secondary minerals in the Ham kimberlite. Primary minerals crystallized directly from fluids in the kimberlite magma. Secondary carbonate formed after the crystallization of the kimberlite groundmass from carbonate-rich fluids which were ascending from the lower regions of the degassing kimberlite during the onset of retrograde serpentinization. Those portions of the diatreme which were more highly carbonatized were also subjected to prograde serpentinization (see below).

CARBONATEPetrography

Primary carbonate occurs as tiny (<0.5 mm long), euhedral, inclusion-free, lath-shaped microphenocrysts (exhibiting flow textures in the Ham dyke) and as monomineralic, inclusion-free, coarse-grained, round to cusp-shaped emulsion textures in the Ham diatreme and dyke. Petrographic examination indicates that microphenocrysts have been incipiently to wholly (Ham diatreme) corroded during alteration of the kimberlite groundmass.

Secondary carbonate occurs as coarse-grained, inclusion-free, carbonate veins (max. 3 cm long) predominantly within the Ham dyke and adjacent to intrusive contacts of the Ham diatreme. These commonly culminate in locally pervasive areas of groundmass carbonatization. These areas and bleached zones adjacent to the veins (max. 1 cm wide) are characterized by a decrease in the concentration of silicate and opaque minerals and a lightening in colour of the groundmass. Secondary carbonate pseudomorphs after olivine, which are coarse-grained and have been extensively replaced by secondary "prograde" serpentine, occur predominantly within Type 1B kimberlite. The extensive corrosion and replacement of carbonate pseudomorphs by secondary serpentine and the crystallization of discrete, euhedral carbonate crystals and successive epitaxial overgrowths of carbonate indicates a multistage mobilization of a carbonate-rich fluid, which was periodically interrupted by the mobilization of a silica- and magnesium-rich fluid which crystallized serpentine minerals.

Inspection of Table 20 shows that Ham carbonates, regardless of paragenesis, are calcite.

#### Carbonate in Kimberlite

Experimental work by Franz and Wyllie (1967) demonstrated that carbonate in kimberlite could be a

TABLE 20  
Representative Analyses of Ham Carbonate

	1	2	3	4	5	6	7	8	9	10	11
MnO	0.12	0.09	0.00	0.14	0.00	0.01	0.16	0.13	0.00	0.03	0.00
FeO*	0.18	0.16	0.10	0.23	0.05	0.04	0.21	0.24	0.11	0.07	0.13
MgO	0.32	0.37	0.37	0.34	0.33	0.32	0.39	0.36	0.45	0.33	0.49
CaO	57.32	57.63	59.40	57.28	58.20	58.72	59.67	58.46	59.46	59.21	59.44
TOTAL	57.94	58.25	59.87	57.99	58.58	59.09	60.43	59.19	60.02	59.64	60.06
<u>Mn</u>											
Mn+Fe+											
Mg+Ca	0.13	0.08	0.00	0.13	0.03	0.00	0.17	0.14	0.00	0.00	0.00
<u>Fe</u>											
Mn+Fe+											
Mg+Ca	0.24	0.19	0.07	0.26	0.03	0.03	0.26	0.28	0.13	0.07	0.14
<u>Mg</u>											
Mn+Fe+											
Mg+Ca	0.74	0.84	0.81	0.80	0.74	0.73	0.86	0.83	0.97	0.70	1.00
<u>Ca</u>											
Mn+Fe+											
Mg+Ca	98.89	98.89	99.12	98.81	99.20	99.24	98.71	98.75	98.90	99.23	98.88

\* Total iron as FeO

Analyses 1-3 - Carbonate emulsion

Analyses 4-6 - Carbonate in serpentine emulsion

Analyses 7-8 - Carbonate replacing olivine

Analyses 9-10- Euhedral carbonate in serpentine replacing olivine

Analysis 11- Euhedral carbonate laths in Ham dyke kimberlite groundmass

primary phase. Mitchell (1979b) proposed that kimberlite magmas may in some circumstances differentiate to late stage immiscible carbonate-rich fluids, a process which Ferguson and Currie (1971) propose might be initiated by extensive fractional crystallization. Ferguson and Currie (1971) found that upon melting an olivine-lamprophyre containing carbonate ocelli, a homogenous silicate phase plus an immiscible CO<sub>2</sub>-rich fluid phase would form. This is consistent with petrographic evidence that suggests that the carbonate-rich segregations were attributable to liquid immiscibility.

Mitchell (1975, 1978a, 1979a) describes round to lobate inclusion-free carbonate segregations in Somerset Island kimberlites similar to those found in the Ham kimberlite (emulsion textures). Mitchell (1978a) asserts that these structures could only have formed after fluidization. That these textures are conclusive evidence of liquid immiscibility between a silicate and carbonate-rich portion of a kimberlite magma and are not a replacement phenomena is supported by the lack of veining between segregations and the lack of gradational contacts between the silicate groundmass and the carbonate segregations. The presence of primary groundmass carbonate in these kimberlites satisfies the criteria for immiscibility, in that,

crystallized droplets (segregations) of one liquid, trapped in another, occur in a rock from which one of the mineral phases (carbonate) is simultaneously crystallizing (Mitchell 1975).

Carbonate in veins and associated groundmass carbonate is considered to have crystallized from ascending fluids during the degassing of structurally lower portions of the kimberlite and is not the result of liquid immiscibility.

## SERPENTINES

### Models of Prograde and Retrograde Serpentinization

Serpentinization of the Ham kimberlite was complex and may be described in terms of a continuing process involving retrograde and prograde serpentinization (Wicks et al. 1977, Wicks and Whittaker 1977 and Wicks and Plant 1979).

Wicks and Whittaker (1979) describe a possible model of the serpentinization process which involves four retrograde and four prograde mineral assemblages. The retrograde processes, excluding those involving shearing events during cooling, from higher to lower temperature assemblages are: Type 1, antigorite + magnetite in pseudomorphic textures and Type 3, lizardite + brucite + magnetite in pseudo-

morphic textures. The prograde processes, excluding those involving shearing during heating, from lower to higher temperature assemblages are: Type 5, chrysotile + lizardite + brucite + magnetite in non-pseudomorphic textures and Type 7, antigorite + brucite + magnetite in non-pseudomorphic textures.

Petrographic examination of the Ham kimberlite indicates that retrograde serpentization began after the crystallization of the kimberlite groundmass and did not develop Type 1 mineral assemblages. Experimental data for the thermal stability limits of lizardite (Caruso and Chernosky 1979) constrains the development of lizardite-bearing Type 3 retrograde assemblages to temperatures below approximately 490°C. Petrographic examination of Type 2 kimberlite (incipient Type 3 serpentization) suggests that serpentization began with the development of multi-layer lizardite veins (Figure 9C, Wicks and Plant 1979) in olivines. Progressive serpentization proceeded with the development of fine-grained, randomly oriented serpentine followed closely by recrystallization to moderately well-oriented, coarse-grained (Plate 9a, this study) lizardite (Wicks and Plant 1979) that formed mesh rims and mesh centres (Figures 5b, c and e of Wicks and Plant 1979) or hourglass textures (Figure

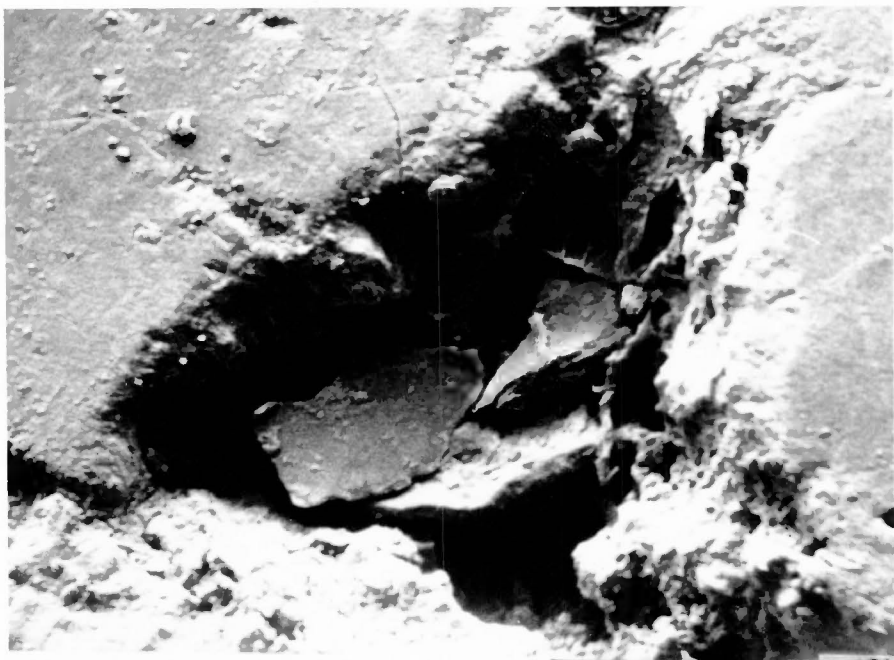


Plate 9a:  
Coarse bladed lizardite in a  
retrograde serpentine pseudomorph  
(S.E.M.)



Plate 9b:  
Spherulitic prograde serpentine in  
a carbonate emulsion texture  
(S.E.M.)

2d of Laurent and Hebert 1979). If the serpentinization process does not proceed to completion (i.e. to a homogenous pseudomorph with coarse magnetite inclusions), mesh centres with anomalously high Si contents (Anal. 2-10, 2-11 of Wicks and Plant 1979) intergrown with relict olivine will remain. Wicks and Plant (1979) contend that the development of hourglass textures is an extension of the development of mesh textures, perhaps the result of thorough Type 3 retrograde serpentinization, or, as a link with prograde Type 7 serpentinization as suggested by minor amounts of secondary antigorite. Highly variable amounts of rod-like chrysotile (Plates 10a and 10b) are commonly intermixed with lizardite in mesh rims and mesh centres.

During prograde serpentinization, Wicks and Plant (1979) indicate that relict olivine may alter directly to chrysotile + brucite or antigorite + brucite (Type 5 and Type 7 prograde serpentinization, respectively). This non-pseudomorphic (Figure 5e, 9b of Wicks and Plant 1979) replacement which occurs predominantly in Ham Type 1B kimberlite, is dominated solely by the development of antigorite blades (Plates 11a and 11b) in the kimberlite groundmass and at the edges of lizardite pseudomorphs after olivine. The growth of antigorite is always accompanied by the

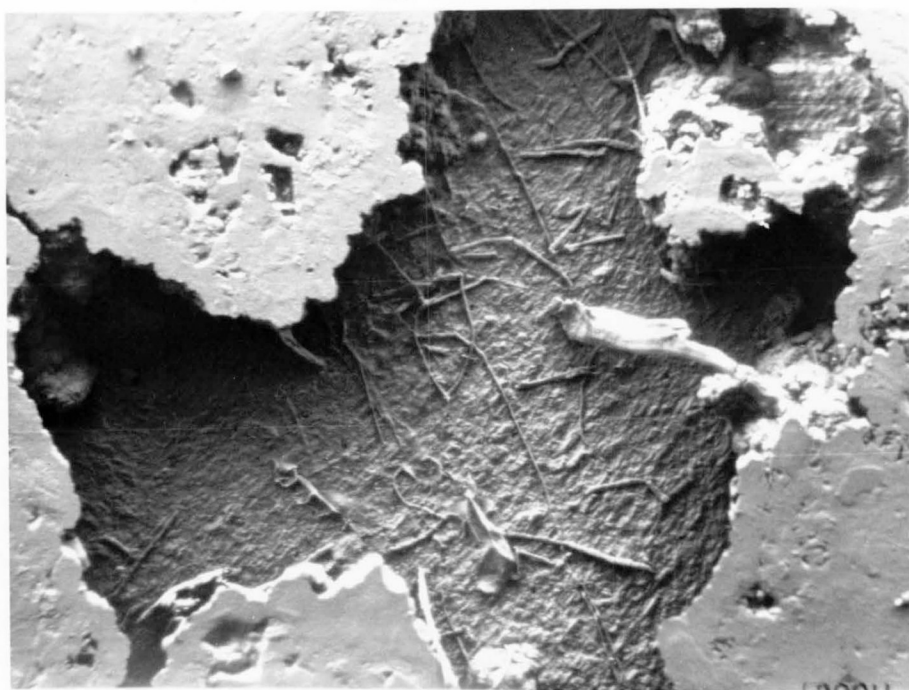


Plate 10a:  
Chrysotile rods in a carbonate (leached  
by HCl) emulsion texture  
(T.E.M.)

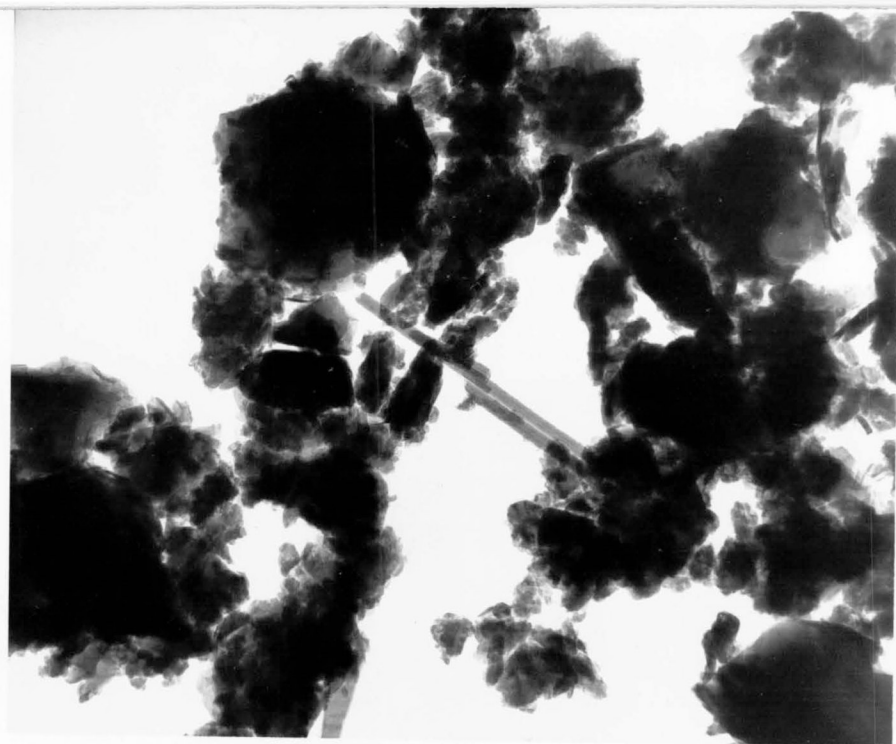
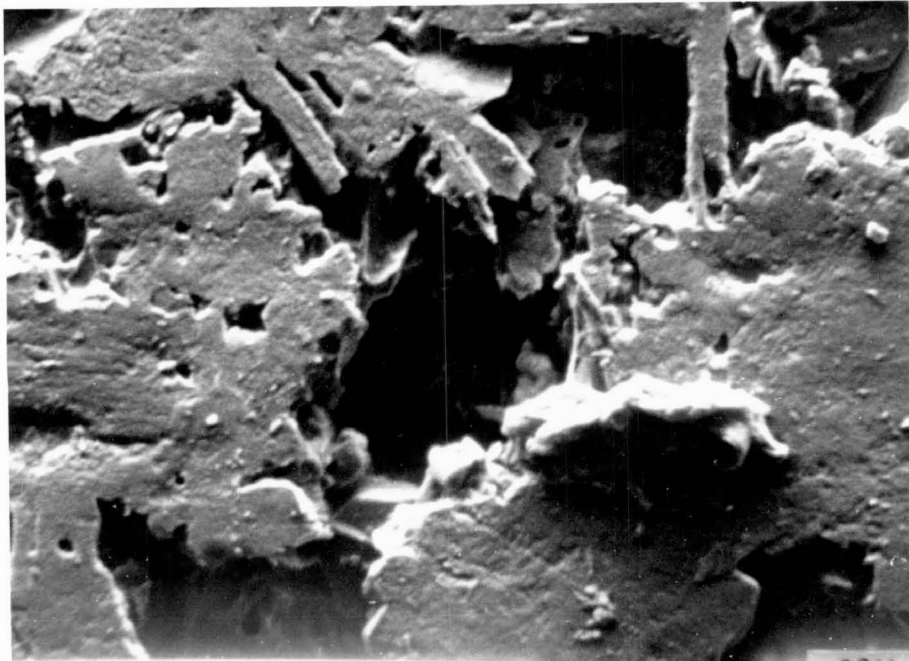
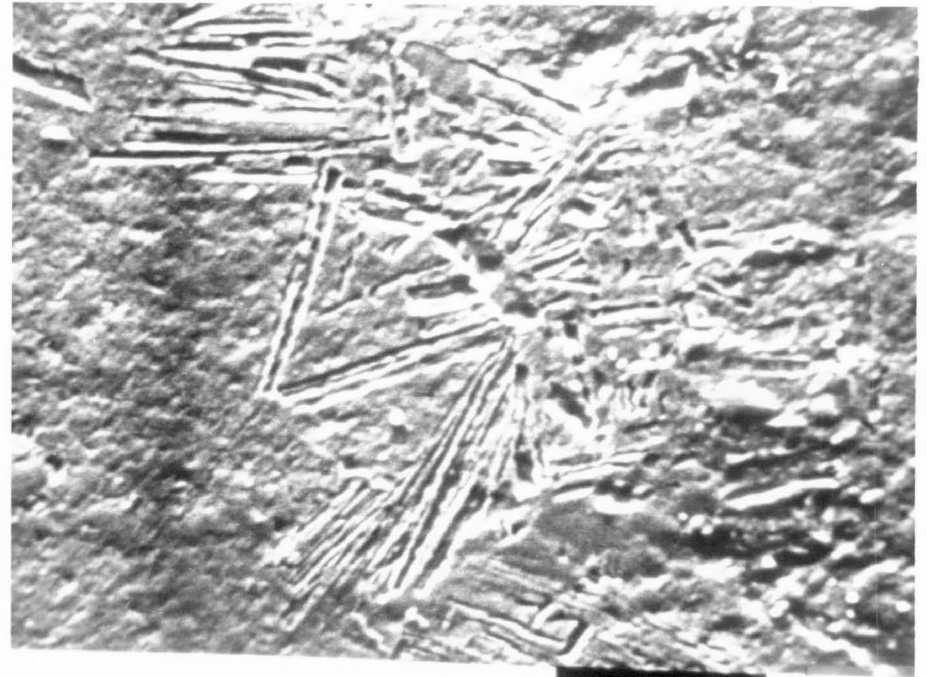


Plate 10b:  
Chrysotile rods with coarse bladed  
lizardite  
(S.E.M.)



100

Plate 11a:  
Antigorite blades protruding into a  
carbonate (leached by HCl) emulsion  
texture  
(S.E.M.)



100

Plate 11b:  
Interlocking antigorite blades in the  
kimberlite groundmass  
(S.E.M.)

extensive recrystallization of lizardite mesh textures to spherulitic (Plate 9b, this study) lizardite (Wicks and Whittaker 1977). The paucity of abundant chrysotile in this prograde mineral assemblage indicates that water was abundant during prograde serpentization (Wicks and Plant 1979). It follows from petrographic examination of Ham Type 1A and Type 1B kimberlite, that portions of the diatreme, where antigorite and granular lizardite are most abundant and chrysotile is scarce, or absent, are coincident with portions of the diatreme which were fluid-rich. Experimental data from Caruso and Chernosky (1979) indicate that fluid temperatures during prograde serpentization do not exceed approximately 550°C.

A comparison of x-ray diffraction data in Table 21 with x-ray diffraction data for serpentines in Maksimovich (1973), Whittaker and Zussman (1955), Brindley and Wan (1975) and Selected Powder Diffraction Data for Minerals, 1st Ed. (1974) indicate that the serpentine assemblages in the Ham diatreme and dyke Type 1A and Type 2 kimberlite include variable proportions of lizardite 10 and chrysotile 2M serpentine with very minor amounts of lizardite 1T. Large proportions of lizardite 1T are conspicuous by their absence. Cressey (1979), Wicks and Plant (1979),

Table 21  
X-ray Diffraction Data for Representative Serpentine  
Samples in the Ham Kimberlite

Type 1A Kimberlite		Type 1B Kimberlite		Type 2 Kimberlite	
d	I/I <sub>0</sub>	d	I/I <sub>0</sub>	d	I/I <sub>0</sub>
7.28	100	7.27	100	7.25	100
4.595	5	4.595	40	4.60	35
4.515	20	4.49	40	3.625	70
4.245	W	4.27	VW	3.35	30
3.911	W	4.231	15	2.62	W
3.88	W	4.009	20	2.45	10
3.85	W	3.879	18	2.165	5
3.65	70	3.63	80	1.750	VW
3.495	10	3.512	40	1.68	VW
2.795	VW	2.788	W	1.44	VW
2.710	VW	2.776	W	1.29	VW
2.497	70	2.759	23	1.15	VW
2.412	VW	2.704	W	1.045	VW
2.291	5	2.652	W		
2.153	VW	2.518	30		
2.093	5	2.504	47		
1.801	5	2.495	88		
1.75	VW	2.430	10		
1.685	VW	2.373	10		
1.54	5	2.147	46		
1.503	VW	2.092	W		
1.458	VW	1.983	W		
1.44	VW	1.793	23		
1.42	VW	1.751	5		
1.315	VW	1.698	W		
1.28	VW	1.660	W		
1.168	VW	1.610	5		
		1.546	10		
		1.534	23		
		1.517	10		
		1.502	26		

W - weak reflection  
VW - very weak reflection

Wicks et al.(1977) and Wicks and Whittaker (1977) indicate lizardite 1T is the most important lizardite polytype in serpentized ultramafic rocks. The serpentine assemblage in Type 1B kimberlite includes chrysotile 2M, lizardite 10 and minor amounts of antigorite 10. Brucite was not detected in any samples.

Scanning and transmission electron micrographs of Ham serpentines are given in Plates 9a to 11b. Plates 9a and 9b illustrate the coarse bladed lizardite found in retrograde Type 3 pseudomorphic assemblages and spherulitic lizardite found in prograde Type 5 and Type 7 non-pseudomorphic assemblages, respectively. Plates 10a and 10b illustrate chrysotile found in carbonate emulsion textures with spherulitic serpentine (not shown) and chrysotile found with coarse bladed lizardite in hourglass structures and mesh rims and mesh centres. Plates 11a and 11b illustrate the bladed form of antigorite in the kimberlite groundmass and in carbonate emulsion textures partially replaced by spherulitic lizardite during Type 5 prograde serpentinization.

Nomenclature for serpentine textures and serpentinization events described below are indicated by " " ,and are from studies by Wicks et al.(1977), Wicks and Whittaker (1977) and Wicks and Plant (1979).

No further references will be made to these authors.

### Serpentine Petrography in the Ham Kimberlite

Primary serpentine occurs in round, discrete, mildly corroded, pale-yellow emulsion textures (max. 0.5 mm diameter) in unaltered Type 1A kimberlite.

Secondary serpentine which formed during "retrograde Type 3" serpentinization and which occurs predominantly in Type 1A and Type 2 kimberlite was recrystallized during prograde "Type 5 and Type 7" serpentinization in Type 1B kimberlite.

### Type 1A Kimberlite

The partial to complete "retrograde Type 3" pseudomorphism of olivine microphenocrysts and megacrysts is characterized by the extensive development of light-yellow, magnetite-free, lizardite + chrysolite "mesh centres and rims" in the former variety of olivine and the progressive development of coarse bladed lizardite in hourglass structures and fine-grained "multi-layer" lizardite + magnetite in veins after "mesh centres and rims" of lizardite + chrysotile + magnetite, in the latter variety of olivine. Serpentine in grain cores and vein margins adjacent to fresh megacryst olivine is brown-yellow changing to orange-yellow at grain margins and at vein cores.

Magnetite (Table 22) may form in irregular masses and as tiny, discrete crystals and fine dustings at grain margins and in vein cores, respectively. Minor recrystallization of serpentine in olivine to spherulitic lizardite is evident along grain fractures and on grain margins.

Primary and secondary serpentine in mono- and bi-mineralic, round to cusp-shaped emulsion textures (the latter replacing carbonate) consists of medium-grained, pale yellow "spherulitic" lizardite. Margins of emulsion textures are commonly corroded and intergrown with pale yellow, optically unidentifiable groundmass serpentine. Scarce antigorite blades occur in the groundmass.

#### Type 1B Kimberlite

The initial serpentinization of Type 1B kimberlite progressed in a manner similar to that described above. Petrographic examination reveals that the "pseudomorphic" serpentinization was preceded by carbonate metasomatism and the development of partial carbonate pseudomorphs after olivine. Petrographic evidence suggests that carbonate metasomatism culminated with the renewal of serpentinization ("prograde Type 5 and Type 7") characterized by the

TABLE 22  
 Representative Analyses of Opaques in Serpentine

	1	2	3	4
TiO <sub>2</sub>	0.93	1.06	0.12	0.12
Al <sub>2</sub> O <sub>3</sub>	0.01	0.33	0.00	0.01
Cr <sub>2</sub> O <sub>3</sub>	0.02	0.00	0.00	0.00
FeO*	83.30	81.04	86.07	87.65
MnO	1.06	0.91	2.17	2.29
MgO	1.65	2.85	0.81	0.58
TOTAL **	86.97	86.19	89.17	90.65

\*Total iron as FeO

\*\*Low totals are due to Fe calculated as FeO, and the small size of the crystals precluding accurate analysis

partial replacement of carbonate pseudomorphs and the recrystallization of relict pseudomorphic "mesh and hourglass" textured serpentine by non-pseudomorphic, pale yellow, "spherulitic" lizardite. Opaques (Table 22) occasionally occur as irregular masses in olivine grain cores and commonly form coarse crystals in the groundmass adjacent to serpentine pseudomorphs.

Monomineralic and bimineralic emulsion textures composed of pale yellow, "spherulitic" lizardite and "spherulitic" lizardite + antigorite + chrysotile replacing carbonate are commonly developed. A similar assemblage occurs in the kimberlite groundmass.

#### Type 2 Kimberlite

Olivine microphenocrysts are incipiently to wholly pseudomorphed by brown-yellow, coarse bladed lizardite in "hourglass" structures and "multi-layer" lizardite in "mesh rims and in veins". Serpentinization of megacryst olivines is confined to the development of medium-grained, brown-yellow to orange-yellow "multi-layer" lizardite veins and scarce lizardite "mesh rims". Opaques are commonly developed in the groundmass adjacent to wholly pseudomorphed olivines or in vein partings associated with orange-yellow serpentine. Partial opaque pseudomorphs (Table 22) after olivine are scarce.

"Spherulitic", pale yellow to pale brown lizardite associated with scarce antigorite blades incipiently replaces carbonate in bimineralic emulsion textures and occurs with optically unidentified pale yellow serpentine in the groundmass.

#### GEOCHEMICAL STUDIES

It is evident from representative analyses in Table 23 that Ham serpentines vary considerably in their silica, iron and magnesium contents and that oxide totals are below ideal. These fluctuations are due to the complex nature of serpentinization in the Ham kimberlite. Low totals occur because of weathering of samples.

Petrographic evidence, Table 23 and Figure 27 indicate that Ham serpentines exhibit a systematic variation in Fe/Fe+Mg ratios dependent upon the extent and nature of serpentinization. Figure 27c illustrates that during pervasive, "retrograde" "pseudomorphic" serpentinization of olivine, pseudomorphism is accompanied by the ejection of iron from the serpentine with its subsequent concentration in grain margins as magnetite (Table 22) crystals or in irregular, spongy masses. Consequently, the Fe/Fe+Mg ratios demonstrate a bimodal distribution between

TABLE 23

 Representative Analysis of Ham Serpentine  
 Type 1A Kimberlite

	1(c)	2(m)	3(c)	4(m)	5(c)	6(m)	7(m)	8	9	10	11
SiO <sub>2</sub>	40.41	39.80	38.71	39.85	39.41	38.31	37.31	38.62	41.32	40.67	40.45
TiO <sub>2</sub>	0.01	0.03	0.00	0.01	0.00	0.03	0.03	0.03	0.00	0.00	0.00
Al <sub>2</sub> O <sub>3</sub>	0.32	0.41	0.70	0.57	0.58	0.46	0.55	0.34	0.74	1.07	1.13
Cr <sub>2</sub> O <sub>3</sub>	0.06	0.06	0.12	0.06	0.12	0.09	0.14	0.09	0.00	0.04	0.02
FeO*	6.32	8.59	5.73	7.23	5.91	7.98	7.60	7.96	2.09	2.45	4.20
MgO	35.93	33.85	36.85	35.60	37.13	33.95	30.98	33.73	40.23	39.23	37.65
CaO	0.09	0.07	0.07	0.07	0.05	0.06	0.18	0.11	0.01	0.05	0.02
MnO	0.07	0.08	0.06	0.10	0.11	0.08	0.11	0.13	0.00	0.00	0.01
NiO	0.18	0.11	0.05	0.30	0.11	0.19	0.51	0.36	0.00	0.00	0.02
Na <sub>2</sub> O	0.00	0.00	0.00	0.00	0.00	0.00	0.00	0.00	0.00	0.00	0.10
K <sub>2</sub> O	0.07	0.05	0.01	0.04	0.01	0.01	0.06	0.01	0.01	0.00	0.00
TOTAL	83.46	84.05	82.30	83.83	83.43	81.16	77.47	81.58	84.40	83.51	83.60
Fe/Fe+Mg	0.089	0.124	0.080	0.102	0.082	0.116	0.121	0.116	0.028	0.033	0.059

## Type 1B Kimberlite

	1(c)	2(m)	3(c)	4(m)	5(c)	6(m)	7(m)	8	9	10	11
SiO <sub>2</sub>	40.91	41.47	38.38	38.84	39.20	38.43	36.58	41.39	39.96	41.25	40.42
TiO <sub>2</sub>	0.04	0.07	0.03	0.12	0.09	0.38	0.34	0.10	0.14	0.03	0.04
Al <sub>2</sub> O <sub>3</sub>	0.36	0.36	0.47	0.71	0.46	1.25	1.92	0.50	0.64	0.37	0.58
Cr <sub>2</sub> O <sub>3</sub>	0.07	0.05	0.08	0.03	0.00	0.06	0.00	0.02	0.02	0.04	0.02
FeO*	2.65	2.76	6.05	7.20	6.20	5.78	6.36	5.57	6.46	3.91	2.53
MgO	38.02	38.11	35.45	33.68	34.01	36.27	35.01	36.82	34.43	37.94	37.14
CaO	0.09	0.17	0.13	0.16	0.25	0.11	0.10	0.10	0.10	0.08	0.08
MnO	0.01	0.03	0.09	0.08	0.09	0.11	0.14	0.08	0.14	0.05	0.00
NiO	0.09	0.05	0.36	0.29	0.04	0.17	0.14	0.05	0.04	0.08	0.02
Na <sub>2</sub> O	0.04	0.00	0.00	0.00	0.00	0.09	0.05	0.05	0.00	0.14	0.02
K <sub>2</sub> O	0.00	0.00	0.00	0.00	0.01	0.07	0.04	0.04	0.00	0.02	0.01
TOTAL	82.28	83.07	81.04	81.11	80.35	82.72	80.68	84.72	81.93	83.91	80.86
Fe/Fe+Mg	0.037	0.39	0.087	0.106	0.093	0.080	0.092	0.078	0.095	0.054	0.037

\*Total iron as FeO

Analyses 1-4 - Large olivine pseudomorph

Analyses 5-7 - Small olivine pseudomorph

Analyses 8-11- Emulsion texture

(c) - core, (m) - margin

TABLE 23 (cont'd)

Representative Analyses of Ham Serpentine  
Type 2 Kimberlite

	1	2	3	4	5(c)	6(m)	7	8	9	10	11
SiO <sub>2</sub>	40.80	41.56	42.11	39.58	40.16	41.83	42.19	41.55	39.79	40.25	42.65
TiO <sub>2</sub>	0.00	0.07	0.13	0.04	0.12	0.21	0.07	0.21	0.05	0.00	0.01
Al <sub>2</sub> O <sub>3</sub>	0.00	0.14	0.55	0.00	0.14	2.63	0.73	3.08	0.21	0.15	0.21
Cr <sub>2</sub> O <sub>3</sub>	0.06	0.01	0.04	0.11	0.07	0.06	0.00	0.00	0.07	0.04	0.04
FeO*	6.55	7.14	8.06	12.78	7.04	6.65	5.53	7.64	12.23	11.13	9.11
MgO	33.63	32.68	33.79	29.70	32.64	32.03	36.41	33.70	30.55	30.96	33.17
CaO	0.10	0.15	0.07	0.45	0.47	0.54	0.13	0.27	0.31	0.25	0.22
MnO	0.04	0.06	0.11	0.09	0.02	0.08	0.31	0.04	0.14	0.15	0.14
NiO	0.38	0.43	0.07	0.63	0.34	0.08	0.02	0.00	0.57	0.60	0.32
Na <sub>2</sub> O	0.00	0.00	0.00	0.00	0.05	0.00	0.00	0.00	0.00	0.00	0.00
K <sub>2</sub> O	0.00	0.00	0.02	0.00	0.00	0.02	0.07	0.04	0.00	0.02	0.02
TOTAL	81.56	82.24	84.95	83.38	81.05	84.13	85.46	86.53	83.92	83.55	85.89
Fe/Fe+Mg	0.098	0.109	0.118	0.241	0.108	0.104	0.075	0.113	0.183	0.168	0.133

\* Total iron as FeO

Analyses 1-3 - Large olivine, grain margin (Anal. 1 - adjacent to fresh olivine, Anal. 3 - grain margin)

Analyses 4-6 - Small olivine pseudomorphs

Analyses 7-8 - Emulsion textures

Analyses 9-11 - Vein serpentine (Anal. 9 - vein core, Anal. 11 vein margin adjacent to fresh olivine)

(c) - core, (m) - margin

grain cores and margins. A similar scenario is suggested by the bimodal distribution of Fe/Fe+Mg ratios in serpentine veins (Figure 27a) where iron is concentrated in vein partings away from fresh olivine. Because serpentinization of olivine in Type 2 kimberlite (Figure 27a) is only incipiently developed, the bimodal distribution of Fe/Fe+Mg ratios characteristic of pseudomorphism in olivines has not occurred. The unimodal distribution of Fe/Fe+Mg ratios in Type 1B kimberlite olivines (Figure 27b), combined with petrographic evidence suggests that prograde recrystallization of pseudomorphic serpentine homogenizes the distribution of iron within the serpentine. Figure 27 also suggests that serpentines in emulsion textures were originally relatively low iron serpentines or that they were very susceptible to iron expulsion. The systematic variation of iron and magnesium in Figure 28 supports these conclusions.

Golightly and Arancibia (1979) and Wicks and Plant (1979) show that the silica content of serpentines, and particularly the  $\text{SiO}_2/\text{MgO}$  ratio may be used to determine the extent and nature of serpentinization. Examination of Figures 1 and 6 of Wicks and Plant (1979) indicate that serpentines formed during incipient "retrograde Type 3" serpentinization are silica-rich and

FIGURE 27  
Histogram of Fe/Fe+Mg Ratios for Ham Serpentine

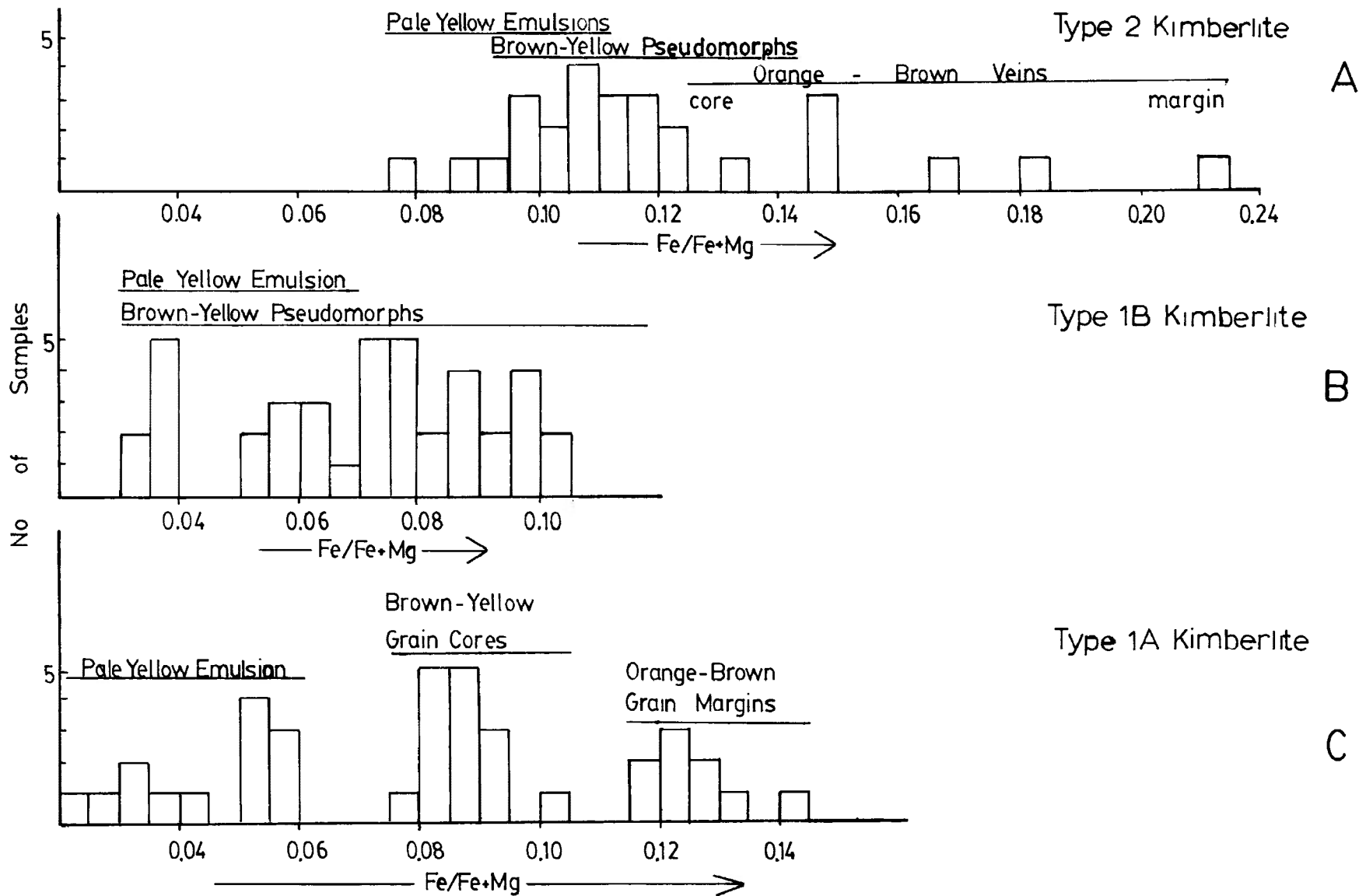
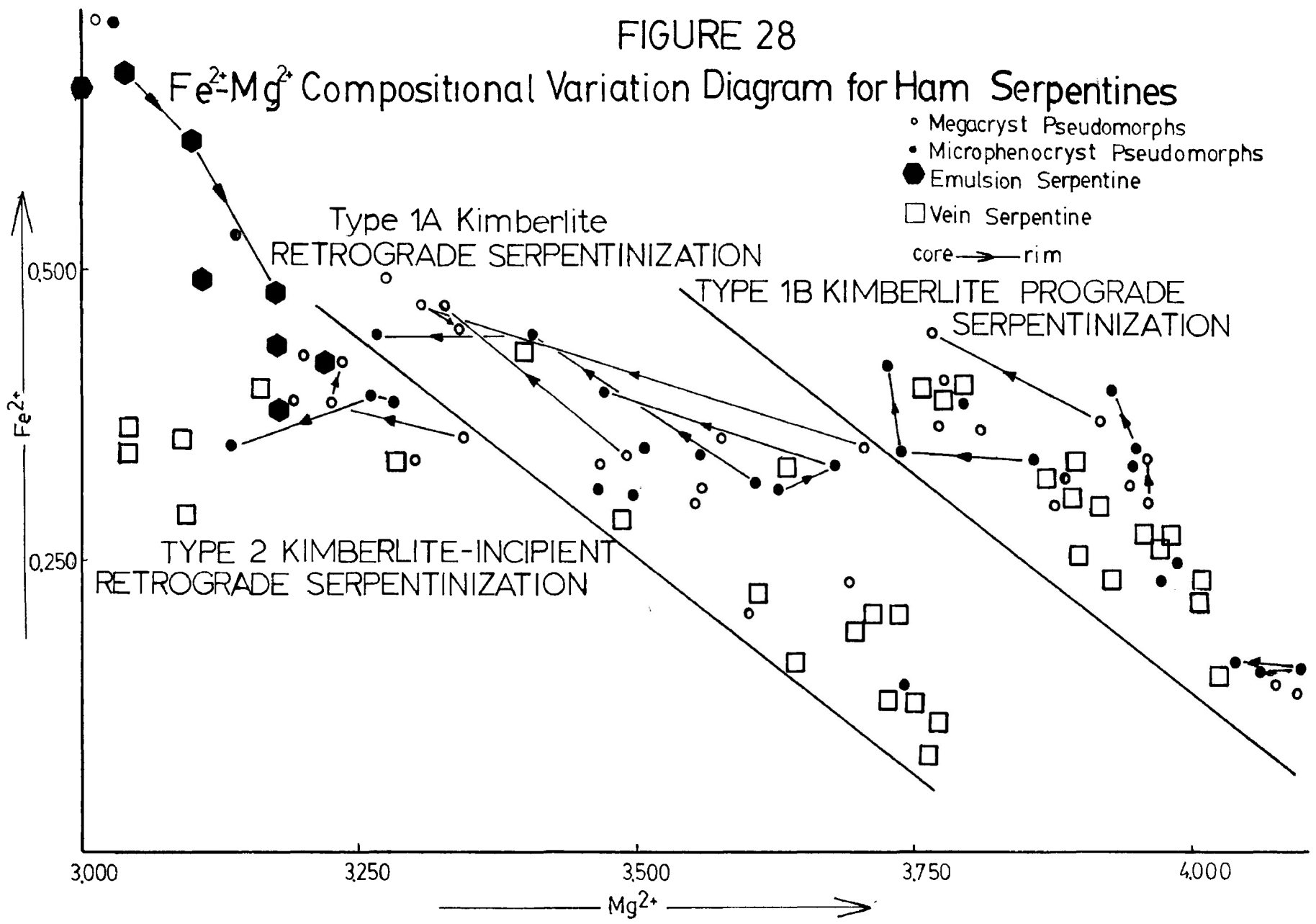


FIGURE 28

Fe<sup>2+</sup>-Mg<sup>2+</sup> Compositional Variation Diagram for Ham Serpentines



plot above the 50% SiO<sub>2</sub> compositional join on a SiO<sub>2</sub>-MgO-FeO plot. In contrast, serpentines (lizardites) analyzed in regions of advanced "Type 3" serpentinization plot below the Mg<sub>3</sub>-Fe<sub>3</sub><sup>2+</sup> join (Wicks and Plant 1979). Serpentines (antigorite and chrysotile assemblages + lizardite) formed during "prograde Type 5 and Type 7" serpentinization plot between the Fe<sub>3</sub><sup>2+</sup>-Mg<sub>3</sub> and Fe<sub>2</sub><sup>3+</sup>-Mg<sub>3</sub> joins and between the Fe<sub>2</sub><sup>3+</sup>-Mg<sub>3</sub> and 50% SiO<sub>2</sub> joins, respectively. In addition, Wicks and Plant (1979) report an expulsion of iron during serpentinization. Data for Ham serpentines (Figure 29, SiO<sub>2</sub>-MgO-FeO) reflect such a serpentinization history in which incipient "Type 3" serpentine assemblages developed in Type 2 kimberlite are silica-rich compared to serpentine assemblages in Type 1A kimberlite which is characterized by a more thorough serpentinization. During "prograde Type 5 and Type 7" serpentinization, the silica content of Ham serpentines (Type 1B kimberlite) increased.

#### Serpentines in Kimberlite

A comparison of Tables 23 and 24 with Table 6 of Smith et al. (1978) reveal that kimberlite serpentines are iron-rich, and contain highly variable SiO<sub>2</sub> and MgO contents. Minor element contents are usually low

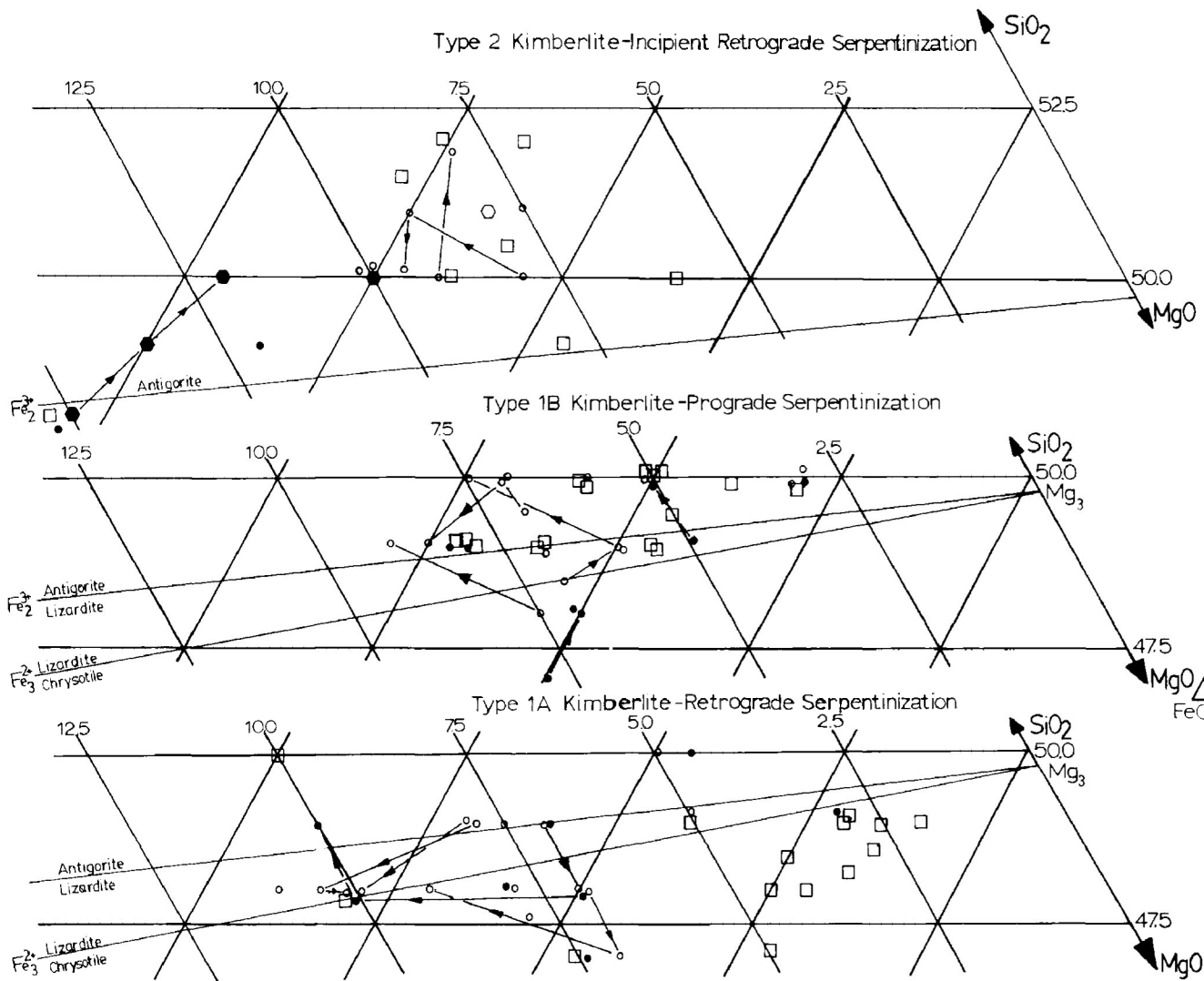
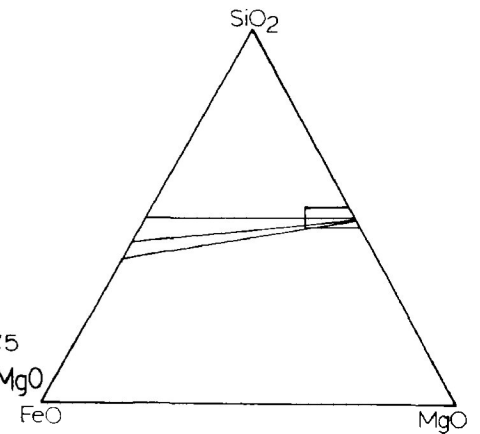


FIGURE 29  
 SiO<sub>2</sub>-MgO-FeO Ternary Plot  
 for  
 Ham Serpentine

- Olivine megacryst pseudomorphs
- Olivine microphenocryst pseudomorphs
- Vein serpentine
- Emulsion serpentine
- core → rim



Serpentine fields from Wicks and Plant (1979).

(<1.0 wt. %), although alumina and chromium may exceed 1.00 weight percent. This is strikingly in contrast with Deer et al.'s (1972) serpentine analyses (Table 3, Anal. 19-21, synthesized serpentines) and supports conclusions of Wicks and Plant (1979), Dungan (1979) and Cressey (1979) who indicate that the chemical composition of pseudomorphic serpentines is similar to that of the primary minerals.

Very little is known of serpentine mineralogy in kimberlite. McCallum (1975) reports single and double layer lizardites and chrysotile with minor Al-serpentine, fibrous chrysotile, antigorite and serpophite in variably altered kimberlites. Emeleus and Andrews (1975) and Pasteris (1980) describe kimberlites with primary and secondary serpentine, in fibrous and structureless patches (serpophite), in "pools" and as antigorite and talc pseudomorphs after olivine, respectively. Mitchell (1978a) reports groundmass serpentine, serpentine pseudomorphs after olivine and serpentine + calcite in emulsion textures. Although serpophite was not observed in the Ham kimberlite, lizardite 10, 1T, chrysotile 2M and antigorite 10 were found. The varied mineralogical assemblages of serpentines in kimberlite indicate that the alteration and serpentinization of kimberlite is a

TABLE 24  
Representative Analyses of Somerset Island and South African Serpentine

	1	2	3	4	5	6	7	8	9	10	11
SiO <sub>2</sub>	39.61	39.96	39.24	37.41	42.10	39.98	40.05	39.99	37.28	44.13	42.01
TiO <sub>2</sub>	0.03	0.00	0.00	0.00	0.01	0.02	0.36	0.00	0.05	0.11	0.13
Al <sub>2</sub> O <sub>3</sub>	0.23	0.53	0.70	0.20	0.22	0.48	0.30	0.95	7.53	0.42	0.47
Cr <sub>2</sub> O <sub>3</sub>	0.00	0.00	0.05	0.00	0.03	0.02	0.07	0.05	0.12	0.03	0.00
FeO*	5.77	3.60	3.50	5.36	3.02	3.58	11.60	5.33	10.90	12.88	14.36
MgO	39.18	39.09	39.84	40.20	38.50	41.68	33.50	38.11	30.21	26.83	27.66
MnO	0.09	0.05	0.08	0.00	0.06	0.12	0.03	0.11	0.13	0.20	0.24
CaO	0.09	0.08	0.09	0.15	0.10	0.05	0.04	0.63	0.48	0.30	0.34
NiO	0.00	0.00	1.02	0.28	0.00	0.00	0.09	0.44	0.46	0.04	0.52
Na <sub>2</sub> O	0.00	0.13	0.21	0.00	0.00	0.09	0.00	0.00	0.00	0.05	0.03
K <sub>2</sub> O	-	-	-	-	-	-	-	0.00	0.04	0.10	0.10
TOTAL	85.00	83.44	84.73	83.60	84.04	86.02	86.04	85.61	87.20	85.09	85.87

\*Total iron as FeO

Analyses 1-2 - Groundmass Serpentine )  
 Analysis 3 - Olivine pseudomorph ) - Elwin Bay kimberlite,  
 Analysis 4 - Blue pleochroic serpentine after olivine ) Mitchell (1978a)  
 Analyses 5-6 - Serpentine in calcite ocelli )  
 Analyses 7 - Isotropic Serpentine - South-west Greenland Kimberlite, Emeleus and Andrews (1975)

TABLE 24 (cont'd)

	12	13	14	15	16	17	18	19	20	21
SiO <sub>2</sub>	45.18	41.81	43.43	42.66	40.21	42.57	42.42	41.83	41.25	43.60
TiO <sub>2</sub>	0.00	0.11	0.02	0.00	0.10	0.02	0.05	0.02	0.02	0.01
Al <sub>2</sub> O <sub>3</sub>	0.00	2.96	0.81	0.29	5.57	0.97	0.74	0.30	0.54	1.03
Cr <sub>2</sub> O <sub>3</sub>	0.03	0.09	0.01	0.00	0.00	0.13	0.02	-	-	0.02
FeO*	7.25	6.67	5.08	3.82	8.92	1.07	4.32	1.37	1.41	1.71
MgO	31.84	37.87	38.45	37.11	29.36	39.46	37.26	41.39	41.84	41.00
MnO	0.15	0.12	0.05	0.09	0.07	0.23	0.20	0.04	0.07	0.04
CaO	0.17	0.29	0.33	0.31	0.61	0.77	0.12	Tr	0.02	0.05
NiO	0.08	0.06	0.00	0.01	0.00	0.00	0.19	-	-	0.16
Na <sub>2</sub> O	0.02	0.20	0.00	0.00	0.05	0.09	-	-	-	0.01
K <sub>2</sub> O	0.01	0.06	0.01	0.00	0.49	0.05	-	-	-	0.03
TOTAL	84.73	90.24	88.19	84.29	85.38	85.36	85.32	84.95	85.15	87.66

\*Total iron as FeO

Analyses 8-12 - Serpentine after olivine - De Beers Pipe, Pasteris (1980)

Analyses 13-16 - Serpentine in "pods" - De Beers Pipe, Pasteris (1980)

Analysis 17 - Serpentine after olivine - Lattavarum (L1) kimberlite - Akella et al. (1979)

Analysis 18 - Serpentine after olivine - Lattavarum (L2) kimberlite - Akella et al. (1979)

Analyses 19-21 - Chrysotile, lizardite, antigorite, Deer et al. (1977)

complex process.

Carbonatization and Serpentinization of the Ham Kimberlite

Petrographic evidence indicates that fluid movement within the Ham diatreme subsequent to "retrograde" serpentinization was responsible for "prograde" serpentine mineral assemblages and carbonatization of the Ham kimberlite. Figure 30 and the following sequence of events summarize the nature of the carbonatization and serpentinization of the Ham diatreme. Stages 1 and 2 are common to both the diatreme and dyke. Stages 3, 4 and 5 occur solely in the diatreme and are associated with the development of Type 1B kimberlite.

- 1) Pseudomorphic "Type 3 retrograde" serpentinization of olivine and the groundmass by deuteric fluids.
- 2) Incipient to extensive replacement of carbonate emulsion textures by MgO-rich deuteric fluids (possibly contemporaneous with (1)).
- 3) Initiation of restricted carbonate metasomatism leading to the development of carbonate pseudomorphs after olivine and euhedral carbonate crystals in serpentinized olivine, (Fluids paths are illustrated in Figure 30).



- 4) Waning of carbonate metasomatism and the introduction of "hotter," metasomatic fluids leading to the development of non-pseudomorphic, "Type 5, prograde" serpentine assemblages in olivines, emulsion textures and in the kimberlite groundmass. This event recrystallizes "Type 3 retrograde" serpentines and partially replaces carbonate emulsion textures and carbonate pseudomorphs after olivine.
- 5) Incipient development of "Type 7 prograde" serpentine assemblages.

Petrographic, geophysical and field studies indicate that Type 1B kimberlite is a highly altered equivalent of Type 1A kimberlite and that if a fluidized, fissure type intrusive event occurring at the intersection of several fracture sets (Chapter 1 and 10) is accepted for the origin of the Ham Diatrema, then the origin of the serpentizing and carbonatizing fluids responsible for the alteration of Type 1A kimberlite is coincident with the intersection of these fracture sets (compare Figure 30 and 31).

CHAPTER 8MISCELLANEOUS MINERALSPerovskite

Perovskite occurs as tiny (<0.01 mm diameter), rounded crystals and thin (<0.001 mm thick), blocky, euhedral overgrowths on post-fluidization spinels in the Ham kimberlite. Petrographic examination indicates that perovskite was unaffected during alteration of the kimberlite groundmass.

Mechanical and heavy liquid separation was used to obtain a perovskite concentrate for the preliminary investigation of its rare earth element (REE) content. Examination of perovskite concentrates indicate they were contaminated by up to 50 percent by spinel grains. REE determination was undertaken by instrumental neutron activation analysis using a hyperpure germanium crystal.

Table 25 compares the REE (La, Ce, Sm, Tb) and Ta, Hf, Co, Sc, Th, and Fe contents of Ham perovskite with perovskite from the Lqhobong (Boctor and Boyd, 1980), Green Mountain (Boctor and Meyer, 1979) and Yakution (Ilupin et al, 1971) kimberlites and with the REE abundance of kimberlite from India (Paul et al. 1975), Greenland (Paul et al. 1976) and Zambia

(Paul et al.1975).

Inspection of Table 25 reveals that perovskites from kimberlites (this study, Boctor and Boyd 1980, Boctor and Meyer 1979) have similar patterns of enrichment in LREE. The magnitude of enrichment in LREE is similar in Green Mountain (Boctor and Meyer 1979) and Lighobong(Boctor and Boyd 1980) perovskite but is up to 20 times greater than that found in Ham perovskite. The lower REE abundances of Ham perovskite reflect the contaminated nature of sample concentrates by rare earth poor spinel grains. The extremely high iron contents of Ham perovskites relative to others is also an indication of the spinel contamination.

Table 25 is considered to indicate that perovskite may be the major source of REE in host kimberlites.

### Ruby

Eleven, tiny (<0.10 mm across), transparent, candy-pink, angular rubies were handpicked from heavy mineral concentrates from Type 1A kimberlite in the Ham diatreme. The angular nature of these very small crystals indicate they may have been larger prior to grinding and mineral separation.

Representative analysis and x-ray diffraction data for Ham rubies are presented in Table 26 (Analyses

TABLE 25  
REE CONTENT OF HAM PEROVSKITE\*

Element	Ham Dyke	Ham Diatreme	Liqhobong Kimberlite	Green Mountain	Yakutian Kimberlite	Indian Kimberlite	Greenland Kimberlite	Zambian Kimberlite
La	2120	959	5489	15451	22	139	128	128
Ce	69	1987	20736	33073	41	381	233	231
Sm	230	299	3198	n.r.	3	40	14	18
Tb	3	5	174	n.r.	n.r.	2.7	0.90	1.4
REE	2422	3250	44204**	65958**	91**	574**	478**	499**
Ta	506	343	n.r.	238	n.r.	15	10	10
Hf	191	122	n.r.	n.r.	n.r.	30	4	6
Co	78	44	n.r.	n.r.	n.r.	n.r.	n.r.	n.r.
Sc	8	6	n.r.	n.r.	n.r.	n.r.	n.r.	n.r.
Th	168	63	n.r.	n.r.	n.r.	199	15	15
Fe	87463	35807	9440	19352	n.r.	n.r.	n.r.	n.r.

\* - in ppm

\*\* - Total REE may include abundances for Pr, Nd, Pm, Eu, Gd, Dy, Ho, Er, Tm, Yb, and Lu

n.r.- not recorded

Ham Diatreme and Dyke - (Perovskite), this study

Liqhobong Kimberlite - (Perovskite), Boctor and Boyd (1980)

Green Mountain Kimberlite - (Perovskite), Boctor and Meyer (1979)

Yakutian Kimberlite - (Perovskite), Ilupin et al (1971)

Indian Kimberlite - (Rock), Paulet al. (1975)

Greenland Kimberlite - (Rock), Paulet al. (1976)

Zambian Kimberlite - (Rock), Paulet al. (1976)

1-10) and in Table 27, respectively.

Table 26 indicates that Ham rubies contain between 94.21 and 99.44 weight percent alumina, 1.52 to 4.05 weight percent chromium (Av. 2.43 wt. %) and up to 0.38 weight percent iron (Av. 0.27 wt. %) and 0.39 weight percent silica (Av. .25 wt. %). Other elements constitute less than 0.16 weight percent of individual analyses.

It is evident from Table 26 that Ham rubies are compositionally similar to secondary corundum found in alkremites (pyrope-garnet, Cr-poor spinel xenoliths, Padovani and Tracey 1981) and to rubies found as inclusions in diamond (Meyer, Person. Comm.) in both major ( $\text{Al}_2\text{O}_3$ ) and minor ( $\text{Cr}_2\text{O}_3$ , FeO,  $\text{SiO}_2$ ) element contents. Rubies from metamorphic terrains in the upper crust (Anal. 12, 14-19) are compositionally different and contain higher  $\text{Al}_2\text{O}_3$  (97.50-99.80 wt. %) and lower  $\text{Cr}_2\text{O}_3$  (0.14-1.71 wt. %), FeO (0.00-0.03 wt. %) and  $\text{SiO}_2$  (0.00 to 0.54 wt. %) contents.

X-ray diffraction data from Ham rubies and synthetic corundum (99.9 wt. %  $\text{Al}_2\text{O}_3$ , <0.1 wt. % K, Na, Si, <0.01 wt. % Ca, Cu, Fe, Mg, Pb and <0.001 wt. % B, Cr, Li, Mn, Ni) are compared in Table 27. Inspection of Table 27 reveals that the substitution

TABLE 26  
Representative Analyses of Ham Rubies

	1	2	3	4	5	6	7	8	9	10
SiO <sub>2</sub>	0.29	0.17	0.23	0.27	0.20	0.26	0.28	0.39	0.23	0.21
TiO <sub>2</sub>	0.00	0.00	0.00	0.00	0.00	0.00	0.00	0.00	0.00	0.00
Al <sub>2</sub> O <sub>3</sub>	97.56	98.44	95.90	97.50	96.86	96.00	96.54	94.21	96.03	97.54
Cr <sub>2</sub> O <sub>3</sub>	1.52	2.12	2.72	1.89	2.41	2.87	2.02	4.05	2.64	2.09
FeO*	0.23	0.24	0.27	0.22	0.27	0.28	0.25	0.38	0.29	0.29
MnO	0.00	0.00	0.01	0.02	0.04	0.02	0.01	0.06	0.01	0.04
MgO	0.02	0.01	0.02	0.03	0.02	0.02	0.02	0.02	0.02	0.01
CaO	0.01	0.01	0.00	0.00	0.00	0.01	0.00	0.02	0.01	0.02
Na <sub>2</sub> O	0.04	0.13	0.00	0.03	0.01	0.08	0.04	0.00	0.06	0.03
K <sub>2</sub> O	0.01	0.01	0.01	0.00	0.01	0.01	0.01	0.00	0.01	0.03
NiO	0.00	0.00	0.00	0.00	0.00	0.00	0.00	0.00	0.00	0.00
TOTAL	99.68	101.13	99.16	99.96	99.82	99.55	99.17	99.13	99.30	100.26

\*Total iron as FeO

	11	12	13	14	15	16	17	18	19	20	21	22
SiO <sub>2</sub>	0.29	0.18	0.00			0.14	0.54			0.00	0.16	0.03
TiO <sub>2</sub>	0.09	0.00	0.00	0.00	0.00	0.00	0.00	-	-	0.05	0.53	0.09
Al <sub>2</sub> O <sub>3</sub>	97.40	99.30	96.18	99.80	98.98	98.80	97.50	99.80	98.98	100.00	100.00	100.00
Cr <sub>2</sub> O <sub>3</sub>	1.30	0.96	3.24	0.14	0.17	0.95	1.81	0.14	0.17	0.03	0.00	0.10
FeO*	0.22	0.00	0.64	0.01	0.01	0.01	0.03	0.01	0.01	0.14	0.53	0.18
MgO	0.13	0.02	0.19	0.00	0.00	0.02	0.03	-	-	0.02	0.13	0.00
CaO	0.02	0.02	0.00	-	-	-	-	-	-	0.00	0.00	0.04
MnO	0.01	0.04	0.00	0.00	0.00	0.00	0.00	-	-	0.00	0.00	0.00
NiO	0.00	0.01	0.00	-	-	0.00	0.00	-	-	-	-	-
Na <sub>2</sub> O	-	0.00	-	-	-	-	-	-	-	0.00	-	-
K <sub>2</sub> O	-	0.01	-	-	-	-	-	-	-	0.00	-	-
TOTAL	99.46	100.54	100.25	99.95	99.16	99.92	99.91	99.95	99.16	100.24	101.35	100.44

\*Total iron as FeO

- Analysis 11 - Ruby inclusion in diamond - H.O.A. Meyer (Person. Comm.)  
 Analysis 12 - Burmese Ruby - H.O.A. Meyer (Person. Comm.)  
 Analysis 13 - Corundum from xenolith - Padavoni and Tracey (1981), (Alkremite)  
 Analyses 14-15 - Corundum from marble - (Kashmir), Okrusch, (1976)  
 Analyses 16-17 - Natural Ruby - Deer, Howie and Zussman, (1977)  
 Analyses 18-19 - Natural Ruby - Bank and Okrusch, (1976)  
 Analysis 20 - Corundum from corundum eclogite, (Av. 4 analyses) - Shee, (1978)  
 Analysis 21 - Corundum from grosopydite xenolith (Ak1/130) - Shee (1978)  
 Analysis 22 - Corundum from garnet-graphite-clinopyroxene rock (Alkremite ?) - Ak1/62 - Shee, (1978)

of chromium (up to 4.05 wt. %) for alumina (Finger and Hazen 1977) into the trigonal structure of corundum does not significantly distort the crystal lattice. Line spacings (d-spacings) of Ham ruby and synthetic ruby agree to within 0.15 percent (mean, stand. dev. = 0.17). Lattice parameters  $a_o$  and  $c_o$  (Table 27) were calculated using equation (1) (Finger and Hazen 1977) below and the (410) and (006) reflections, respectively.

$$\sin^2 \theta = \frac{\lambda}{3a_o^2} \cdot (h^2 + hk + k^2) + \frac{\lambda}{4c_o^2} l^2 \quad \text{Equation (1)}$$

Equations (2) and (3) derived by Finger and Hazen (1977) can be used as a geobarometer using the unit-cell parameters  $a_o$  and  $c_o$ .

$$a_o = 4.7607 - 8.1 \times 10^{-4} P + 3.5 \times 10^{-6} P^2 \quad \text{Equation (2)}$$

and

$$c_o = 12.995 - 1.3 \times 10^{-3} P - 1.1 \times 10^{-5} P^2 \quad \text{Equation (3)}$$

(P = kbars)

From equation (1),  $a_o = 4.752A^\circ$  and  $C_o = 12.989 A^\circ$ . Solving equations (2) and (3), pressures of formation are 3.33 and 3.57 kilobars, respectively. The difference in pressure results from systematic deviations during pressure calibration of a best-fit curve for experimental runs (Finger and Hazen 1977).

TABLE 27  
X-ray Diffraction Data for Ham Ruby

Ham		Synthetic Corundum (<0.001 Cr)		Ham		Synthetic	
d Spacing	I/I <sub>o</sub>	d Spacing		d Spacing		d Spacing	
3.466	75	3.479		0.906	4	0.9052	
2.556	90	2.552		0.898	8	0.8991	
2.376	40	2.379		0.881	<1	0.8884	
2.165	<1	2.165		0.880	<1	with 11 lines	
2.083	100	2.085		0.871	<1	to 0.7931	
1.968	2	1.964		0.869	<1		
1.737	45	1.740		0.849	5		
1.600	80	1.601		0.845	<1		
1.542	4	1.546		0.825	3		
1.514	6	1.514		0.818	<1		
1.512	8	1.510		0.815	<1		
1.405	30	1.404		0.813	<1		
1.376	50	1.374		0.802	<1		
1.339	2	1.337		0.779	<1		
1.274	4	1.276		0.777	<1		
1.240	16	1.239		0.775	<1		
1.236	8	1.2343		$a_o$ calc using (410) reflection=4.752 $c_o$ calc using (006) reflection=12.989 $c = c_o/a_o = 2.7333$			
1.184	8	1.1898		$a_o$ syn = 4.758 $c_o$ syn = 12.991 $c_{syn} = c/a_o = 2.7303$			
1.158	<1	1.1600		Ham Ruby - <sup>o</sup> this study			
1.145	6	1.1470		Synthetic Ruby - from Selected			
1.138	2	1.1382		Powder Diffraction Data for Minerals,			
1.126	6	1.1255		1st Edition. Joint Committee on Powder			
1.125	4	1.1246		Diffraction Standards, (1974)			
1.100	8	1.0988					
1.081	4	1.0831					
1.079	8	1.0781					
1.040	14	1.0426					
1.019	2	1.0175					
0.998	12	0.9976					
0.986	<1	0.9857					
0.982	4	0.9819					
0.943	<1	0.9431					
0.941	<1	0.9413					
0.936	4	0.9345					
0.917	4	0.9178					
0.909	14	0.9076					

CONCLUSIONS

The paragenesis of Ham ruby is uncertain. Ruby has been found as inclusions in diamond (Meyer, person. comm.), as secondary minerals in corundum eclogite (Sobolev 1964, Shee 1978) and alkremite xenoliths (Padovini and Tracey 1981), in plagioclase-bearing metaperidotites (Lasnier 1974) and in various upper crustal metamorphic terrains (Wells 1956, Bank and Okrusch 1976, Piat 1974, Gubelin 1974, Bank 1978 and Males 1976) characterized by alkaline intrusions in metalimestones.

Chemical data (Cr contents) suggests that Ham rubies did not crystallize in an upper crustal metamorphic-metasomatic terrain but may have formed as a secondary mineral in ultra-basic xenoliths. Pressure of formation calculations limit this reaction to less than 3.5 to 4.5 kbars depth, although at present, it cannot be ascertained whether or not ruby is a quenched mineral phase from a magma or a re-equilibrated phase in a mantle mineral assemblage. The paucity of requisite mantle host rocks for Ham rubies (corundum eclogite, alkremite or plagioclase-bearing peridotite) suggest that either they were fragmented during the fluidized intrusion of the kimberlite or that an

alternate source for the rubies must be found.

This is the second documented occurrence of ruby in Canada, the other being ruby in stream concentrates of the Tulameen River in British Columbia (Sinkankas 1959).

CHAPTER 9HEAVY MINERAL DISPERSION PATTERN

The study of the dispersion pattern of kimberlite indicator minerals (pyrope-garnet, chrome-diopside and magnesian-ilmenite) is the foremost exploration technique utilized during the initial stages of exploration for kimberlite intrusions. Satterly (1971), Lampietti and Sutherland (1978) and Mosig (1979) discuss stream sampling procedures in the U.S.S.R., South Africa, South America and Australia. Satterly (1971) emphasizes the relative successes of stream sampling procedures in glaciated versus unglaciated terrains. Lee (1965) and Brown et al. (1967) summarize glacio-focus and basal till sampling programs conducted in the James Bay Lowlands in Northern Ontario. The former technique led to the discovery of a one metre wide kimberlite dyke in the Upper Canada Mine, Gauthier Township, Ontario.

The stream dispersion pattern of pyrope-garnet and chrome-diopside derived from the Ham diatrema was studied to evaluate the effectiveness of stream sediment sampling as an exploration tool in the Canadian Arctic.

The Ham diatrema (Map 1) is located at the headwaters of the Cunningham River. The diatrema (Map 1D) is exposed on a gently sloping plain dissected by several small tributaries of the Cunningham River. Stream sediment transport is greatest during late May to early July when spring runoff is at a peak.

One kilogram stream sediment samples were taken at 100 metre intervals (Map 1D) downslope from the Ham diatrema (stream gradient 40m/km) to the Cunningham River. The sampling interval in the Cunningham River (average stream gradient 6.6 m/km) was increased to approximately 0.5 kilometres (Map 1C) and subsequently to approximately 1.5 kilometres. Thirty-two samples were collected; no preconcentration was attempted in the field.

In the laboratory, samples were screened to remove rock fragments larger than 9 mesh. The reject was inspected for ultra-basic xenolith fragments, pyrope and chrome-diopside megacrysts and kimberlite rock fragments. Minus 9 mesh sand grains were washed in dilute hydrochloric acid to remove calcareous cement. Heavy mineral separation was performed using tetrabromoethane (sp. gr. 2.65) and

methylene iodide (sp. gr. 3.33). Mineral concentrates were dried and weighed, then inspected to determine the number of pyrope and chrome-diopside grains present. Grain morphologies and textures were also noted. Identification criteria for kimberlite indicator minerals are briefly outlined in Table 28. The number of grains in each concentrate was normalized to a 10 gram concentrate weight to compensate for the variable sample sizes. Table 29 presents raw and normalized grain counts. Table 30 outlines the grain morphology and records the persistence of kimberlite minerals and associated rock fragments. Table 31 presents the results of a similar study in Australia (Mosig 1979) and in the U.S.S.R. (Bobrievich 1957).

The results of this study presented in Table 29 reveal that the number of pyrope and chrome-diopside grains decreases with distance across the outwash plain downslope from the Ham diatreme and within a small stream draining the outwash plain, (samples D-1 to D-19). Morphologies and textures of grains (Table 30) proximal to the Ham kimberlite are similar to those encountered at random sample sites over the Ham diatreme. Grains demonstrate a broad size range and may be angular to rounded and frosted. These characteristics were developed during the

TABLE 28  
Distinctive Characteristics of Heavy Minerals

Mineral	Distinguishing Characteristics
Pyrope	Mauve, Red, Wine-Red, kelyphite rim may be present
Almandine	Orange, candy pink, no kelyphite
Chrome-diopside	Chrome green colour, prismatic crystals, rightangle cleavage - fibrous alteration with white clay present

TABLE 29  
Concentrations of Indicator Minerals in Stream Sediment Samples

Sample N <sup>o</sup> /*	Concentrate Weight (gr)	No. of Pyrope Garnet	No. of Chrome- diopside	No. of Pyropes/ 10 gr.	No. of Chrome- Diopside/10 gr.
D-1	3.6361	350	197	962	542
D-2	5.8366	265	176	454	302
D-3	2.2316	147	165	659	739
D-4	0.4618	51	109	1104	2360
D-5	0.6196	2	6	32	97
D-6	0.6234	3	1	48	16
D-7	0.2250	4	2	178	89
D-8	0.7622	13	0	171	0
D-9	0.2875	5	2	174	70
D-10	0.2038	1	3	49	147
D-11	0.1787	3	0	168	0
D-12	0.2213	1	2	45	90
D-13	0.1538	2	0	130	0
D-14	1.0753	15	2	139	19
D-15	0.2465	1	3	41	122
D-16	0.2829	4	0	141	0
D-17	0.4309	2	3	46	70
D-18	0.1281	3	0	234	0
D-19	0.2477	1	4	40	160
D-20	0.4376	0	0	0	0
D-21	0.2650	0	0	0	0
D-22	0.9077	1	0	11	0
D-23	0.9954	2	0	20	0
D-24	0.3362	2	0	59	0
D-25	0.7376	1	1	14	14
D-26	0.6414	2	2	31	31
D-27	0.3058	2	1	65	33
D-28	0.9747	1	1	10	10
D-29	0.3737	0	7	0	187
D-30	0.6894	3	4	44	58
D-31	0.6744	4	3	59	44
D-32	0.1707	0	18	0	1054

\*See location maps 1c and 1d.

fluidized intrusion of the Ham diatrema. Changes in grain morphology and texture by detrital processes are not evident immediately downslope from the diatrema (up to 500m), however, grains become sub-angular to sub-rounded at distances greater than 500 metres downslope from the kimberlite. Table 30 indicates that the degree of rounding and frosting increases with distance from the source kimberlite.

Within the Cunningham River system sampling results do not show a decrease in the number of pyrope and chrome-diopside grains with distance from the source area. Table 29 indicates that several areas along the Cunningham River are points of anomalous grain concentration or grain absence. Table 30 indicates that most grains are angular to sub-angular which suggests only a short transport distance. However, Mosig (1979), Satterly (1971) Lampietti and Sutherland (1979), Brown et al.(1967) and Lee (1968) suggest grain morphology and texture can be correlated with distance from the source area and that grain roundness and frosting should be enhanced with increased distance from the source area. Also, Mosig (1979) (Table 31) and Lampietti and Sutherland (1979) indicate chrome-diopside may not be present in stream sediment beyond 4 kilometres from the source

TABLE 30  
Grain Morphologies of Indicator Minerals in Stream Sediment Samples

Distance from HAM DIATREME	Pyrope	Chrome-Diopside	Comments
Proximate <500m	-angular to rounded and fractured grains - some frosted - no kelyphite rims even in samples taken directly over kimberlite	-angular to subangular with minor frosting, quickly developing subangular to sub-rounded grain morphology-some grains may appear rotten	- abundant subangular-rounded ol, scarce phlogopite and bleached opx; kimberlite frags absent >400m; xenoliths present in stream up to 250m
500m-1km	-few angular grains- most grains subangular to sub-rounded and frosted	-subangular to sub-rounded grains - often frosted and rotten (fibrous with clay alteration)	- 10% cl, well-rounded to 700m - scarce >700m - phlogopite - opx absent
1km-1.5km	-angular to subangular and frosted	-few angular - most grains subangular to rounded, frosted and rotten (fibrous with clay alteration)	- scarce rounded olivine
1.5km-2.0km	-angular to subangular and frosted	-subangular and subangular to sub-rounded and rotten (fibrous with clay alteration)	- very scarce olivine
2.0-5.0km	-angular - not frosted	-very scarce - subangular to sub-rounded and rotten (fibrous with clay alteration)	- very scarce olivine
5.0-10km	-angular to subangular and frosted	-abundant angular grains and subangular to sub-rounded and rotten (fibrous with clay alteration) grains	- olivine absent
10-16km	-angular to rounded and frosted	-abundant sub-angular and sub-rounded grains, sub-rounded grains may be rotten (fibrous with clay alteration)	- olivine absent

area. The angularity of pyrope grains and the angularity and anomalous concentration of chrome-diopside grains within the Cunningham River suggest that a second source of kimberlite minerals may be present. The area surrounding the Ham dyke (Maps 1C and 1D) is also drained by a tributary of the Cunningham River. Inspection of Table 29 reveals that this stream bears pyrope and chrome-diopside grains but not in sufficient quantity to produce the anomalous concentrations noted above.

An alternate source is mantle-derived garnet-lherzolite xenoliths which may have been transported downstream from the Ham diatreme and disaggregated during transportation; this latter source is the more probable.

The effects of weathering on the persistence of a mineral species within a fluvial system has important implications for exploration in various climates. Tables 30 and 31 present grain textures and morphologies and persistence criteria of kimberlite indicator minerals in various climates. A comparison of these tables reveals that pyrope-garnet and magnesian-ilmenite are the most persistent kimberlite indicator minerals in detrital sediments regardless of climate. Within sub-Arctic (Bobrievich 1957) and

TABLE 31  
Comparison of Grain Morphologies and Mineral Abundances with Data from Russian  
and Australian Kimberlites

Mineral	Morphology of mineral up to 4 km from kimberlite	Mosig (1979)		Bobrievich (1957)
		Morphology of mineral greater than 4 km from kimberlite		Mineral Persistence
Phlogopite	Grains become bleached with increasing travel	Absent		N.R.
Chrome-diopside	Grains lose green colour intensity with increasing travel. Grains rapidly become finer with travel and decompose.	Generally absent		Absent >30 km
Composite-grains (e.g. nodules)	Grains usually found only close by kimberlite.	Absent		N.R.
Picroilmenite	Grains lose leucoxene rims with travel.	Grains become worn.		persist >125 km
Pyrope	Kelyphite removed with increasing travel.	Frosted surface to grains.		90-125 km
Olivine	Grains rapidly decompose to nontronite clay. Rarely found unaltered.	Absent		N.R.

N.R. - not reported

Arctic (this study) climates, chrome-diopside persists up to 30 kilometres and at least 16 kilometres, respectively, from the source kimberlite, although Mosig (1979) reports that chrome-diopside is generally absent greater than 4 kilometres from the source kimberlite in sub-tropical, semi-arid climates. The effect of disaggregation of garnet-lherzolite xenoliths within the fluvial system has not been considered previously. Olivines, in Arctic, sub-arid climates (this study) persist up to 5.0 kilometres from the source kimberlite. In contrast, olivine rapidly decomposes to nontronite clay and is absent greater than 4 kilometres from the source in sub-tropical semi-arid climates (Mosig 1979). Phlogopite is physically and chemically unstable regardless of climate and is broken down within several hundred metres of the source kimberlite.

In conclusion, heavy mineral dispersion patterns are a useful exploration tool for kimberlite prospecting in a semi-arid, Arctic climate. The appearance of easily weathered minerals such as olivine and phlogopite and kimberlite rock fragments is a useful indicator of proximity to the source kimberlite. However, grain morphologies and textures of persistent indicator minerals are not a particularly useful

indicator of proximaty to source if heavy mineral concentrates are contaminated with minerals derived from locally disaggregated mantle-derived xenoliths.

CHAPTER 10MAGNETIC EXPRESSION AND STRUCTURAL CONTROL

Prospecting for kimberlites has traditionally involved studying the mineral dispersion pattern of kimberlite indicator minerals, (Chapter 9). Recently, geophysical prospecting has become the foremost exploration technique once a target area of about 25 km<sup>2</sup> in size (Janse 1975) has been delineated by other methods. Gerryts (1967), Macnee (1979) and Nixon (1979) reviewed the application of current airborne and ground geophysical methods including magnetic, electro-magnetic, gravity, resistivity, induced-polarization, seismic and scintillometer surveys to exploration for kimberlite. Magnetic surveys, which are relatively easy to perform and interpret, are the most useful airborne and ground exploration technique, although recently, electro-magnetic surveys (Macnee 1979) conducted in conjunction with magnetic surveys have been gaining prominence.

Gerryts (1967) reports that magnetic anomalies associated with kimberlite intrusions range up to 7000 gammas, although some Sierra Leone, Tanzanian and South African kimberlites have no magnetic expression. It is important to note that the magnetic

susceptibility contrast between rock types determines the strength of the anomaly. If the magnetic susceptibilities are similar, then no anomaly will be determined. Gerryts (1967) reports that typical magnetic susceptibilities for Yakutian kimberlites range from  $1 \times 10^{-4}$  to  $6 \times 10^{-3}$  c.g.s. Magnetic susceptibilities of Lesotho kimberlites range from  $6 \times 10^{-3}$  to  $5 \times 10^{-5}$  c.g.s. (Nixon 1979).

Kimberlite usually contains 5 to 10 percent iron as iron oxides and magnesian ilmenite. In fresh kimberlite, magnetite and magnesian ilmenite will dominate the magnetic response and produce a detectable anomaly. In contrast, deep weathering and deuteric alteration will alter the magnetite iron oxides to non-magnetic iron oxides in the top portion of the kimberlite, resulting in a deepening of the magnetic source and a retardation of the magnetic response. If retardation is large enough and the magnetic contrast between the kimberlite and host rock is not high, a detectable anomaly may not be found.

A detailed ground magnetometer survey was conducted over the Ham diatreme and dyke utilizing a Sharpe MF-1 Fluxgate magnetometer. The total magnetic field was determined; accuracy was  $\pm 200$  gammas. Readings were recorded at 15 metre intervals along

grid lines spaced 15 metres apart. Intermediate readings were recorded if changes in the magnetic response exceeded 200 gammas. Diurnal variation was not calculated because pre-survey, mid-survey and post-survey base station readings differed by less than 100 gammas. Regional background was determined to be 6800 gammas. Magnetic susceptibility was not determined. The susceptibility of the host rock limestone is essentially zero.

The magnetic expression (Figure 31a) of the Ham diatrema and dyke correlate closely with areas of kimberlite regolith. The magnetic expression of the Ham diatrema is a complex bell-shaped anomaly approximately 255 metres long and up to 165 metres wide. The anomaly consists of highly magnetic flanks (peak response 2400 gammas) enclosing a weakly magnetic core characterized by several magnetic depressions and a magnetic response of approximately 600 gammas above background. Figures 31 and 32 illustrate the close relationship between the magnitude of magnetic response and the type of kimberlite present. The highly magnetic (>1200 gammas) flanks of the anomaly correspond to Type 1A kimberlite regolith. Magnetic anomalies less than 1200 gammas are coincident with Type 1B and Type 2 kimberlite regolith.

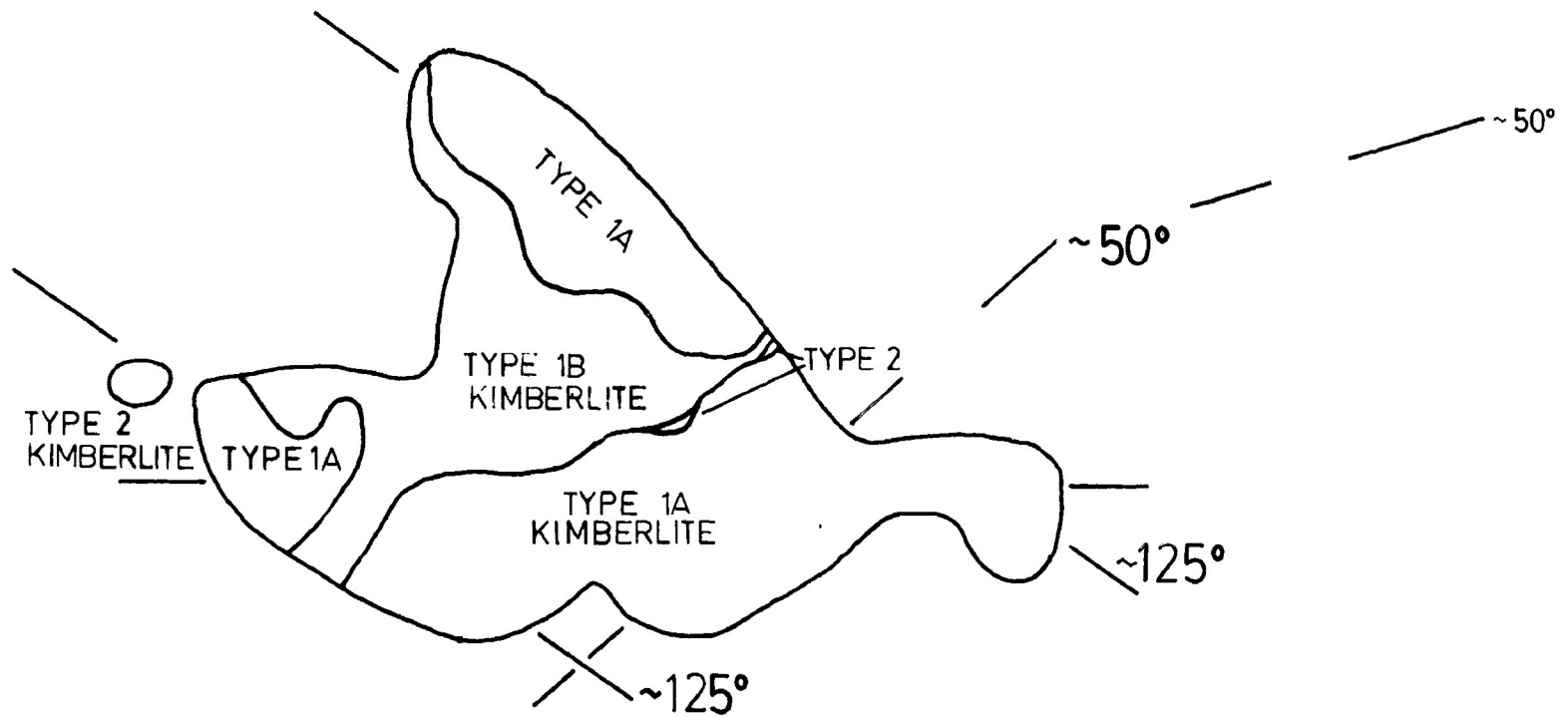


FIGURE 31B  
GEOLOGICAL AND STRUCTURAL INTERPRETATION OF THE HAM KIMBERLITE

FIGURE 31A  
MAGNETIC EXPRESSION OF THE HAM KIMBERLITE

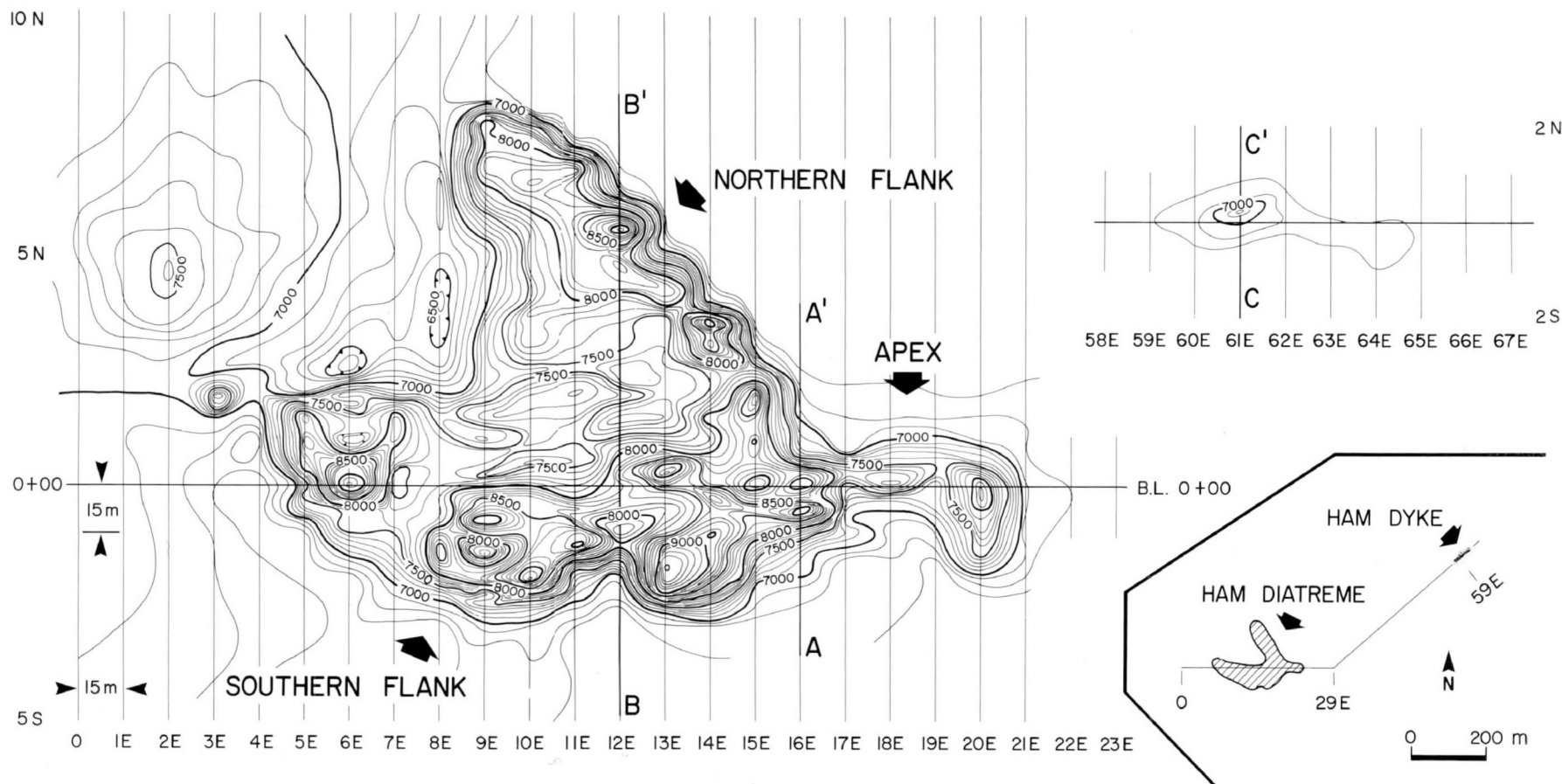
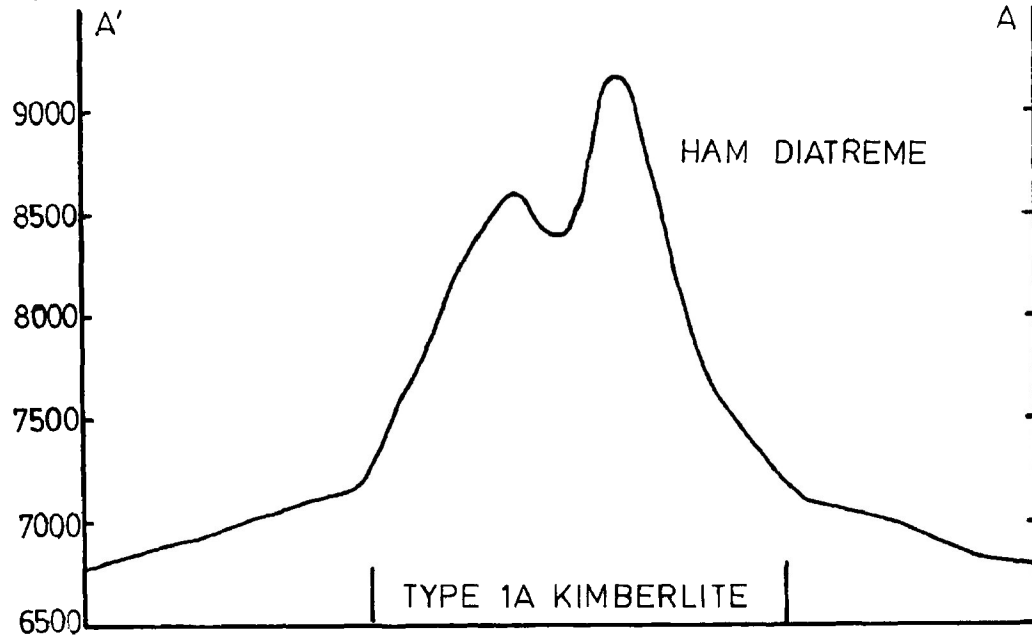
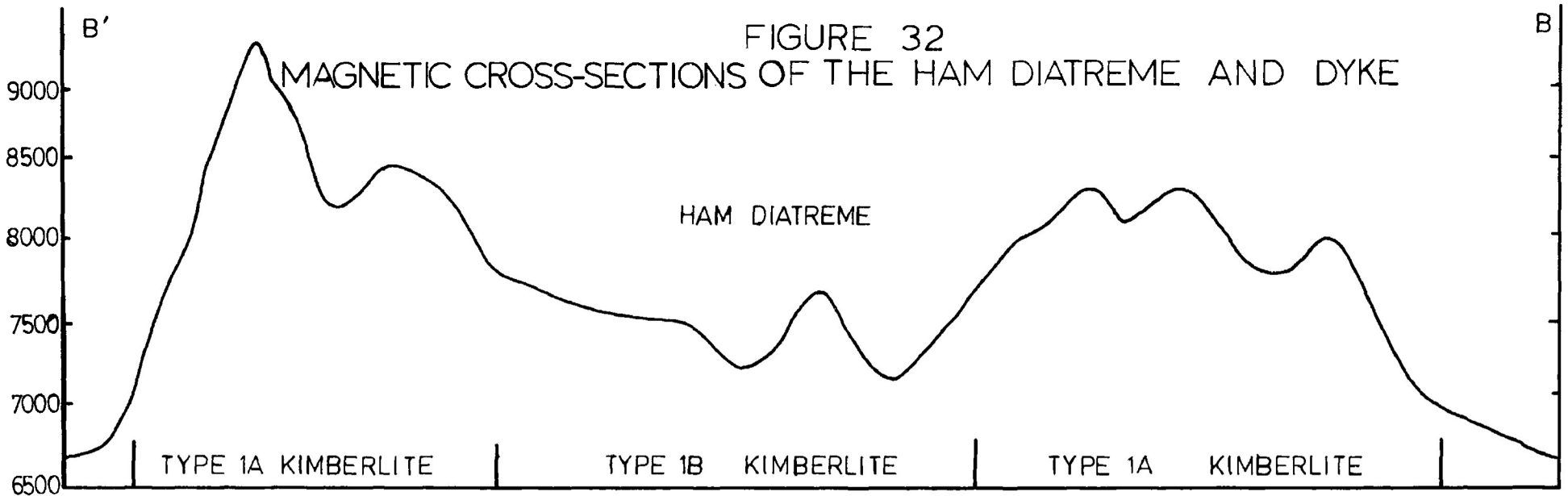
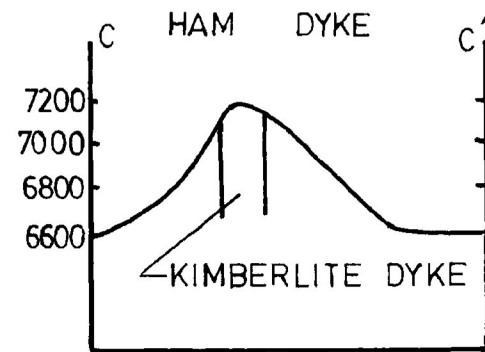


FIGURE 32

MAGNETIC CROSS-SECTIONS OF THE HAM DIATREME AND DYKE



A - see figure 31a for location of sections  
- readings in gammas



15m

Chapter 7 has shown that Type 1A kimberlite is relatively unaltered compared to Type 1B kimberlite and that Type 1A kimberlite contains substantially more opaque minerals as primary iron-bearing oxides in the groundmass and as secondary magnetite associated with the serpentinization of olivine compared to Type 1B and Type 2 kimberlite.

The magnetic anomaly associated with the Ham dyke is roughly lenticular and approximately 75 metres long and up to 10 metres wide. The peak magnetic anomaly (400 gammas) is associated with the heaviest concentration of kimberlite regolith. Lesser concentrations of kimberlite regolith located to the east are coincident with a lower magnetic anomaly (100 gammas). The decrease in concentration of kimberlite regolith and the lower magnitude of the magnetic anomaly along strike to the east suggest a narrowing of the kimberlite dyke or a deepening of the magnetic source. Figures 31 and 32 suggest that the Ham dyke is a vertically dipping lenticular body of kimberlite with a maximum thickness of 2 metres and strike length of approximately 60 metres. The uniform nature of the anomaly and petrographic examination suggest that the Ham dyke is a single unaltered intrusion.

Inspection of Figure 31a and Figures 2, 6 and 7 of Mitchell (1975) suggest that the complex magnetic expression of the Ham diatreme is similar to that of the petrographically complex Peuyuk kimberlite. Mitchell (1975) attributes the peak magnetic anomalies associated with Peuyuk Phase B kimberlite to a higher magnetite content than Peuyuk Phase A and C kimberlite. The uniform magnetic expression of the Ham dyke is similar to that of the Korvik and Selatiavak (Mitchell 1975) kimberlites and the Inugpasugsuk and Ameyersuk kimberlite (Batty Bay, Somerset Island, Figure 33, this study). These kimberlites have a relatively uniform distribution of magnetite and are not complexly altered.

Table 32 indicates that the magnetic intensities of all the Somerset Island kimberlites are similar (400-2400 gammas) although that of the Inugpasugsuk (Figure 33) intrusion is anomalously high (10,000 gamms) compared to other Somerset Island, American, Russian and South African kimberlites. This can be attributed to an unusually high concentration of magnetite in the groundmass of this intrusion.

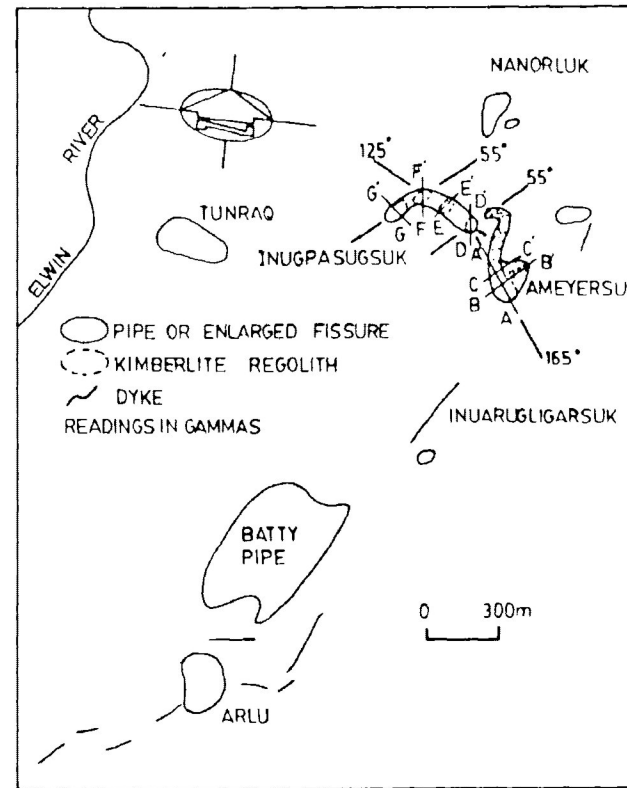
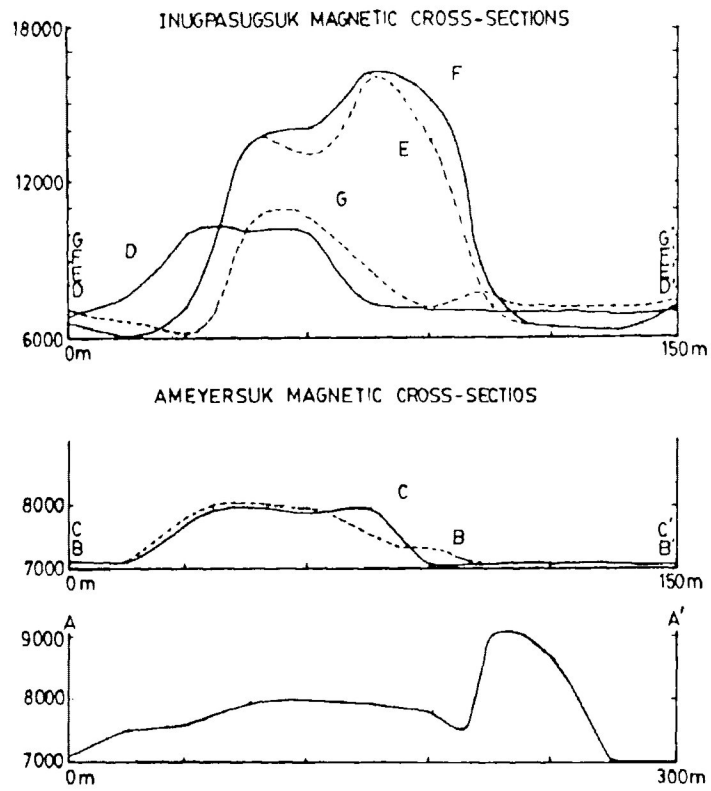
#### STRUCTURAL CONTROL

The pattern of the magnetic expression of a kimberlite in areas of limited outcrop and where

TABLE 32  
 Magnetic Intensities of Somerset Island, American,  
 South African and Russian Kimberlites

Kimberlite	Maximum Anomaly	Source
Ham Diatrema	2400 gammas	This study )
Ham Dyke	400	This study )
Korvik	800	Mitchell, 1975) Somerset
Selatiavak	600	Mitchell, 1975) Island
Peuyuk	1800	Mitchell, 1975)
Amayersuk	2000	This study )
Inugpasugsuk	10000	This study )
Batty Pipe	5600	This study )
Pipe 205	2000	Macnee (1979) )
Kolo	6000	Nixon (1979) (Vertical)South field) )African
Mali	1550	Gerryts (1967) )
Prairie Creek	900	Bolivar and Brookins (1977)
Russian Kimberlite	3000-5000	Gerryts (1967)

FIGURE 33  
MAGNETIC CROSS-SECTIONS OF THE BATTY BAY KIMBERLITES



solifluction of regolith occurs is often useful in determining the subcrop pattern of the kimberlite and relating its emplacement to structural features.

Inspection of Figures 31 and 33 indicate that the emplacement of the Ham diatreme and dyke may have been structurally controlled by the same structural elements which controlled the emplacement of other Somerset Island kimberlites. Mitchell (1975) interprets the Central Somerset Island kimberlites to be enlarged fissure fillings formed by a series of fluidized intrusions (blows) along fracture sets. These were developed in the Paleozoic sediments deposited on the flanks of the Boothia Uplift. These fractures are a reflection of structures developed in the Precambrian basement which was subject to three phases of Cornwallis folding (Brown et al. 1969). Mitchell (1975) recognizes three distinct fractures which are developed as major lineaments on airphotos and which correspond to lineaments present in exposed Boothia granulite terrains on the west coast of Somerset Island. These include approximately north-south (strike  $175^{\circ}$ ), north-east (strike  $50^{\circ}$ ) and south-east (strike  $125^{\circ}$ ) striking fracture sets. Figure 33 shows that these three fracture sets may have structurally controlled the emplacement of the Inugpasugsuk, Amayersuk and Arlu

kimberlites at Batty Bay, Somerset Island. Geophysical data (this study) and the linear distribution of the Inugpasugsuk intrusions suggest that although they are not joined at the surface, they are joined at depth and formed as a series of fluidized intrusions along pre-existing fractures striking approximately  $50^{\circ}$  and  $125^{\circ}$ .

Figures 3la and b illustrate a geological, geophysical and structural interpretation of the Ham diatreme and dyke in relation to two postulated fracture sets striking  $50^{\circ}$  and  $125^{\circ}$ . Geological reconnaissance in the Cunningham River suggests that at least two fracture sets are present in the host limestone. Although direct measurements of the strike could not be obtained, the angle between the fractures was approximately  $75^{\circ}$ . Airphoto interpretation suggests that the Ham dyke is linearly coincident with an elongate petroleum seep and formed along a fracture striking  $50^{\circ}$ . In addition, the regional drainage scheme may also be structurally controlled by fractures in the Paleozoic limestones which strike approximately north-south ( $175^{\circ}$ ) and south-east ( $125^{\circ}$ ). These postulated fracture sets and their relationship to the Ham diatreme are presented in Figures 3la and b. It is evident that the northern flank and the western portion of the southern flank of the magnetic anomaly

may have formed along parallel fractures striking approximately  $125^{\circ}$ . The eastern portion of the southern flank may have formed along a fracture striking  $50^{\circ}$ . The intersection of these two fractures at the eastern end of the anomaly is coincident with the bulk of the intrusion. Petrographic examination of the Ham kimberlite suggests that the area of the intersection of these two fractures may also have been the source of carbonate-rich deuteric fluids which invaded portions of the Ham diatreme.

In conclusion, the Ham diatreme forms a roughly bell-shaped magnetic anomaly composed of strongly magnetic flanks of unaltered kimberlite enclosing a weakly magnetic core of highly altered kimberlite. Geophysical and structural evidence suggests that the Ham diatreme formed by a series of fluidized intrusions along several intersecting fracture sets striking  $50^{\circ}$  and  $125^{\circ}$  and eventually coalesced to form a roughly bell-shaped intrusion.

The Ham dyke forms a uniformly magnetized lenticular anomaly, which, is interpreted to have formed as a single stage, unaltered intrusion along a fracture striking  $50^{\circ}$ . Geophysical reconnaissance indicates that the Ham diatreme and dyke intrusive systems are not connected.

CHAPTER 11SUMMARY

The mineralogy and petrology of the Ham diatreme and dyke indicate that they are relatively carbonate-poor kimberlites belonging to the least evolved type of Mitchell's (1979b) kimberlite clan. Pressure-temperature estimates indicate that the depth of origin of the kimberlite magma was in excess of 110-120 km (1031-1146<sup>o</sup>C) in agreement with experimental studies by Wyllie and Huang (1976) which show that similar magmas may be generated in the upper mantle at similar depths by small degrees of partial melting of garnet lherzolite. The Ham kimberlites initially crystallized garnet and olivine and scarce alumina-rich AM-chromite as pre-fluidization, liquidus phases. As the magma ascended and pressure decreased, olivine continued to crystallize but garnet ceased to be a liquidus phase; its place being taken by increasing amounts of AM-chromite which evolved from relatively Al-rich to relatively Cr-rich compositions and by later crystallizing Ti- and Cr-rich phlogopite. Complex normal and reverse zoning exhibited by olivine and phlogopite, the occurrence of post-fluidization Ti-rich phlogopite and Mg-rich olivine and the lack of reverse zoning in post-fluidization spinels indicates that

magma mixing occurred prior to the fluidized intrusion of the Ham kimberlites.

Intrusion of the Ham diatreme (Type 1A kimberlite) probably occurred as a series of repeated "blows" or fluidized intrusions along a series of intersecting fractures which eventually coalesced to form the Ham diatreme. The relatively unaltered nature of Type 2 kimberlite indicates that it was intruded subsequent to the final crystallization of Type 1A kimberlite. The single intrusion which formed the Ham dyke may or may not have been contemporaneous with the intrusion of the Ham diatreme.

Olivine, phlogopite and perovskite formed as post-fluidization liquidus phases together with spinel and later crystallizing carbonate, serpentine, and apatite. Spinel, which formed as discrete crystals or mantles upon pre-existing spinel evolved from Ti-bearing,  $\text{Fe}^{2+}$ - and Cr-rich titan-MA-chromite to Ti- $\text{Fe}^{3+}$ -rich MU-magnetite at approximately constant Fe/Fe+Mg ratios. These were later replaced by Ti-free magnetite which crystallized epitaxially upon cores of titan-MA-chromite and MU-magnetite. Atoll spinels are believed by Mitchell and Clarke (1976) to have formed by extensive resorption of early spinels by later crystal-liquid interaction. This process was not arrested in

the Ham diatreme prior to the extensive resorption of MU-magnetite and titan-MA-chromite. In contrast, the persistence of atoll spinel in the Ham dyke indicates that this kimberlite was fully crystallized before extensive spinel resorption could occur. As post-fluidization crystallization proceeded, late stage volatile-rich fluids separated as immiscible carbonate-rich liquids (to crystallize later as emulsion textures). Olivine, mica, spinel and apatite ceased to be liquidus phases and the serpentine-carbonate groundmass eventually crystallized. Late stage residual fluids partially chloritized phlogopite and initiated the retrograde serpentinization of olivine in the Ham diatreme and dyke. Subsequent degassing of structurally lower portions of the Ham diatreme released carbonate-rich fluids which ascended along the conduit formed by the intersection of feeder dykes to the Ham diatreme. These fluids were responsible for the prograde serpentinization and carbonatization of the Ham diatreme and for the formation of Type 1B kimberlite from Type 1A kimberlite. Petrographic studies show that olivines were initially replaced by carbonate and subsequently were replaced by non-pseudomorphic prograde serpentine mineral assemblages which also pervaded Type 1B groundmass. The smaller volume of the Ham dyke

precluded the release of ascending fluids from lower portions of the kimberlite and its subsequent alteration.

That the proportion of xenocrystal garnets over phenocrystal garnets in the Ham diatreme is greater than in the Ham dyke where garnet phenocrysts predominate, indicates that intrusive conditions favoured the incorporation and disaggregation of xenoliths in the Ham diatreme and that petrogenetic conditions favoured the crystallization of garnet phenocrysts in the Ham dyke. A comparison of statistical and chemical petrogenetic classification methods for Ham garnets shows that multiple discriminant analysis must be used to distinguish between groups of chemically similar garnets within a paragenesis and that cluster analysis is only useful to distinguish between garnets of grossly distinct chemistry and paragenesis.

The mineralogy and petrology and chemical evolutionary path of the Ham kimberlite is similar to that of the Peuyuk (Mitchell 1975, Mitchell and Clarke 1976) kimberlite rather than to that of the micaceous Tunraq (Mitchell 1979a) or Jos (Mitchell and Meyer 1980) kimberlite. However, the differences that do exist demonstrate that each kimberlite follows a distinct chemical evolutionary trend during crystallization.

## References

- Akella, J., 1976. Garnet pyroxene equilibria in the system  $\text{CaSiO}_3\text{-MgSiO}_3\text{-Al}_2\text{O}_3$  and in natural mineral mixtures. *American Mineralogist*, 61, 589-598.
- Bank, H., 1978. Rubine aus Alipur, Mysore. *Deutsche Gemmologischen Gesellschaft. Zeitschrift*, 27, 211.
- Bank, H. and Okrusch, M., 1976. Über rubin vorkommen in Marmoren von Hunza (Pakistan). *Deutsche Geomologische. Zeitschrift*, 25, 67-85.
- Bobrievich, A. P., 1957. The diamonds of Siberia. Moscow, 158 p. reviewed in *Economic Geology*, 53, 220-221.
- Boctor, N. Z. and Boyd, F. R., 1980. Oxide minerals in the Liphobong kimberlite, Lesotho. *American Mineralogist*, 65, 631-638.
- Boctor, N. Z. and Meyer, H. O. A., 1979. Oxide and sulphide mineralogy in kimberlite from Green Mountain, Colorado. In, *Kimberlites, Diatremes and Diamonds: Their Geology, Petrology and Geochemistry* (F.R. Boyd and H. O. A. Meyer, eds), American Geophysical Union Special Paper SPO024, 161-171.
- Bolivar, S. L. and Brookins, D. G., 1979. Geophysical and Rb-Sr study of the Prairie Creek, AK kimberlite. In, *Kimberlites, Diatremes and Diamonds: Their Geology, Petrology and Geochemistry* (F.R. Boyd and H.O.A. Meyer eds), American Geophysical Union Special Paper SPO024, 289-299.
- Boyd, F. R., 1970. Garnet peridotite and the system  $\text{CaSiO}_3\text{-MgSiO}_3\text{-Al}_2\text{O}_3$ . *Mineralogical Society America Special Paper*, 3, 63-75.
- Boyd, F. R., 1973. A pyroxene geotherm. *Geochimica Cosmochimica Acta*, 37, 2533-2546.
- Boyd, F. R. and Clement, C. R., 1977. Compositional zoning of olivines in kimberlite from the DeBeers Mine, Kimberley, South Africa. *Carnegie Institute Washington, Yearbook* 76, 485-493.
- Boyd, F. R. and Dawson, J. B., 1972. Kimberlite garnets and pyroxene-ilmenite intergrowths. *Carnegie Institute Washington, Yearbook* 71, 373-378.

- Boyd, F. R. and Nixon, P. H., 1975. Origins of ultramafic nodules from some kimberlites of northern Lesotho and the Monastery Mine. *Physics Chemistry Earth*, 9, 431-454.
- Brindley, G. W. and Wan, H., 1975. Composition, structure and thermal behaviour of Ni-containing minerals in the lizardite-nepouite series. *American Mineralogist*, 60, 863-871.
- Brown, D. D., Bennett, G. and George, P. T., 1967. The source of alluvial kimberlite indicator minerals in the James Bay Lowland. Ontario Department Mines, MP7, 1-35.
- Brown, R. L., Dalziel, I.W.D. and Rust, B., 1969. The structure, metamorphism and development of the Boothia Arch, Arctic Canada. *Canadian Journal Earth Sciences*, 6, 525-534.
- Carmichael, I. S. E., 1967. The iron-titanium oxides of salic volcanic rocks and their associated ferromagnesian silicates. *Contributions Mineralogy and Petrology*, 14, 36-64.
- Carswell, D. A., 1975. Primary and secondary phlogopites and clinopyroxenes in garnet lherzolite xenoliths. *Physics Chemistry Earth*, 9, 417-429.
- Carswell, D. A., Clarke, D. B. and Mitchell, R. H. 1979. The petrology and geochemistry of ultramafic xenoliths from Pipe 200, Northern Lesotho. In, *The Mantle Sample: Inclusions in Kimberlites and Other Volcanics* (F.R. Boyd and H.O.A. Meyer, eds) American Geophysical Union Special Paper SPO024, 127-144.
- Carswell, D. A., and Gibb, F. G. F., 1980. Geothermometry of garnet lherzolite nodules with special reference to those from the kimberlites of Northern Lesotho. *Contributions Mineralogy Petrology*, 74, 403-416.
- Caruso, L. J. and Chernosky Jr., J. V., 1979. The stability of lizardite. *Canadian Mineralogist*, 17, 757-769.
- Clarke, D. B. and Mitchell, R. H., 1975. Mineralogy and petrology of the kimberlites from Somerset Island, N.W.T., Canada. *Physics Chemistry Earth*, 9, 123-136.

- Cooley, W. W. and Lohnes, P. R., 1962. Multivariate procedures for the behavioural sciences. J. Wiley and Sons, New York.
- Cressey, B. A., 1979. Electron microscopy of serpentine textures. *Canadian Mineralogist*, 17, 741-756.
- Danchin, R. V. and Wyatt, B. A., 1979. Statistical cluster analysis of garnets from kimberlites and their xenoliths. *Cambridge Kimberlite Symposium II*, 22-27.
- Dawson, J. B., 1967. A review of the geology of kimberlite. In, *Ultramafic and Related Rocks* (P.J. Wyllie ed), J. Wiley and Sons, New York, 241-251.
- Dawson, J. B. and Hawthorne, J. B., 1973. Magmatic sedimentation and carbonatite differentiation in kimberlite sills at Benfontein, South Africa. *Journal Geological Society London*, 129, 61-85.
- Dawson, J. B. and Smith, J. V., 1975. Chemistry and origin of phlogopite megacrysts in kimberlite. *Nature*, 253, 336-338.
- Dawson, J. B. and Smith, J. V., 1977. The MARID (mica-amphibole-rutile-ilmenite-diopside) suite of xenoliths in kimberlite. *Geochimica Cosmochimica Acta*, 41, 309-323.
- Dawson, J. B. and Stephens, W. F., 1975. Statistical classification of garnets from kimberlite and associated xenoliths. *Journal Geology*, 83, 589-607.
- Dawson, J. B. and Stephens, W. E., 1976. Statistical classification of garnets from kimberlite and associated xenoliths - Addendum, *Journal Geology*, 84, 495-496.
- Davidson, C. F., 1964. On diamondiferous diatremes. *Economic Geology*, 59, 1368-1380.
- Davidson, C. F., 1967. The so-called "cognate xenoliths" of kimberlite. In, *Ultramafic and Related Rocks* (P.J. Wyllie, ed), J. Wiley and Sons, New York, 342-345.
- Davis, B. T. C. and Boyd, F. R., 1966. The join  $Mg_2Si_2O_6$ - $CaMgSi_2O_6$  at 30 kb pressure and its application to pyroxenes from kimberlite. *Journal Geophysical Research*, 71, 3567-3576.

- Davis, J. C., 1973. Statistics and data analysis in geology. J. Wiley and Sons, New York.
- Deer, W. A., Howie, R. A. and Zussman, J., 1977. An introduction to the rock forming minerals. Longman, London.
- Delaney, J. S., Smith, J. V., Carswell, D. A. and Dawson, J. B., 1980. Chemistry of micas from kimberlites and xenoliths - II. Primary-and-secondary-textured micas from peridotite xenoliths. *Geochimica Cosmochimica Acta*, 44, 857-872.
- Dungan, M. A., 1979. Bastite pseudomorphs after orthopyroxene, clinopyroxene and tremolite. *Canadian Mineralogist*, 17, 729-740.
- Emeleus, C. H. and Andrews, J. R., 1975. Mineralogy and petrology of kimberlite dyke and sheet intrusions and included peridotite xenoliths from South West Greenland. *Physics Chemistry Earth*, 9, 179-197.
- Ferguson, J. and Currie, K. L., 1971. Evidence of liquid immiscibility in alkaline ultrabasic dykes at Callendar Bay, Ontario. *Journal Petrology*, 12, 561-585.
- Finger, L. W. and Hazen, R. M., 1977. Crystal structure and compressibility of ruby to 80 kbar. *Carnegie Institute Washington, Yearbook*, 76, 523-528.
- Franz, G. W. and Wyllie, P. J., 1967. Experimental studies in the system  $\text{CaO-MgO-CO}_2\text{-H}_2\text{O}$ . In, *Ultramafic and Related Rocks* (P. J. Wyllie, ed) *Inter-science*, New York, 323-326.
- Gerryts, E., 1967. Diamond prospecting by geophysical methods - a review of current practice. *Mining and Groundwater Geophysics, Geological Survey Canada, Economic Geology Report*, 26, 439-446.
- Golightly, J. P. and Arancibia, O. N., 1979. The chemical composition and infrared spectrum of nickel- and iron-substituted serpentine from a nickeliferous laterite profile, Soroaka, Indonesia. *Canadian Mineralogist*, 17, 719-728.
- Gubelin, E. J., 1974. Im tal der rubine. *Lapis*, 2, 19-26.

- Gurney, J. J., Jakob, W. R. O., and Dawson, J. B., 1979. Megacrysts from the Monastery kimberlite pipe, South Africa. In, *The Mantle Sample: Inclusions in Kimberlite and Other Volcanics* (F.R. Boyd and H.O.A. Meyer, eds), American Geophysical Union Special Paper SPO024, 227-243.
- Haggerty, S. E., 1972. Luna 16. An opaque mineral study and a systematic examination of compositional variations of spinels from Mare Fecunditatis. *Earth Planetary Science Letters*, 13, 328-352.
- Haggerty, S. E., 1973. Spinel of unique composition associated with ilmenite reaction mantles in the Lihobong kimberlite pipe, Lesotho. In, *Lesotho Kimberlites* (P.H. Nixon, ed), Lesotho National Development Corporation, Maseru, Lesotho, 149-158.
- Haggerty, S. E., 1975. The chemistry and genesis of opaque minerals in kimberlites. *Physics Chemistry Earth*, 9, 295-307.
- Haggerty, S. E., 1976. Opaque mineral oxides in terrestrial igneous rocks. In, *Oxide Minerals* (D. Rumble III, ed) Mineralogical Society America Short Course Notes, 3, Hg 101-300.
- Hearne, B. C. and Boyd, F. R., 1975. Garnet peridotite xenoliths in Montana, U.S.A., Kimberlite. *Physics Chemistry Earth*, 9, 247-255.
- Ilupin, I. P., Khomyakov, A. P., and Balashov, Yu. A., 1970. Rare-earths in accessory minerals of Yakutian kimberlite. *Akademiia Nauk S.S.S.R. Doklady*, 201, 272-274.
- Irvine, T. N., 1965. Chromian spinel as a petrogenetic indicator. Part 1, Theory. *Canadian Journal Earth Sciences*, 2, 648-672.
- Janse, A. J. A., 1975. Kimberlite and related rocks from the Nama Plateau of South-West Africa. *Physics Chemistry Earth*, 9, 81-94.
- Kim, J., 1975. Factor analysis and the construction of factor scales: Procedure factor. In, *A User's Guide to the SCSS Conversational System* (N.H. Nie, C.H. Hull, M. N. Franklin, J. G. Jenkins, K. J. Sours, M. J. Norusis and V. Beadle, eds), McGraw-Hill, New York, 457-578.

- Klecka, W. R., 1975. Discriminant analysis. In, Statistical Package for the Social Sciences, 2nd Ed. (N.H. Nie, C.H. Hull, J.G. Jenkins, K. Steinbrenner and D.H. Bent, eds), McGraw-Hill, New York, 434-462.
- Lampietti, F. M. J. and Sutherland, D., 1978. Prospecting for diamonds - some current aspects. Mining Magazine, 139, 117-123.
- Lasnier, B., 1974. Origine du corindon secondaire dans les gabbros, norites et pyroxenolites a spinelle du Pont de Lowen. Societe Geologique et Mineralogique de Bretagne, Bulletin Rennes, 6, 109-130.
- Laurent, R. and Hebert, Y., 1979. Paragenesis of serpentine assemblages in harzburgite, tectonite and dunite cumulate from the Quebec Appalachians. Canadian Mineralogist, 17, 857-888.
- Lee, H. A., 1965. Investigation of eskers for mineral exploration. Geological Survey Canada, Paper 65-14, 1-17.
- Le Maitre, R. W. E., 1968. Chemical variation within and between volcanic rock series - A statistical approach. Journal Petrology, 9, 220-252.
- Lewis, R. D., 1977. Mineralogy, petrology and geophysical aspects of the Prairie Creek kimberlite, near Murfreesboro, Arkansas. Unpubl. M.Sc. Thesis, Purdue University.
- MacGregor, I. D., 1974. The system  $MgO-Al_2O_3-SiO_2$ : solubility of  $Al_2O_3$  in enstatite for spinel and garnet peridotite compositions. American Mineralogist, 59, 110-119.
- MacGregor, I., 1979. Mafic and ultramafic xenoliths from the Kao kimberlite pipe. In, The Mantle Sample: Inclusions in Kimberlites in Other Volcanics (F.R. Boyd and H.O.A. Meyer, ed) American Geophysical Union Special Paper SPO024, 156-172.
- Macnae, J. C., 1979. Kimberlites and exploration geophysics. Geophysics, 44, 1395-1416.
- Maksimovich, Z., 1973. The isomorphous series lizardite-nepouite. International Geological Review, 17, 1035-1040.
- Males, P. A., 1976. Ruby corundum from the Harts Range, N. T., Australian Gemmologist, 12, 310-312.

- McCallum, M. E., Egglar, D. H. and Burns, L. K., 1975. Kimberlite diatremes in Northern Colorado and Southern Wyoming. *Physics Chemistry Earth*, 9, 149-162.
- Meyer, H. O. A. and Boyd, F. R., 1969. Inclusions in diamond. *Carnegie Institute Washington, Yearbook* 66, 315-320.
- Meyer, H. O. A. and Boyd, F. R., 1972. Composition and origin of crystalline inclusions in natural diamonds. *Geochimica Cosmochimica Acta*, 36, 1255-1273.
- Mitchell, R. H., 1970. Kimberlite and related rocks - a critical reappraisal. *Journal Geology*, 78, 686-704.
- Mitchell, R. H., 1973. Composition of olivine, silica activity and oxygen fugacity in kimberlites. *Lithos*, 6, 65-81.
- Mitchell, R. H., 1975. Geology, magnetic expression and structural control of the central Somerset Island Kimberlites. *Canadian Journal Earth Sciences*, 12, 757-764.
- Mitchell, R. H., 1977. Ultramafic xenoliths from the Elwin Bay kimberlite: the first Canadian paleogeotherm. *Canadian Journal Earth Sciences*, 14, 1202-1210.
- Mitchell, R. H., 1978a. Mineralogy of the Elwin Bay Kimberlite, Somerset Island, N.W.T., Canada. *American Mineralogist*, 63, 47-57.
- Mitchell, R. H., 1978b. Garnet lherzolites from Somerset Island, Canada and aspects of the nature of perturbed geotherms. *Contributions Mineralogy Petrology*, 67, 341-347.
- Mitchell, R. H., 1979a. Mineralogy of the Tunraq kimberlite, Somerset Island, N.W.T., Canada. In, *Kimberlites, Diatremes and Diamonds: Their Geology, Petrology and Geochemistry* (F.R. Boyd and H.O.A. Meyer, eds), *American Geophysical Union Special Paper* SPO024, 161-171.
- Mitchell, R. H., 1979b. The alleged kimberlite-carbonatite relationship: Additional contrary mineralogical evidence. *American Journal Science*, 279, 570-589.

- Mitchell, R. H., Carswell, D. A., and Clarke, D. B., 1980. Geological implications and validity of calculated equilibrium conditions for ultramafic xenoliths from the Pipe 200 kimberlite, Northern Lesotho. *Contributions Mineralogy Petrology*, 72, 205-217.
- Mitchell, R. H. and Clarke, D. B., 1976. Oxide and sulphide mineralogy of the Peuyuk kimberlite, Somerset Island, N.W.T., Canada. *Contributions Mineralogy Petrology*, 56, 157-172.
- Mitchell, R. H. and Fritz, P. 1973. Kimberlite from Somerset Island, District of Franklin, N.W.T., Canada. *Canadian Journal Earth Sciences*, 10, 384-393.
- Mitchell, R. H. and Meyer, H. O. A., 1980. Mineralogy of micaceous kimberlite from the Jos dyke, Somerset Island, N.W.T., Canada. *Canadian Mineralogist*, 18, 241-250.
- Mori, T. and Green, P. H., 1975. Pyroxenes in the system  $Mg_2Si_2O_6$ - $CaMgSi_2O_6$  at high pressure. *Earth Planetary Science Letters*, 26, 277-286.
- Mosig, R. W., 1979. Morphology of indicator minerals as a guide to proximity of source. In, *Kimberlites and Diamonds*, Publication No. 5, issued jointly by the Geology Department and the Extension Service, the University of Western Australia, 81-88.
- Nixon, D. H., 1979. Regional diamond exploration-theory and practice. In, *Kimberlites and Diamonds*, Publication No. 5, issued jointly by the Geology Department and the Extension Service, the University of Western Australia, 64-80.
- Nixon, P. H., and Boyd, F. R., 1973a. The discrete nodule association in kimberlite from Northern Lesotho. In, *Lesotho Kimberlites* (P.H. Nixon, ed), Lesotho National Development Corporation, Maseru, Lesotho, 67-75.
- Nixon, P. H. and Boyd, F. R., 1973b. Petrogenesis of the granular and sheared ultrabasic nodule suite in kimberlite. In *Lesotho Kimberlites* (P.H. Nixon, ed) Lesotho National Development Corporation, Maseru, Lesotho, 48-56.

- Nixon, P. H., von Knorring, O. and Rooke, J. N., 1963. Kimberlites and associated inclusions of Basutoland, a mineralogical and geochemical study. *American Mineralogist*, 48, 1090-1132.
- O'Hara, M. J., and Mercy, E. L. P., 1966. Eclogite, peridotite and pyrope from the Navajo Country, Arizona and New Mexico. *American Mineralogist*, 51, 336-352.
- O'Hara, M. J. and Schairer, J. F., 1963. The join diopside-pyrope at atmospheric pressure. *Carnegie Institute Washington, Yearbook* 62, 107-115.
- Okrusch, M., Burch, T. E., and Bank, H., 1976. Paragenesis of a corundum bearing marble at Hunza (Kashmir). *Mineralium Deposita*, 11, 278-279.
- Padovani, E. R., and Tracey, R. J., 1981. A pyrope-spinel (alkremite) xenolith from Moses Rock Dike: first known North American occurrence. *American Mineralogist*, 66, 741-745.
- Parks, J. M., 1970. Fortran IV program for Q-mode cluster analysis on distance function with printed dendrogram. *Computer contribution* 46, Kansas State Geological Survey, University of Kansas, Lawrence.
- Pasteris, J. D., 1980. Opaque oxides of the DeBeers pipe kimberlite (Kimberley, South Africa) and their petrologic significance. Unpublished Ph.D. Thesis, Yale University.
- Paul, D. K., Potts, P. J., Gibson, I. L. and Harris, P. G., 1975. Rare-earth abundances in Indian Kimberlite. *Earth Planetary Science Letters*, 25, 151-158.
- Paul, D. K., and Potts, P. J., 1976. Rare-earth abundance in kimberlite from Greenland and Zambia. *Chemical Geology*, 18, 161-167.
- Pearce, J. A., 1976. Statistical analysis of major element patterns in basalts. *Journal of Petrology*, 17, 15-43.
- Piat, D., 1974. Le rubis Himalayen d'Hunza. *Association Francaise de Gemnologie. Bulletin*, 41, 5.

- Poldervaart, A. and Hess, H. H., 1951. Pyroxenes in the crystallization of a basaltic magma. *Journal of Geology*, 59, 472-489.
- Reid, A. M., Donaldson, C. H., Dawson, J. B., Brown, R. W., and Ridley, W. J., 1975. The Igwisi Hills extrusive "kimberlites". *Physics Chemistry Earth*, 9, 199-218.
- Reid, A. M., and Hanor, J. S., 1970. Pyrope in Kimberlite. *American Mineralogist*, 55, 1374-1379.
- Reynolds, D. L., 1954. Fluidization as a geological process and its bearing on the problem of intrusive granites. *American Journal Science*, 252, 577-613.
- Satterly, J., 1971. Diamond: U.S.S.R. and North America, a target for exploration in Ontario. Ontario Department of Mines, Miscellaneous Paper 48.
- Scott, B. H. and Skinner, E. M. W., 1979. Petrography, mineral chemistry and geochemistry of kimberlite and associated lamprophyre dykes near Swartruggens, Western Transvaal, R.S.A. Cambridge Kimberlite Symposium II, 6-12.
- Shee, S. R., 1978. The mineral chemistry of xenoliths from the Orapa kimberlite pipe, Botswana. Unpublished M.Sc. Thesis, University of Cape Town, South Africa.
- Simkin, T. and Smith, J. V., 1970. Minor element distribution in olivine. *Journal Geology*, 78, 304-325.
- Sinkankas, J., 1959. Gemstones of North America. D. Van Nostrand and Co., New York.
- Smith, J. V., Breensholtz and Dawson, J. B., 1978. Chemistry of micas from kimberlites and xenoliths-I, Micaceous Kimberlites. *Geochimica Cosmochimica Acta*, 42, 959-971.
- Smith, J. V. and Dawson, J. B., 1975. Chemistry of Ti-poor spinels, ilmenites and rutiles from peridotite and eclogite xenoliths. *Physics Chemistry Earth*, 9, 309-322.
- Sobolev, N. V., 1964. Eclogite xenolith with ruby. *Akademiia Nauk. S.S.S.R., Doklady*, 157, 1382-1384.

- Stephens, W. E. and Dawson, J. B., 1977. Statistical comparison between pyroxenes from kimberlite and their associated xenoliths. *Journal Geology*, 85, 433-449.
- Selected Powder Diffraction Data for Minerals, 1st edition, 1974. Joint Committee on Powder Diffraction Studies. Publication, DBM-1-23, Swarthmore, Pennsylvania.
- Warner, R. D., and Luth, W. C., 1973. Two phase data for the join monticellite ( $\text{CaMgSiO}_4$ ) -forsterite ( $\text{Mg}_2\text{SiO}_4$ ) experimental results and numerical analysis. *American Mineralogist*, 58, 998-1008.
- Wells, A. J., 1956. Corundum from Ceylon. *Geology Magazine*, 93, 25-31.
- Wells, P. R. A., 1977. Pyroxene thermometry in simple and complex systems. *Contributions Mineralogy Petrology*, 62, 129-139.
- Whittaker, E. J. W., and Zussman, J., 1956. The characterization of serpentine minerals by x-ray diffraction, *Mineralogical Magazine*, 31, 107-126.
- Wicks, F. J. and Plant, A. G., 1979. Electron-microprobe and x-ray-microbeam studies of serpentine textures. *Canadian Mineralogist*, 17, 785-830.
- Wicks, F. J. and Whittaker, E. J. W., 1977. An idealized model for serpentine textures after olivine. *Canadian Mineralogist*, 15, 446-458.
- Wicks, F. J., Whittaker, E. J. W., and Zussman, J., 1977. Serpentine textures and serpentinization. *Canadian Mineralogist*, 15, 459-488.
- Wishart, D., 1969. Fortran II programmes for 8 methods of cluster analysis CLUSTAN I. Computer contribution 30, Kansas State Geological Survey, University of Kansas, Lawrence.
- Wood, B. J., 1977. The solubility of alumina in orthopyroxene coexisting with garnet. *Contributions Mineralogy Petrology*, 46, 1-5.
- Wood, B. J., and Banno, S., 1973. Garnet-orthopyroxene and orthopyroxene-clinopyroxene relationships in simple and complex systems. *Contributions Mineralogy Petrology*, 42, 109-124.

Wyllie, P. J., and Huang, W. L., 1976. Carbonation and melting reactions in the system  $\text{CaO-MgO-SiO}_2\text{-CO}_2$  at mantle pressure with geophysical and petrological applications. *Contributions Mineralogy Petrology*, 54, 79-107.

## APPENDIX A

## HAM DIATREME AND DYKE GARNETS

## HAM DIATREME GARNETS

SIO2	TIO2	AL2O3	CR2O3	FeO	MNO	MGO	CAO
40.69	0.06	20.07	5.17	6.91	0.50	20.76	5.18
40.61	0.00	18.91	6.68	7.26	0.43	19.30	6.16
40.44	0.00	19.49	5.70	7.67	0.60	19.26	5.97
41.22	0.00	19.81	5.46	6.94	0.52	20.41	5.23
40.84	0.15	19.20	5.86	6.98	0.26	20.61	5.49
40.71	0.09	19.03	6.58	7.26	0.43	20.25	5.23
40.60	0.00	18.17	7.35	6.77	0.39	19.55	6.56
40.93	0.21	19.67	5.07	7.28	0.29	20.58	5.03
40.79	0.00	19.10	6.54	7.26	0.47	19.61	6.92
40.65	0.68	18.37	6.21	7.17	0.34	19.76	6.42
41.36	0.14	20.92	4.24	7.67	0.50	20.37	4.95
41.25	0.24	19.70	4.77	7.22	0.38	20.46	5.19
41.49	0.28	19.71	4.95	7.26	0.33	20.79	5.29
41.41	0.19	19.97	4.74	6.92	0.24	20.62	5.10
41.03	0.27	19.86	4.96	6.83	0.43	20.76	5.21
41.33	0.35	19.91	4.87	7.06	0.50	20.91	5.22
41.41	0.13	19.58	4.98	7.22	0.41	20.67	5.28
40.55	0.33	17.99	7.21	6.70	0.31	20.08	5.79
40.80	0.00	18.84	6.52	7.28	0.53	19.77	6.43
41.03	0.28	19.83	4.83	7.43	0.41	20.71	5.19
41.46	0.26	19.81	4.96	7.14	0.25	21.09	5.22
40.83	0.43	17.85	7.20	6.94	0.45	20.21	5.99
41.17	0.25	19.80	4.98	6.99	0.43	20.63	5.20
40.95	0.49	18.07	7.03	6.99	0.30	20.28	6.26
40.87	0.00	16.94	8.91	6.58	0.38	18.86	7.77
40.89	0.37	18.14	7.18	6.88	0.33	20.16	5.92
40.15	0.20	19.93	3.94	6.58	0.39	20.22	4.94
41.08	0.18	19.72	4.88	7.12	0.34	20.54	5.29
41.32	0.09	19.87	4.68	7.08	0.38	20.35	5.29
40.59	0.46	17.92	7.27	6.98	0.37	20.27	6.14
41.13	0.11	20.04	5.01	7.01	0.29	20.76	5.26
40.71	0.22	19.05	5.91	6.79	0.29	20.41	5.84
40.94	0.17	19.84	4.67	7.07	0.37	20.90	5.14
40.52	0.48	17.98	7.12	6.76	0.33	19.91	6.19
40.76	0.50	18.15	7.14	6.93	0.35	20.48	5.86
41.02	0.41	17.91	7.15	6.85	0.41	20.34	6.15
40.74	0.22	18.88	5.83	6.99	0.29	20.30	5.57
39.89	0.05	16.71	8.48	6.31	0.33	18.95	7.66
41.04	0.00	19.01	6.07	6.88	0.36	20.57	5.76
40.52	0.27	19.24	5.84	6.89	0.26	20.38	5.75
40.31	0.35	17.94	6.96	6.72	0.35	20.02	6.12
40.96	0.34	19.61	4.88	7.28	0.49	20.61	5.36
40.98	0.21	18.91	5.57	6.87	0.40	20.52	5.73
40.28	0.36	17.83	7.13	6.75	0.32	19.74	6.11

41.22	0.12	19.08	6.09	7.05	0.37	20.42	5.71
41.17	0.25	19.05	5.81	6.74	0.37	20.52	5.86
40.47	0.53	17.95	7.05	7.03	0.32	20.14	6.08
41.13	0.20	19.69	4.86	7.08	0.35	20.39	5.17
40.46	0.34	17.90	7.04	6.62	0.43	19.88	6.04
40.95	0.32	19.21	5.94	6.77	0.34	20.24	5.72
41.07	0.47	19.74	4.73	6.71	0.22	21.14	5.36
41.07	0.42	18.08	6.96	6.78	0.29	19.84	6.12
40.52	0.47	17.88	6.97	6.68	0.34	19.98	6.02
40.82	0.22	19.32	5.70	6.68	0.39	20.45	5.70
41.06	0.23	19.97	4.65	6.97	0.43	20.69	5.34
40.55	0.42	18.20	7.03	6.84	0.39	20.05	6.15
40.71	0.13	18.35	6.36	6.66	0.24	20.35	5.35
40.61	1.04	17.85	6.63	6.76	0.43	20.15	6.51
40.53	0.49	17.94	7.09	6.71	0.25	19.98	6.04
41.27	0.31	21.63	2.26	7.44	0.34	21.23	4.62
40.58	0.24	18.77	5.83	6.92	0.24	20.24	5.62
40.81	0.00	19.74	4.82	6.98	0.21	20.37	5.20
40.79	0.09	19.70	4.99	7.19	0.19	20.29	5.34
40.79	0.15	19.37	4.98	6.62	0.27	21.15	5.11
41.11	0.54	18.31	7.23	6.96	0.35	20.53	5.99
41.00	0.19	19.42	5.89	7.13	0.35	20.61	5.77
41.21	0.24	19.25	5.88	6.82	0.36	20.69	5.73
41.08	0.06	19.94	5.04	7.02	0.39	20.72	5.21
41.63	0.21	19.37	4.88	6.51	0.32	21.16	5.11
41.11	0.22	19.33	4.72	6.65	0.34	21.14	5.00
41.04	0.41	18.34	7.16	6.89	0.35	20.30	6.04
41.53	0.25	19.88	5.00	7.38	0.48	20.73	5.23
41.29	0.12	19.13	5.69	6.75	0.20	20.21	5.76
41.81	0.23	20.12	4.98	6.86	0.53	21.15	5.32
41.04	0.50	18.15	7.12	6.93	0.50	20.21	5.93
41.30	0.35	19.23	6.14	6.71	0.35	20.81	5.80
40.54	0.51	17.98	4.82	6.95	0.40	20.62	5.31
41.19	0.28	19.88	5.02	6.97	0.53	20.95	5.16
40.88	0.00	18.61	6.70	7.01	0.49	19.54	6.36
40.72	0.37	18.09	7.15	6.66	0.37	20.19	6.15
40.76	0.29	19.15	5.76	6.65	0.32	20.15	5.76
40.86	0.09	18.71	6.50	7.35	0.50	19.48	6.29
41.50	0.43	20.74	3.67	6.60	0.26	21.72	4.94
41.09	0.13	19.28	5.88	6.64	0.41	20.66	5.74
41.41	0.27	19.83	4.95	7.03	0.35	20.99	5.34
41.16	0.42	18.16	7.02	7.03	0.39	20.20	5.93
41.40	0.29	19.86	4.98	7.22	0.41	20.59	5.33
41.65	0.35	19.59	4.92	6.55	0.22	21.22	4.94
41.45	0.28	19.14	5.84	6.95	0.41	20.47	5.85
41.40	0.12	19.81	4.94	7.35	0.36	20.85	5.38
42.01	0.13	20.79	3.76	6.70	0.46	21.57	4.90
41.79	0.18	19.96	4.85	6.96	0.38	20.67	5.43
42.10	0.26	20.90	4.04	6.97	0.43	21.63	4.95
41.72	0.13	20.03	5.04	7.31	0.38	21.02	5.34
41.95	0.23	20.14	4.91	7.22	0.39	21.09	5.23
42.20	0.17	21.81	2.39	7.52	0.30	21.40	4.52
41.29	0.18	19.56	5.81	6.81	0.42	20.77	5.64

41.43	0.21	19.83	4.89	7.29	0.29	20.90	5.26
41.60	0.16	19.96	4.96	7.14	0.42	20.71	5.44
40.90	0.46	18.38	7.12	6.91	0.29	20.45	6.11
40.95	0.34	18.16	7.35	6.77	0.32	20.22	6.01
41.78	0.00	20.74	4.19	6.97	0.34	21.26	5.18
41.48	0.21	19.86	4.82	7.25	0.33	20.76	5.21
41.62	0.25	19.97	5.12	7.60	0.41	21.00	5.28
41.77	0.09	20.72	3.83	6.80	0.32	21.08	4.99
41.54	0.23	19.92	4.79	7.22	0.40	20.92	5.33
41.36	0.30	20.21	4.93	7.28	0.43	21.08	5.18
41.71	0.25	20.30	5.03	7.28	0.47	20.81	5.34
41.69	0.23	19.69	4.99	6.99	0.34	21.05	5.12
41.63	0.27	20.54	4.32	6.61	0.32	21.27	5.27
41.75	0.00	20.60	4.22	6.94	0.36	21.10	5.11
41.94	0.41	20.20	4.82	6.70	0.31	21.31	5.44
41.90	0.26	20.78	4.04	7.06	0.36	21.30	4.99
41.59	0.30	19.36	5.84	7.01	0.38	20.51	5.72
41.36	0.22	19.18	6.08	6.99	0.35	20.62	5.80
41.05	0.45	18.12	7.40	6.56	0.36	20.25	6.29
41.50	0.38	19.66	4.98	6.80	0.33	21.30	4.95
41.70	0.11	20.47	4.29	6.96	0.40	21.13	5.13
41.70	0.19	19.44	6.01	7.15	0.35	20.72	5.83
41.04	0.37	17.91	7.05	6.78	0.40	20.33	5.71
41.51	0.09	20.08	4.91	7.18	0.34	20.99	5.25
41.35	0.15	19.36	5.79	6.86	0.39	20.51	5.71
41.52	0.00	19.88	5.05	7.06	0.29	20.95	5.42
41.34	0.35	18.92	6.56	6.90	0.34	20.87	5.57
41.82	0.16	20.77	3.99	6.80	0.35	21.74	4.93
41.96	0.00	20.54	5.70	7.11	0.37	21.21	5.07
41.36	0.22	19.18	6.08	6.99	0.35	20.62	5.80
41.31	0.10	20.47	4.41	7.46	0.36	20.57	5.19
40.64	0.47	18.38	6.79	6.73	0.38	20.16	6.21
41.21	0.58	18.45	7.23	6.85	0.43	20.12	6.34
41.06	0.18	19.23	5.78	6.91	0.37	20.51	5.67
41.40	0.12	19.77	5.13	7.15	0.32	20.46	5.36
41.89	0.27	21.07	3.56	6.23	0.28	21.74	5.47
41.49	0.00	19.87	4.89	7.40	0.26	20.48	5.28
41.41	0.27	19.36	6.00	6.88	0.34	20.69	5.86
41.34	0.19	19.87	4.98	7.25	0.53	20.67	5.19
41.73	0.11	20.14	5.20	7.23	0.38	20.95	5.56
41.65	0.06	20.48	4.13	7.01	0.33	21.06	5.01
41.73	0.19	20.08	5.04	7.41	0.34	20.90	5.44
41.66	0.13	20.50	3.85	6.79	0.31	21.28	4.92
41.65	0.00	20.64	4.38	7.08	0.46	20.46	5.17
41.54	0.00	19.39	5.91	7.04	0.39	20.79	5.81
41.79	0.20	20.47	3.92	6.90	0.36	21.41	4.89
41.77	0.48	19.58	5.05	6.54	0.35	21.45	5.26
41.08	0.57	18.31	7.20	6.87	0.29	20.22	6.46
41.74	0.21	20.25	4.33	6.63	0.18	21.29	5.38
41.46	0.21	19.98	4.84	7.11	0.41	20.84	5.31
41.50	0.26	19.97	5.01	7.23	0.40	20.90	5.23
42.07	0.23	21.01	3.76	6.66	0.50	21.89	4.87
41.66	0.00	20.75	3.96	6.68	0.26	21.39	4.93

41.15	0.45	18.07	7.49	6.54	0.29	20.56	6.12
41.84	0.27	20.69	4.09	5.85	0.27	22.23	4.64
40.94	0.33	20.47	4.01	6.15	0.18	21.11	5.33
41.30	0.43	20.83	3.74	6.06	0.37	21.09	5.49
40.99	0.55	21.05	1.89	7.71	0.32	20.51	4.95
41.53	0.53	22.76	0.66	7.25	0.42	21.61	4.36
41.06	0.13	19.92	4.88	7.15	0.36	20.89	5.11
40.67	0.22	19.54	4.91	6.96	0.39	20.71	4.98
40.69	0.66	20.70	2.48	8.93	0.36	19.59	5.32
40.97	0.59	20.64	2.61	9.02	0.29	19.79	5.19
40.54	0.85	20.46	2.56	9.05	0.24	19.83	5.43
40.68	0.80	20.65	2.53	9.09	0.36	19.81	5.31
41.09	0.00	19.85	5.06	6.89	0.49	20.75	5.02
41.43	0.57	19.85	0.62	7.27	0.32	21.58	4.27
41.45	0.42	22.62	0.59	7.29	0.34	21.60	4.35
41.27	0.29	20.88	3.51	6.69	0.39	21.35	4.55
41.28	0.46	22.47	0.66	7.13	0.31	21.42	4.32
41.48	0.43	22.53	0.66	7.07	0.34	21.44	4.40
41.39	0.38	22.63	0.77	6.98	0.38	21.51	4.52

## HAM DYKE GARNETS

SIO2	TIO2	AL2O3	CR2O3	FEO	MNO	MGO	CAO
41.29	0.53	21.31	1.96	7.90	0.34	20.74	5.04
40.87	0.50	21.37	1.93	7.79	0.27	20.59	5.11
41.07	0.61	21.46	1.98	7.86	0.37	20.75	5.00
40.80	0.74	21.19	1.36	8.74	0.34	19.85	5.06
40.66	0.44	20.18	3.77	6.79	0.27	20.88	5.43
40.95	0.52	21.37	1.86	7.79	0.34	20.69	5.01
41.34	0.56	21.43	1.97	7.72	0.35	20.81	5.05
41.57	0.35	21.52	1.77	7.58	0.28	21.39	4.77
40.03	1.48	19.33	2.56	8.01	0.29	19.17	6.55
41.06	0.52	21.25	1.89	7.79	0.36	20.55	5.11
41.07	0.51	21.45	1.87	7.91	0.28	20.81	4.98
41.14	0.72	20.84	2.41	7.58	0.29	20.50	5.23
40.08	0.51	21.42	1.83	7.87	0.33	20.76	4.93
40.64	0.81	21.23	1.26	9.06	0.34	19.55	5.09
40.71	0.78	20.62	2.46	8.62	0.22	20.08	5.02
41.12	0.41	21.35	1.87	7.88	0.26	20.56	4.95
40.84	0.49	21.46	1.93	8.02	0.33	20.69	4.99
40.90	0.79	20.86	2.66	7.89	0.24	20.45	5.20
40.55	0.83	21.37	1.26	9.19	0.37	19.59	5.15
40.81	0.62	21.41	1.91	7.93	0.37	20.68	4.99
41.02	0.51	21.21	1.97	7.87	0.23	20.63	5.01
41.04	0.65	21.25	1.88	7.99	0.38	20.63	5.00
40.78	0.56	21.27	1.81	8.15	0.29	20.63	5.02
41.01	0.58	21.13	2.08	7.67	0.32	20.69	5.13
40.62	0.75	21.24	1.23	8.99	0.32	19.19	5.18
40.87	0.62	21.30	1.93	7.93	0.48	20.60	5.01
40.95	0.62	21.30	1.93	7.84	0.19	20.73	5.11
40.50	0.82	21.36	1.31	8.90	0.41	19.82	5.01
41.26	0.77	20.81	2.42	7.67	0.28	20.61	5.21

41.17	0.57	21.46	1.93	7.75	0.40	20.64	5.12
41.04	0.20	20.98	3.21	8.28	0.39	20.21	4.76
41.24	0.56	21.58	1.86	8.11	0.33	20.59	5.07
41.05	0.58	21.45	1.94	8.07	0.39	20.73	5.09
41.35	0.51	21.11	1.90	8.00	0.37	20.63	5.05
41.01	0.60	21.85	1.46	9.29	0.28	20.17	4.99
40.76	0.62	21.02	1.85	7.65	0.28	20.66	5.06
40.93	0.46	21.19	1.94	8.07	0.41	20.87	4.91
41.33	0.48	21.42	1.83	7.98	0.33	20.54	5.03
40.45	0.70	20.88	2.34	8.60	0.25	19.85	4.97
41.08	0.55	21.50	1.88	7.68	0.22	20.71	4.97
41.29	0.60	21.54	1.88	7.75	0.33	20.64	5.07
41.25	0.39	21.31	1.89	7.99	0.30	20.42	5.04
40.73	0.00	21.60	2.30	9.13	0.58	19.18	4.78
40.89	0.08	19.61	4.83	7.02	0.55	20.22	5.35
40.62	0.15	21.14	3.26	8.17	0.56	19.91	4.88
40.73	0.06	21.48	2.46	9.26	0.62	19.37	4.99
40.66	0.14	20.13	4.71	7.14	0.47	20.40	5.17
40.62	0.23	21.06	3.28	8.42	0.40	19.95	4.78
40.89	0.27	19.62	4.83	7.12	0.48	20.19	5.16
40.78	0.24	21.50	2.38	9.16	0.53	19.27	4.93
40.73	0.19	21.62	2.41	9.32	0.64	19.66	4.90
40.88	0.20	21.48	2.51	9.19	0.64	19.34	4.92
40.40	0.06	19.71	5.00	7.30	0.35	20.46	5.29
40.79	0.24	21.47	2.44	9.38	0.59	19.46	4.89
40.64	0.23	19.60	4.94	7.04	0.42	20.22	5.27
40.31	0.15	21.34	2.39	9.27	0.47	19.21	4.89
40.49	0.00	20.79	3.79	7.46	0.45	20.06	5.11
40.65	0.17	21.49	2.48	9.60	0.49	19.26	4.97
41.29	0.13	21.01	3.10	8.37	0.43	20.15	4.99
41.25	0.13	21.04	3.26	8.44	0.41	20.17	4.77
40.72	0.23	20.76	3.40	8.34	0.45	19.70	4.82
40.96	0.25	20.03	4.68	7.00	0.35	20.48	5.32
41.01	0.17	19.85	4.78	7.03	0.37	20.33	5.31
41.00	0.16	21.70	2.51	9.32	0.60	19.57	5.03
40.93	0.23	21.05	3.29	8.45	0.36	19.83	4.89
40.60	0.13	21.61	2.49	9.30	0.39	19.40	4.81
40.64	0.23	20.99	3.25	8.27	0.45	20.06	5.05
40.57	0.25	20.94	3.25	8.51	0.54	19.76	5.03
40.79	0.23	19.96	4.80	7.28	0.35	20.71	5.36
40.64	0.13	21.23	2.62	9.24	0.41	19.54	5.03
40.74	0.31	19.73	4.75	7.16	0.45	20.49	5.54
40.87	0.09	21.05	3.28	8.28	0.53	20.31	5.00
41.08	0.12	21.14	2.41	9.17	0.48	19.41	5.04
40.83	0.15	21.61	2.49	9.24	0.54	19.60	5.19
40.74	0.23	21.54	2.38	9.14	0.47	19.17	5.09
41.05	0.19	20.80	3.24	8.10	0.42	20.18	5.04
40.77	0.13	21.25	2.49	9.24	0.39	19.24	5.05
40.75	0.15	21.37	2.44	9.34	0.51	19.27	5.03
40.79	0.10	20.99	3.29	8.17	0.46	19.83	4.92
40.60	0.23	19.54	4.82	7.17	0.34	20.64	5.44
40.90	0.29	19.73	4.62	7.08	0.47	20.61	5.44
40.84	0.09	21.28	2.55	9.45	0.41	19.53	5.07

41.20	0.14	21.36	2.42	9.55	0.51	19.47	5.08
40.68	0.17	21.52	2.45	9.31	0.49	19.42	5.06
40.53	0.13	21.43	2.34	9.27	0.55	19.51	5.13
41.08	0.10	21.57	2.27	9.33	0.58	19.53	5.07
40.76	0.31	20.95	3.27	8.30	0.53	20.28	4.96
40.84	0.24	21.39	2.40	9.24	0.48	19.45	5.19
41.10	0.28	19.74	4.76	7.29	0.45	20.60	5.44
40.67	0.23	19.61	4.91	6.96	0.37	20.70	5.45
40.77	0.00	21.45	2.38	9.06	0.49	19.68	5.09
41.02	0.21	19.78	4.83	7.06	0.37	20.54	5.61
41.10	0.10	21.34	2.51	9.41	0.56	19.52	5.06
40.83	0.30	21.60	2.63	9.37	0.60	19.78	5.23
40.83	0.22	21.84	2.20	9.48	0.57	19.38	5.06
40.84	0.21	20.97	3.43	8.45	0.43	20.12	5.14
41.02	0.15	21.43	2.40	9.33	0.45	19.51	5.06
41.14	0.19	20.93	3.29	8.35	0.54	20.43	5.11
40.78	0.12	21.80	2.40	9.31	0.49	19.43	5.14
41.06	0.20	21.48	2.45	9.20	0.55	19.90	5.16
40.95	0.11	19.87	4.33	6.82	0.28	20.90	5.76
41.00	0.40	21.90	2.19	9.19	0.54	19.48	4.95
40.81	0.16	20.85	3.28	8.46	0.38	19.97	5.07
40.66	0.06	21.35	2.19	9.27	0.40	19.35	4.99
41.21	0.16	20.99	3.26	8.28	0.44	20.13	5.10
40.59	0.24	19.70	4.87	7.19	0.41	20.53	5.55
40.85	0.06	21.44	2.47	9.21	0.55	19.90	5.07
40.90	0.22	21.34	2.44	9.39	0.47	19.35	5.15
40.76	0.10	21.52	2.56	9.48	0.49	19.63	5.23
41.30	0.31	19.93	5.17	7.43	0.38	20.08	5.39
41.64	0.18	20.48	4.92	7.55	0.46	20.20	5.42
41.31	0.16	19.94	4.89	7.32	0.30	20.73	5.48
41.80	0.18	20.41	4.70	7.61	0.42	20.50	5.44
41.50	0.16	20.46	4.64	7.54	0.48	20.25	5.24
41.57	0.00	20.54	4.92	7.22	0.50	20.45	5.66
41.27	0.08	20.25	4.80	7.44	0.30	19.99	5.33
41.41	0.12	20.30	4.75	7.60	0.47	20.13	5.35
41.53	0.00	20.20	4.93	7.50	0.47	20.36	5.45
41.27	0.00	20.09	4.80	7.66	0.45	20.21	5.38
41.61	0.19	20.08	5.04	7.58	0.53	20.16	5.48
41.69	0.11	20.15	4.83	7.57	0.49	20.03	5.36
41.30	0.00	19.86	4.99	7.66	0.45	20.30	5.24
41.53	0.20	20.54	4.83	7.58	0.58	20.29	5.40
41.22	0.13	20.08	4.88	7.56	0.39	20.24	5.42
41.54	0.00	20.59	4.73	7.65	0.44	20.32	5.43
41.21	0.15	20.88	3.81	7.55	0.36	20.32	5.43
41.21	0.15	20.88	3.81	7.55	0.36	20.32	5.25
41.09	0.21	20.03	5.05	7.79	0.43	20.07	5.55
41.32	0.00	20.73	3.79	7.56	0.43	19.94	5.18
40.90	0.00	20.29	4.83	7.16	0.45	20.06	5.66
41.33	0.05	21.02	3.98	7.62	0.41	20.24	5.29
41.07	0.00	20.87	3.77	7.61	0.49	19.97	5.33
40.96	0.00	20.00	4.84	7.42	0.43	19.99	5.39
40.96	0.00	19.77	4.71	7.41	0.27	19.96	5.33
40.84	0.23	20.06	5.09	7.63	0.47	20.02	5.62

40.88	0.12	20.00	4.98	7.66	0.36	20.07	5.56
41.10	0.16	19.94	4.88	7.02	0.41	20.46	5.38
40.99	0.15	19.90	4.94	7.27	0.42	20.01	5.61
41.16	0.13	19.92	4.87	7.62	0.45	20.00	5.50
41.18	0.10	20.72	4.01	7.54	0.60	20.37	5.42
41.10	0.14	20.30	4.86	7.48	0.56	20.24	5.37
41.23	0.19	20.34	4.61	7.45	0.56	20.23	5.27
41.23	0.16	19.99	5.04	7.41	0.52	19.88	5.50
41.04	0.00	20.06	5.18	7.41	0.42	19.97	5.41
41.18	0.16	20.11	4.71	7.25	0.45	20.68	5.39
41.07	0.00	19.81	4.94	7.43	0.45	20.05	5.51
40.56	0.45	15.49	9.91	6.89	0.24	18.80	7.73
41.43	0.20	20.01	4.99	7.32	0.38	20.56	5.49
41.34	0.17	19.91	4.74	7.22	0.37	20.76	5.50
41.43	0.07	20.08	4.71	7.46	0.40	20.08	5.34
40.57	0.69	15.66	9.99	6.26	0.41	19.92	7.08
41.35	0.13	19.90	4.72	7.32	0.45	20.75	5.36
40.92	0.18	19.88	4.95	7.10	0.43	20.66	5.40
41.67	0.17	20.14	4.88	7.39	0.34	20.95	5.45
41.41	0.10	19.98	4.72	6.94	0.45	20.85	5.49
41.45	0.14	19.99	4.85	7.13	0.42	20.47	5.42
41.72	0.00	21.77	2.48	9.75	0.42	19.46	5.09
41.82	0.32	19.80	4.90	7.25	0.43	20.84	7.25
41.25	0.29	20.02	4.87	7.19	0.48	20.66	5.60
41.71	0.30	20.02	4.99	7.30	0.33	20.69	5.45
41.38	0.23	19.99	4.95	7.20	0.37	20.73	5.43
41.28	0.22	19.87	4.95	7.24	0.37	20.78	5.52
41.08	0.16	20.01	4.83	7.27	0.39	20.77	5.37
41.26	0.20	19.83	4.93	6.97	0.45	20.89	5.63
41.55	0.19	19.82	4.87	7.18	0.42	20.78	5.54
41.39	0.19	19.79	5.02	7.18	0.39	20.61	5.50
41.48	0.27	19.88	4.87	7.26	0.45	20.74	5.45
41.77	0.24	21.23	3.26	8.57	0.51	20.26	5.09
41.77	0.22	20.08	4.64	7.15	0.54	20.74	5.43
41.39	0.16	20.13	5.07	7.21	0.40	20.77	5.55
41.38	0.13	19.87	4.90	7.19	0.37	20.84	5.38
41.98	0.29	20.88	3.77	6.83	0.25	21.23	4.84
41.37	0.27	19.95	4.84	7.16	0.43	20.69	5.54
41.35	0.21	20.08	4.81	7.22	0.46	20.80	5.49
41.72	0.17	20.17	4.73	7.31	0.51	20.71	5.48
41.33	0.25	20.07	5.00	7.40	0.37	20.65	5.42
41.26	0.27	19.83	4.93	7.01	0.50	20.71	5.52
40.97	0.12	20.55	4.60	7.33	0.53	20.18	5.22
41.32	0.23	18.56	6.61	7.00	0.31	20.32	6.37
41.71	0.56	21.39	1.93	8.07	0.28	20.94	5.25
40.86	0.26	17.69	7.67	6.68	0.41	19.74	7.19
41.37	0.06	20.02	4.82	7.48	0.50	20.19	5.44
40.88	0.24	17.84	8.05	6.45	0.43	19.58	7.18
41.15	0.20	20.02	4.98	7.11	0.43	20.69	5.52
41.48	0.08	20.27	4.84	7.60	0.49	20.45	5.48
41.57	0.20	20.11	5.00	6.95	0.23	20.64	5.41
41.39	0.09	19.97	4.99	7.62	0.33	20.37	5.44
41.60	0.00	20.53	4.71	7.37	0.50	20.39	5.50

40.96	0.14	20.13	4.86	7.53	0.44	20.14	5.49
41.30	0.07	19.96	4.74	7.56	0.40	20.17	5.37
41.06	0.19	20.59	4.38	7.61	0.55	20.60	5.21
41.21	0.22	20.43	4.96	7.69	0.56	20.29	5.50
40.67	0.00	20.45	4.27	7.34	0.39	20.38	5.12
40.99	0.10	20.07	4.90	7.50	0.42	20.14	5.39
41.04	0.10	20.00	4.93	7.57	0.43	20.22	5.40
41.16	0.14	19.78	4.81	7.08	0.33	20.67	5.51
41.20	0.06	20.08	4.58	7.64	0.41	20.08	5.32
40.99	0.18	20.00	5.14	7.60	0.47	20.28	5.61
40.67	0.11	19.62	4.99	7.58	0.36	19.97	5.47
40.63	0.06	17.01	8.41	6.46	0.28	19.62	7.22
40.98	0.00	20.34	4.73	7.22	0.52	20.17	5.64
41.14	0.18	20.12	4.91	7.58	0.46	20.12	5.52
41.16	0.10	20.25	4.43	7.41	0.34	20.43	5.34
41.15	0.30	20.40	4.82	7.59	0.50	20.59	5.60
40.92	0.09	20.05	5.08	7.49	0.41	20.01	5.38
40.77	0.24	19.88	5.10	7.37	0.42	20.21	5.42
41.21	0.06	21.10	3.34	8.46	0.35	20.14	4.97
40.91	0.07	20.83	3.77	7.42	0.46	20.43	5.29
40.78	0.11	21.05	3.32	8.26	0.45	20.41	5.08
40.98	0.19	19.80	5.13	7.44	0.44	20.16	5.57
40.93	0.20	20.05	4.89	7.64	0.46	20.17	5.49
41.02	0.20	20.24	4.89	7.46	0.37	20.13	5.47
41.23	0.00	19.89	4.83	7.01	0.47	20.80	5.49
41.23	0.21	20.06	5.03	7.66	0.43	20.12	5.40
40.75	0.14	19.97	4.90	7.22	0.39	20.11	5.37
40.95	0.23	20.31	4.77	7.32	0.53	20.27	5.26
40.90	0.08	20.91	3.96	7.62	0.48	20.37	5.40
40.80	0.13	19.91	4.92	7.65	0.46	20.09	5.44
40.84	0.00	20.63	3.77	7.72	0.51	20.36	5.34
40.75	0.12	19.96	4.90	7.32	0.34	20.38	5.40
41.09	0.07	20.08	3.76	7.34	0.42	20.43	5.31
41.19	0.00	20.94	3.93	7.54	0.48	20.46	5.27
40.78	0.12	20.62	3.82	7.50	0.43	20.14	5.26
40.44	0.00	19.89	5.06	7.61	0.48	20.21	5.35
40.91	0.00	20.23	4.78	7.12	0.41	19.98	5.65
40.55	0.18	19.73	4.79	7.04	0.32	20.65	5.36
40.64	0.07	19.62	4.99	7.41	0.42	20.03	5.33
41.19	0.12	20.99	3.86	7.57	0.63	20.39	5.30
41.01	0.16	20.18	4.78	7.43	0.48	20.17	5.45
40.70	0.09	20.67	4.04	7.44	0.52	20.20	5.30
40.81	0.12	19.91	4.93	7.61	0.52	20.23	5.38
40.79	0.21	20.12	4.78	7.52	0.40	20.14	5.48
40.60	0.16	19.54	4.74	6.98	0.40	20.43	5.39
40.74	0.12	19.95	4.87	7.43	0.38	20.20	5.43
40.56	0.07	20.67	3.86	7.32	0.44	20.17	5.24
41.33	0.10	20.14	4.87	7.57	0.42	20.13	5.47
40.88	0.10	20.20	5.11	7.42	0.42	20.15	5.39
41.09	0.11	20.21	4.85	7.35	0.47	20.57	5.32
41.01	0.00	20.23	4.75	7.33	0.31	20.01	5.37
41.01	0.13	19.90	4.72	7.30	0.35	20.85	5.28
40.67	0.16	20.15	4.98	7.58	0.39	20.40	5.54

41.21	0.28	20.11	4.85	7.29	0.46	20.78	5.31
41.25	0.23	19.98	4.87	7.03	0.32	20.93	5.58
41.04	0.19	20.31	4.79	7.52	0.46	20.35	5.54
40.93	0.00	20.28	4.76	7.01	0.43	20.20	5.66
41.48	0.06	20.31	4.69	7.45	0.43	20.38	5.24
40.93	0.07	19.84	4.94	7.36	0.38	20.12	5.32
40.78	0.00	20.34	4.27	7.42	0.34	20.47	5.11
41.61	0.17	20.90	3.80	7.48	0.51	20.52	5.37
41.02	0.13	20.10	4.74	7.54	0.51	20.14	5.40
41.34	0.13	20.98	3.97	7.51	0.46	20.56	5.46
41.12	0.25	20.36	4.90	7.34	0.43	20.62	5.49
41.30	0.00	20.89	4.14	7.40	0.53	20.47	5.42
40.91	0.09	20.86	4.01	7.62	0.44	20.22	5.34
41.31	0.00	20.33	4.80	7.34	0.54	20.23	5.76
40.99	0.00	20.97	3.76	7.46	0.40	20.44	5.28
41.12	0.09	20.85	3.82	7.62	0.43	20.49	5.26
40.17	0.09	20.17	5.05	7.48	0.45	20.09	5.60
41.18	0.11	21.01	3.89	7.70	0.45	20.44	5.53
41.06	0.11	20.01	4.88	7.25	0.37	21.02	5.46
41.04	0.00	19.74	4.79	6.94	0.34	20.67	5.62
41.18	0.20	19.99	4.74	7.20	0.44	20.70	5.44
40.76	0.20	20.13	4.80	7.49	0.48	20.20	5.45
40.93	0.15	20.07	4.94	7.44	0.45	20.35	5.57
41.02	0.00	20.93	3.94	7.52	0.41	20.44	5.39
40.84	0.10	20.22	4.95	7.19	0.41	20.25	5.47
40.96	0.23	20.03	4.94	7.55	0.48	20.28	5.56
41.13	0.00	20.36	4.93	7.56	0.41	20.33	5.43
41.36	0.20	19.76	4.95	7.07	0.40	20.47	5.52
41.27	0.00	20.29	4.85	7.14	0.46	20.29	5.76
41.45	0.00	20.34	4.85	7.48	0.46	20.18	5.68
41.15	0.14	20.39	4.57	7.54	0.45	20.38	5.32
40.55	0.15	16.06	9.99	5.99	0.20	19.93	7.16
40.71	0.19	19.71	4.92	7.08	0.38	20.52	5.52
41.02	0.10	19.99	4.85	7.77	0.44	20.21	5.52
41.38	0.00	20.51	4.81	7.26	0.63	20.34	5.77

## APPENDIX B

## HAM DIATREME CLINOPYROXENES

SIO2	TIO2	AL2O3	CR2O3	FEO	MNO	MGO	CAO	NA2O	K2O	NIO
53.79	0.25	2.41	2.71	2.35	0.08	16.51	18.59	2.27	0.00	0.00
53.82	0.47	2.37	1.82	2.63	0.10	17.94	18.46	1.74	0.04	0.04
54.18	0.45	2.62	1.20	3.37	0.11	19.20	16.92	1.60	0.00	0.08
52.86	0.25	4.97	1.13	1.43	0.07	15.25	21.77	1.72	0.00	0.04
54.56	0.53	2.67	1.22	3.02	0.10	18.20	18.29	1.68	0.00	0.07
54.03	0.38	2.08	1.50	2.38	0.11	18.39	18.92	1.57	0.00	0.03
54.73	0.06	1.98	1.82	2.36	0.08	17.98	19.86	1.56	0.00	0.05
54.60	0.14	2.60	2.14	2.32	0.10	17.47	18.65	2.20	0.00	0.05
54.52	0.18	2.92	2.28	2.09	0.09	15.87	19.02	2.71	0.00	0.04
54.61	0.24	3.04	1.62	2.78	0.08	16.42	18.64	2.40	0.00	0.03
54.17	0.17	2.72	2.06	2.33	0.11	16.83	18.56	2.20	0.00	0.03
53.94	0.50	2.73	1.12	3.11	0.10	18.22	18.42	1.61	0.00	0.02
53.23	0.22	3.67	1.22	1.09	0.04	16.16	22.26	1.64	0.00	0.01
53.65	0.00	3.44	1.03	1.31	0.05	16.47	22.63	1.22	0.00	0.02
53.87	0.18	3.73	1.01	1.10	0.06	16.23	22.48	1.50	0.00	0.06
54.45	0.23	3.17	1.02	1.16	0.07	16.46	22.32	1.52	0.00	0.06
54.58	0.20	0.76	0.93	1.19	0.13	16.60	22.64	1.49	0.00	0.06
54.32	0.20	3.25	1.18	1.13	0.06	16.22	21.30	1.56	0.00	0.04
53.89	0.44	4.24	1.33	1.33	0.09	15.23	20.98	1.94	0.00	0.00
54.03	0.20	3.61	1.04	1.15	0.06	16.21	22.45	1.52	0.00	0.06
54.16	0.23	3.60	1.72	1.52	0.07	15.34	20.68	2.38	0.00	0.00
54.49	0.23	3.42	1.80	1.28	0.51	15.95	21.30	2.07	0.00	0.00
54.55	0.21	3.46	1.69	1.28	0.05	15.14	21.18	2.43	0.00	0.00
54.35	0.24	3.60	1.73	1.38	0.06	15.47	20.39	2.16	0.00	0.00
54.43	0.21	3.49	0.75	1.26	0.01	15.97	21.97	1.73	0.00	0.00
54.17	0.23	3.29	0.49	1.40	0.03	16.25	22.67	1.72	0.00	0.00
54.09	0.21	3.47	0.66	1.30	0.03	16.12	22.40	1.71	0.00	0.00
54.23	0.22	3.49	0.67	1.29	0.03	16.21	22.39	1.73	0.00	0.00
54.03	0.33	3.43	1.13	1.10	0.04	16.28	21.63	1.87	0.00	0.00
53.94	0.35	5.53	1.24	1.07	0.07	15.73	21.26	1.72	0.00	0.00
54.53	0.31	3.43	1.13	1.18	0.01	15.98	21.61	1.39	0.00	0.00
54.37	0.34	4.47	0.76	1.21	0.07	15.42	20.34	2.46	0.00	0.00
54.18	0.14	3.57	1.09	1.40	0.05	15.79	21.94	1.81	0.00	0.00
54.95	0.06	2.17	3.32	2.41	0.11	18.24	18.82	1.74	0.02	0.05
55.44	0.32	2.37	1.04	2.52	0.09	18.59	18.67	1.52	0.02	0.06
53.92	0.23	3.05	1.53	2.62	0.09	17.89	18.08	2.10	0.06	0.04
54.63	0.29	3.02	1.32	2.62	0.11	18.09	17.29	2.24	0.02	0.04
55.18	0.16	2.13	1.49	2.51	0.06	17.87	19.28	1.57	0.03	0.05
54.31	0.07	1.87	1.77	2.64	0.13	19.17	18.56	1.54	0.03	0.05
55.00	0.11	2.27	1.99	2.47	0.12	18.39	18.05	1.61	0.00	0.06
54.10	0.04	2.08	1.46	2.38	0.10	18.59	19.15	1.45	0.03	0.03
54.53	0.02	1.67	1.39	2.42	0.11	19.04	20.11	1.08	0.03	0.05
54.69	0.15	2.47	1.34	2.76	0.11	18.80	18.15	1.72	0.00	0.05
54.16	0.13	1.90	1.50	2.51	0.11	18.62	19.99	1.21	0.04	0.03
53.46	0.10	2.21	2.11	2.14	0.09	17.87	19.45	1.91	0.02	0.04
53.95	0.06	1.92	1.60	2.22	0.10	18.01	19.72	1.63	0.02	0.08
54.71	0.13	2.07	1.92	2.23	0.08	17.58	19.16	1.76	0.03	0.06
53.90	0.27	2.88	2.51	2.20	0.09	15.59	19.12	2.75	0.01	0.05
54.28	0.16	1.17	2.21	1.96	0.06	17.16	22.17	1.09	0.00	0.03
53.23	0.00	2.43	0.75	1.49	0.06	17.80	23.75	0.60	0.00	0.00
53.70	0.38	4.31	1.26	1.36	0.08	15.69	21.19	2.08	0.00	0.04
53.70	0.02	1.82	0.84	1.20	0.06	17.08	23.81	0.91	0.00	0.04
54.28	0.00	2.06	0.80	1.24	0.05	18.12	23.14	0.79	0.03	0.06

## APPENDIX C

## CLUSTER ANALYSIS PROGRAM FOR HAM GARNETS

```

C      THIS PROGRAM IS SETUP FOR USE WITH A 276 X 8 DATA MATRIX
C      WHICH, IF TRANSPOSED, THE ITYPE WILL EQUAL 2
C
C      THIS PROGRAM IS COMMENTED SUCH THAT NEITHER THE DATA
C      MATRIX OR SIMILARITY MATRIX WILL BE OUTPUTTED
C
C      ENTER SIZE OF DATA MATRIX (N,M) AT TOP OF DATA MATRIX
C      DIMENSION X(N,M),IPAIR(2,N),XLEV(N),A(N,N)
C
C      DIMENSION X(444,6),IPAIR(2,444),XLEV(444),A(444,444)
C
C      DATA=N(M)
C
C      DATA X/2664*0.0/
C      MD, WHERE MD=M OR N
C      MD=6
C      ND, WHERE ND=N
C      ND=444
C      MM, WHERE MM=N
C      MM=444
C
C      FORMAT OF INPUT DATA MATRIX FOUND IN SUBROUTINE READM
C      CHANGE IF NECESSARY
C
C      OPEN (UNIT=5, FILE='WDELW.IN',STATUS='OLD',ERR=995)
C      OPEN (UNIT=6, FILE='WDELW.OUT',STATUS='NEW',ERR=994)
C
C      ITYPE, ISIM PROGRAM CONTROL VALUES
C      ITYPE
C      COLUMNS 1 - 3,1= INPUT A DATA MATRIX
C      2= INPUT A DATA MATRIX AND TRANSPOSE IT
C      3= INPUT A SIMILARITY MATRIX
C      ISIM
C      COLUMNS 4 - 6,1= CORRELATION MATRIX
C      2= DISTANCE MATRIX
C
C      TYPE 6
C      FORMAT(1H , 'ENTER VALUES OF ITYPE,ISIM (3 digits for each) :')
C      ACCEPT 1000, ITYPE,ISIM
C      IF(ITYPE .LE. 0) CALL EXIT
C      INPUT SIMILARITY MATRIX
C      IF(ITYPE .NE. 3) GOTO 2
C      CALL READM(A,N,M,MM,MM)
C      GOTO 4
C      READ AND PRINT INPUT DATA MATRIX
C      CALL READM(X,N,M,ND,MD)
C      CALL PRINTM(X,N,M,ND,MD)
C      WRITE(6,2001)
C

```

```

C      TRANSPOSE DATA MATRIX FOR OBSERVATIONS SIMILARITY IF ITYPE =2
C
      IF (ITYPE .NE. 2) GOTO 3
      MT=M
      IF (N .GT. M) MT=N
      DO 110 I=1,MT
      DO 110 J=I,MT
      XS=X(I,J)
      X(I,J)=X(J,I)
      X(J,I)=XS
110    CONTINUE
      MT=M
      M=N
      N=MT

C
C      CALCULATE SIMILARITY MATRIX
C
3      IF (ISIM .EQ. 1) CALL RCCEF (X,N,M,ND,MD,A,MM)
      IF (ISIM .EQ. 2) CALL DIST (X,N,M,ND,MD,A,MM)
C      PRINT SIMILARITY MATRIX
C4     CALL PRINTM (A,M,M,MM,MM)
C      WRITE (6,2002)
C      CALCULATE AND PRINT LINKAGE TABLE
      CALL WPGA (A,M,MM,IPAIR,XLEV,ISIM)
C      PRINT DENDOGRAM
      CALL DENDRO (IPAIR,XLEV,M,MM,ISIM)
      GOTO 5
1000   FORMAT(2I3)
C2001  FORMAT(1H0,4X,'INPUT DATA MATRIX -',1X,
C      1 'COLUMNS = VARIABLES, ROWS = OBSERVATIONS')
C2002  FORMAT(1H0,4X,'SIMILARITY MATRIX')
995    TYPE 993
993    FORMAT(1H , 'Cannot open input file: Garnet.in')
      STOP
994    TYPE 992
992    FORMAT(1H , 'Cannot open output file: Garnet.out')
      STOP
      END

C
      SUBROUTINE READM (A,N,M,N1,M1)
C      SUBROUTINE TO READ A MATRIX HAVING N ROWS AND M COLUMNS
C
      DIMENSION A (N1,M1)
C      READ SIZE OF MATRIX
      READ (5,1000) N,M
C      READ MATRIX ONE ROW AT A TIME
      DO 100 I=1,N
      READ (5,1001) (A(I,J),J=1,M)
C      DO 998 J=1,M
C998   TYPE 999, I,J,A(I,J)
C999   FORMAT(1H , 'DEBUG (1) : I= ',I3,' J= ',I3,' A(I,J)= ',F5.2)
100    CONTINUE
      DO 101 I=1,N

```

```

SUM=0.0
DO 102 J=1,M
SUM=SUM+A(I,J)
102 CONTINUE
C   TYPE 990,SUM
C990  FORMAT(1H , 'SUM= ',F10.3)
DO 103 K=1,M
XMULT=1.0/SUM
C   TYPE 989,I,K,MULT,A(I,K)
C989  FORMAT(1H ,I3,I3,F9.3,F12.3)
A(I,K)=A(I,K)*XMULT
C   TYPE 988,A(I,K)
C988  FORMAT(1H , 'A(I,K) after = ',F12.3)
103 CONTINUE
101 CONTINUE
RETURN
1000  FORMAT(2I3)
1001  FORMAT(F3.2,F6.2,F5.2,F5.2,F6.2,F5.2)
END

C
SUBROUTINE PRINTM(A,N,M,N1,M1)
C   SUBROUTINE TO PRINT A MATRIX HAVING N ROWS AND M COLUMNS
C
DIMENSION A(N1,M1)
C   TYPE 991, N,M,N1,M1
C991  FORMAT(1H , 'N= ',I3, ' M= ',I3, ' N1= ',I3, ' M1= ',I3)
C   PRINT OUT MATRIX IN BLOCKS OF 10 COLUMNS
DO 100 IB=1,M,10
IE=IB+9
IF(IE - M) 2,2,1
1   IE=M
C   PRINT HEADING
2   WRITE(6,2000) (I,I=IB,IE)
DO 101 J=1,N
C   PRINT ROW OF MATRIX
C   TYPE 997, IB,IE
C997  FORMAT(1H , 'DEBUG (2) : IB= ',I3, ' IE= ',I3)
WRITE(6,2001) J,(A(J,K),K=IB,IE)
101 CONTINUE
100 CONTINUE
RETURN
2000  FORMAT(1H1,1X,10I12)
2001  FORMAT(1H0,15,10F12.6)
END

C
SUBROUTINE WPGA(X,M,M1,IPAIR,XLEV,ISIM)
C   SUBROUTINE TO PERFORM WEIGHTED PAIR-GROUP AVERAGE CLUSTERING
C
DIMENSION X(M1,M1),IPAIR(2,M1),XLEV(M1)
C   M1 EQUALS N
DIMENSION I1(444),I2(444),XSIM(444)
C   INITIALIZE
WRITE(6,2001)

```

```

DO 110 I=1,M
  I1(I)=I
110 CONTINUE
  XXXX=-9.0E+35
  IF (ISIM .NE. 1) XXXX=+9.0E+35
  M3=M-1
  IC=0

C
C   FOR A CORRELATION MATRIX FIND LARGEST SIMILARITY IN EACH COLUMN
C
C   FOR A DISTANCE MATRIX FIND SMALLEST SIMILARITY IN EACH COLUMN
C
1 DO 100 I=1,M
  IF (I1(I) .LE. 0) GOTO 100
  IX=0
  XX=XXXX
  DO 101 J=1,M
    IF (I .EQ. J) GOTO 101
    IF (I1(J) .LE. 0) GOTO 101
    GOTO(11,12), ISIM
11  IF (X(J,I)-XX) 101,101,13
12  IF (X(J,I)-XX) 13,101,101
13  XX=X(J,I)
    IX=J
101 CONTINUE
    I2(I)=IX
    XSIM(I)=XX
100 CONTINUE

C
C   FOR A CORRELATION MATRIX FIND MUTUALLY HIGH PAIRS
C   FOR A DISTANCE MATRIX FIND MUTUALLY LOW PAIRS
C
DO 102 I=1,M3
  IF (I1(I) .LE. 0) GOTO 102
  J=I2(I)
  IF (I1(J) .LE. 0) GOTO 102
  IF (J .LE. I) GOTO 102
  IF (I1(J) .EQ. I) GOTO 14
  IF (ABS(XSIM(I)-XSIM(J)) .GT. 0.00001) GOTO 102
C   SAVE PARAMETERS FOR A CLUSTER
14  IC=IC+1
    IPAIR(1,IC)=I
    IPAIR(2,IC)=J
    XLEV(IC)=XSIM(I)
    WRITE(6,2002) I,J,XSIM(I)
    I1(I)=J
    I1(J)=0

C   AVERAGE THE TWO COLUMNS
DO 103 K=1,M
  X(K,I)=(X(K,I)+X(K,J))/2.0
103 CONTINUE
102 CONTINUE
C   AVERAGE ROWS THAT WERE CLUSTERED ON THIS ITERATION

```

```

DO 105 I=1,M3
IF (I1(I) .LE. 0) GOTO 105
IF (I1(I) .EQ. I) GOTO 105
J=I1(I)
C AVERAGE TWO ROWS IN THE NEW CLUSTER
DO 106 K=1,M
IF (I1(K) .LE. 0) GOTO 106
X(I,K)=(X(I,K)+X(J,K))/2.0
106 CONTINUE
I1(I)=I
105 CONTINUE
IF (IC .LT. M3) GOTO 1
WRITE (6,2003)
RETURN
2001 FORMAT (1H1)
2002 FORMAT (6X,2I5,F15.6)
2003 FORMAT (1H0,4X,'COLUMNS 1 AND 2 -',1X,
1 'OBSERVATIONS COMBINED INTO CLUSTERS',/,
2 5X,'COLUMN 3 - SIMILARITY LEVEL OF CLUSTERING')
END

C
SUBROUTINE DENDRO(IPAIR,XLEV,M,M1,ISIM)
C SUBROUTINE TO PRINT A DENDROGRAM
C
DIMENSION IPAIR(2,M1),XLEV(M1)
C M1 WHEN MATRIX IS TRANSPOSED EQUALS N
DIMENSION I1(444),I2(444)
DIMENSION IOUT(61),XX(13)
DATA IBLNK,ICI,ICP,ICM/1H ,1H1,1H.,1H-/

C
C DETERMINE ORDER THAT BRANCHES WILL BE PRINTED IN
C
M2=M-1
DO 100 I=1,M
I1(I)=0
I2(I)=0
100 CONTINUE
DO 101 I=1,M2
J=I-1
11 IF (J .LE. 0) GOTO 12
IF (IPAIR(1,I) .EQ. IPAIR(1,J)) GOTO 13
J=J-1
GOTO 11
12 I2(I)=1
GOTO 15
13 K=I1(J)
IF (K .EQ. 0) GOTO 14
J=K
GOTO 13
14 I1(J)=I
15 DO 102 J=1,I
K=J
IF (IPAIR(2,I) .EQ. IPAIR(1,J)) GOTO 16

```

```

102  CONTINUE
      GOTO 101
16   I2(K)=0
      I1(I)=K
101  CONTINUE
C    FIND STARTING CLUSTER
      DO 103 I=1,M2
      JS=I
      IF (I2(I) .NE. 0) GOTO 20
103  CONTINUE
      CALL EXIT
20   NODE=IPAIR(1,JS)
C
C    FIND LARGEST AND SMALLEST SIMILARITY COEF.
C
      XMIN=XLEV(1)
      XMAX=XMIN
      DO 104 I=1,M2
C     TYPE 996, XMIN,XMAX,XLEV(I)
C996  FORMAT(1H , 'XMIN= ',F10.3,' XMAX= ',F10.3,' XLEV(I)= ',F10.3)
      IF (XLEV(I) .LT. XMIN) XMIN=XLEV(I)
      IF (XLEV(I) .GT. XMAX) XMAX=XLEV(I)
104  CONTINUE
      DX=(XMAX-XMIN)/25.0
      XMIN=XMIN-DX
      XMAX=XMAX+DX
      DX=(XMAX-XMIN)/60.0
      IF (ISIM .NE. 2) GOTO 21
      DX=-DX
      XMIN=XMAX
C
C    BLANK OUT PRINT LINE ARRAY
C
21   DO 105 I=1,61
      IOUT(I)=IBLNK
105  CONTINUE
C
C    PRINT DENDOGRAM
      X=XMIN
      DO 106 I=1,13
      XX(I)=X
      X=X+DX*5.0
106  CONTINUE
      WRITE(6,2000)
      WRITE(6,2001) (XX(I),I=2,12,2)
      WRITE(6,2002) (XX(I),I=1,13,2)
      WRITE(6,2003)
22   X=XMIN
      IF (JS .NE. 0) X=XLEV(JS)
      IS=IFIX((X-XMIN)/DX)+1
      DO 110 I=IS,61
      IOUT(I)=ICM
110  CONTINUE

```

```

IOUT(IS)=ICP
IF (JS .NE. 0) WRITE(6,2004) IOUT,NODE,X
IF (JS .EQ. 0) WRITE(6,2004) IOUT,NODE
IF (JS .EQ. 0) GOTO 31
DO 111 I=IS,61
IOUT(I)=IBLNK
111 CONTINUE
IOUT(IS)=ICI
WRITE(6,2004) (IOUT(I),I=1,IS)
NODE=IPAIR(2,JS)
JS=I1(JS)
GOTO 22
31 WRITE(6,2003)
WRITE(6,2002) (XX(I),I=1,13,2)
WRITE(6,2001) (XX(I),I=2,12,2)
WRITE(6,2005)
RETURN
2000 FORMAT(1H1)
2001 FORMAT(6X,6F10.4)
2002 FORMAT(1X,7F10.4)
2003 FORMAT(6X,'+',12('----+'))
2004 FORMAT(6X,61A1,1X,I3,F10.4)
2005 FORMAT(1H0,4X,'DENDOGRAM - ',1X,
1 'VALUES ALONG X-AXIS ARE SIMILARITIES')
END

C
SUBROUTINE DIST(X,N,M,N1,M1,A,M2)
C SUBROUTINE TO CALCULATE THE MATRIX OF DISTANCE COEFFICIENTS
C BETWEEN COLUMNS OF DATA MATRIX X
C
DIMENSION X(N1,M1),A(M2,M2)
AN=N
C CALCULATE DISTANCE COEFFICIENT BETWEEN COLUMNS I AND J
DO 100 I=1,M
DO 100 J=I,M
C ZERO SUM AND CALCULATE DISTANCE
DISTX=0.0
DO 101 K=1,N
DISTX=DISTX+(X(K,I)-X(K,J))**2
101 CONTINUE
C CALCULATE DISTANCE COEFFICIENT AND STORE IN A MATRIX A
A(I,J)=SQRT(DISTX/AN)
A(J,I)=A(I,J)
100 CONTINUE
RETURN
END

C
SUBROUTINE RCOEF(X,N,M,N1,M1,A,M2)
DIMENSION X(N1,M1),A(M2,M2)
AN=N
C
C CALCULATE CORRELATION COEFFICIENT BETWEEN COLUMNS I AND J
C

```

```

DO 100 I=1,M
DO 100 J=I,M

C
C ZERO SUMS
C
SX1=0.0
SX2=0.0
SX1X1=0.0
SX2X2=0.0
SX1X2=0.0

C
C CALCULATE SUMS,SUMS OF SQUARES AND SUM OF CROSS-PRODUCT
C OF COLUMNS OF I AND J
C
DO 101 K=1,N
SX1=SX1+X(K,I)
SX2=SX2+X(K,J)
SX1X1=SX1X1+X(K,I)**2
SX2X2=SX2X2+X(K,J)**2
SX1X2=SX1X2+X(K,I)*X(K,J)
101 CONTINUE
C
C CALCULATE CORRELATION COEFFICIENT AND STORE IN MATRIX A
C
R=(SX1X2-SX1*SX2/AN)/
1 SQRT((SX1X1-SX1*SX1/AN)*(SX2X2-SX2*SX2/AN))
A(I,J)=R
A(J,I)=R
100 CONTINUE
RETURN
END

C FOR LISTING OF SUBROUTINES, SEE STATISTICS AND DATA
C ANALYSIS IN GEOLOGY " BY JOHN C. DAVIS,
LIB. REF. QE 48.8 .D26
END

```

## APPENDIX D

## MULTIPLE DISCRIMINANT ANALYSIS PROGRAM FOR HAM GARNETS

```

FILE NAME          SPSS MDA CALC
VARIABLE LIST     TIO2,AL2O3,CR2O3,FEO,MGO,CAO
INPUT MEDIUM      DISK
N OF CASES        505
SUBFILE LIST      HW1 (4) HW2 (10) HW3 (32) HW4 (28) HW5 (53)
                  HW6 (31) HW7 (8) HD1 (1) HD4 (32) HD7 (2)
                  HD6 (5) HD2 (40) HD3 (24) HD5 (172)
                  ELWLHZ (20) ELWMEG (43)
INPUT FORMAT      FIXED(F4.2,F7.2,F6.2,F6.2,F7.2,F6.2)
READ INPUT DATA
RUN SUBFILES      ALL
RAW OUTPUT UNIT   16
DISCRIMINANT      GROUPS = SUBFILES/VARIABLES = TIO2 TO CAO/
                  ANALYSIS = TIO2 TO CAO/
                  METHOD = MAXMINF/
                  TOLERANCE = .000001/
                  MAXSTEPS = 9/
                  FIN = 0.00/
                  FOUT = 0.00/
                  FUNCTIONS = (1,99.9,0.99)/
                  PRIORS = SIZE/
OPTIONS           5,6,7,11,12,17,18,19
STATISTICS        ALL
FINISH

```

FOR DOCUMENTATION OF THIS PROGRAM SEE "KLECKA,W.R., 1975  
DISCRIMINANT ANALYSIS. IN, STATISTICAL PACKAGE FOR THE  
SOCIAL SCIENCES, 2ND ED. (N.H. NIE, C.H. HULL, JG. JENKINS,  
K. STEINBRENNER AND D.H. BENT, EDS), MCGRAW-HILL, NEW YORK,  
434-462.

## APPENDIX E

### MICROPROBE OPERATING CONDITIONS

Garnets were analysed by energy dispersive analysis at Dalhousie University. Mineral analyses were obtained by Cambridge Mk V microprobe using synthetic and natural standards. Raw x-ray intensities were corrected for atomic number, fluorescence and absorption effects by the correction program EMPADR VII (Rucklidge 1967). Microprobe voltage and beam current were 15 kv and 5 nanoamps, respectively. The detection limits of all elements except magnesium and sodium were 0.1 percent. The detection limits of magnesium and sodium were 0.2 and 0.3 percent, respectively.

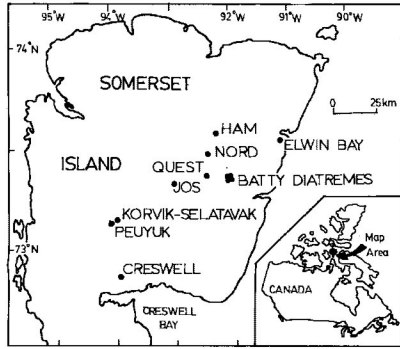
All other mineral analyses were obtained at Purdue University using a fully automated, MAC 500, wavelength dispersive microprobe (Finger and Hadidiacus 1972) and synthetic and natural standards. Raw x-ray-count data were processed by the Bence-Albee (1968) alpha-factor method. Microprobe voltage and beam current were 15 kv and 25 nanoamps, respectively. Detection limits are not available for this microprobe.

Bence, A.E. and Albee, R.V., 1968. Empirical correction factors for electron microanalyses of silicates and oxides. *Journal of Geology*, 76, 382-403.

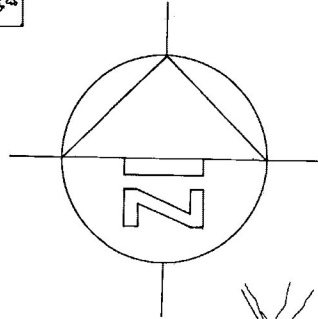
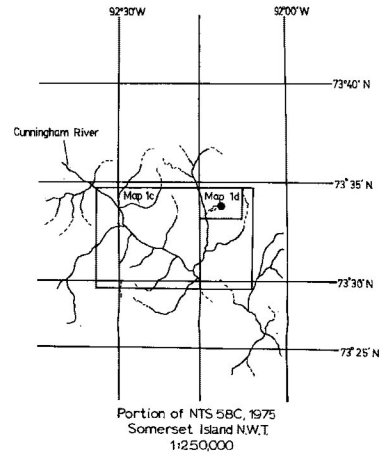
Finger, L.E. and Hadidiacus, C.Q., 1972. Electron microprobe automation. *Carnegie Institute Washington, Yearbook* 71, 598-600.

Rucklidge, J.C., 1967. A computer program for processing microprobe data, *Journal of Geology*, 75, 126.

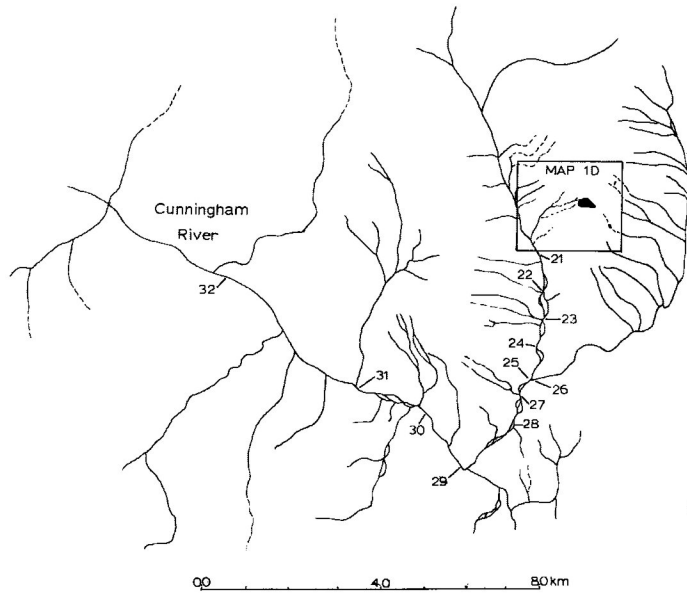
MAP IA



MAP IB



MAP IC



MAP 1D

